VOLUME 2

ILLUSTRATIONS AND APPENDICES

PLATES

(Abbreviated title)

FIGURES

(Abbreviated title)

APPENDICES CONTENTS

Fig. 1.1 Location of study area showing B.G.S. 1:250,000 offshore mapping areas relevant to this study.

LITHOFACIES CODE

DIAMICT

Dm - = massive
Ds - = stratified
Dd - = deformation structures
D-c = >5 % clasts
D-d = ⩽5 % clasts
D--(f) = >5 % shell material

SANDS = S
Sm - = massive
Sh - = horizontal lamination
Sr - = ripples
Sf - = flaser or wavey lamination
Sg - = graded
Sd - = deformation structures
S-c = > 5 % clasts
S-d = ⩽5 % clasts
S--(f) = >5 % shell material
(m)S--- = muddy

FINE GRAINED (mud) = F
Fm - = massive
Fl - = horizontal lamination
Fd - = deformation structures
Ff - = flaser or wavey lamination
F-d = dropstones
F--(f) = >5 % shell material
(s)F--- = sandy
Fl/Sh = interlaminated mud - sand
Fb/Sb = Thinly interbedded mud-sand

SYMBOLS FOR LOGS

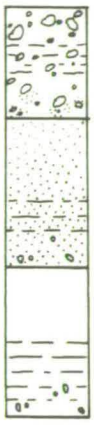

DIAMICT
massive
stratified
sandy
SAND
massive
laminated
pebbly
MUD
massive
laminated
dropstones

Ripple cross-lamination
Sand lenses
Convolute lamination
Deformation structures
Monosulphides
Clay balls
Wood fragments
Bioturbation
Whole shells
Shell fragments
Iron concretions
Carbonate concretions
Phosphatic horizon
Conformable contact
Erosional contact
Gradational contact
Monosulphides

Fig. 1.2. Lithofacies code and symbols used for borehole logs.

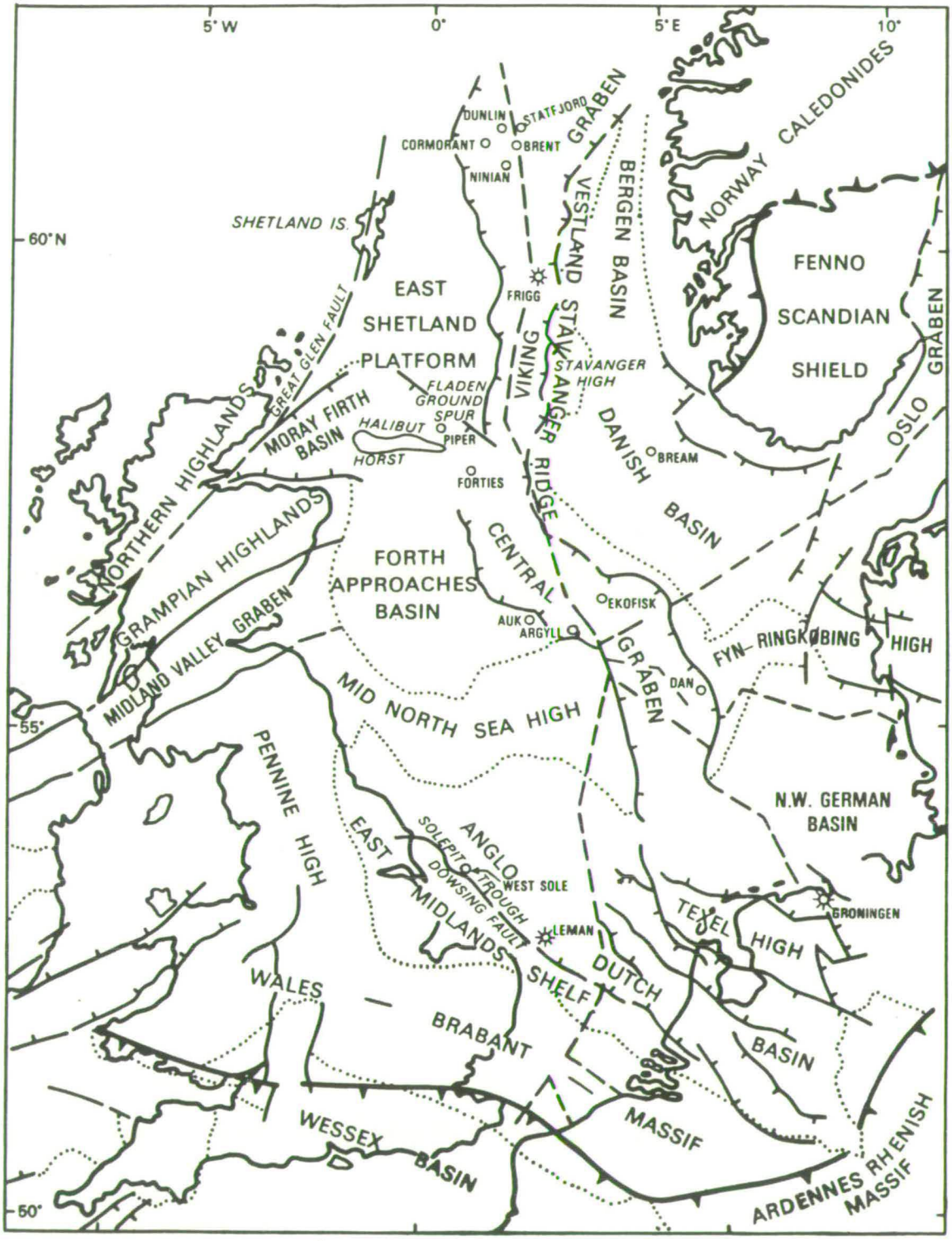

Fig. 1.3. Structural features in the North Sea (after Kent,1975).

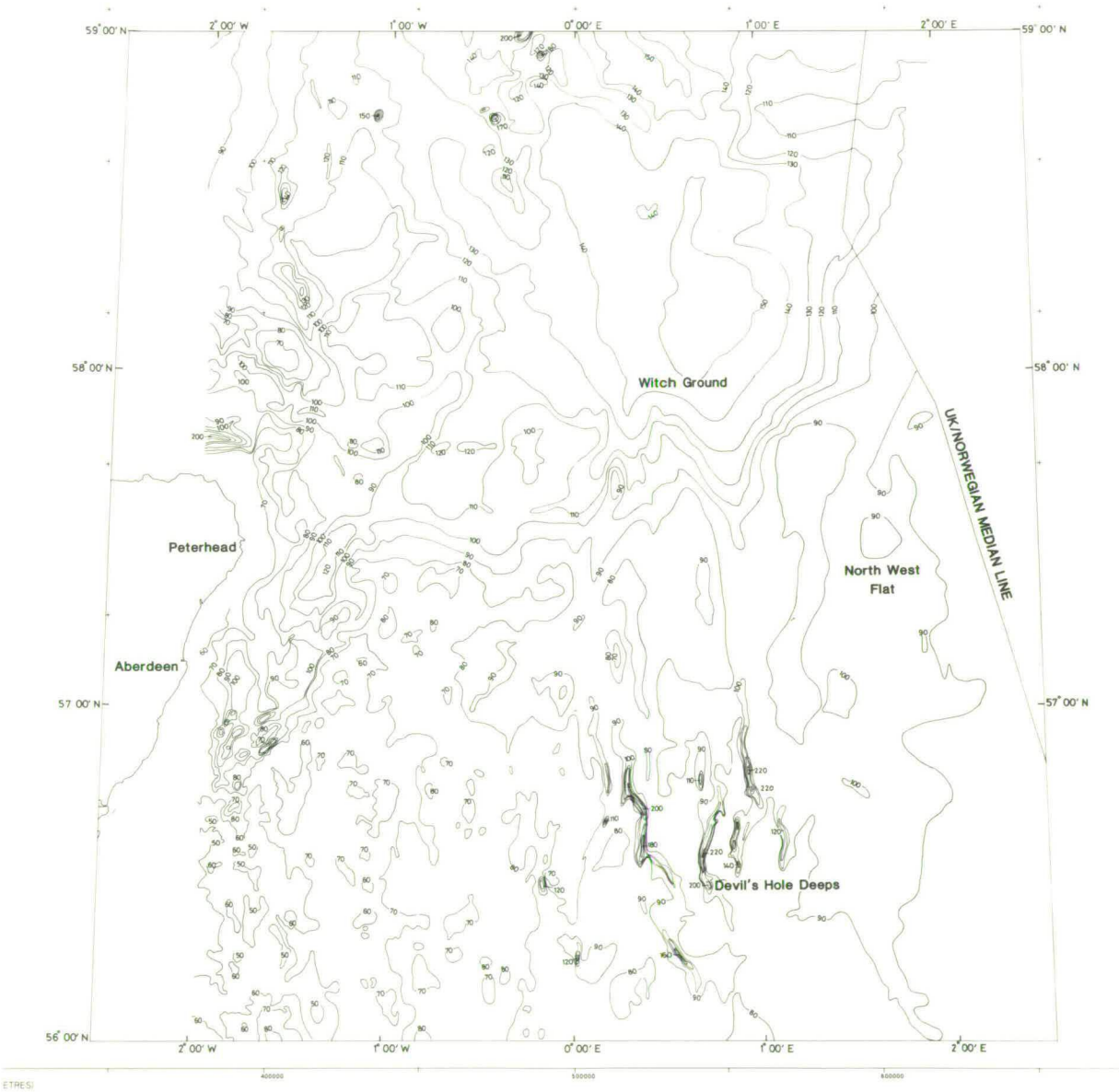

Fig. 1.4. Bathymetry of the study area.

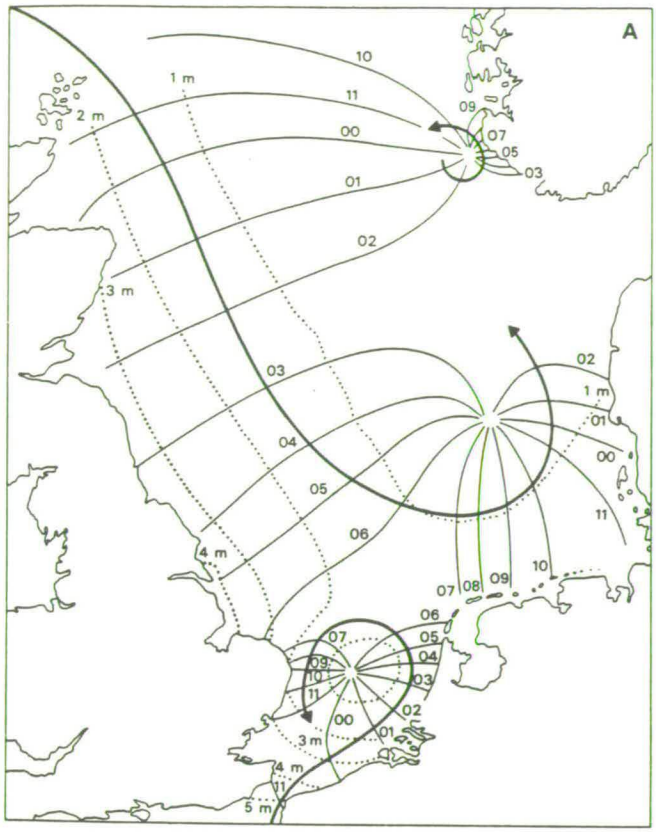

Fig. 1.5. The amphidromic tidal system in the North Sea illustrating the circulation of tidal waves around amphidromic points (after Reading,1978).

Fig. 1.6. Superficial sediments distribution (after Owens, 1977).

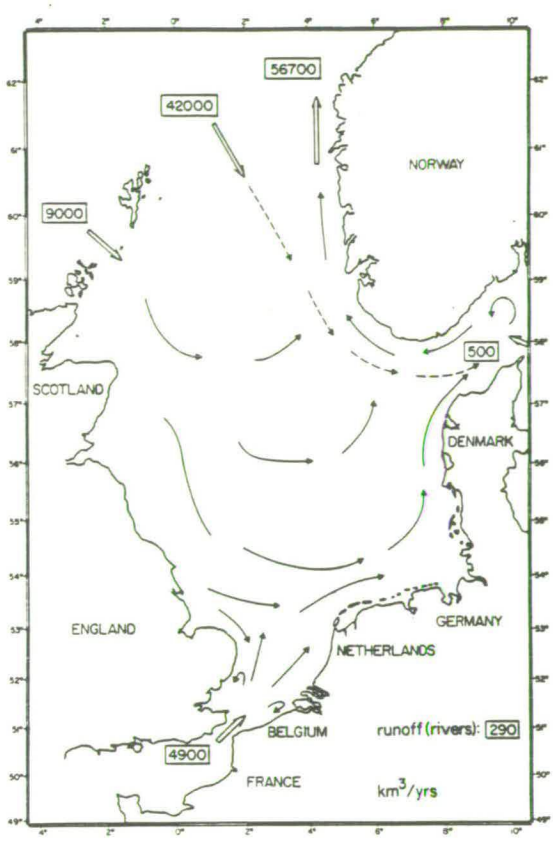

Fig. 1.7. Inflow of water into the North Sea (numbers indicate Km yr-1) and the general water circulation, arrows indicate direction of flow and broken arrows subsurface flow (after Eisma,1981).

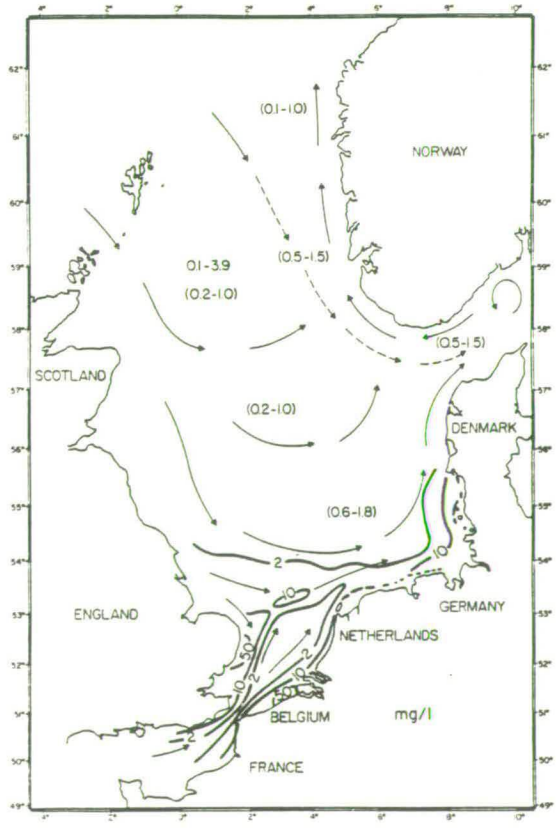

Fig. 1.8. Distribution of suspended matter and water circulation in the North Sea (suspended matter concentrations in mg,1), (after Eisma,1981).

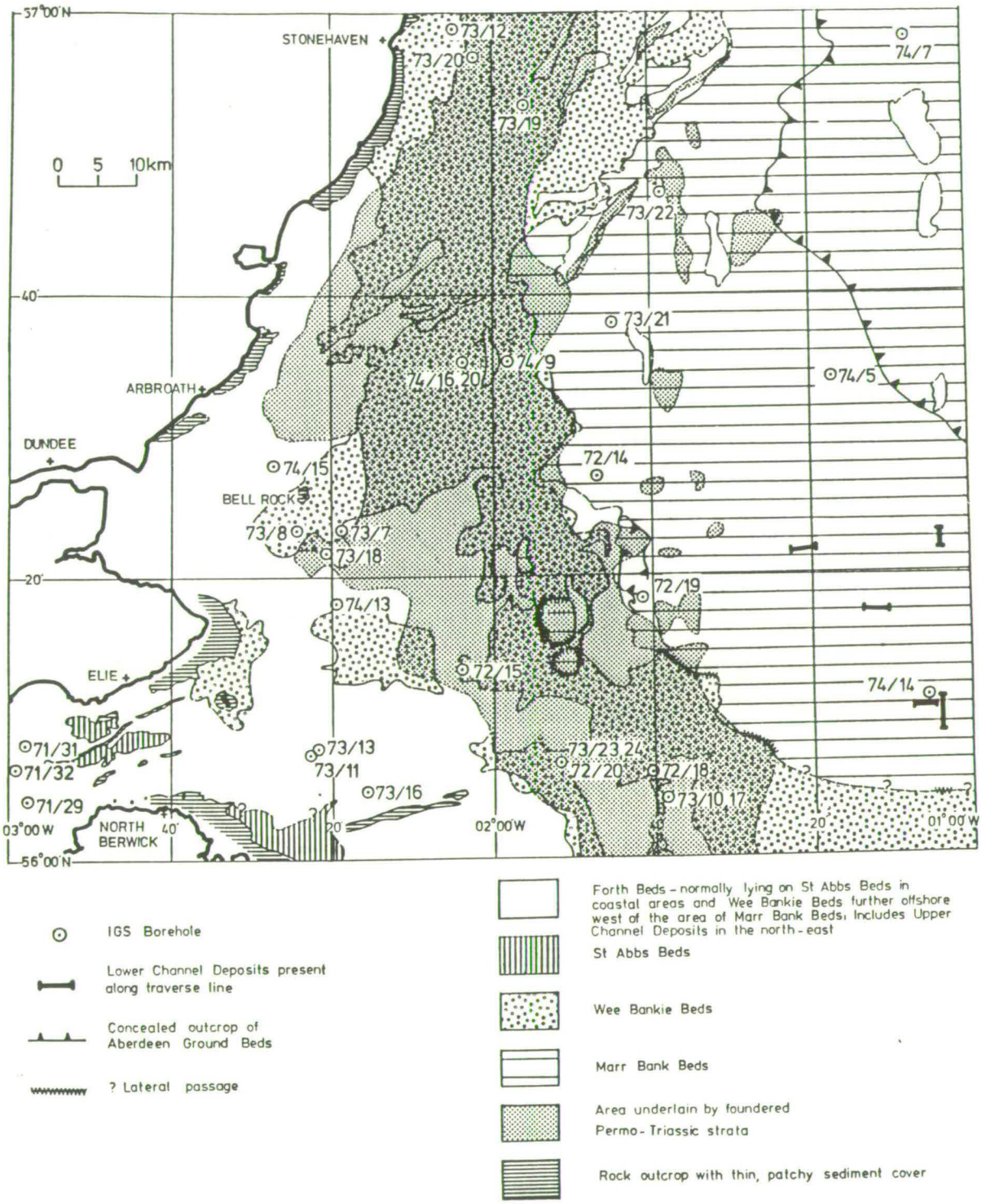

Fig. 1.9. Main geomorplological features of the west central North Sea (after Thomson and Eden,1977).

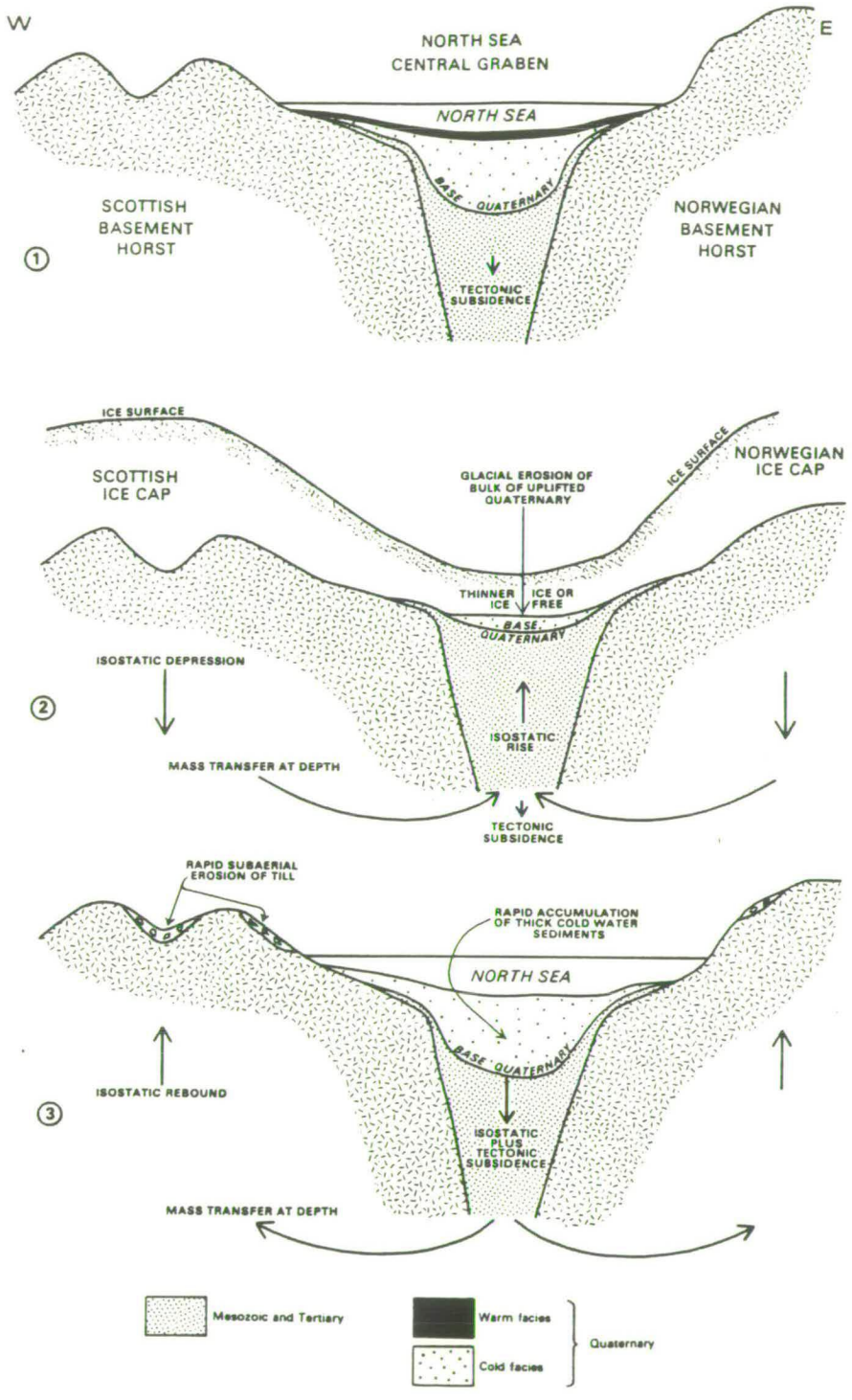

Fig. 1.10. Isostatic model to explain rapid subsidence and sedimentation in the North Sea (after Eden et al., 1978).

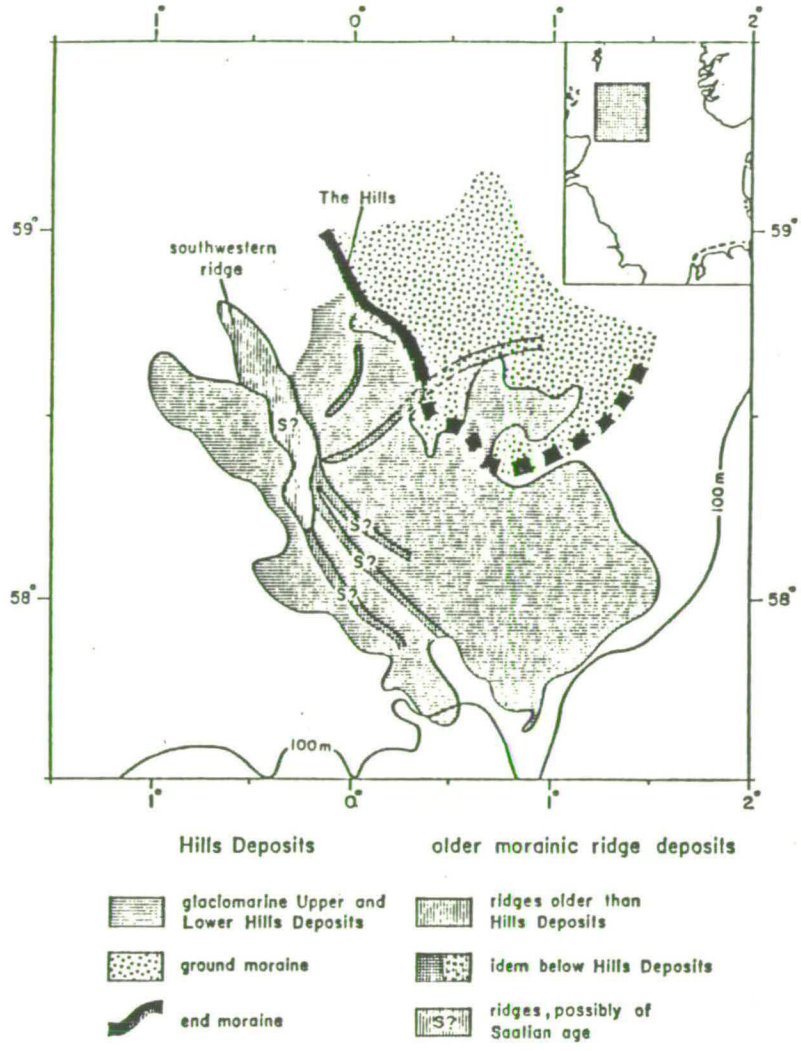

Fig. 1.11. Distribution of subglacial and glaciomarine sediments and moraine ridges in the Fladen Ground area (after Jansen, 1976).

Fig. 1.12. The maximum extension of the ice margin during the last Weichselian glaciation (after Jansen,1976).

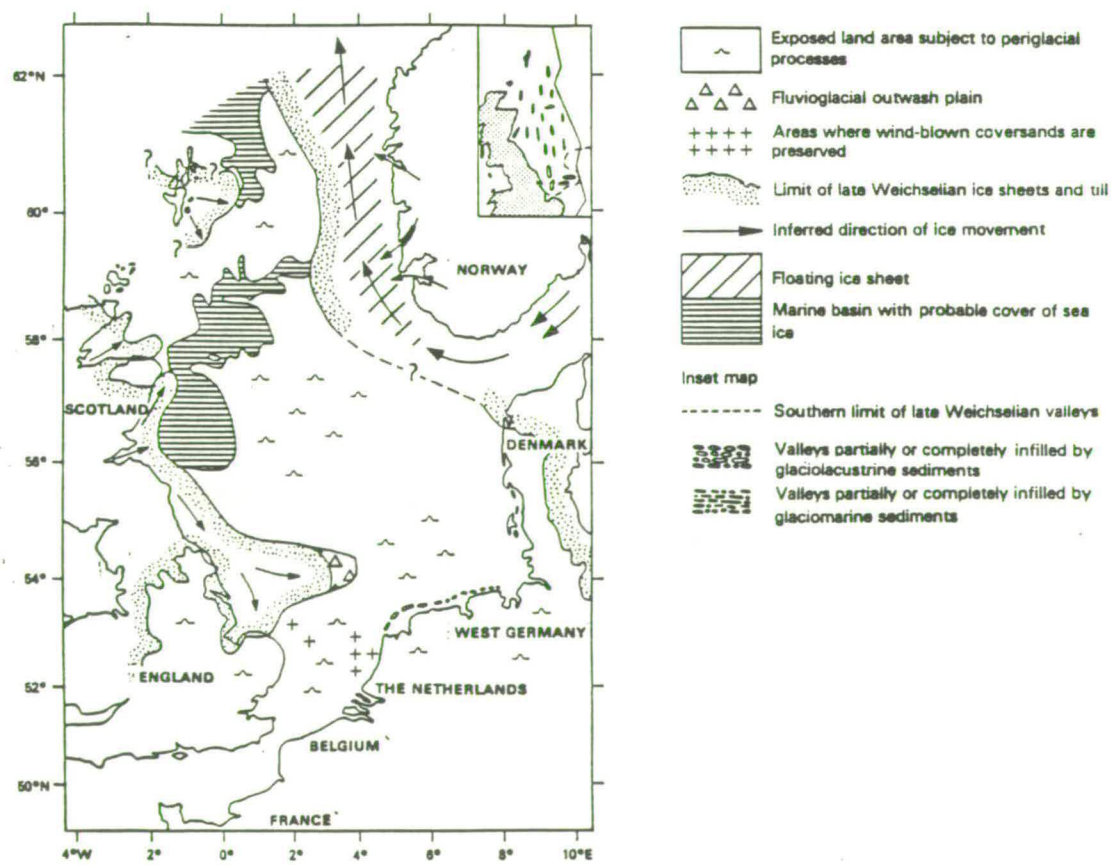

Fig. 1.13. Palaeogeography of the North Sea during the maximum offshore extension of the late Weichselian ice sheet (after Cameron et al.,1986).

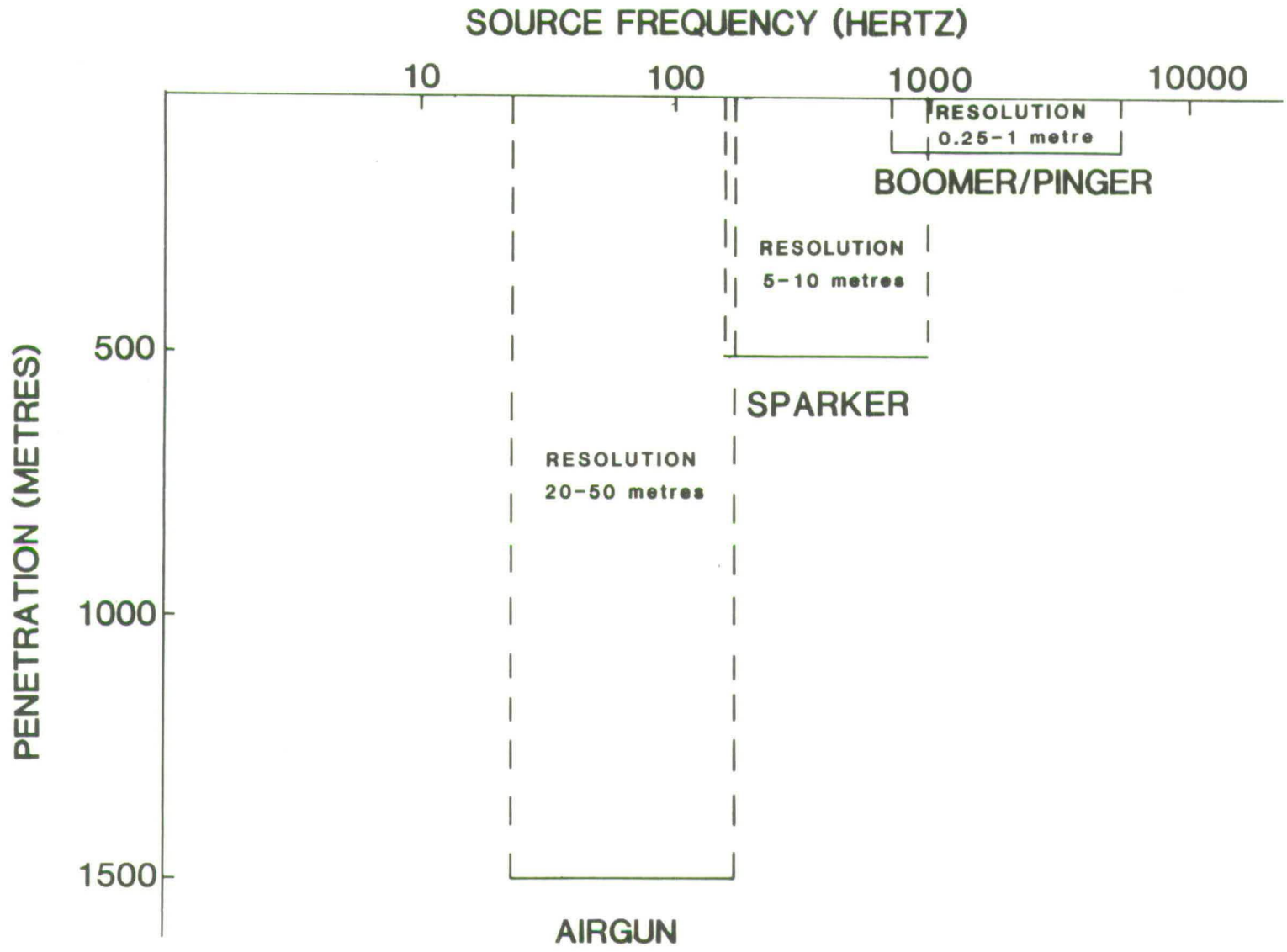

Fig. 1.14. operational capabilities of B.G.S. acoustic profiling equipment.

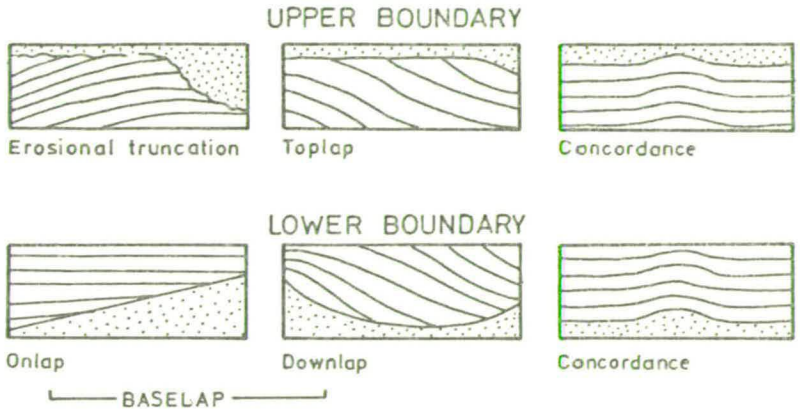

Fig. 2.1. Relations of reflectors to sequence boundaries (after Mitchum et. al., 1977a).

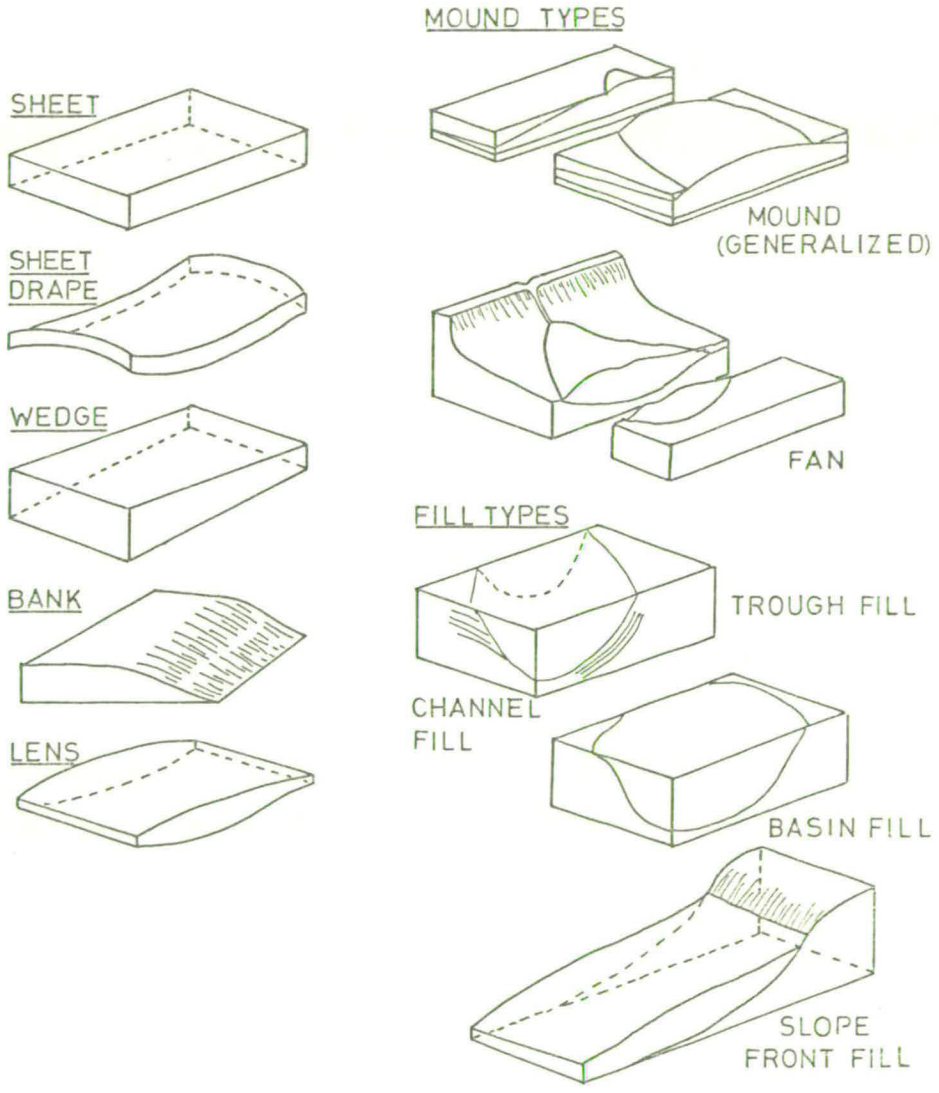

Fig. 2.2 External forms of some seismic facies units (after Mitchum et. al., 1977b).

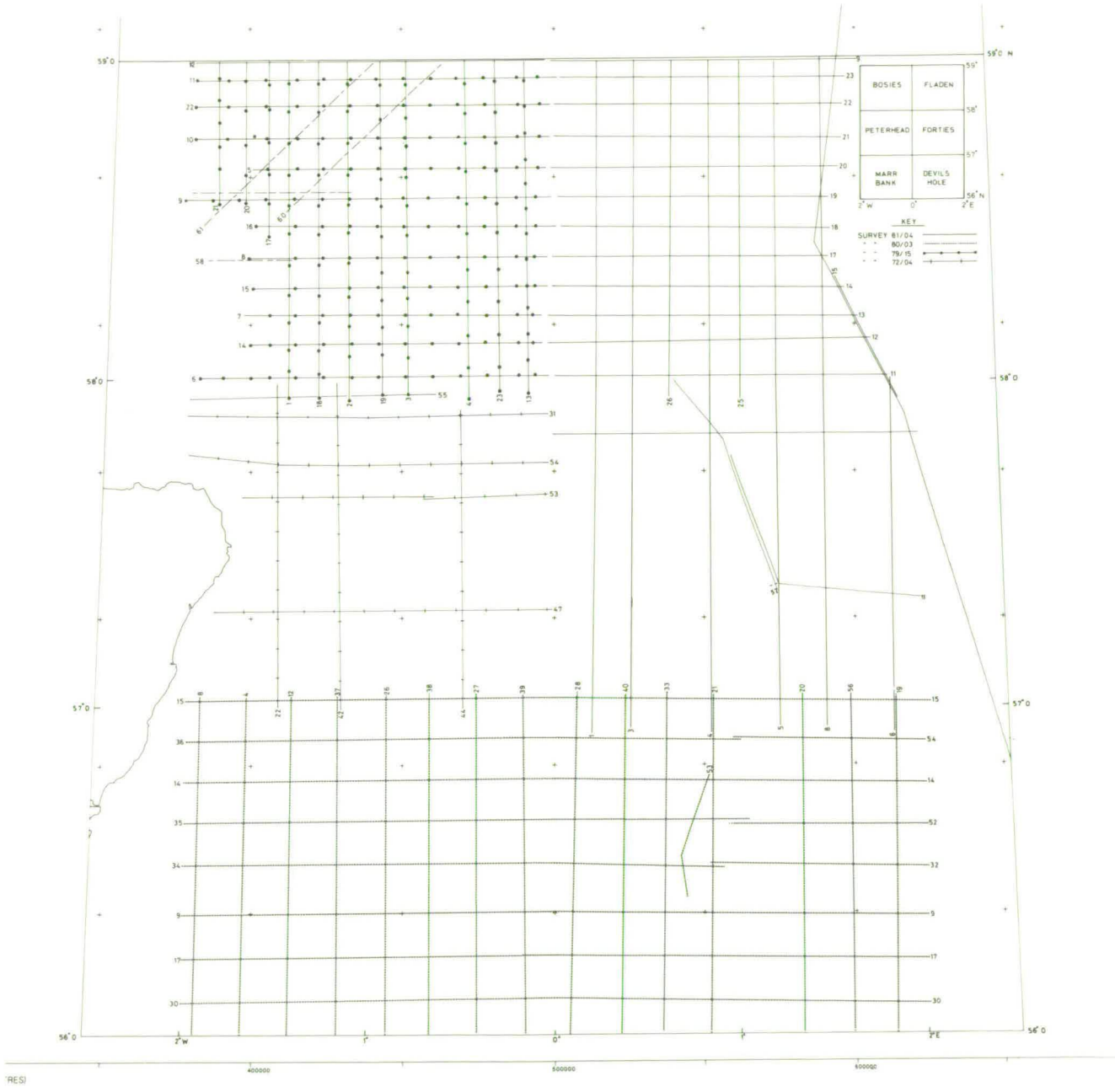

Fig. 2.3. Location of seismic survey lines.

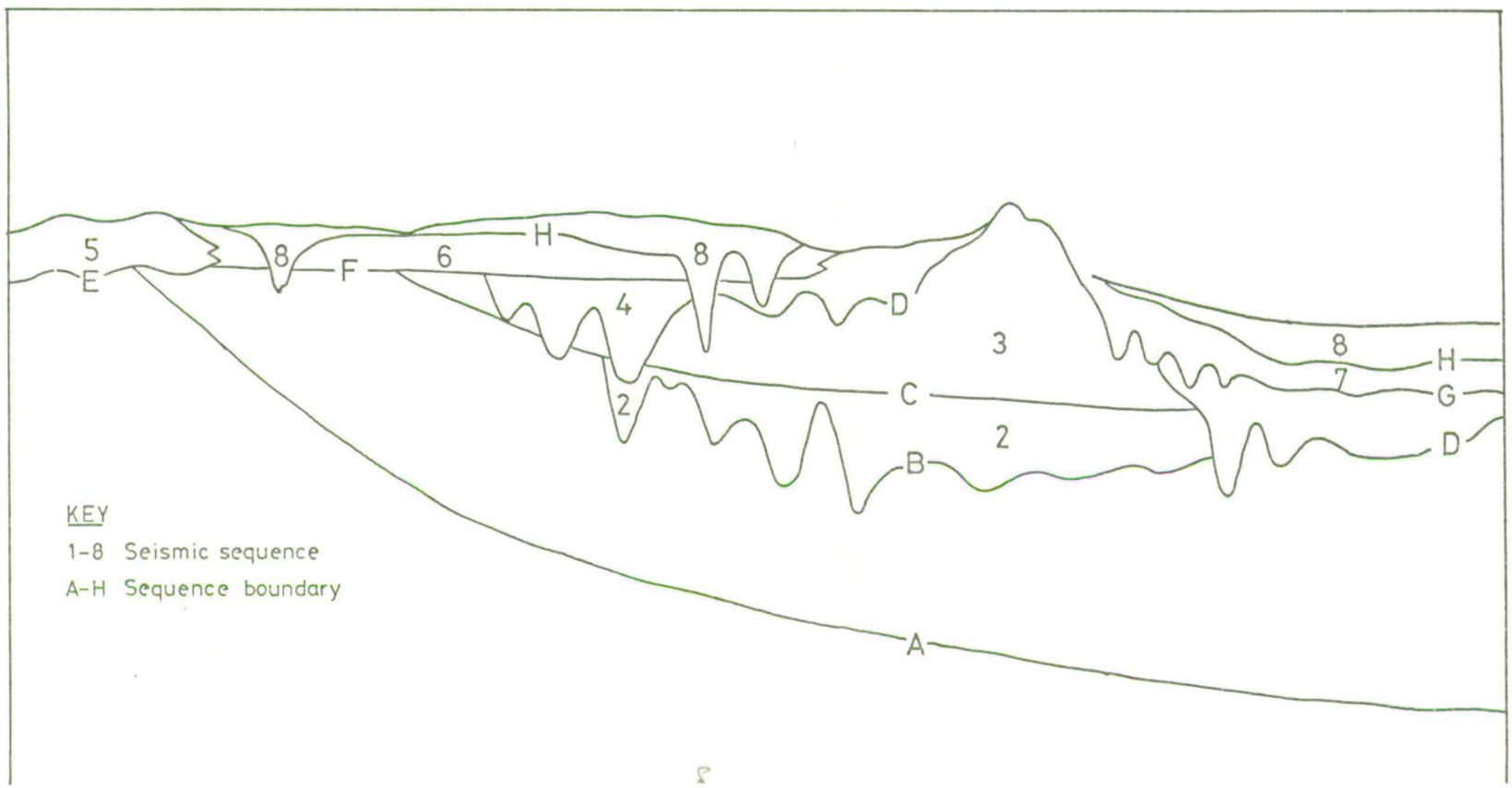

Fig. 2.4. Schematic diagram depicting the eight seismic sequences (1-8), their lateral and vertical relationships, and the bounding surfaces (A-H).

Fig. 2.5. East-west seismic line interpretations (see back pocket).

Fig. 2.6. North-south seismic line interpretations (see back pocket)

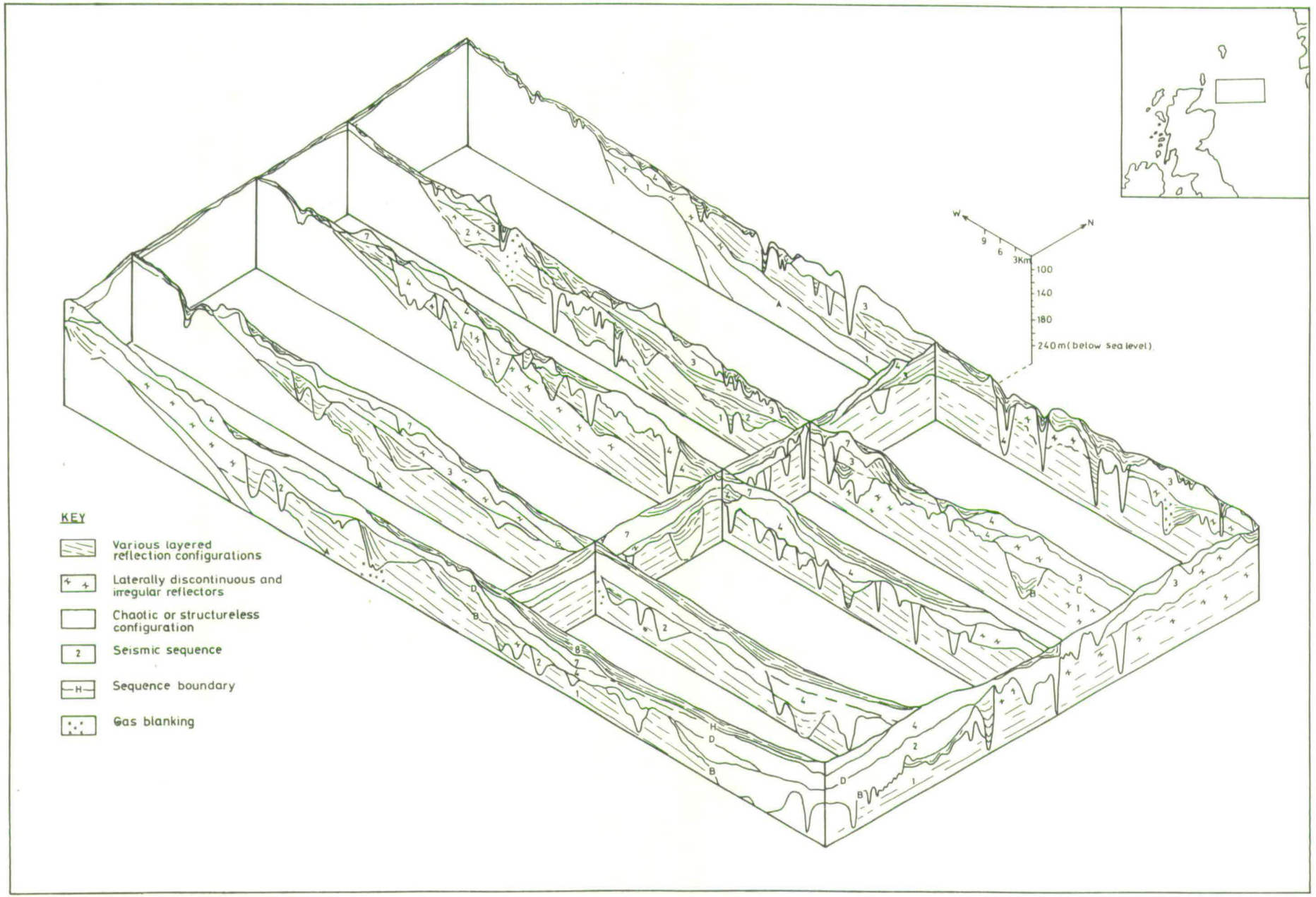

Fig. 2.7 Fence diagram depicting interpretations of various lines shot in the Bosies Bank and Fladen areas, and not shown in figs. 2.5–2.6.

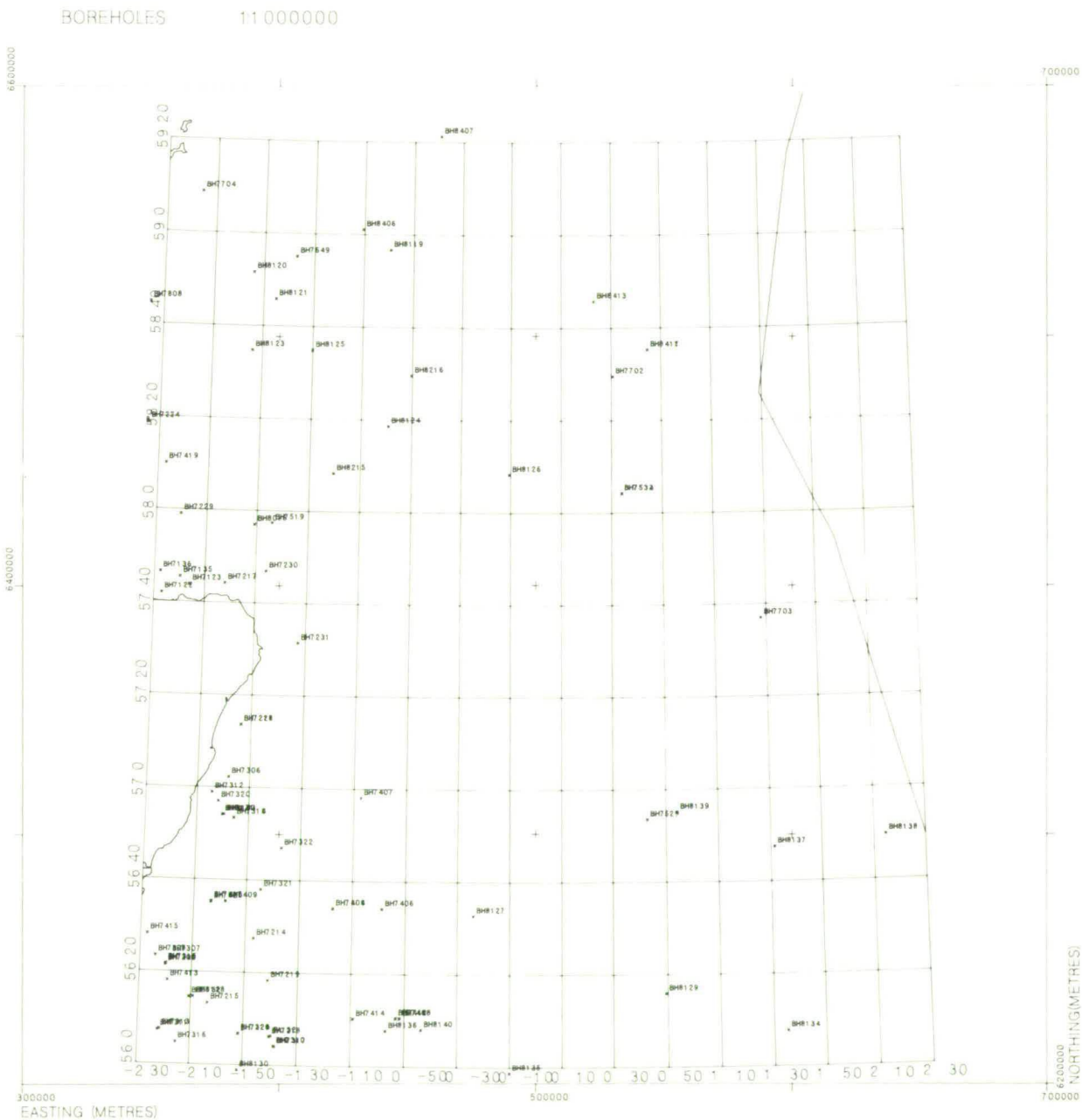

Fig. 2.8. Location of boreholes in the study area.

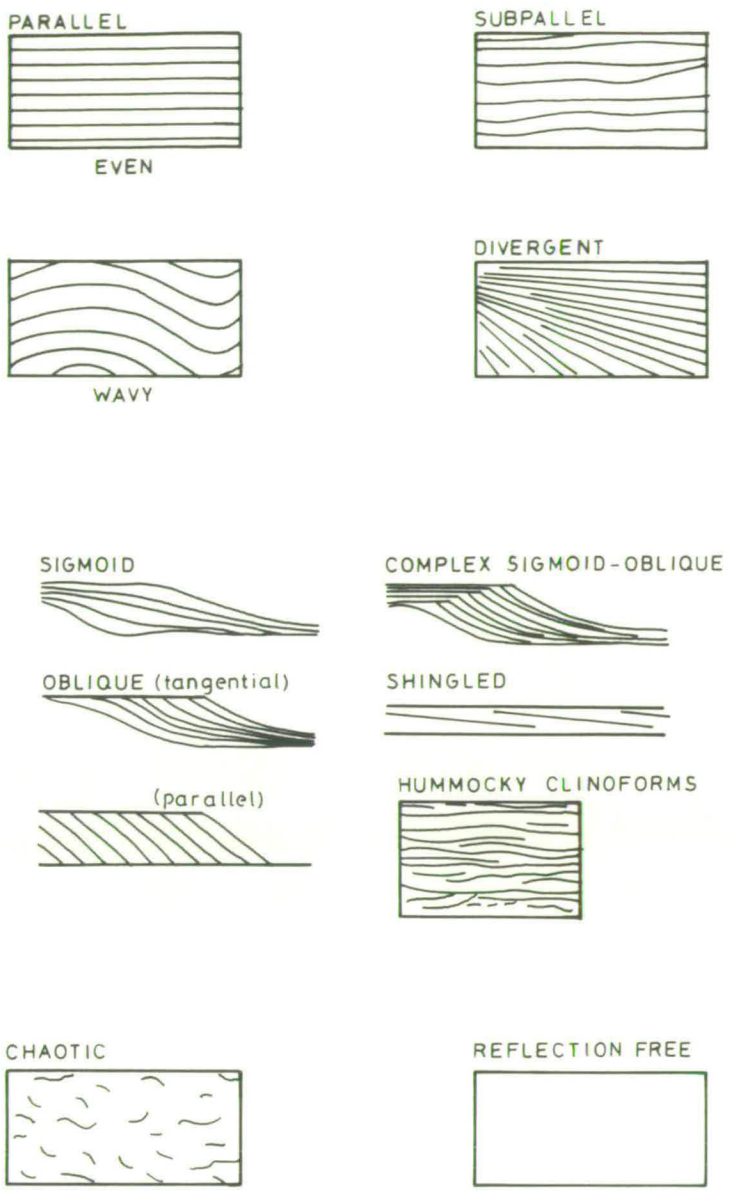

Fig. 2.9. Various reflection configurations (after Mitchum et. al., 1977b)

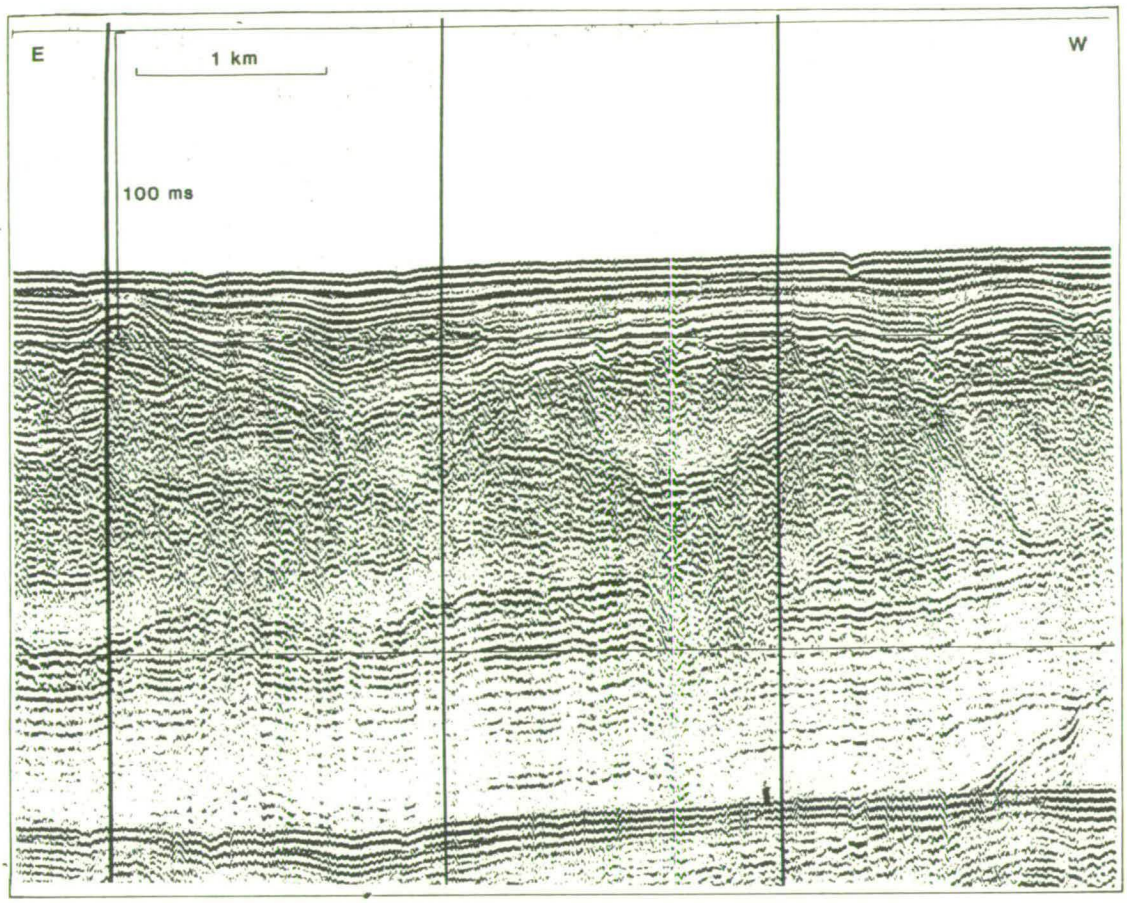

Fig 2.10a Sparker record from the Bosies Bank area.

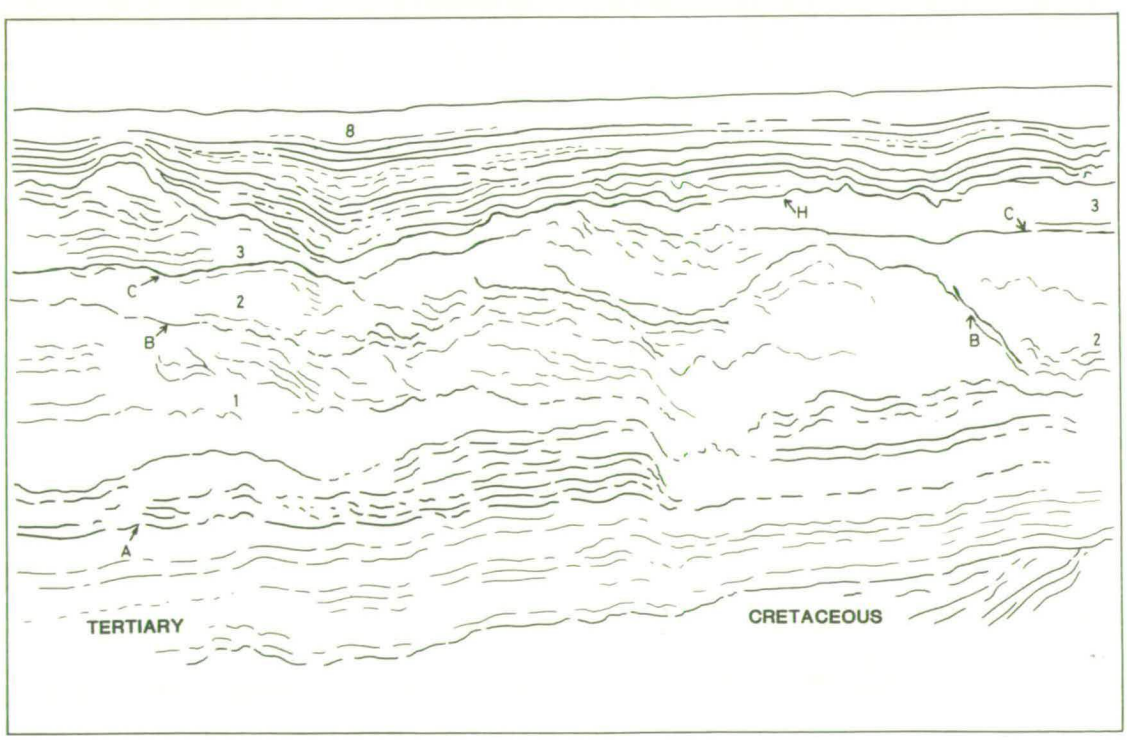

Fig. 2.10b. Line interpretation of the above record depicting the seismic sequences and boundaries.

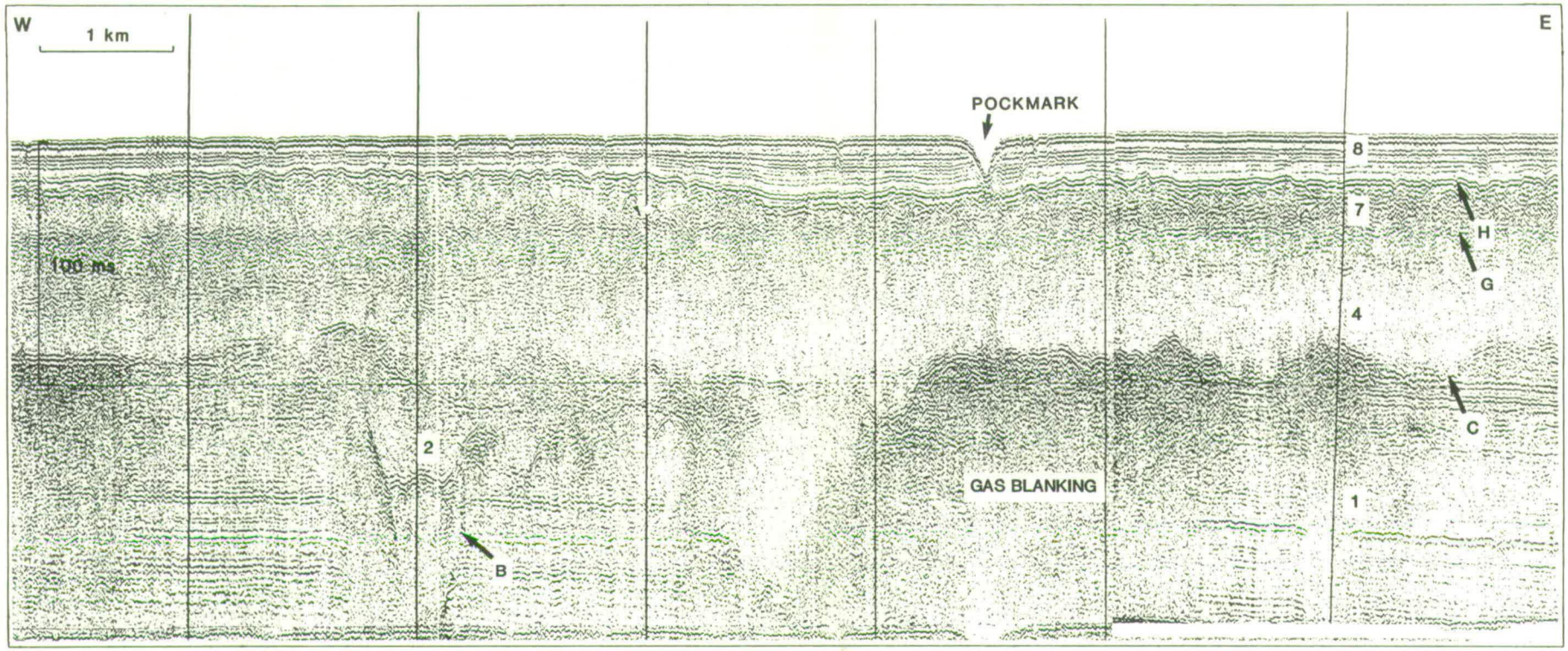

Fig. 2.11. Sparker record from the Fladen area, note the 'V' shaped pockmark at the seabed associated with an underlying zone of gas blanking.

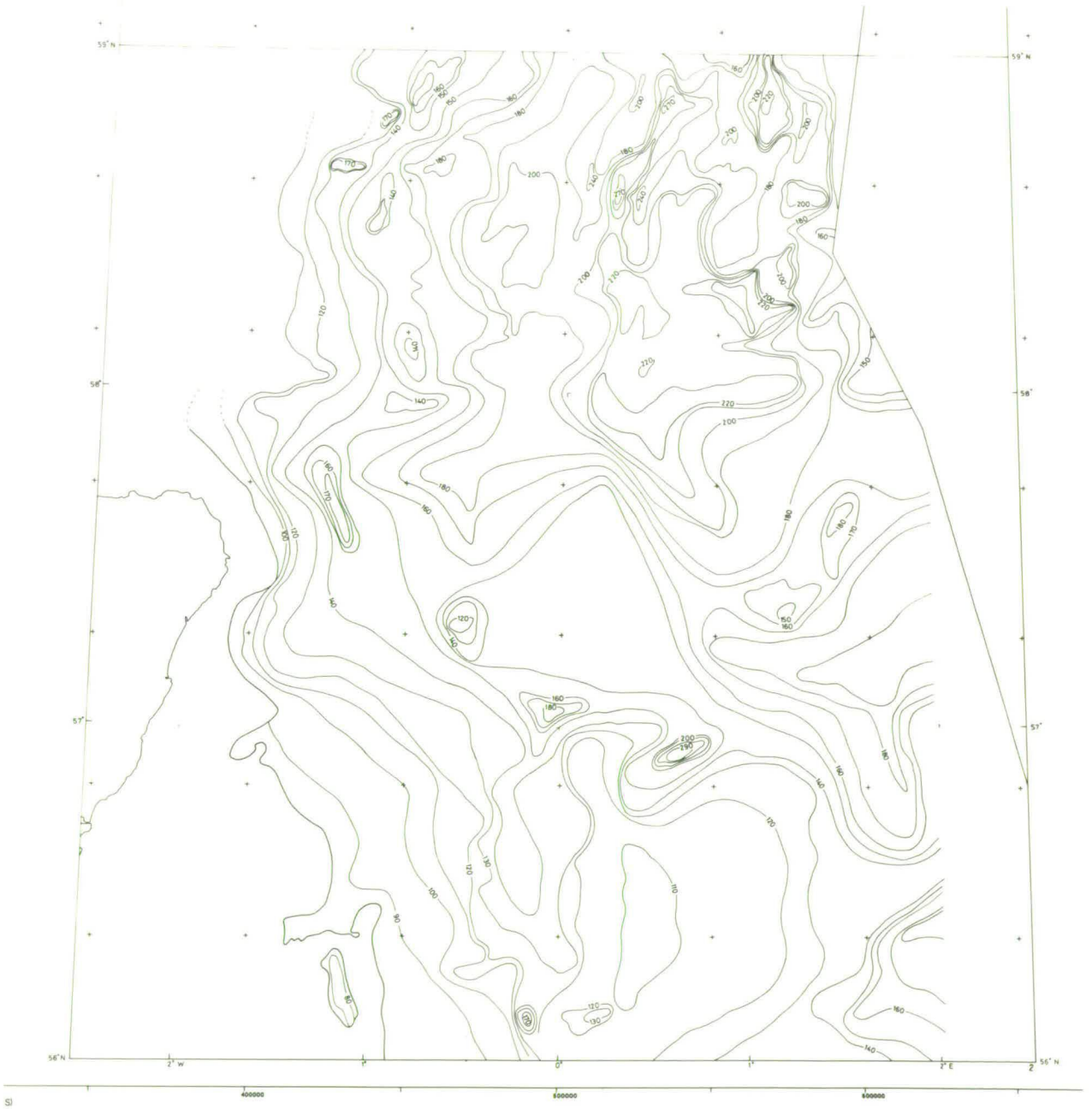

Fig. 2.12. Contours below sea level to the top of seismic sequence 1.

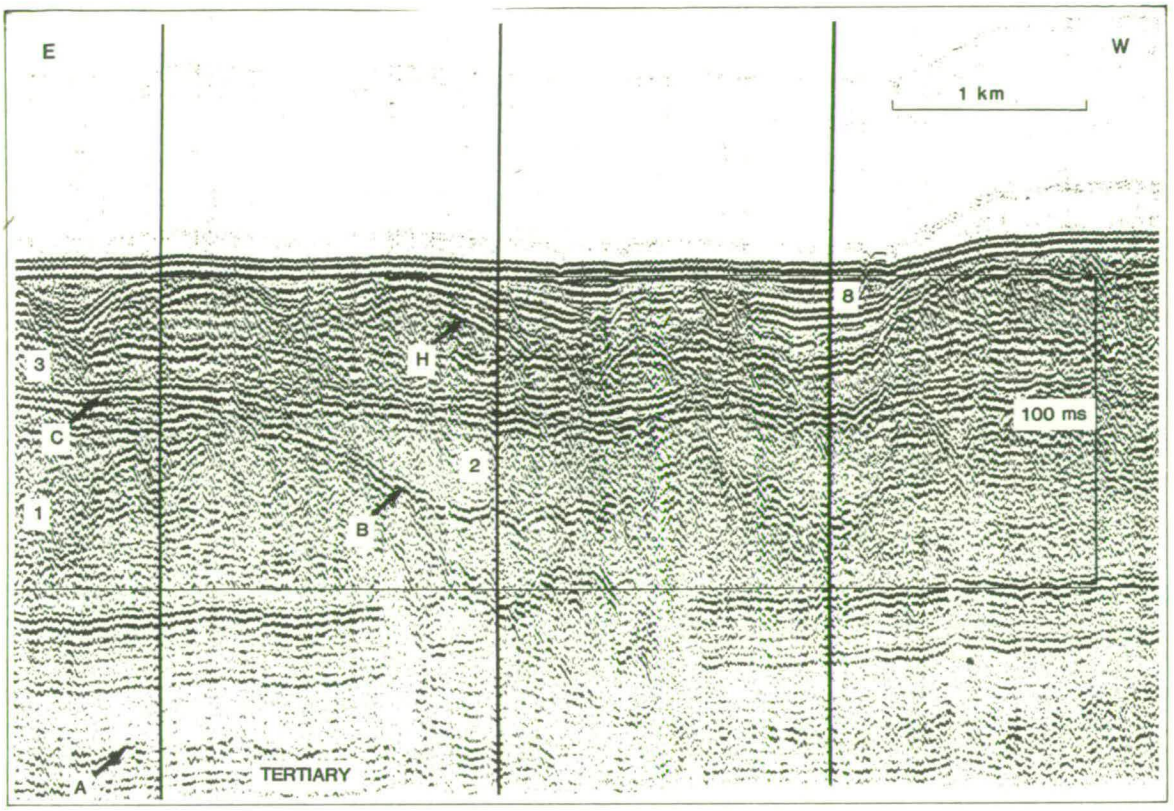

Fig. 2.13. Sparker record from the Bosies Bank area showing the highly irregular basal boundary of sequence 2 and the relatively even upper boundary, reflector C.

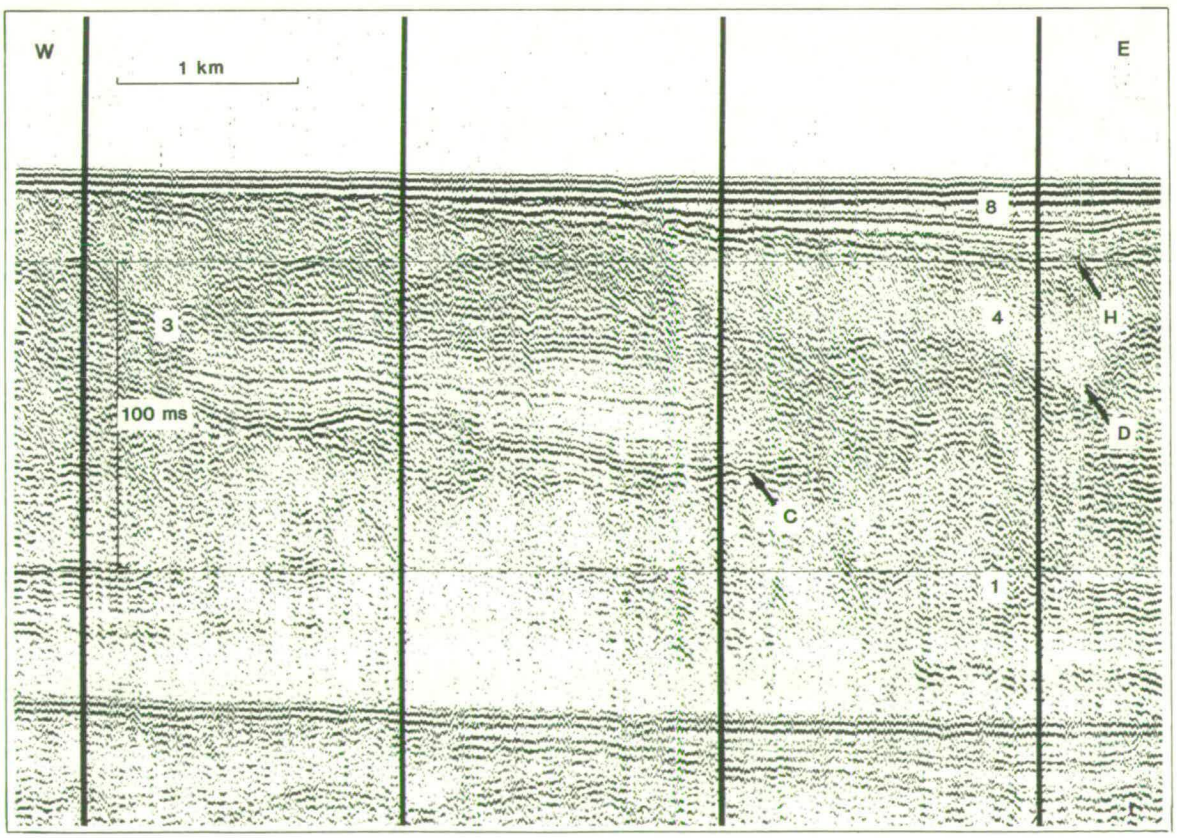

Fig. 2.14. Sparker record from the Bosies Bank area showing the sub-parallel configurations in sequences 2 and 3, and the irregular base to sequence 4.

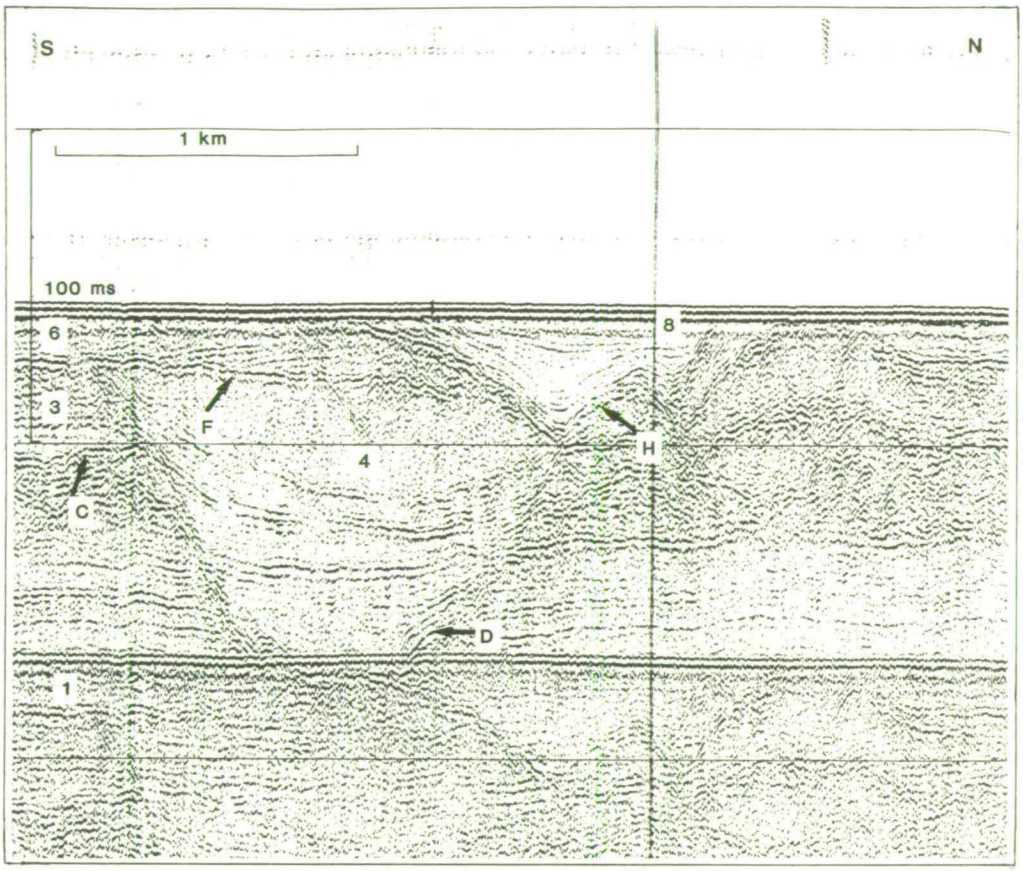

Fig. 2.15. Sparker record from the Forties area showing the inclined reflectors in sequence 6 and the planar base (F). Note also the two sequences of channel fill, 4 and 8.

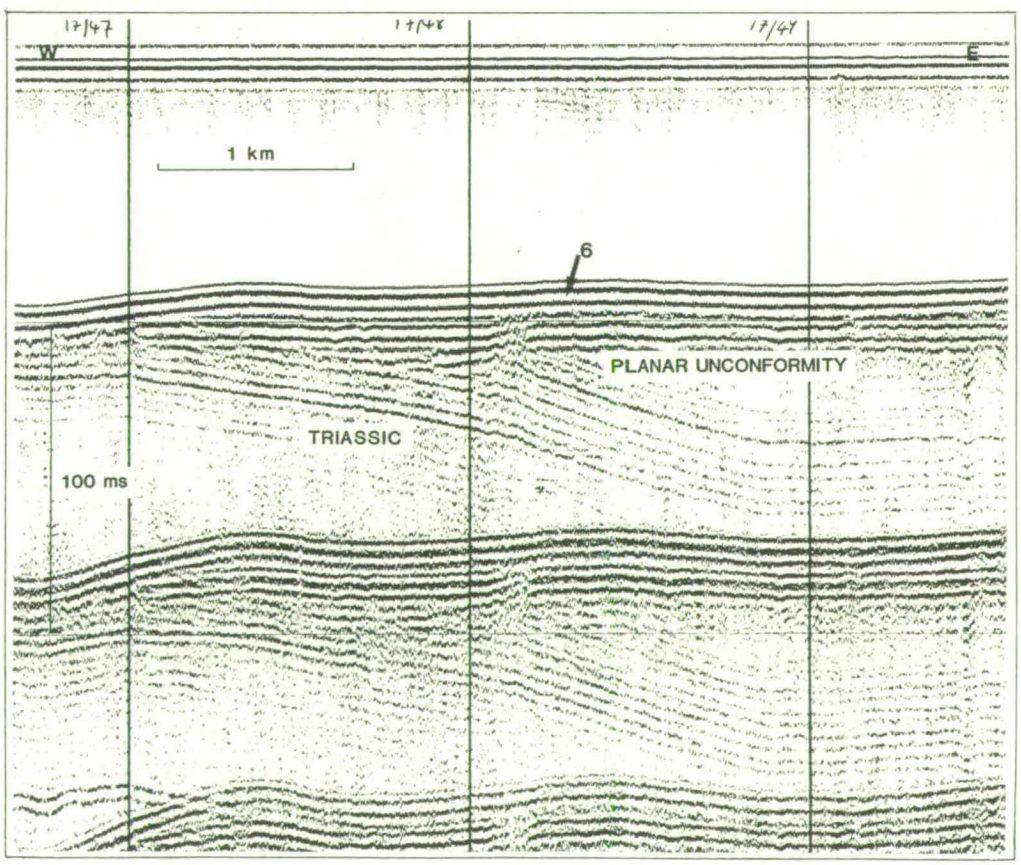

Fig. 2.16. Sparker record from the Marr Bank area showing the planar base of sequence 6.

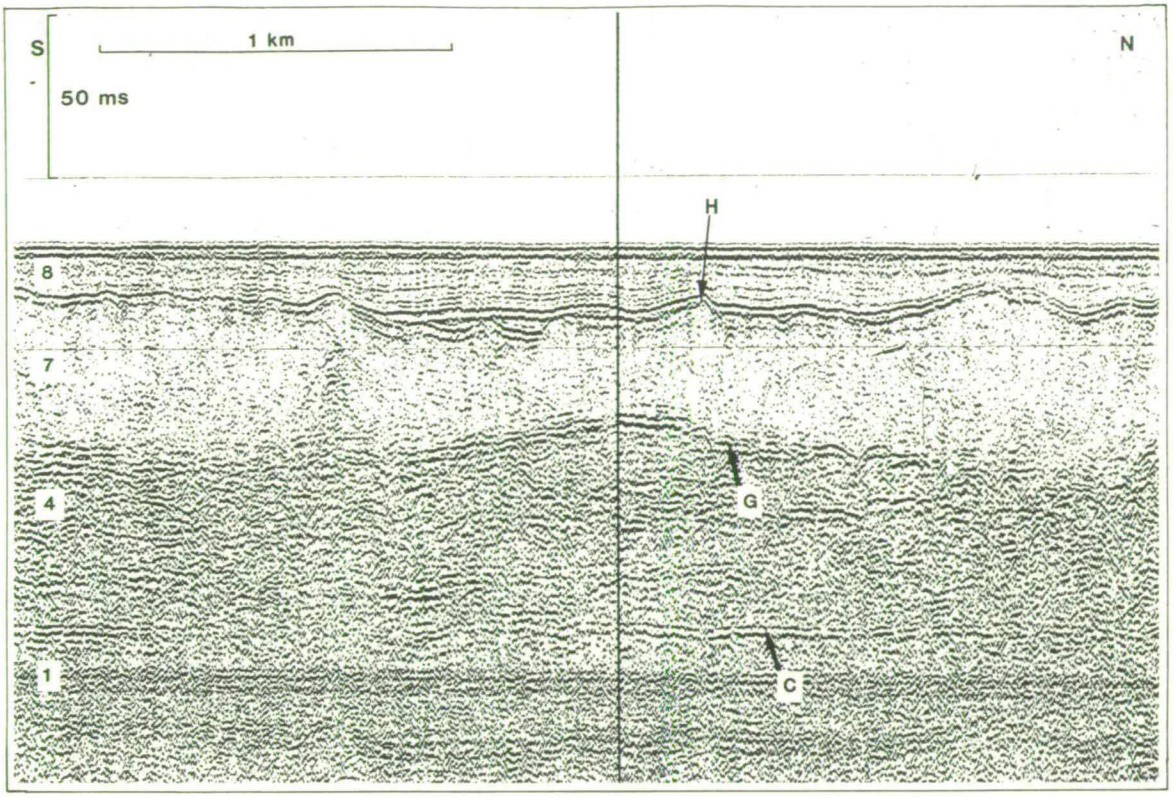

Fig. 2.17. Sparker record from the Fladen area showing the structureless configuration and blanket like form of sequence 7.

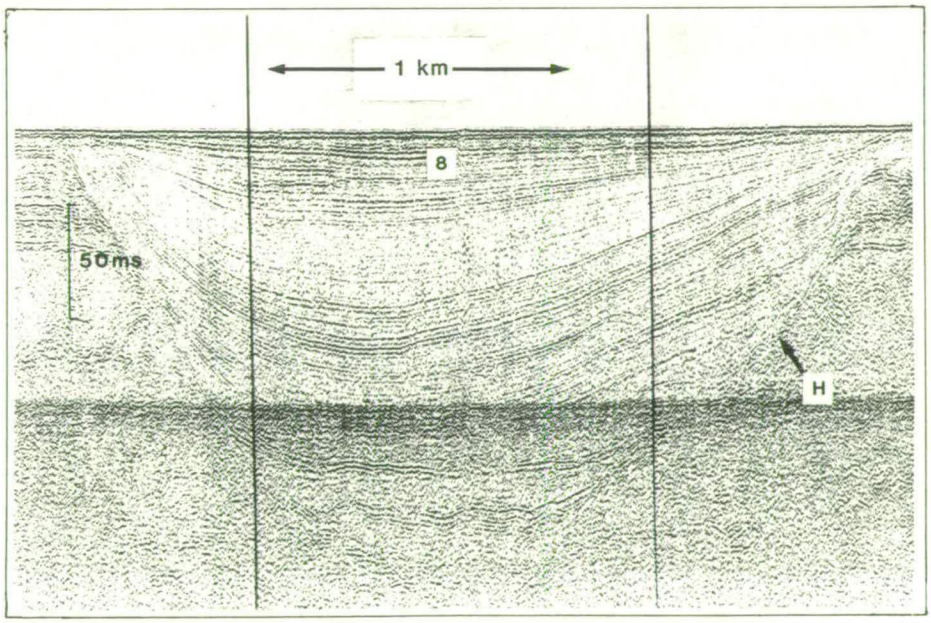

Fig. 2.18. Sparker record from the Forties area showing a divergent channel infill pattern in sequence 8.

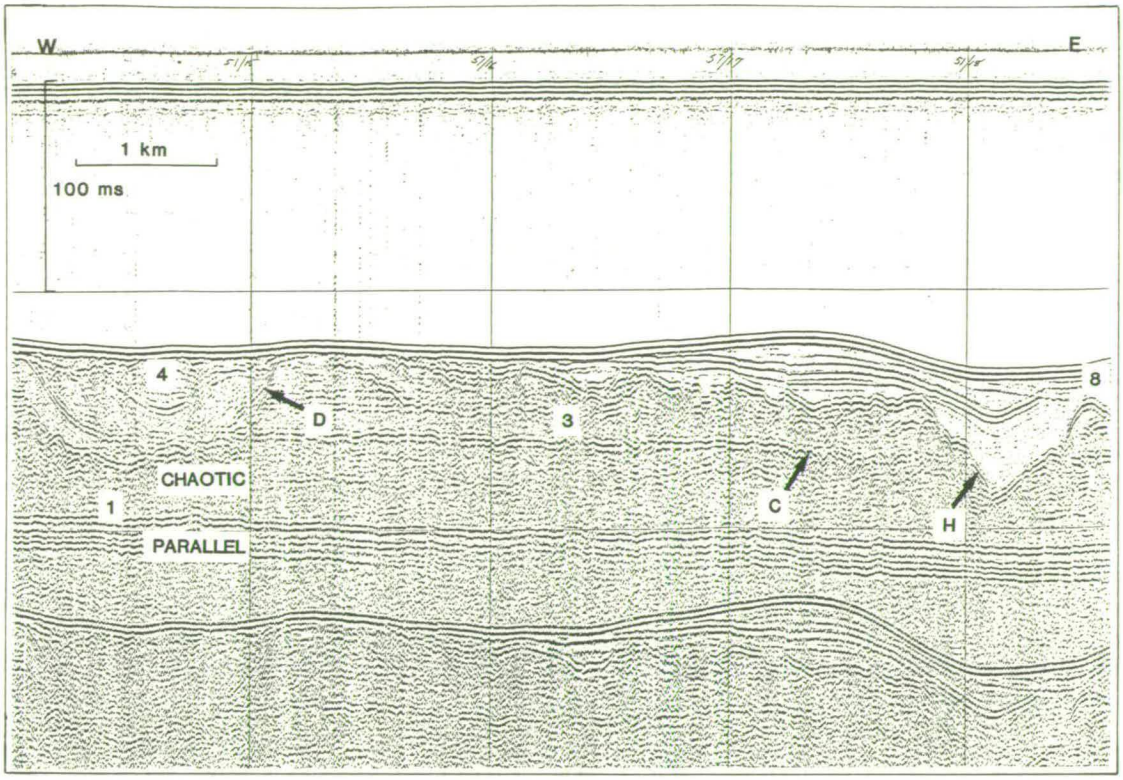

Fig. 2.19. Sparker record from the Devils Hole area showing the upper chaotic and lower layered seismic facies within sequence 1.

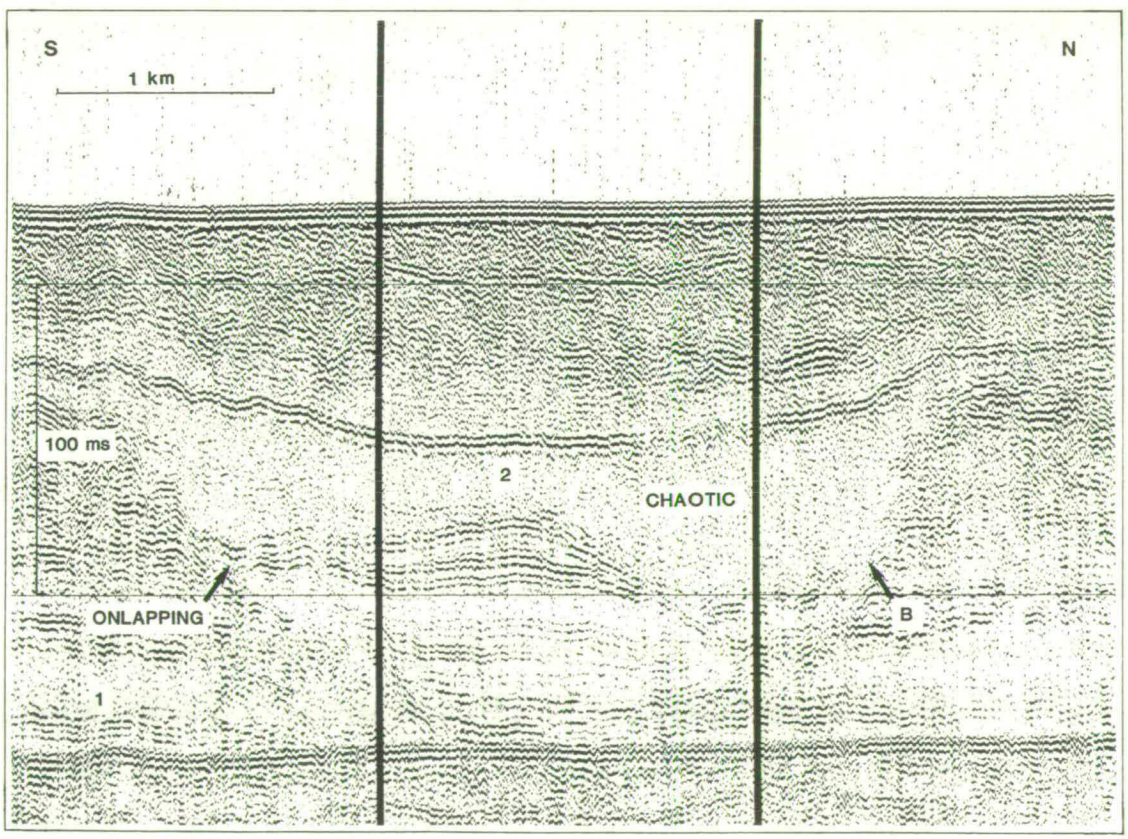

Fig. 2.20. Sparker record from the Bosies Bank area showing a complex channel infill in sequence 2.

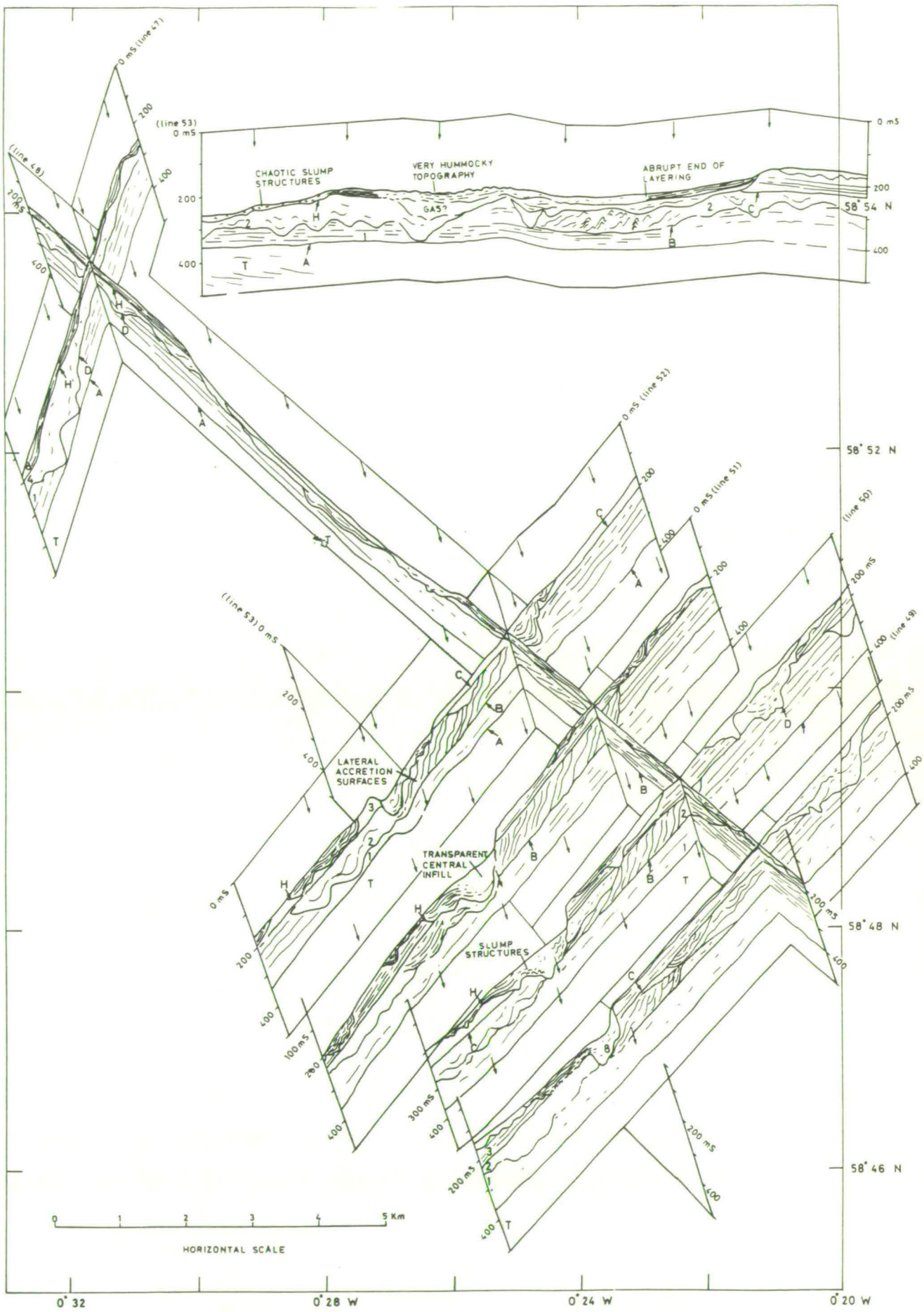

Fig. 2.21. Fence diagram from a detailed survey (85/01) shot across a partially infilled channel in the north–east corner of the Bosies Bank area. Vertical scale is given in milliseconds (two–way time), depth equivalents in the sediments are 90m per 100 mS.

Fig. 2.22. Seismic section across a partially infilled channel
(see back pocket)

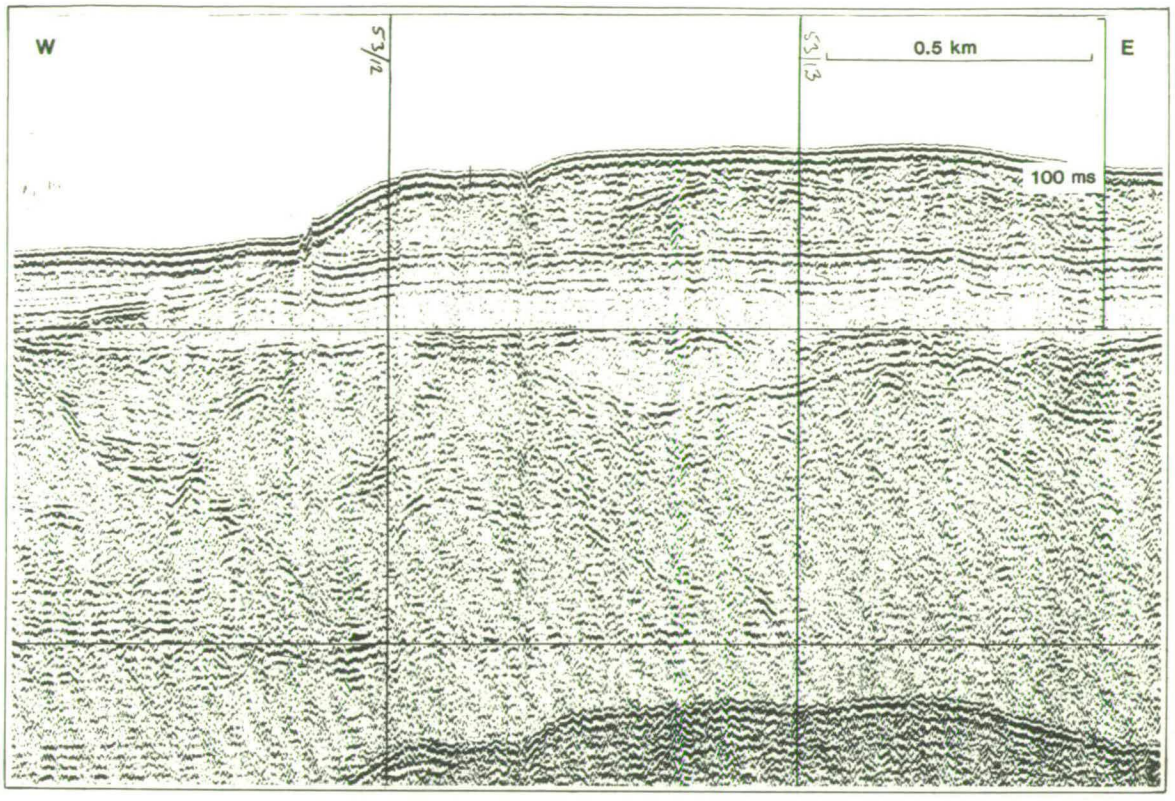

Fig. 2.23a. Sparker record from the Bosies Bank area.

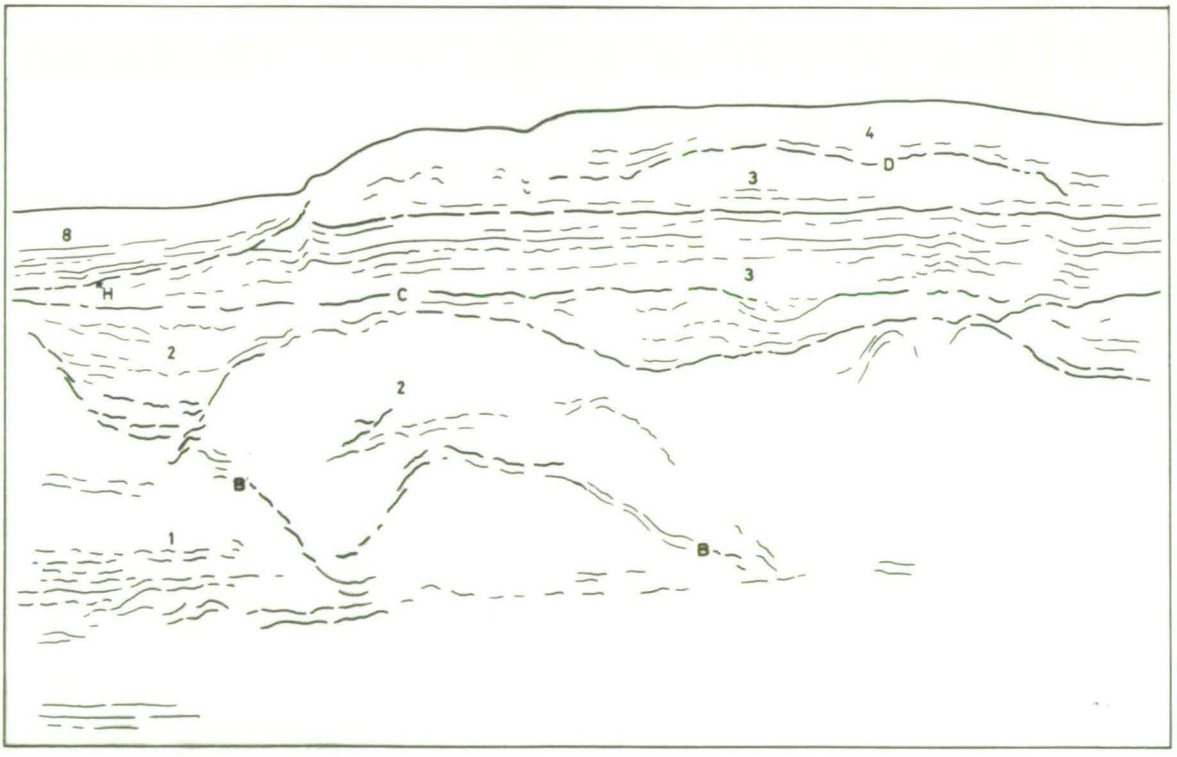

Fig. 2.23b. Line interpretation of the above record, note the lower layered and upper chaotic seismic facies within sequence 3.

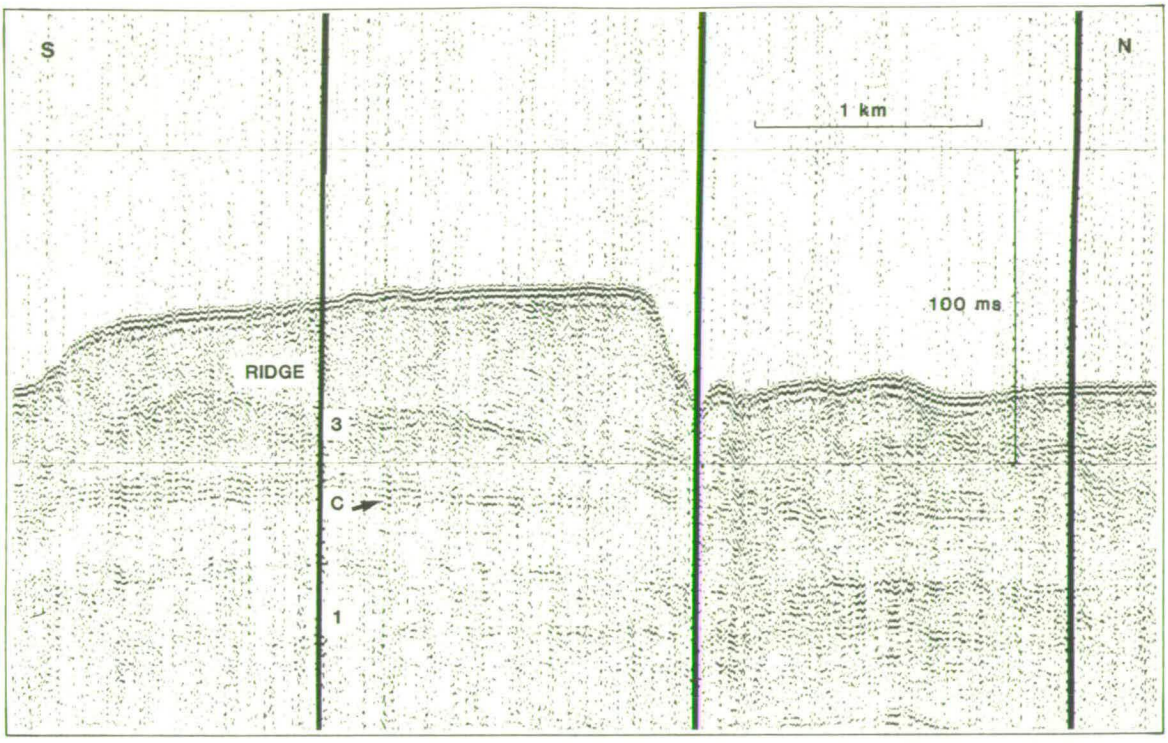

Fig. 2.24. Sparker record from the Bosies Bank area showing an acoustically structureless ridge within sequence 3.

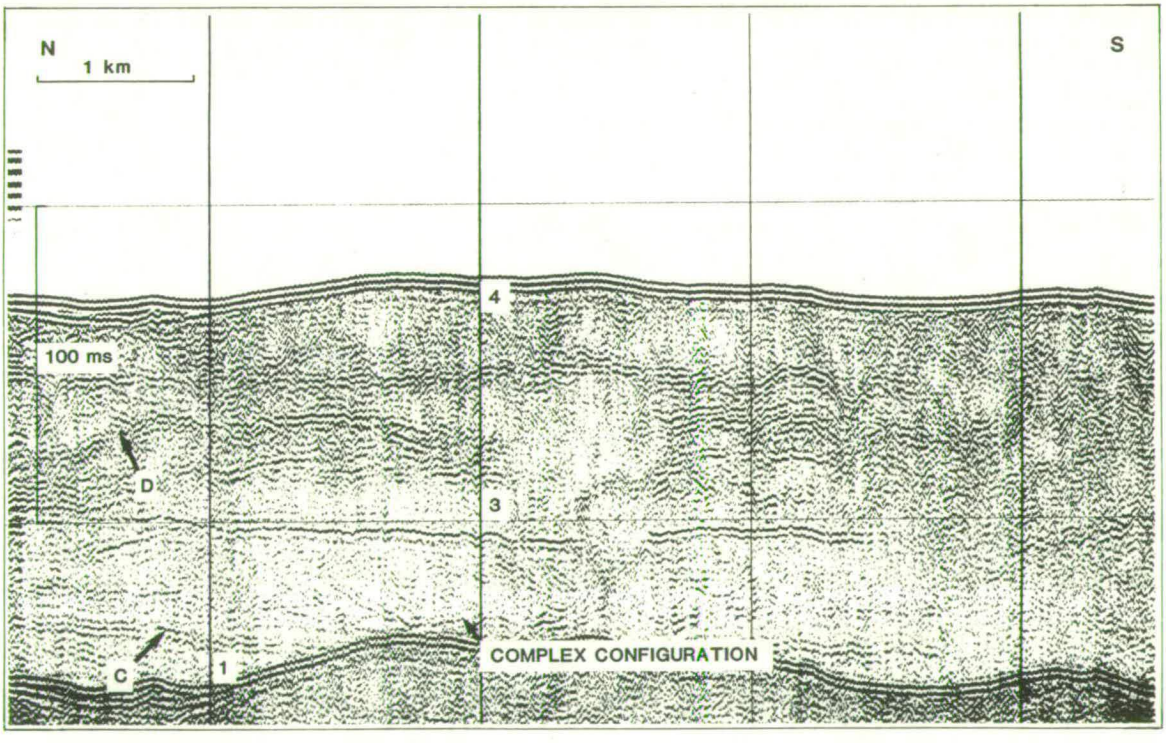

Fig. 2.25 Sparker record from the Devils Hole area showing a complex configuration layer at the base of sequence 3.

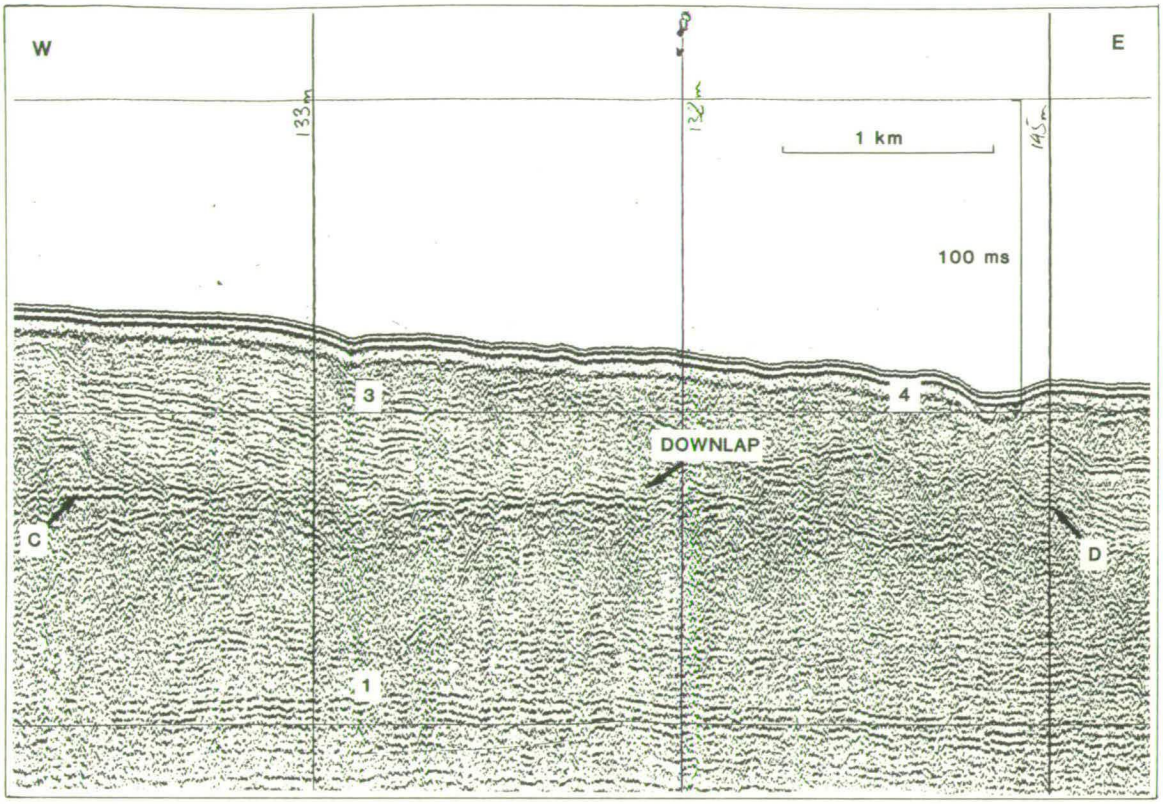

Fig. 2.26. Sparker record from the Fladen area showing downlapping reflectors in sequence 3.

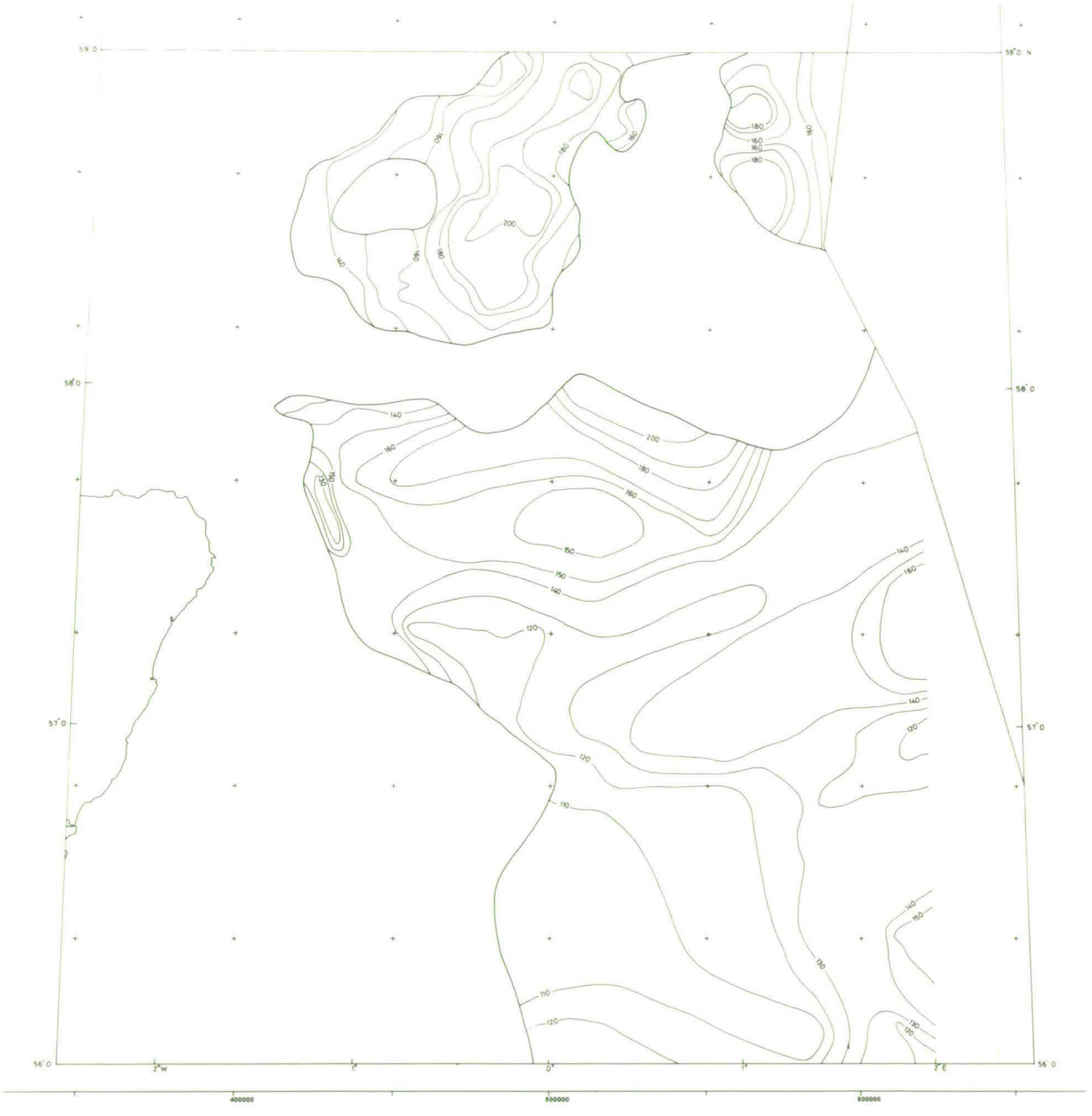

Fig. 2.27. Contours below sea level to the base of seismic sequence 3.

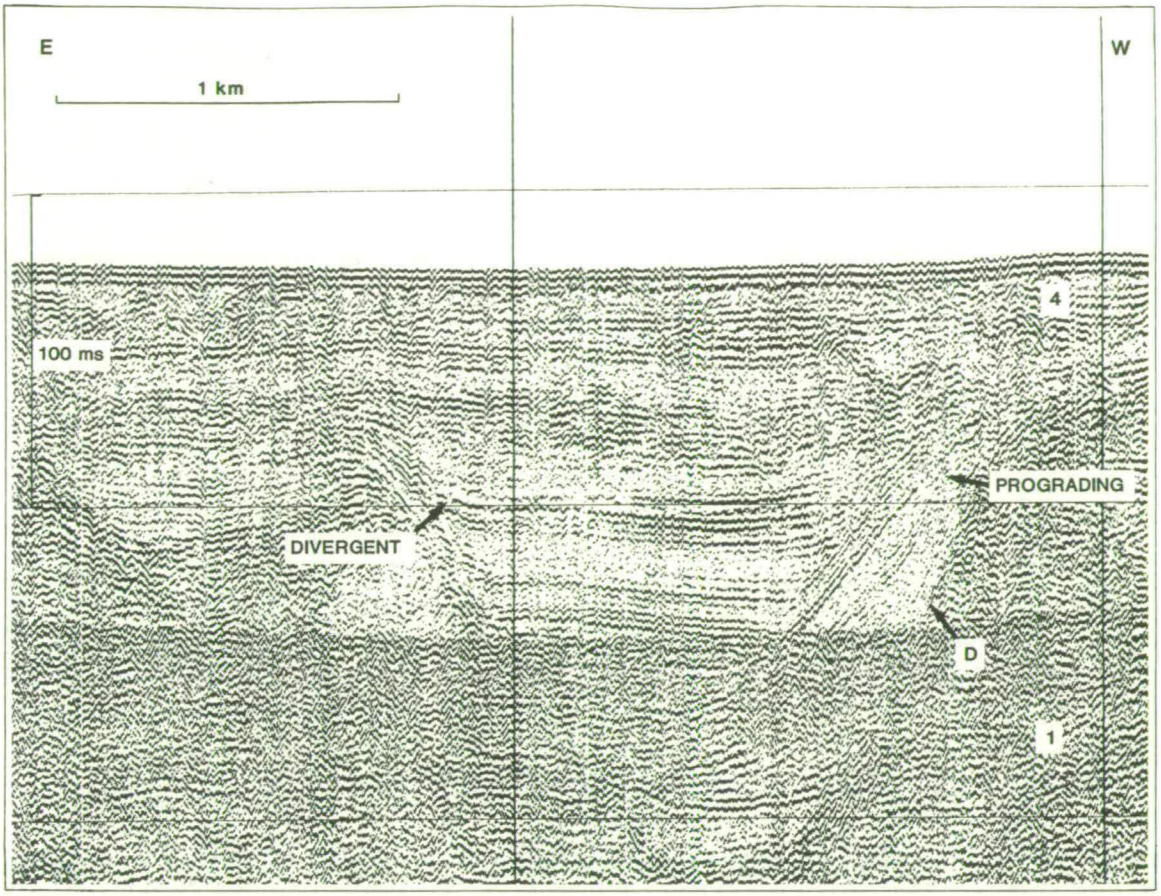

Fig. 2.28. Sparker record from the Devils Hole area showing a complex channel fill sequence, 4, with a lower prograding and an upper diverging facies.

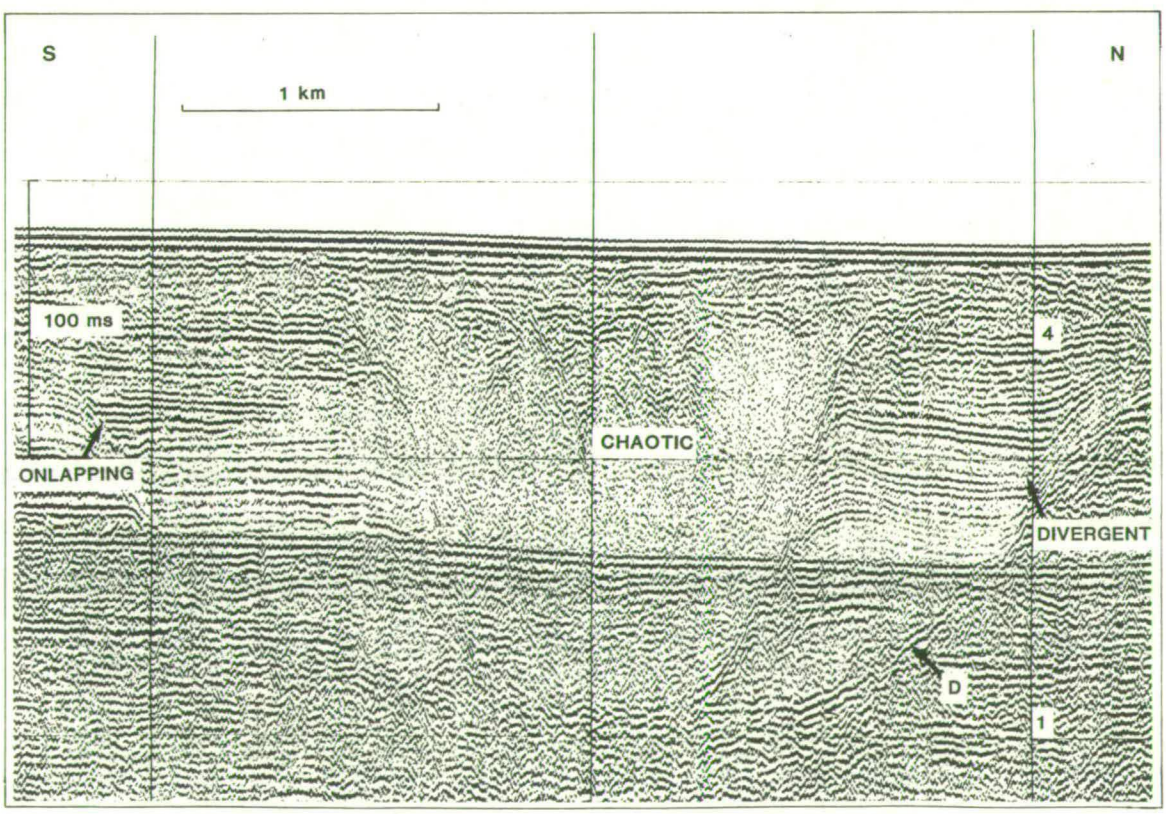

Fig. 2.29. Sparker record from the Devils Hole area showing a divergent fill facies cut by a chaotic fill facies, sequence 4.

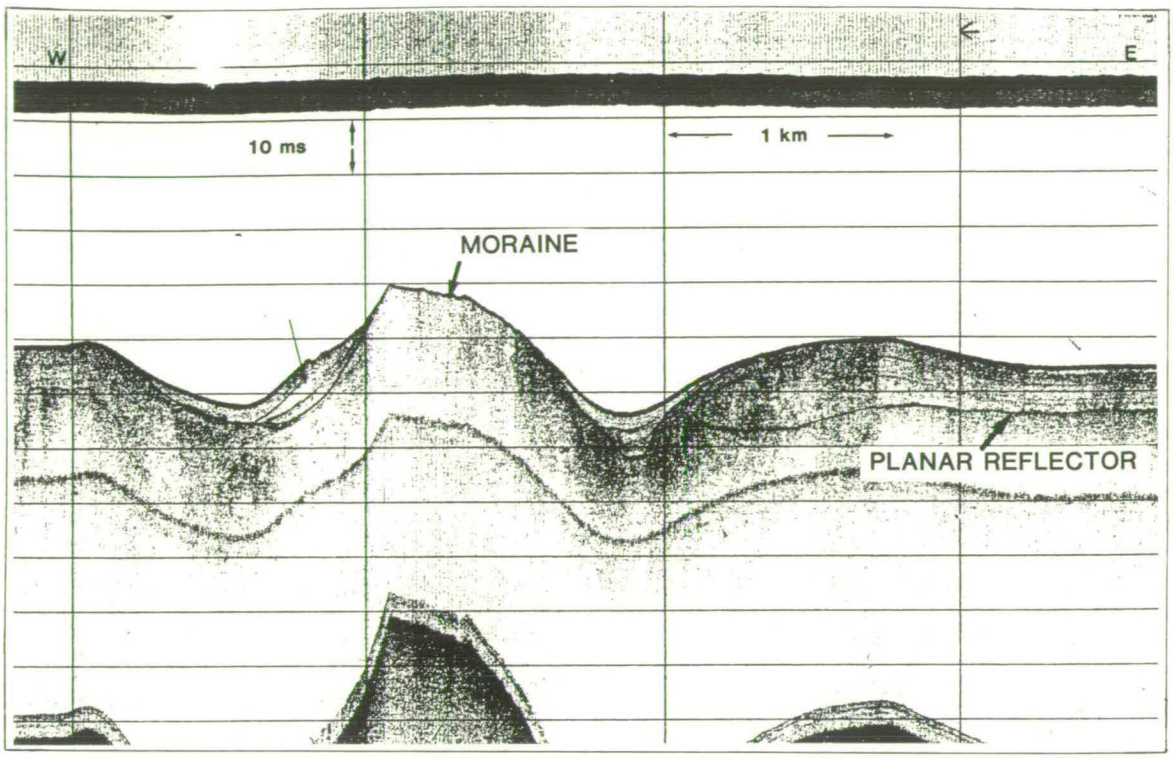

Fig. 2.30. Boomer record from the Marr Bank area showing the hummocky upper surface of sequence 5, and to the east, the planar basal reflector of sequence 6.

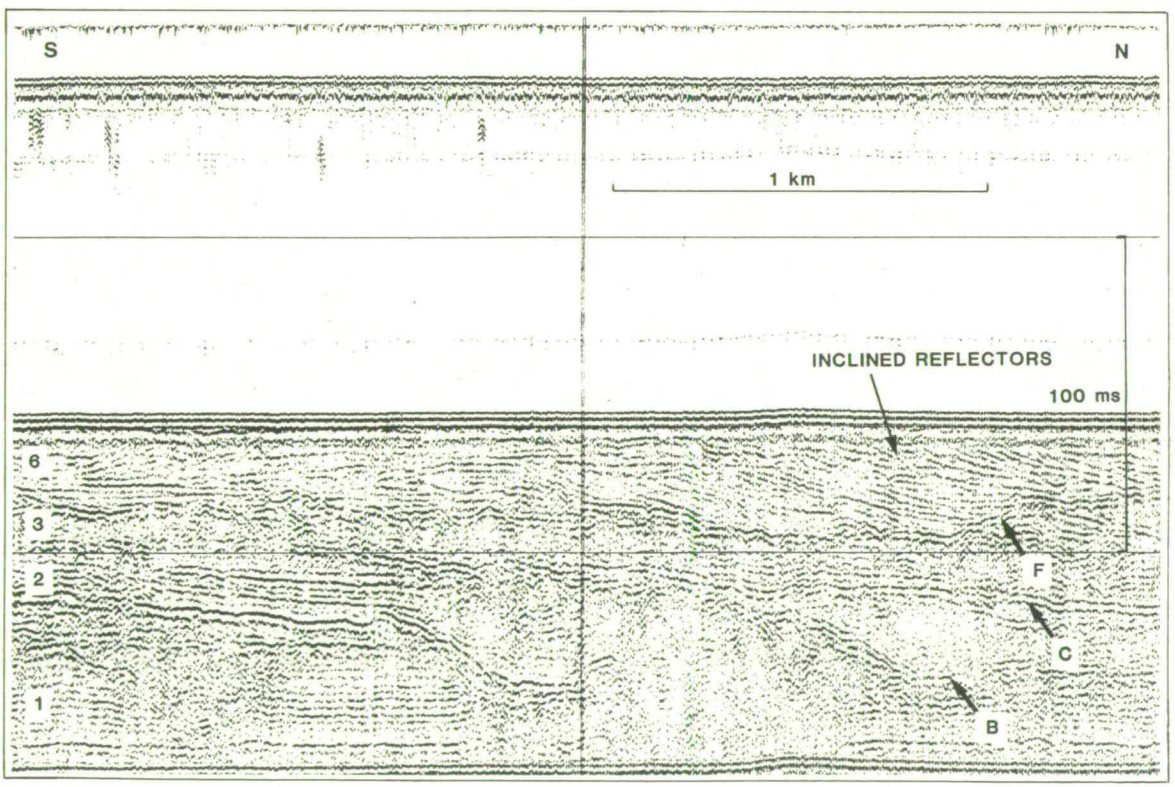

Fig. 2.31. Sparker record from the Forties area showing bi-directional, inclined reflectors in sequence 6.

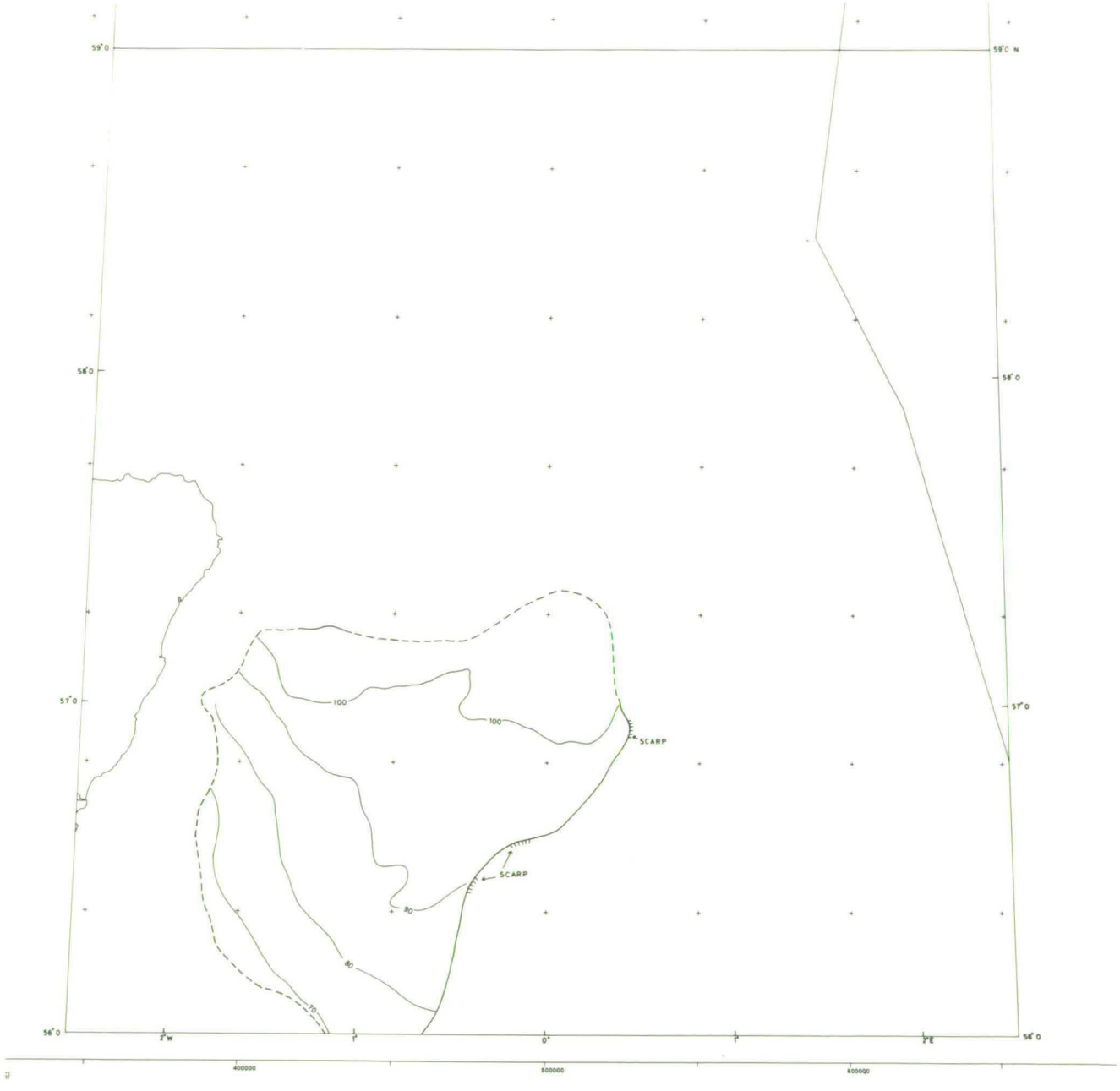

Fig. 2.32. Contours below sea level to the base of seismic sequence 6.

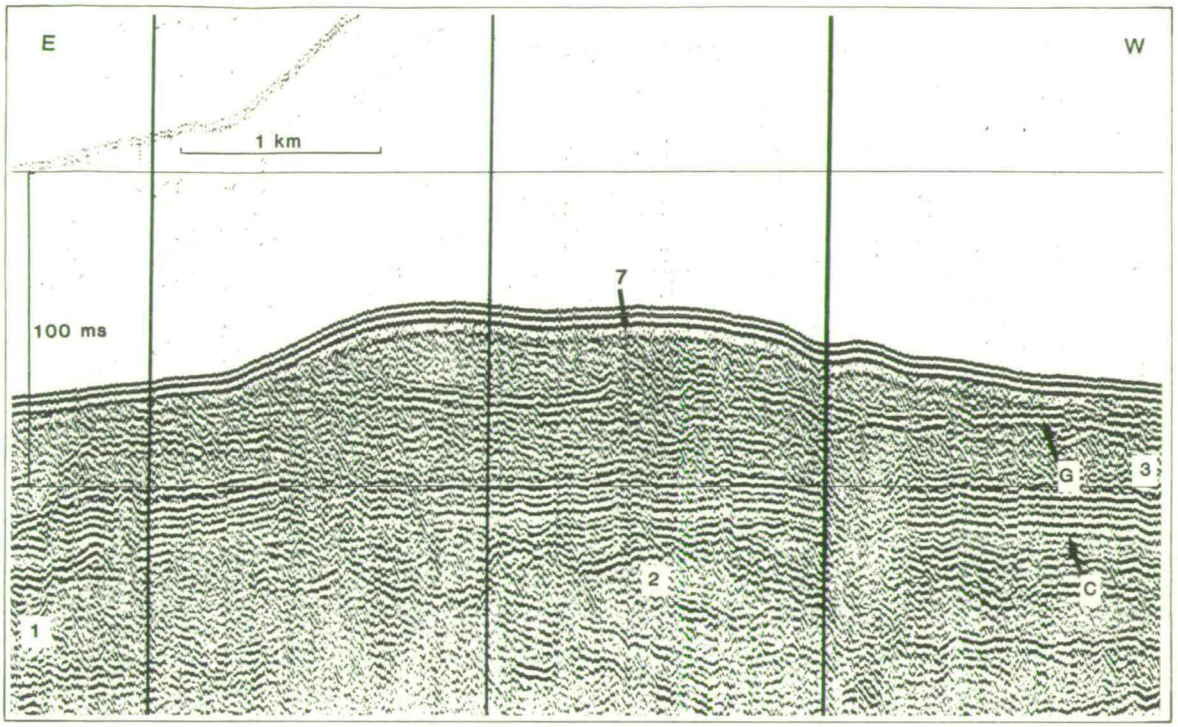

Fig. 2.33. Sparker record from the Bosies Bank area showing an internally chaotic ridge within sequence 7.

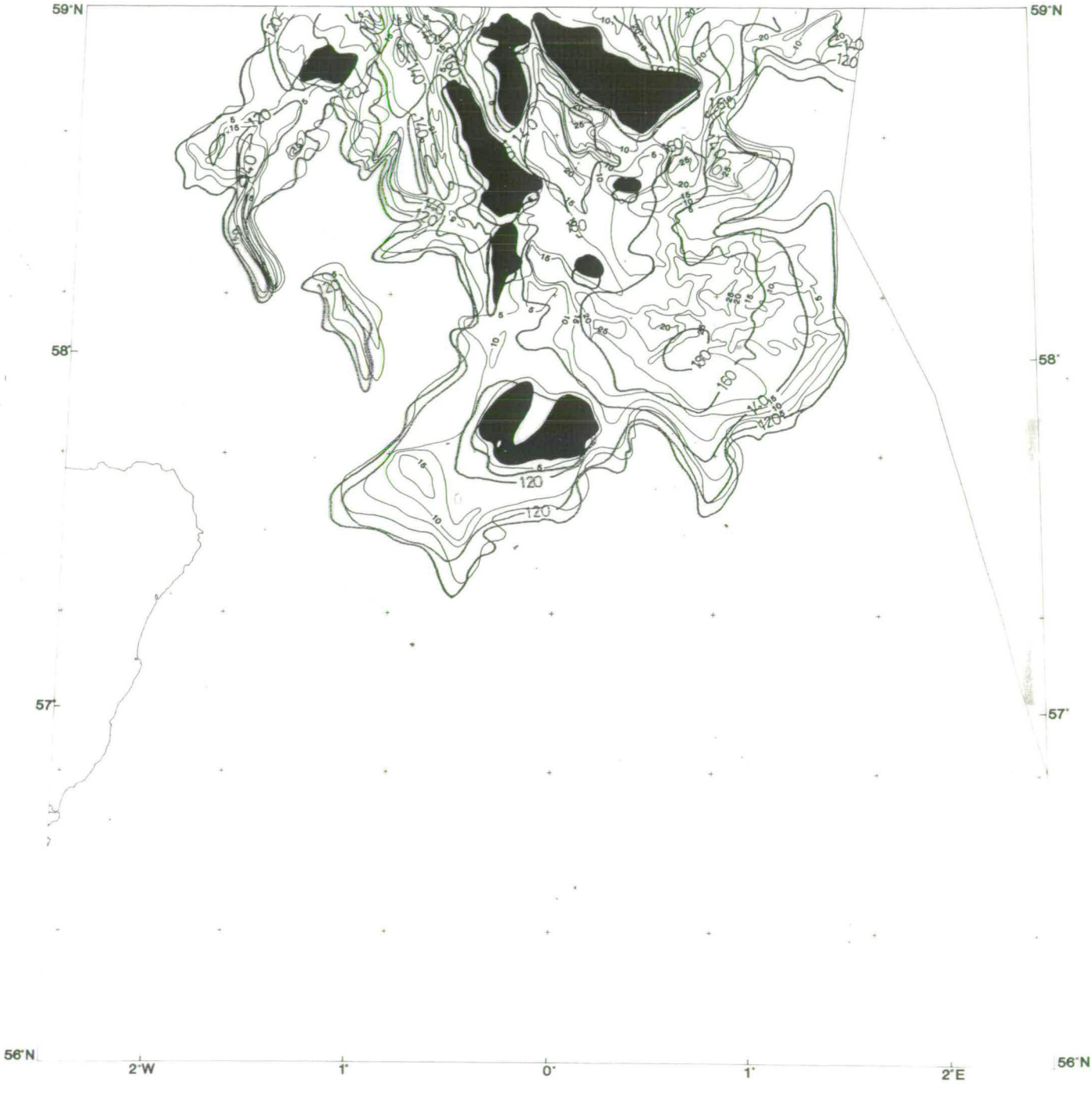

Fig. 2.34. Isopachytes and contours below sea level (overlay) to the base of seismic sequence 8 in the Witch Ground Basin.

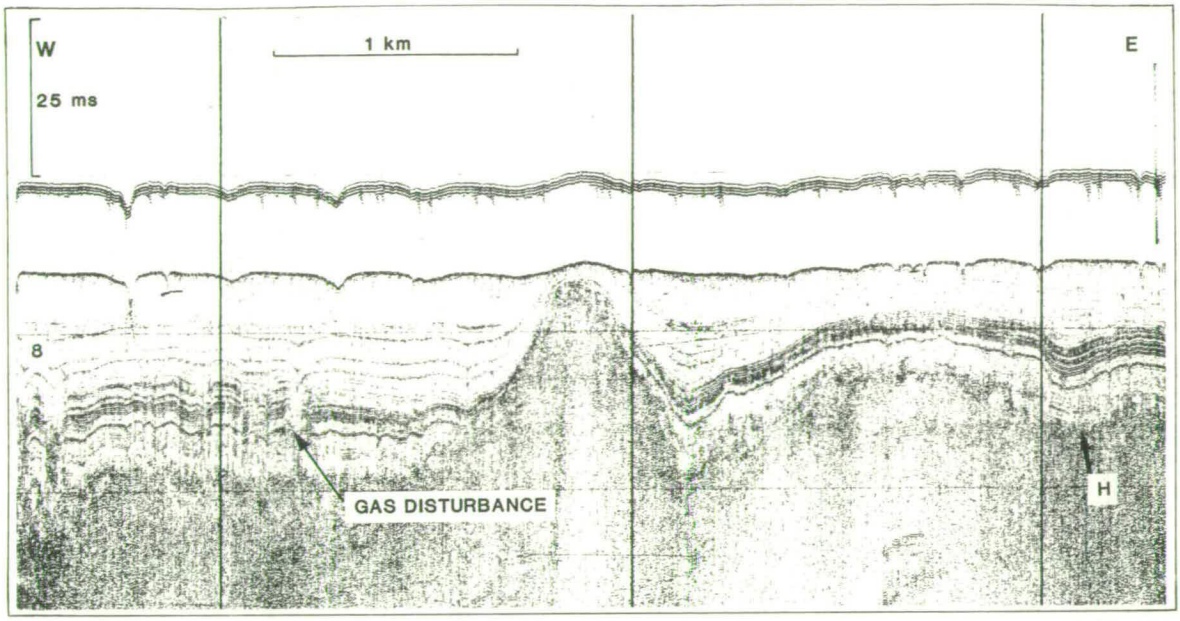

Fig. 2.35. Boomer record from the Witch Ground Basin, in the Fladen area, showing the well layered and basally concordant facies within sequence 8.

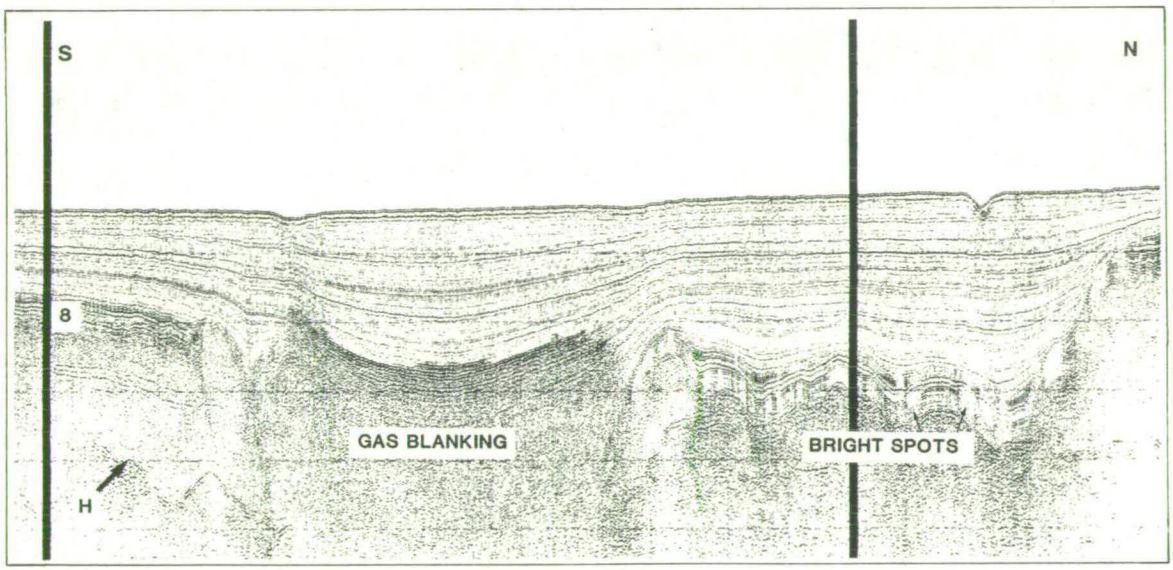

Fig. 2.36. Boomer record from the edge of the Witch Ground Basin, in the Bosies Bank area, showing the occurence of gas blanking in the well layered seismic facies, sequence 8.

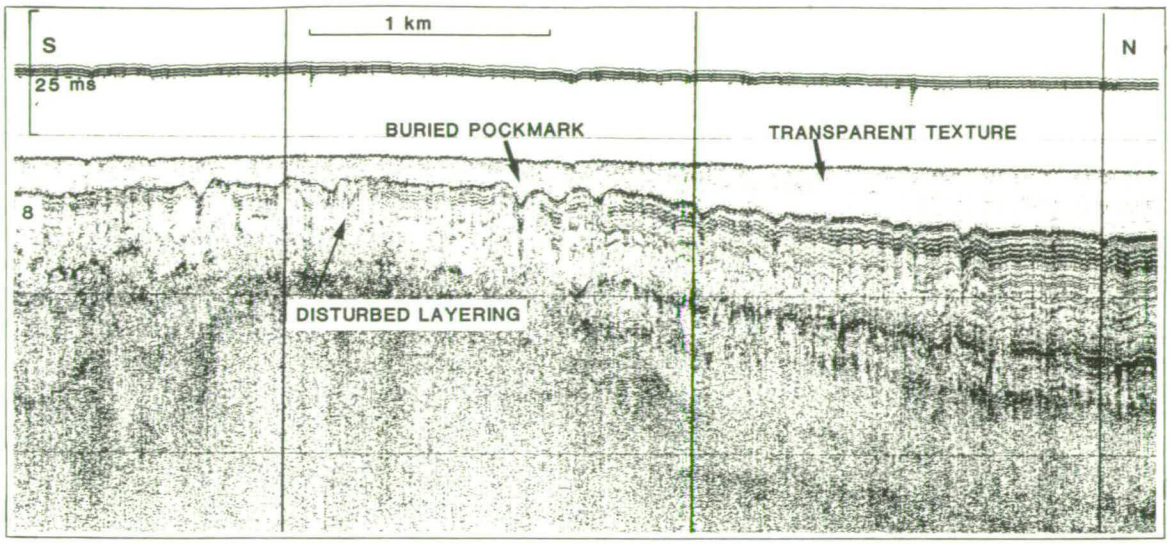

Fig. 2.37. Boomer record from the edge of the Witch Ground Basin in the Bosies Bank area showing lateral variations over highs within the lower, layered facies, sequence 8.

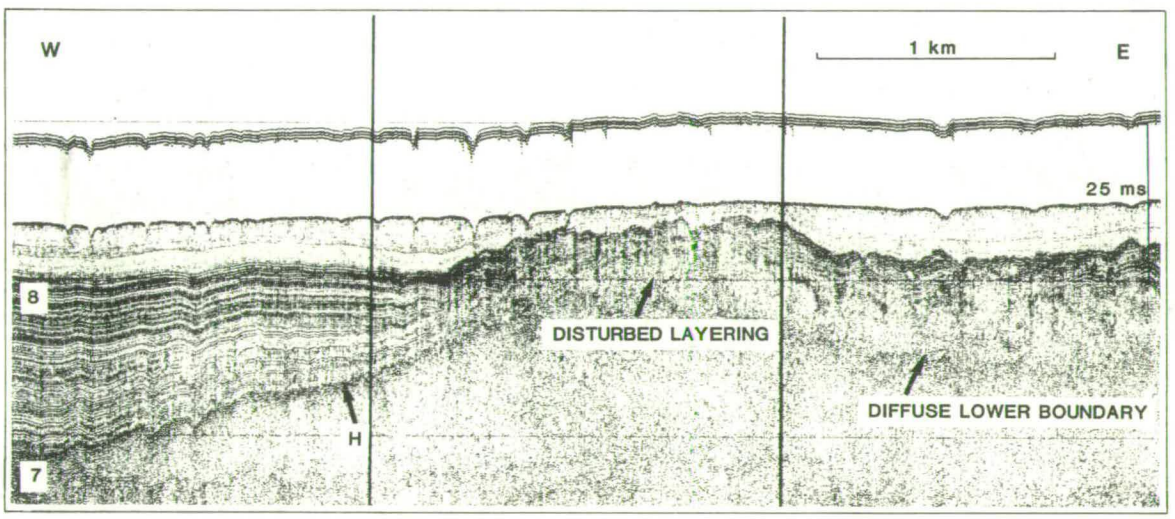

Fig. 2.38. Boomer record from the Witch Ground Basin, Fladen area, showing the well layered lower facies contrasting with the more transparent texture of the upper facies, sequence 8.

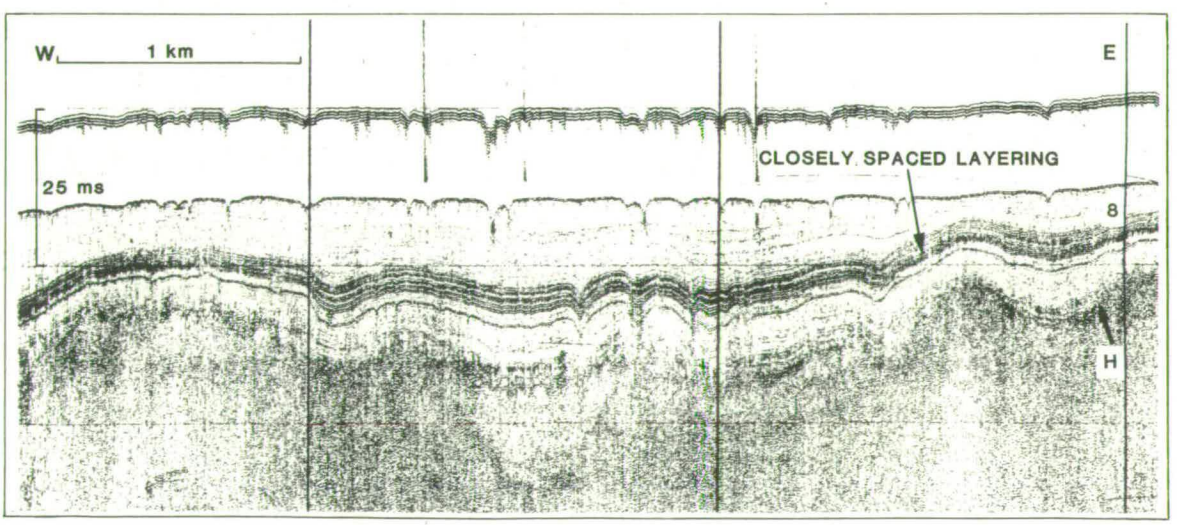

Fig. 2.39. Boomer record from the Witch Ground Basin, Fladen area, showing a band of closely spaced reflectors overlying a transparent basal layer.

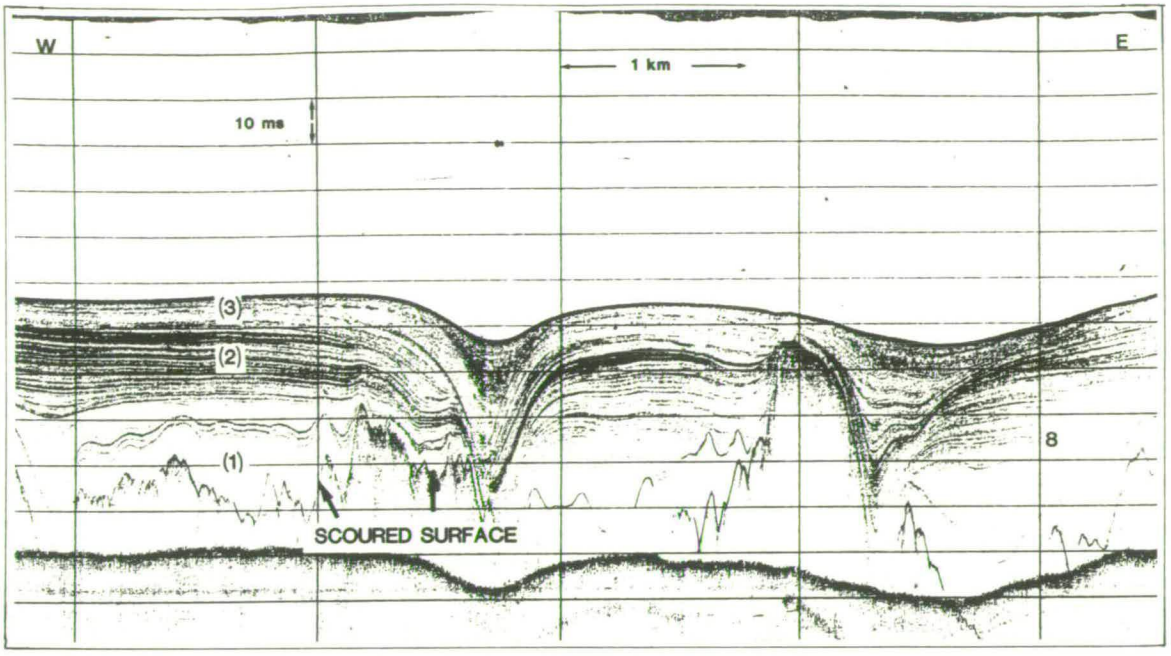

Fig. 2.40. Boomer record from the Devils Hole area, showing various seismic facies within the southern subdivision of sequence 8.

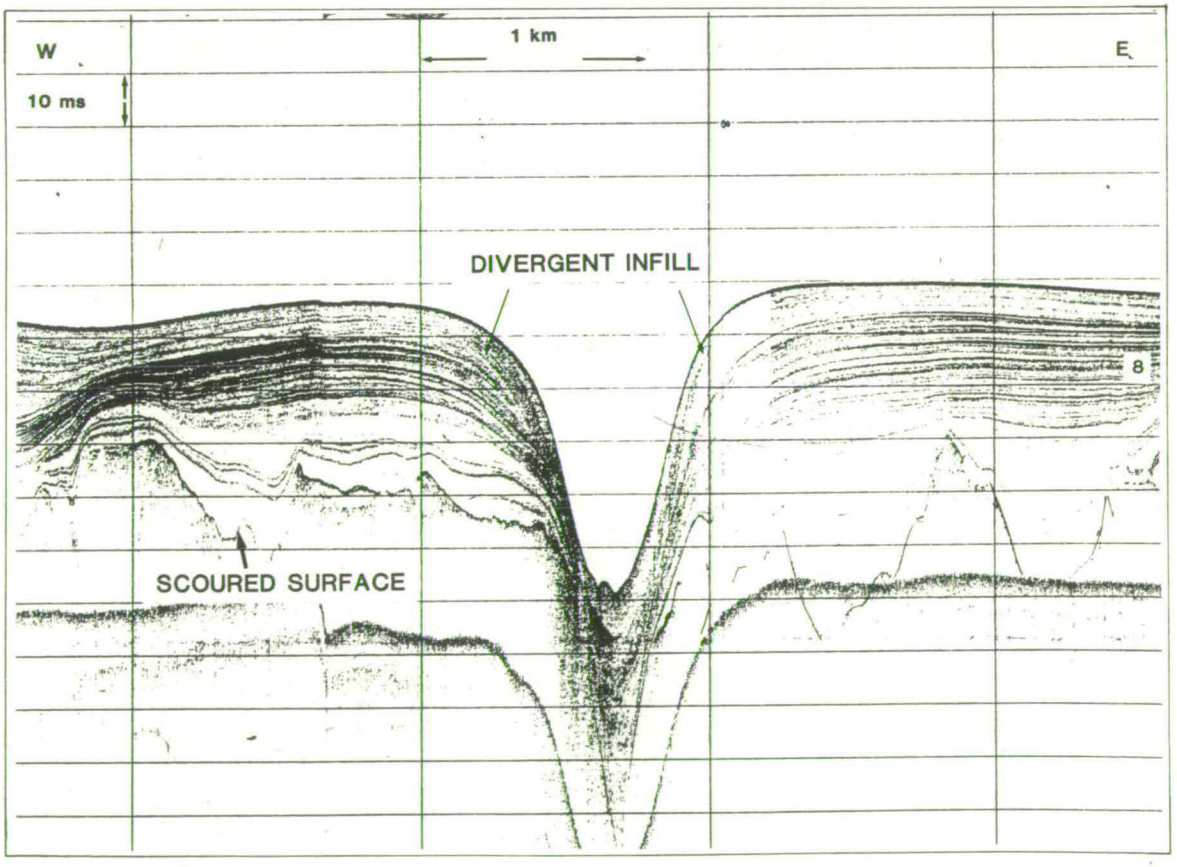

Fig. 2.41. Boomer record from the Devils Hole area showing a channel partially infilled by various seismic facies within sequence 8.

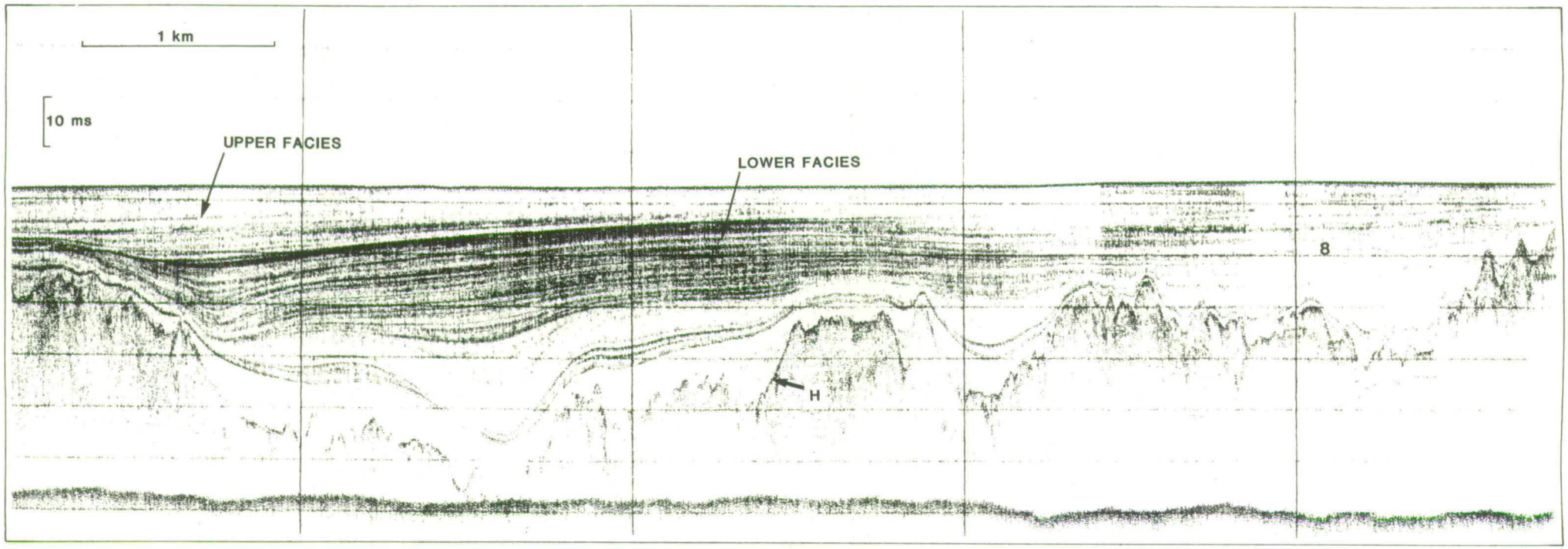

Fig. 2.42. Boomer record from the Devils Hole area showing the lower and upper channel infill facies within sequence 8.

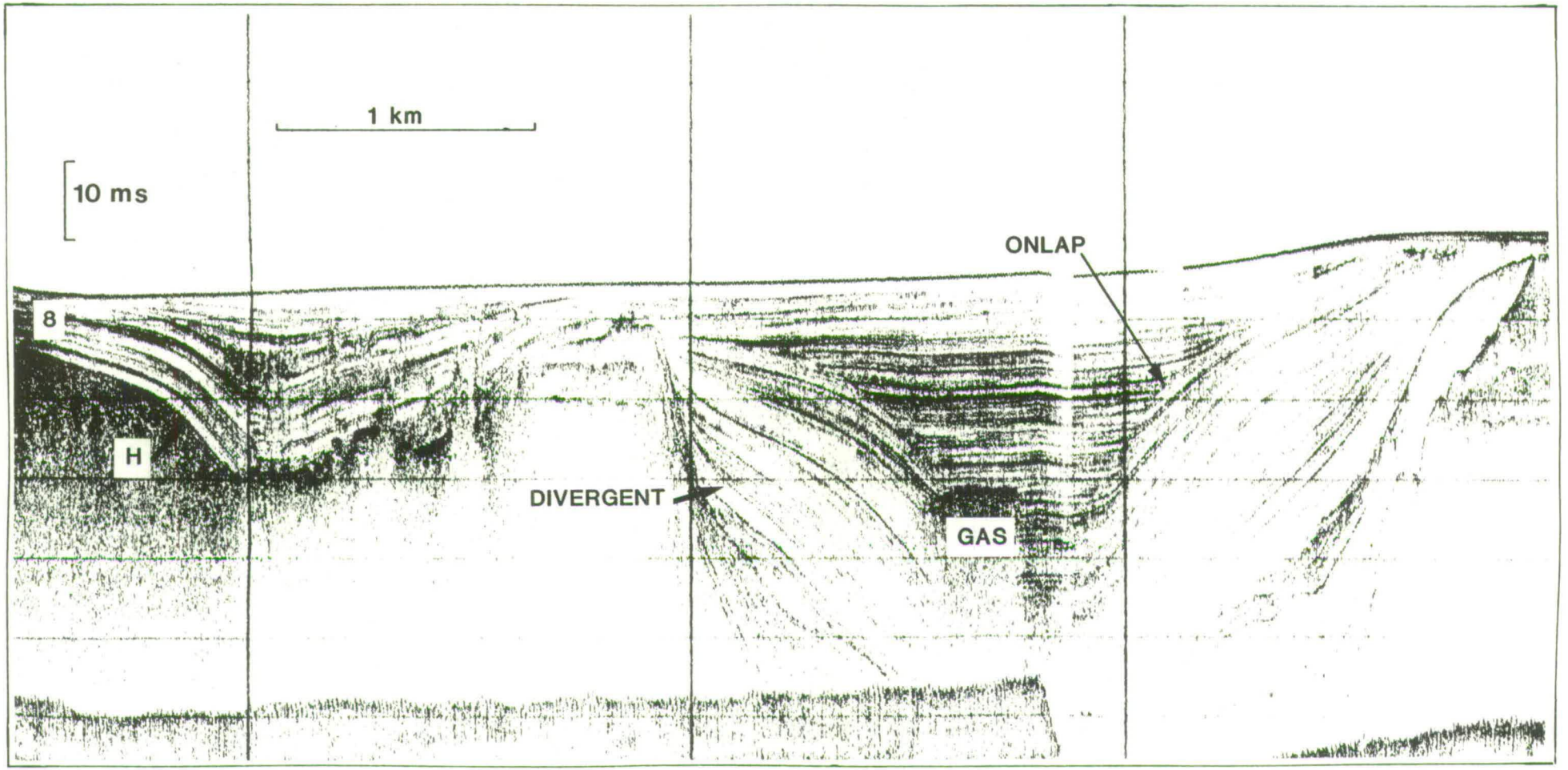

Fig. 2.43. Boomer record from the Devils Hole area showing the discordant relationship between the lower and upper seismic facies, sequence 8.

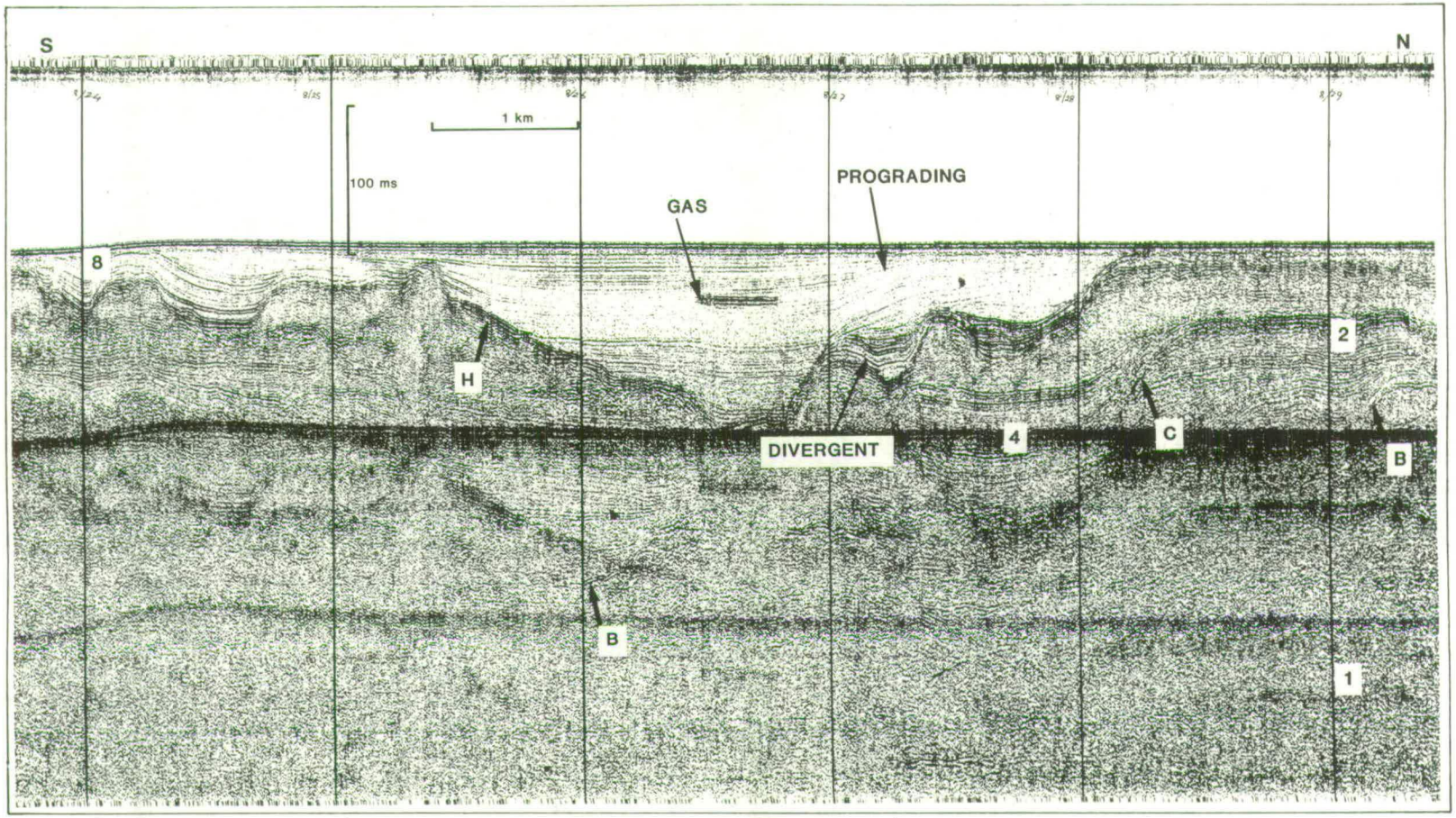

Fig. 2.44. Sparker record from the Forties area showing a lower divergent configuration overlain by prograding and onlapping reflectors infilling a large channel feature within sequence 8. Note also the presence of older sequence 4 and 2, divergent channel infillls.

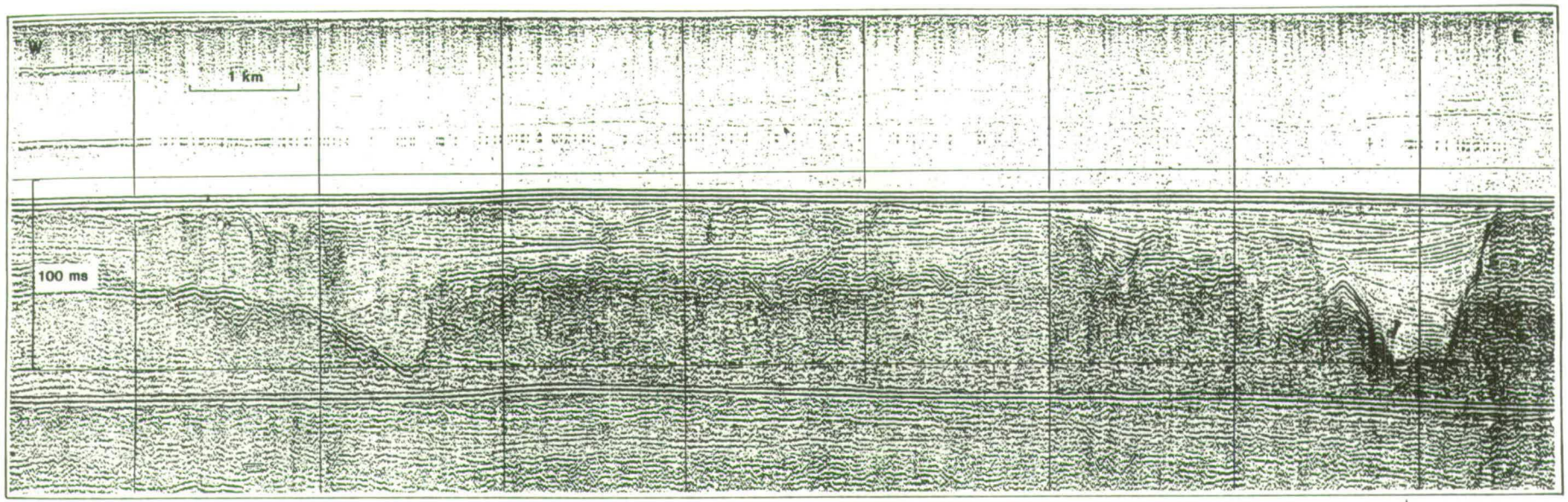

Fig. 2.45a. Sparker record from the Devils Hole area.

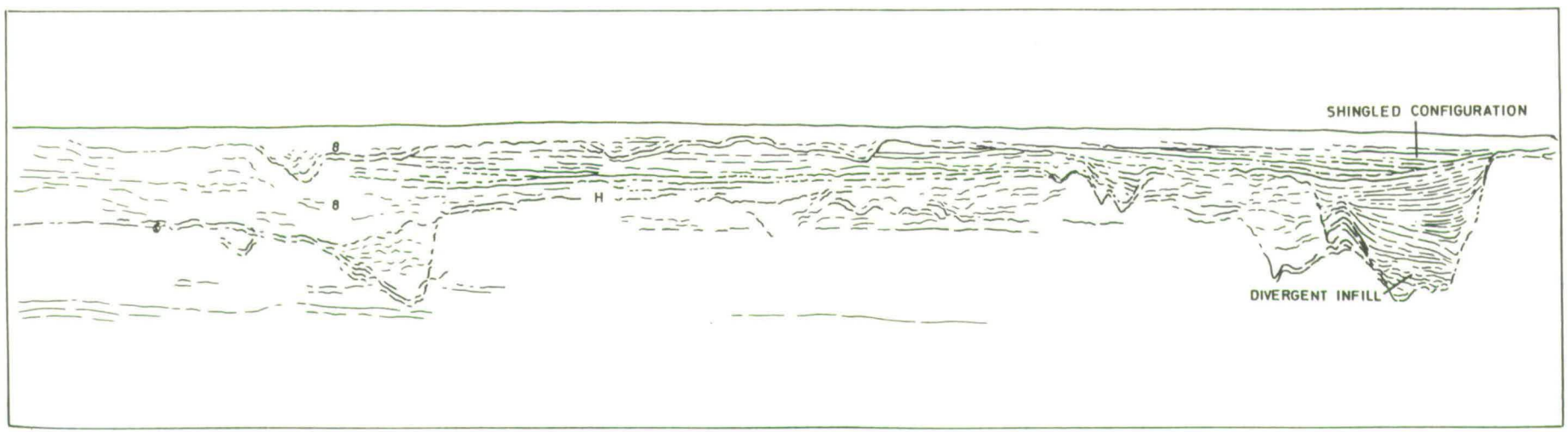

Fig. 2.45b. Line interpretation of the above record showing an upper shingled configuration terminating against a lower divergent infill, sequence 8.

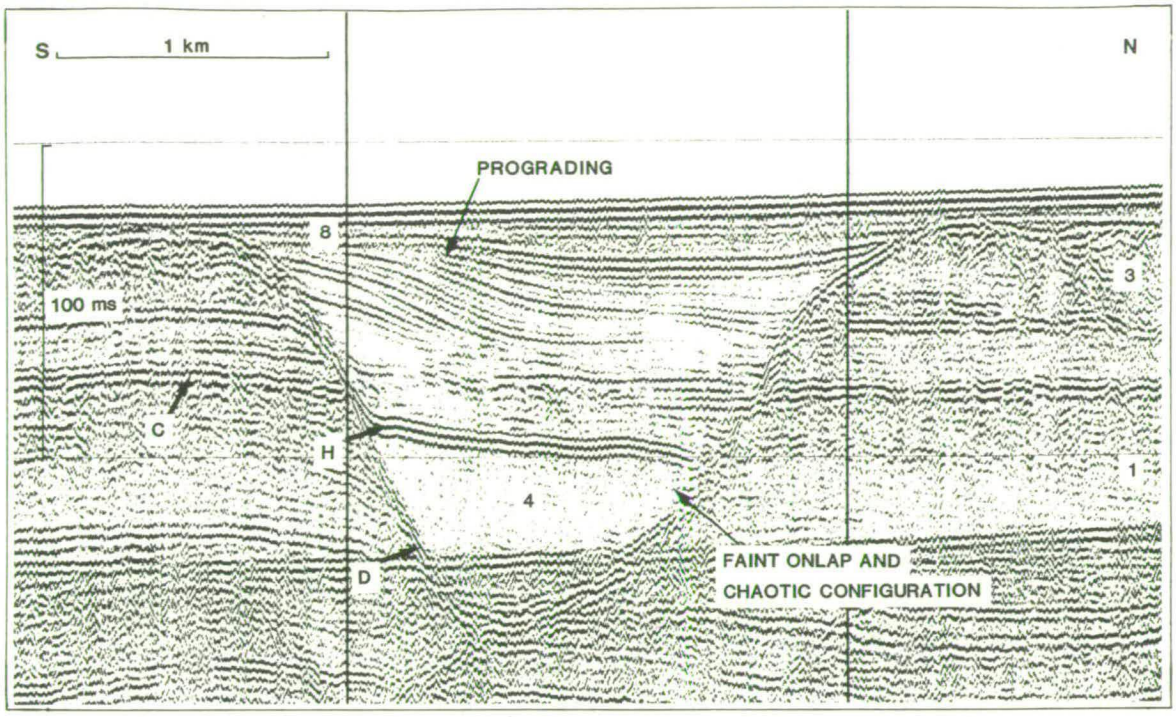

Fig. 2.46. Sparker record from the Devils Hole area showing a complex channel infill. The upper prograding reflectors occur within sequence 8, the lower onlapping and chaotic facies belong to sequence 4.

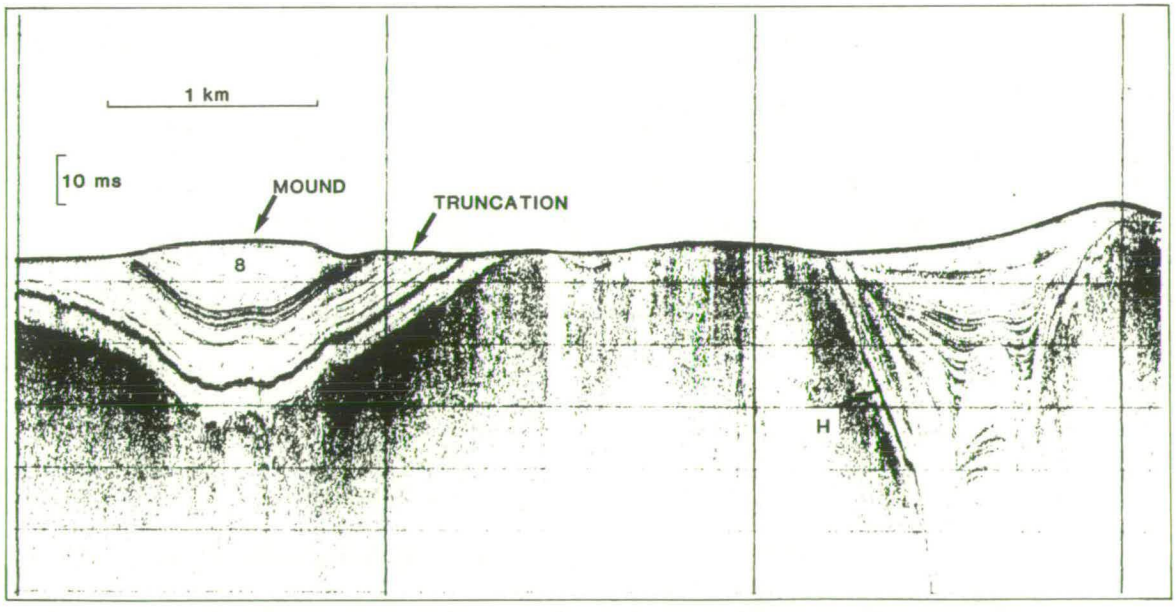

Fig. 2.47. Boomer record from the Devils Hole area showing a mounded type infill within sequence 8.

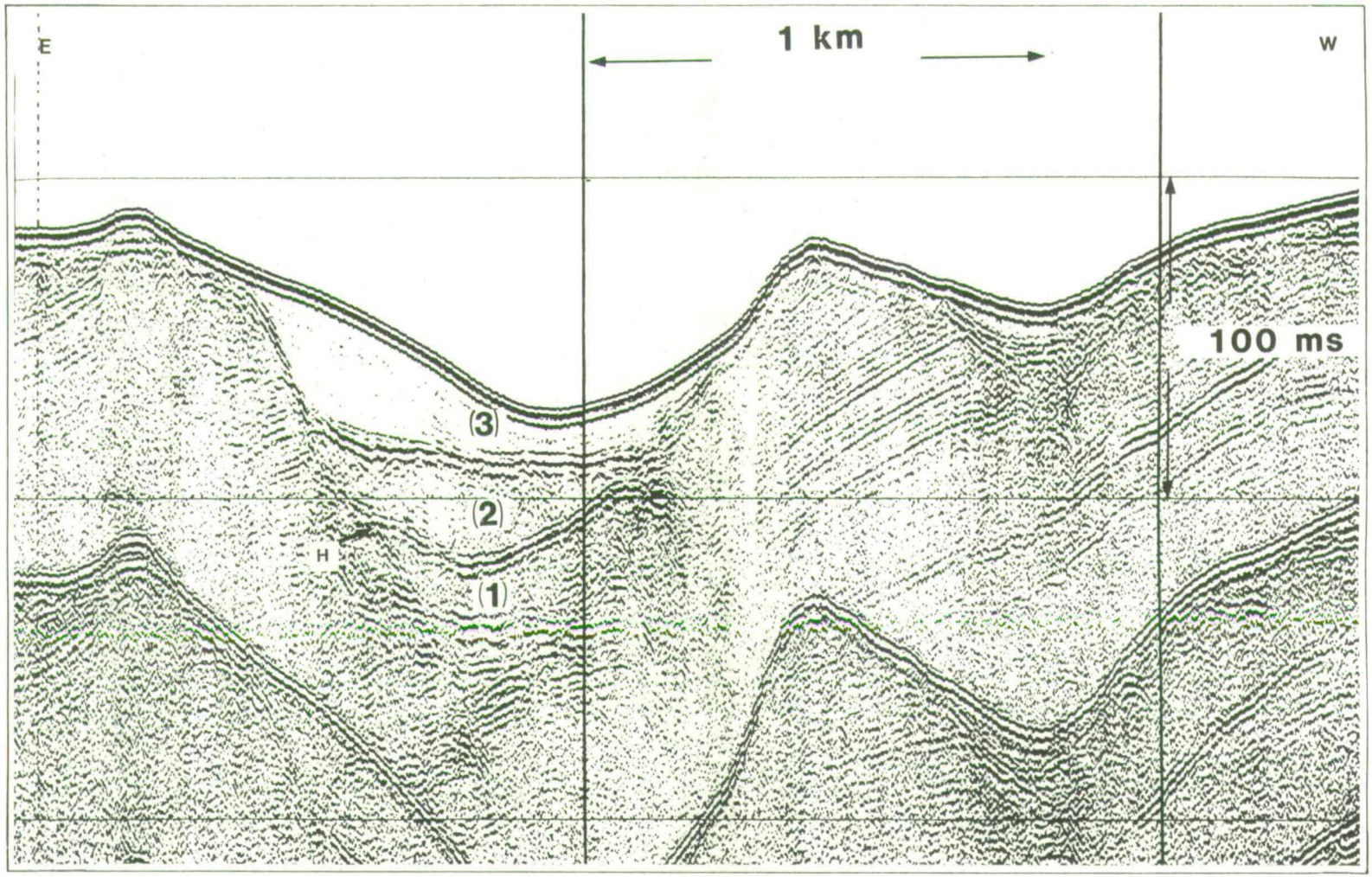

Fig. 2.48. Sparker record from the Peterhead area showing a complex channel infill within sequence 8.

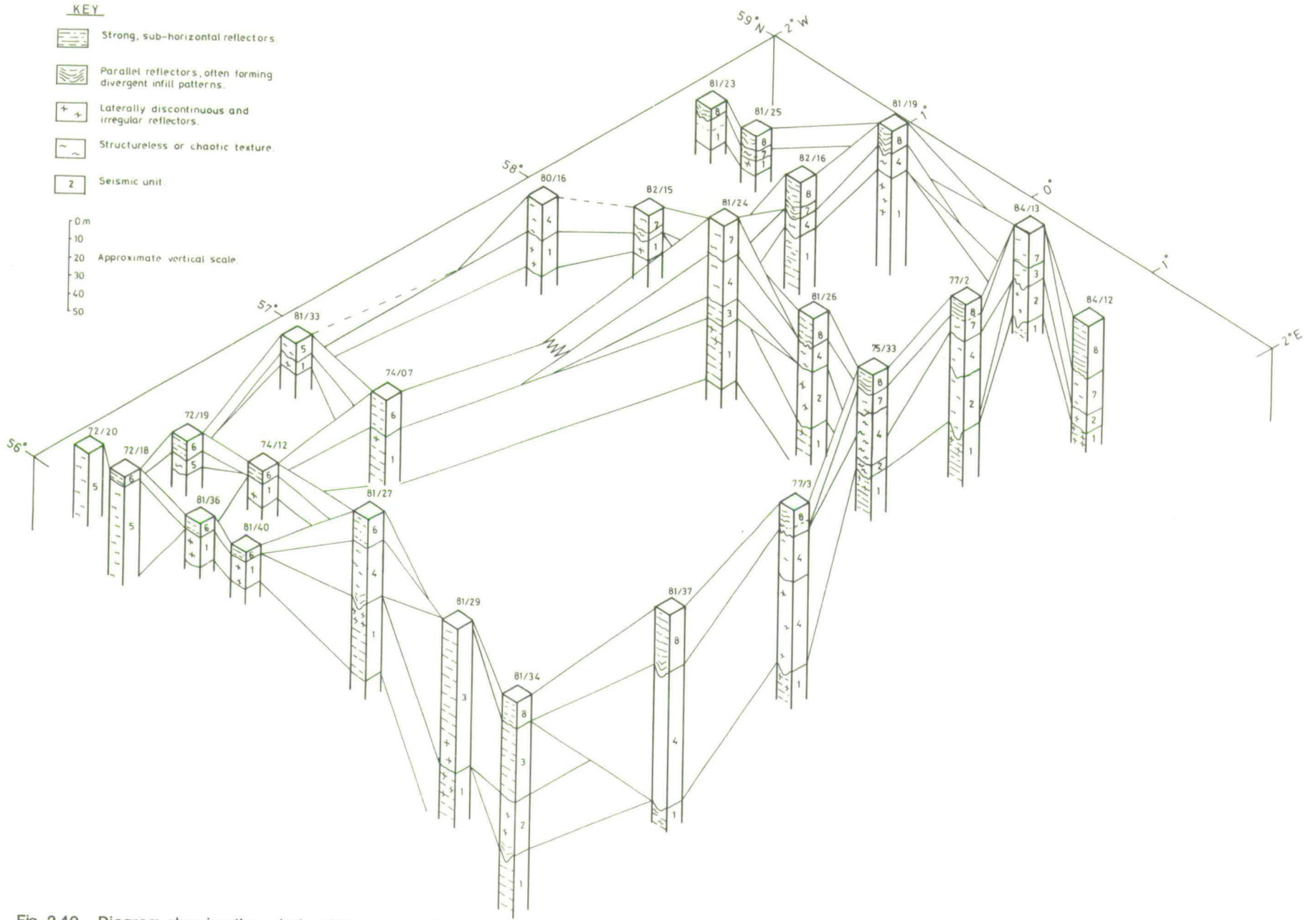

Fig. 2.49. Diagram showing the relationships and positions of various boreholes in the seismic stratigraphy.

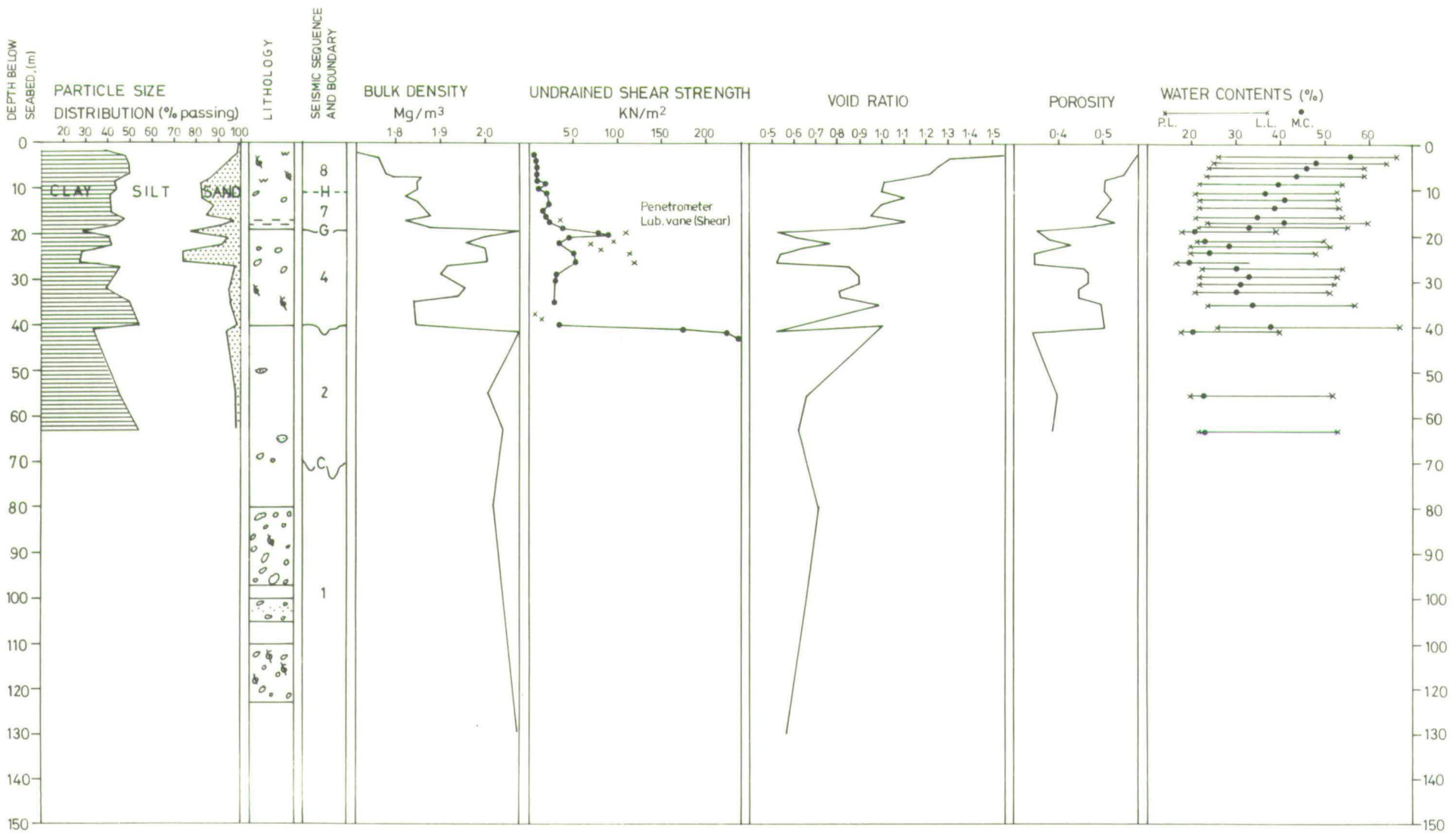

Fig. 2.50. Geotechnical properties of BH 77/2 and their relationship to seismic sequence boundaries, (compiled from raw data in Long and Hobbs, 1979).

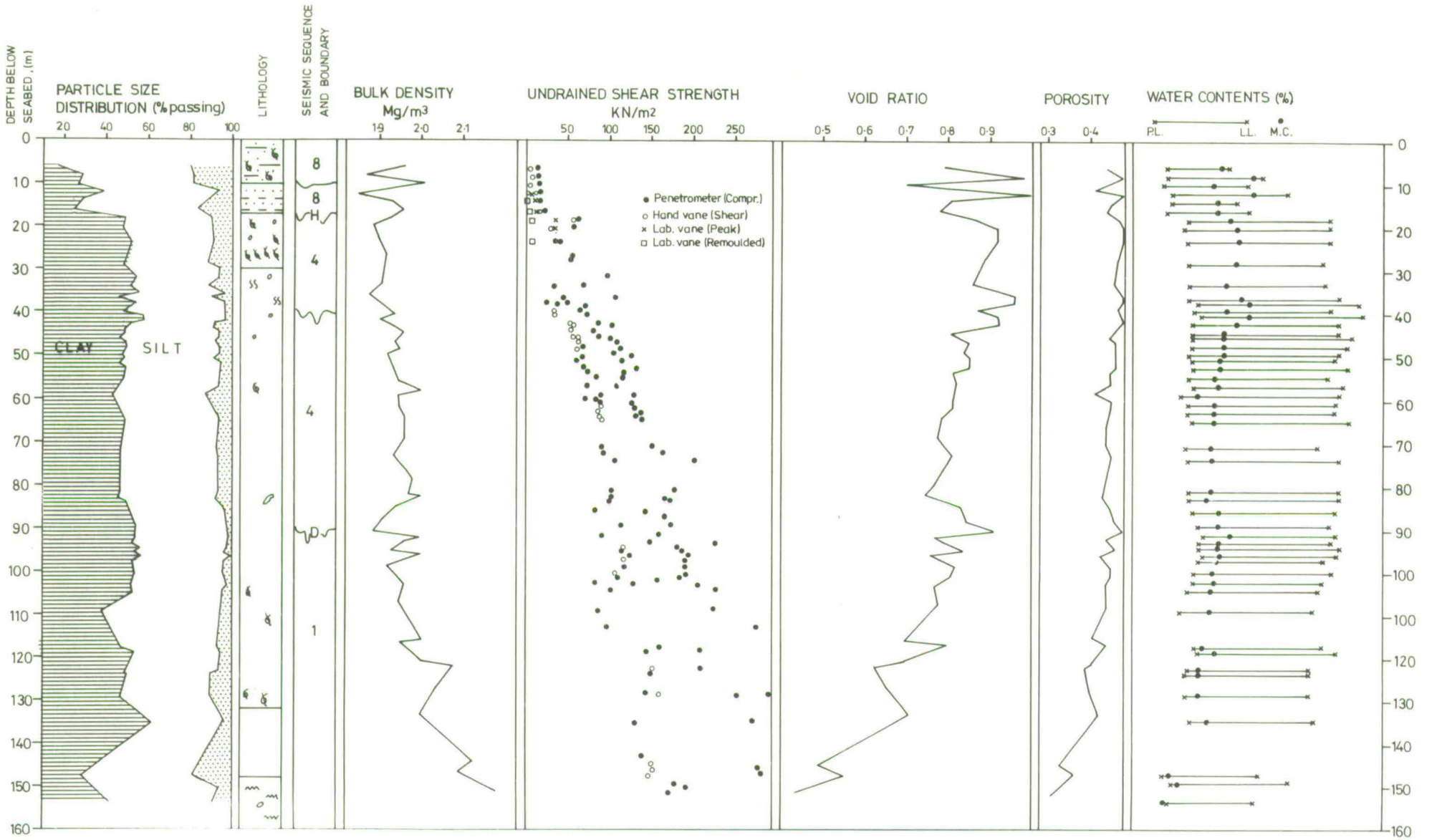

Fig. 2.51. Geotechnical properties of BH 77/3 and their relationship to seismic sequence boundaries, (compiled from raw data in Hobbs and Long, 1978)

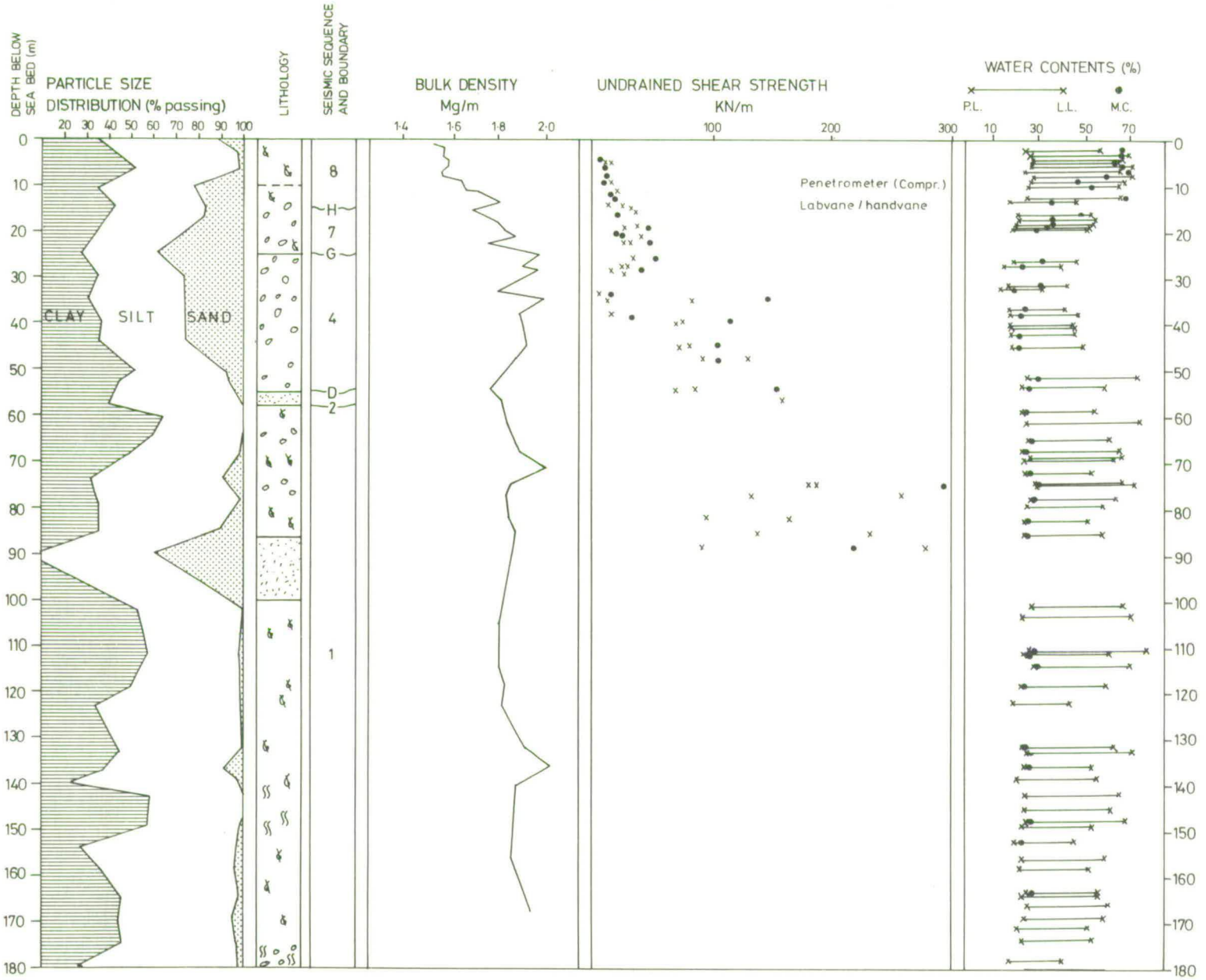

Fig. 2.52. Geotechnical properties of BH 75/33 and their relationship to seismic sequence boundaries, (compiled from raw data in Hobbs, 1978).

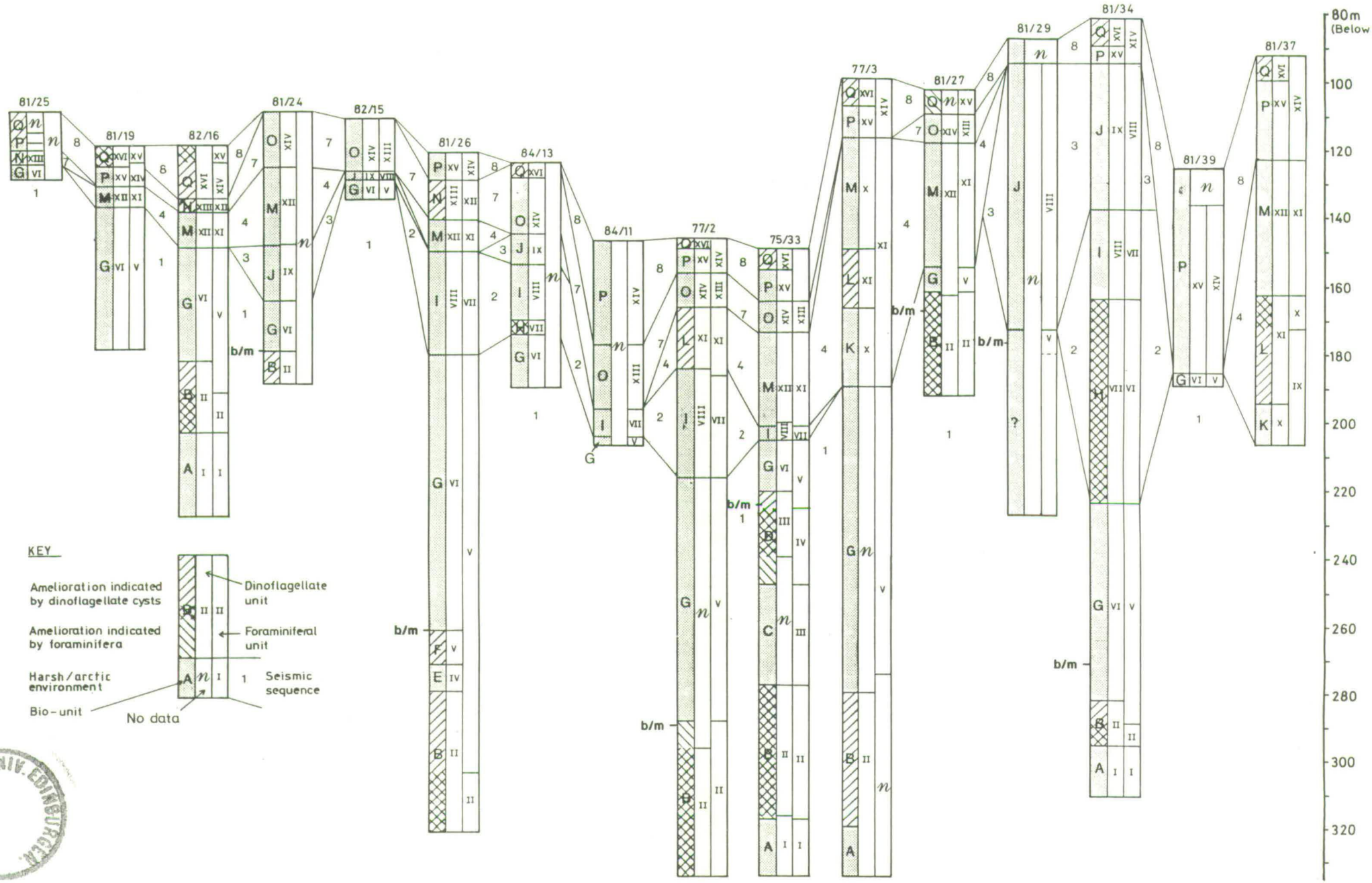

Fig. 3.1 Diagram showing the occurence of the various micropalaeontological units, their position within the seismic framework and the location of the Brunhes Matuyama boundary (b/m).

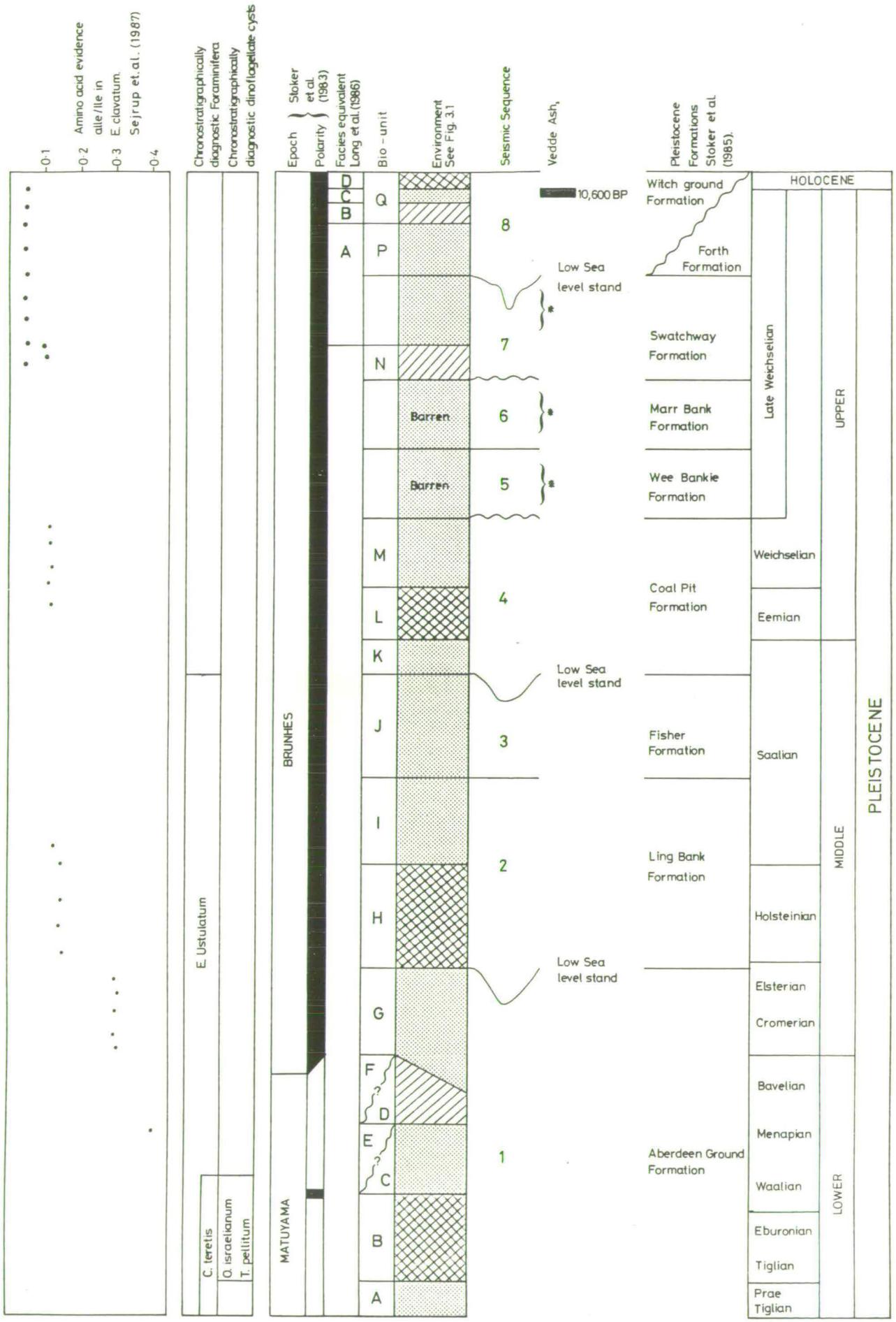

Fig. 3.2 Diagram summarising the stratigraphy of the sequence and relevant evidence used in its construction. Information regarding the Vedde Ash (Long et. al.,1986) and amino acid ratios (Sejrup et. al.,1987) is given in Appendices 8 and 9.*Lateral equivalents.

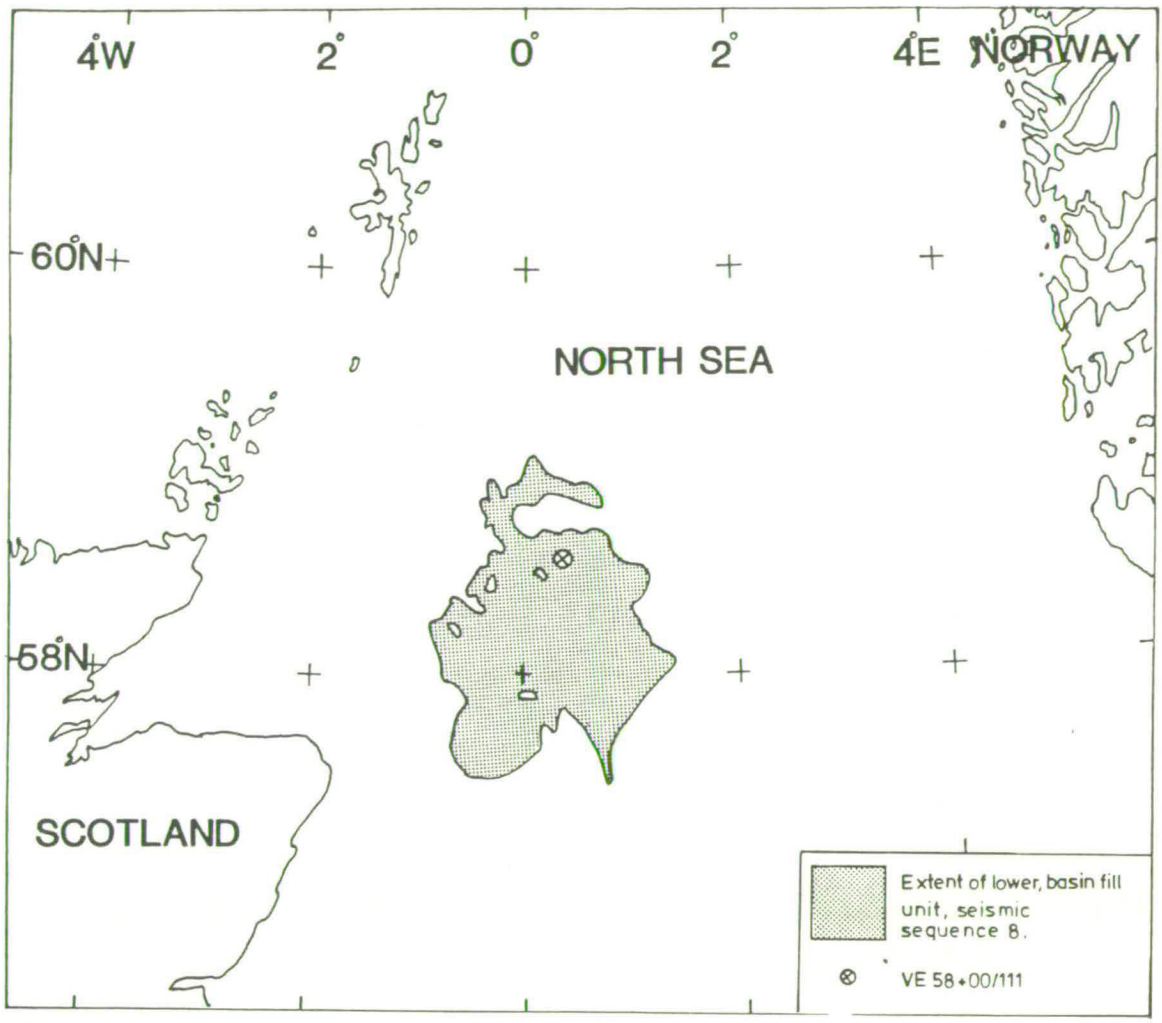

Fig. 3.3a Map showing the position of V.E 58-00/111

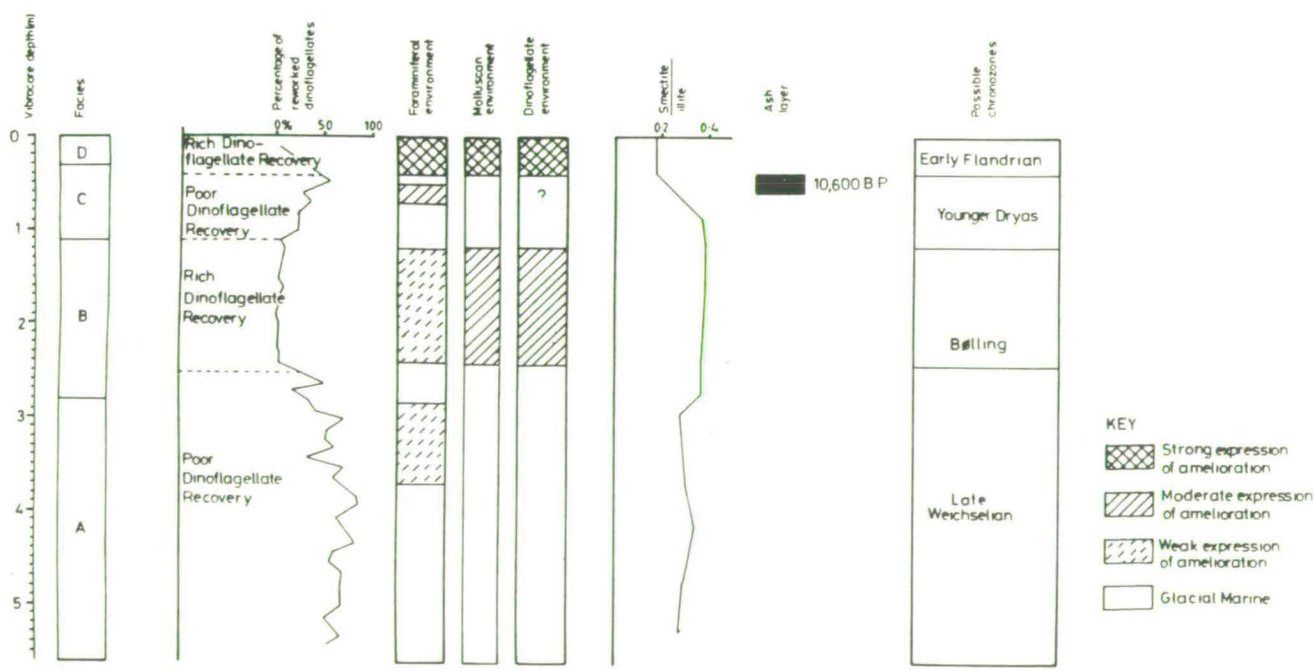

Fig. 3.3b Palaeoenvironmental interpretation and stratigraphy of V.E 58-00/111 (Long et. al.,1986, Appendix 8)

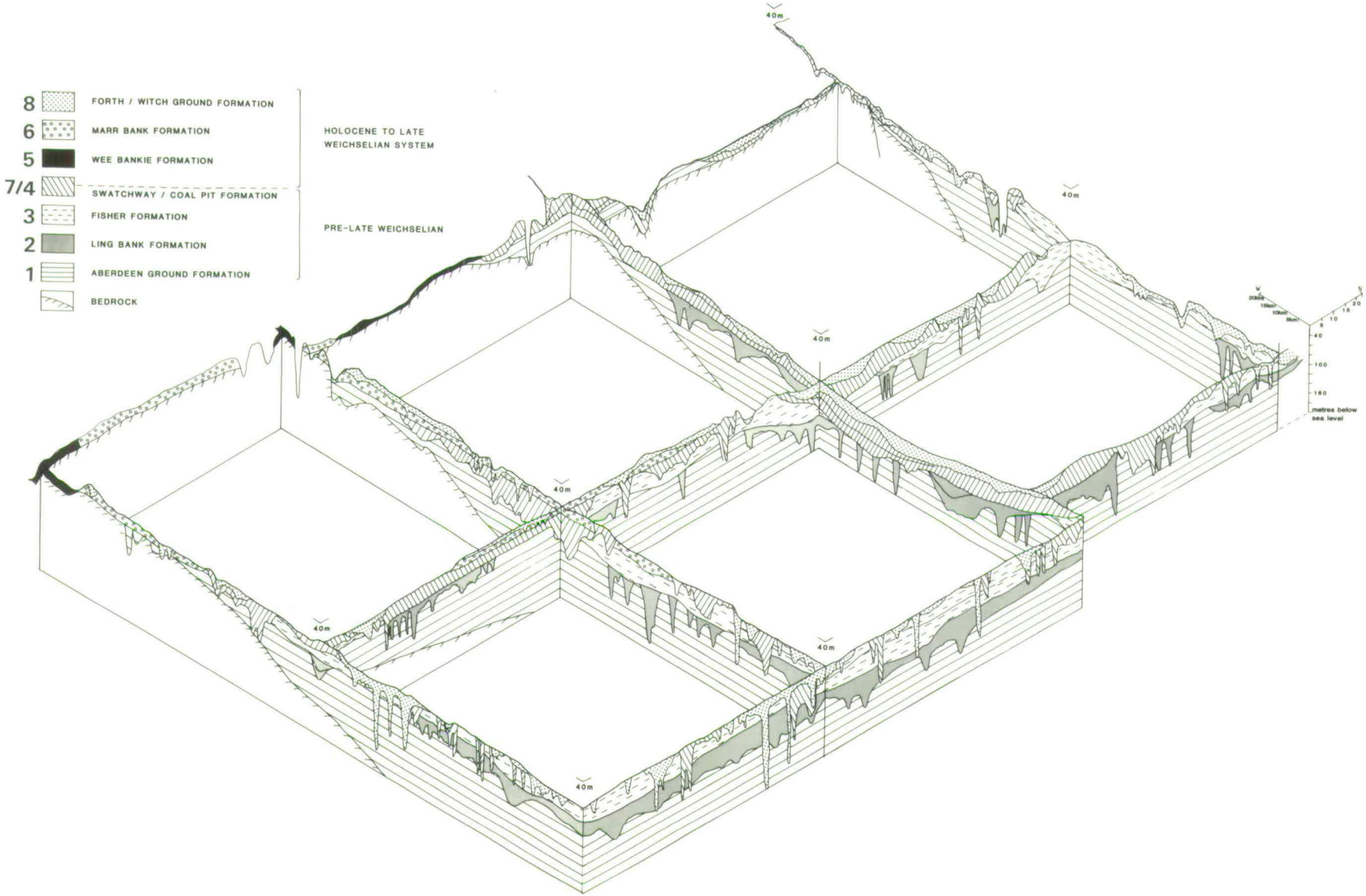

Fig. 3.4 Fence diagram showing the spitial distribution of the 8 seismic sequences and their relationship to the stratigraphy of Stoker et al. (1985).

Figs. 4.1.–4.4. Borehole logs from the Bosies Bank, Fladen, Marr Bank, and Devils Hole areas. Seismic boundaries, sequences, and micropalaeontological units are also indicated.

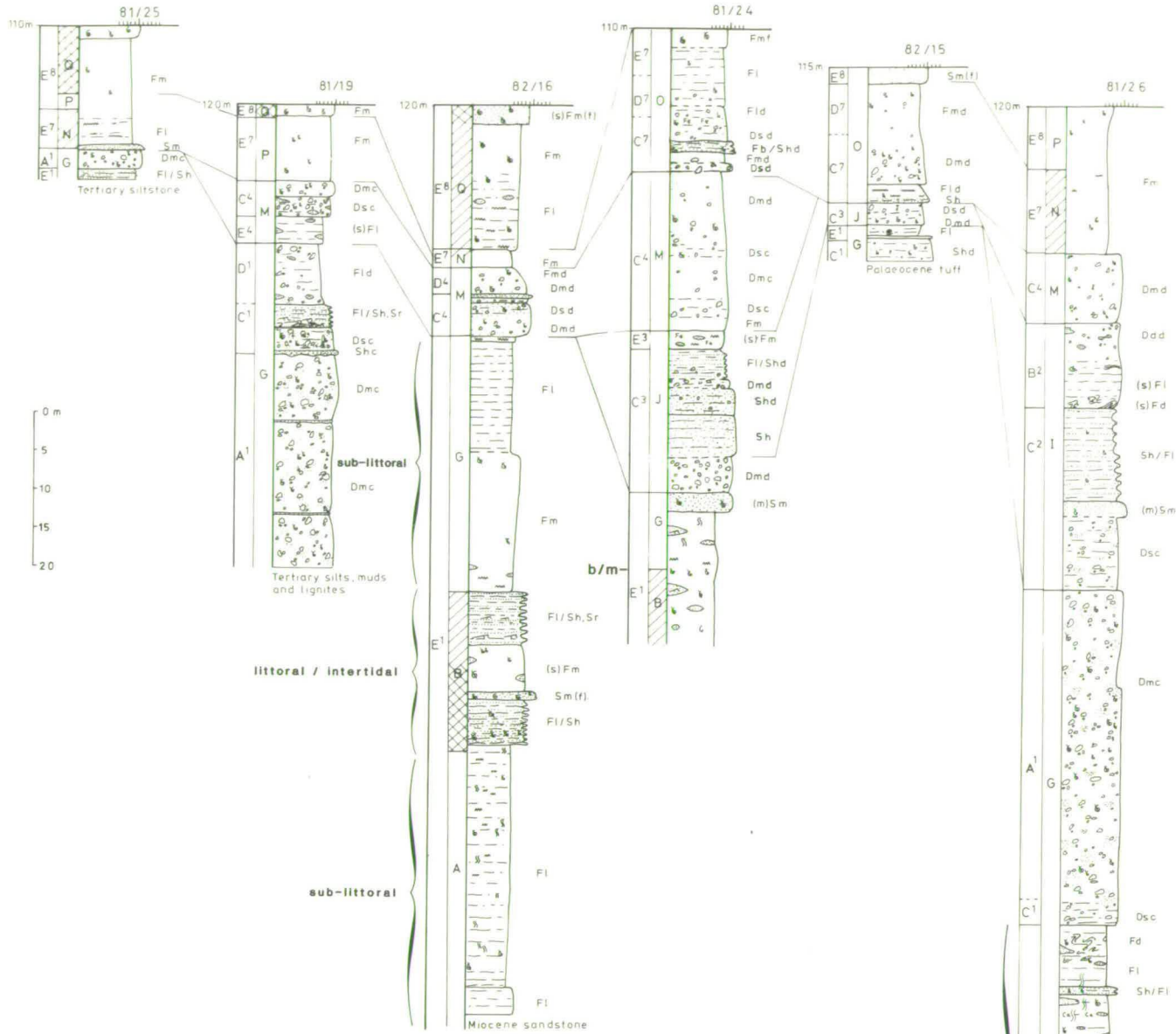

LITHOFACIES CODE

DIAMICT

Dm - : massive
Ds - : stratified
Dd - : deformation structures
D-c : >5 % clasts
D-d : <5 % clasts
D--(f) : >5 % shell material

SANDS : S

Sm - : massive
Sh - : horizontal lamination
Sr - : ripples
Sf - : flaser or wavey lamination
Sg - : graded
Sd - : deformation structures
S-c : >5 % clasts
S-d : <5 % clasts
S--(f) : >5 % shell material
(m)S--- : muddy

FINE GRAINED (mud) : F

Fm - : massive
Fl - : horizontal lamination
Fd - : deformation structures
Ff - : flaser or wavey lamination
F-d : dropstones
F--(f) : >5 % shell material
(s)F--- : sandy
Fl/Sh : interlaminated mud - sand
Fb/Sb : Thinly interbedded mud-sand

SYMBOLS FOR LOGS

DIAMICT
massive
stratified
sandy
SAND
massive
laminated
pebbly
MUD
massive
laminated
dropstones

Ripple cross-lamination
Sand lenses
Convolute lamination
Deformation structures
Monosulphides
Clay balls
Wood fragments
Bioturbation
Whole shells
Shell fragments
Iron concretions
Carbonate concretions
Phosphatic horizon
Conformable contact
Erosional contact
Gradational contact
Monosulphides

MICROPALAEONTOLOGY

Strong expression of amelioration
Moderate expression of amelioration
Harsh / arctic conditions
Barren

FACIES ANALYSIS

E7 Facies and seismic sequence

MEAN GRAIN SIZE

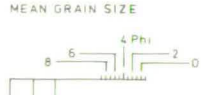

Fig. 4.1.

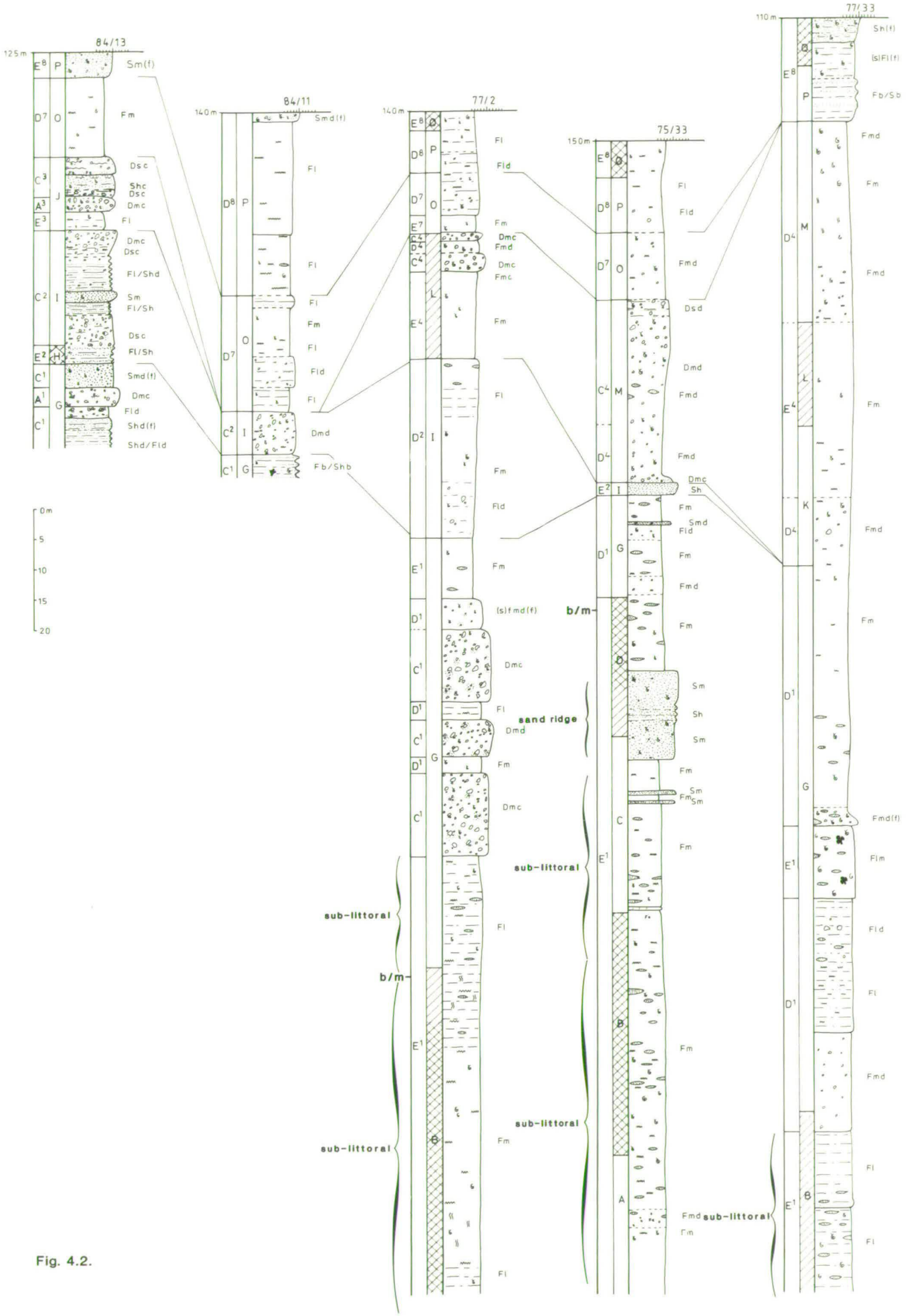
84/13
125m
84/11
140m
77/2
140m
75/33
150m
77/33
110m
0m
5
10
15
20
sand ridge
sub-littoral
b/m

Fig. 4.2.

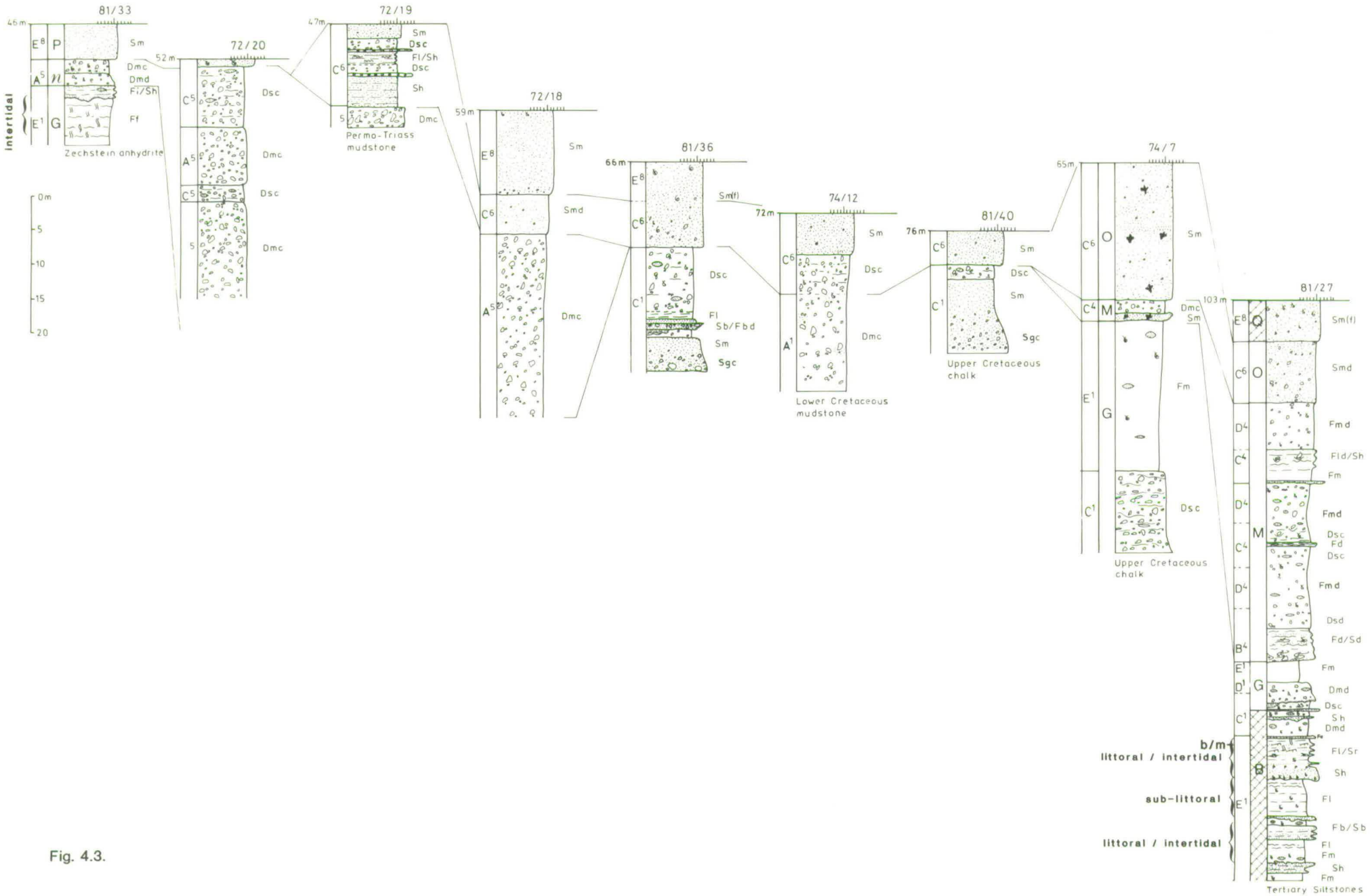
81/33
46m
Sm
Dmc
Dmd
Fl/Sh
Ff
Intertidal
Zechstein anhydrite
72/20
52m
Dsc
Dmc
Dsc
Dmc
72/19
47m
Sm
Dsc
Fl/Sh
Dsc
Sh
Dmc
Permo-Triass mudstone
72/18
59m
Sm
Smd
Dmc
81/36
66m
Sm(f)
Dsc
Fl
Sb/Fbd
Sm
Sgc
74/12
72m
Sm
Dsc
Dmc
Lower Cretaceous mudstone
81/40
76m
Sm
Dsc
Sm
Sgc
Upper Cretaceous chalk
74/7
65m
Sm
Fm
Dsc
Upper Cretaceous chalk
81/27
103m
Dmc
Sm
Sm(f)
Smd
Fmd
Fld/Sh
Fm
Fmd
Dsc
Fd
Dsc
Fmd
Dsd
Fd/Sd
Fm
Dmd
Dsc
Sh
Dmd
Fl/Sr
Sh
Fl
Fb/Sb
Fl
Fm
Sh
Fm
b/m
littoral / intertidal
sub-littoral
littoral / intertidal
Tertiary Siltstones

Fig. 4.3.

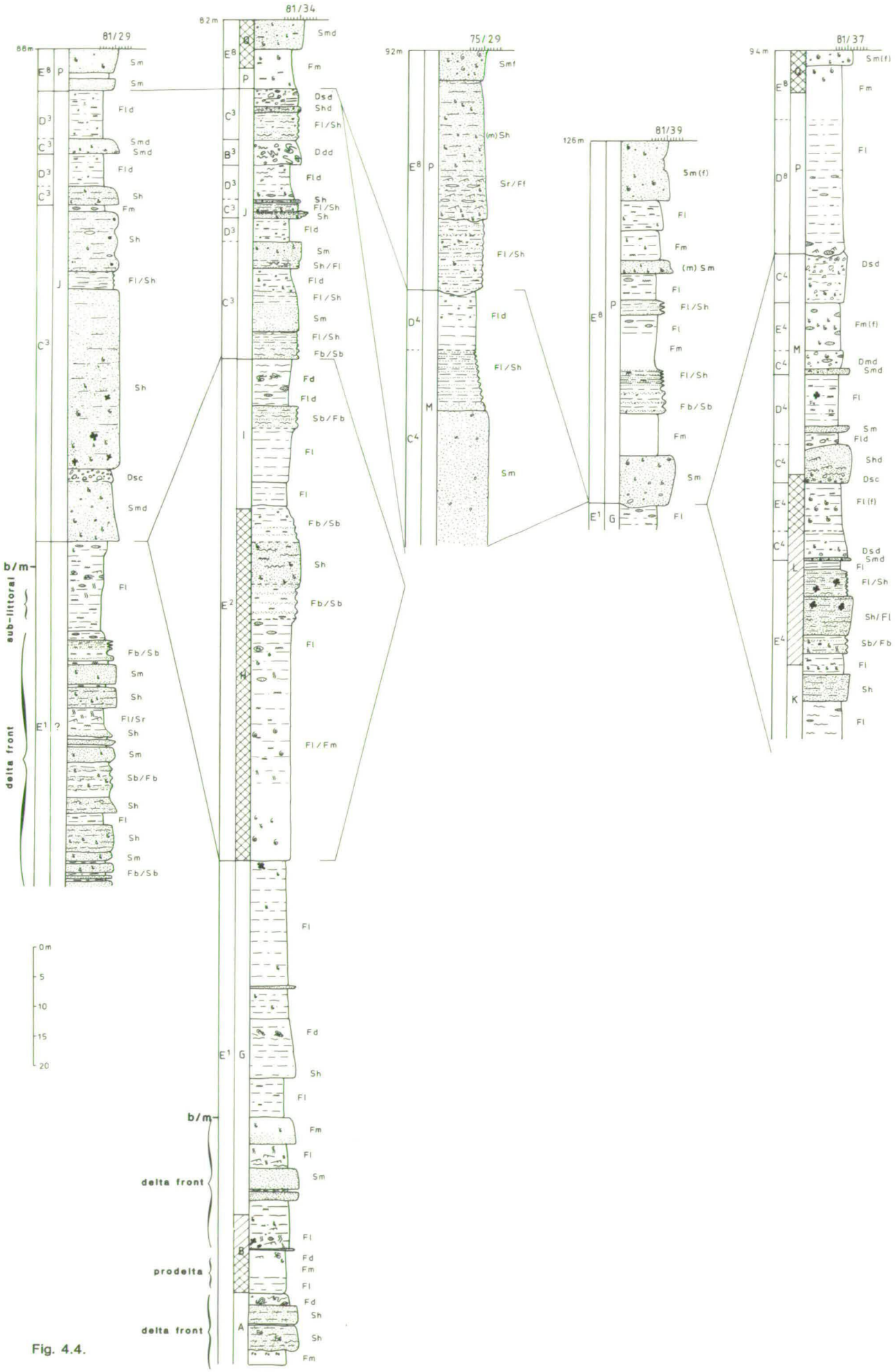
81/29
88m
81/34
82m
75/29
92m
81/39
126m
81/37
94m
b/m
sub-littoral
delta front
prodelta
0m
5
10
15
20

Fig. 4.4.

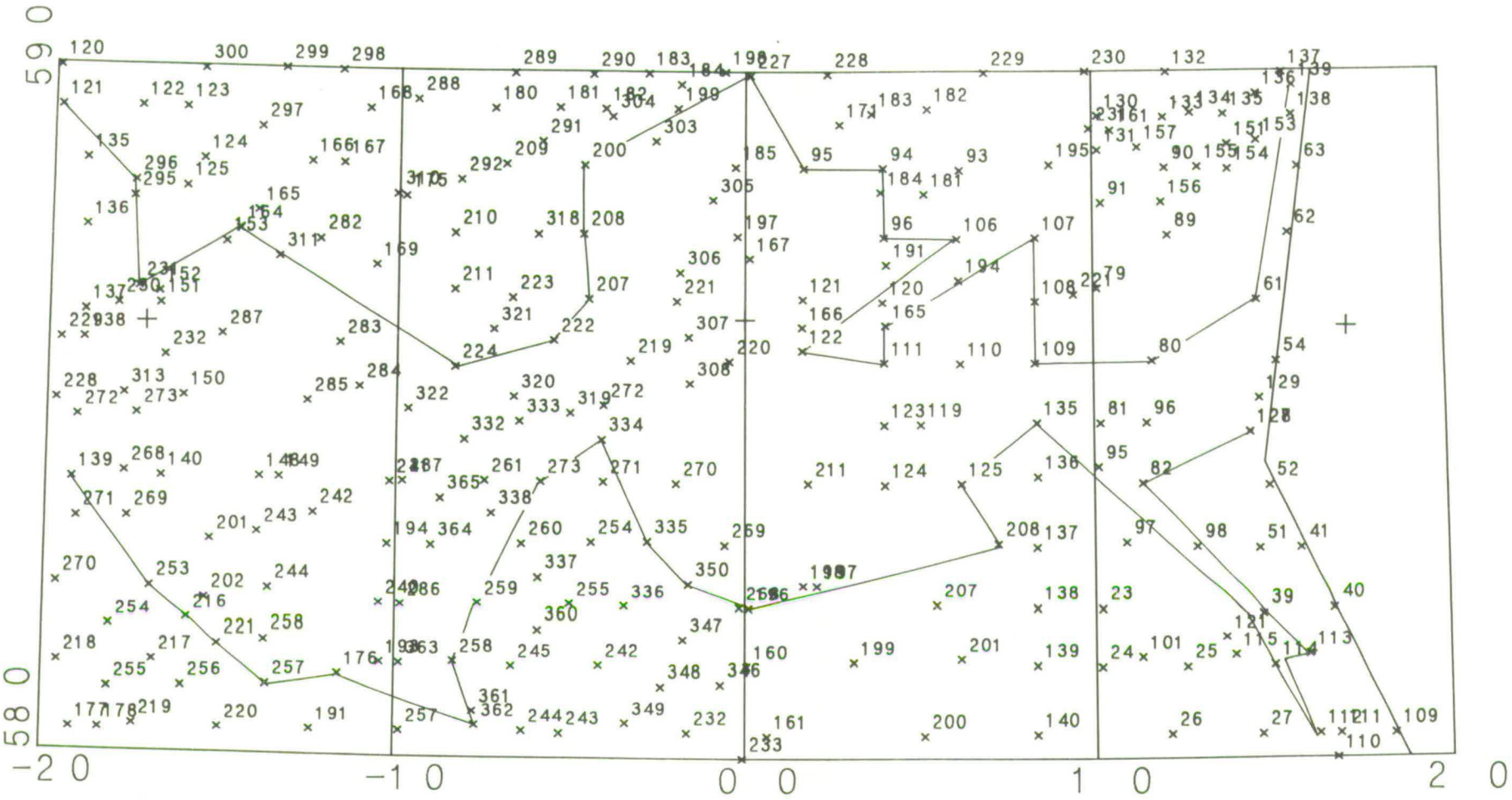

Fig. 4.5. Vibrocore sites in the Bosies Bank (00 to 02W) and Fladen (00 to 02E) areas. The line joins selected vibrocores depicted in Fig. 4.6.

Fig. 4.6. Vibrocore logs from the Bosies Bank and Fladen areas.

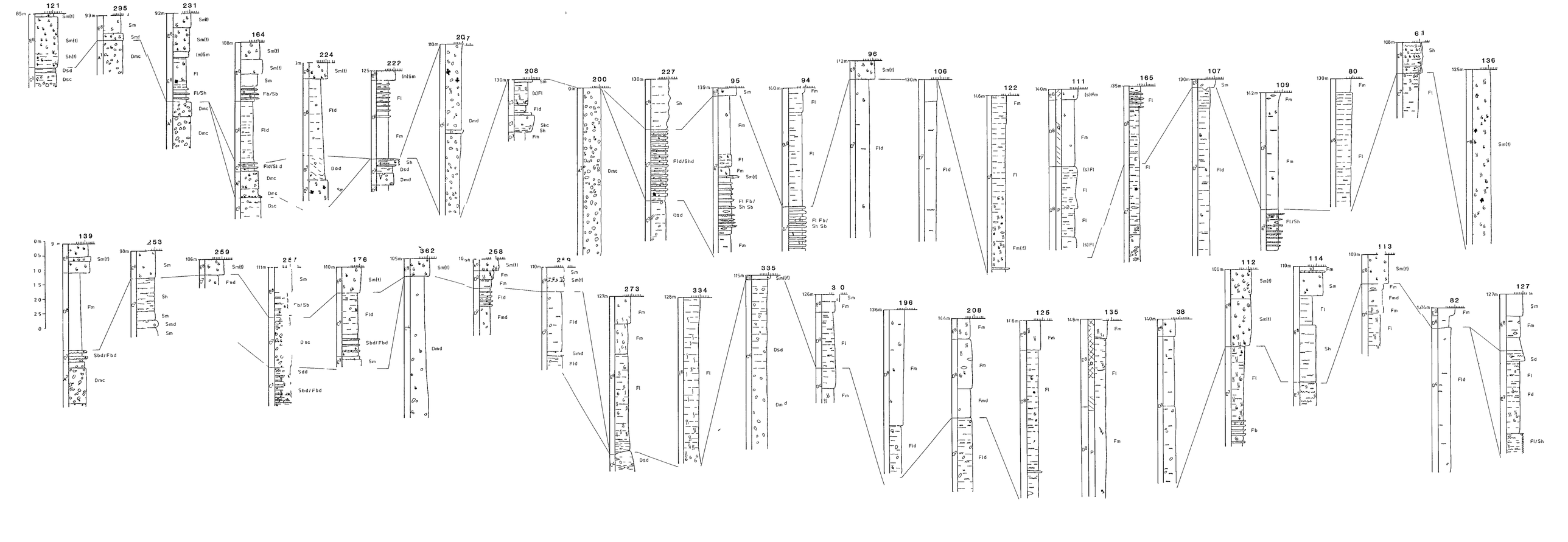
121
85m
Sm(f)
Sm(f)
Shf(f)
Dsd
Dsc
295
93m
Sm
Smf
Dmc
231
92m
Sm(f)
Sm(f)
(m)Sm
Fl
Fl/Sh
Dmc
Dmc
164
108m
Sm(f)
Sm(f)
Sm
Fb/Sb
Fld
Fld/Sld
Dmc
Dmc
Dsc
224
Sm(f)
Fld
Ddd
222
125
(m)Sm
Fl
Fm
Sh
Dsd
Dmd
207
110m
Dmd
208
130m
Sm
(s)Fl
Fld
Shc
Sh
Fm
200
0m
Dmc
227
130m
Sh
Fld/Shd
Dsd
95
139m
Sm
Fm
Ff
Fm
Sm(f)
Fl Fb/
Sh Sb
Fm
94
140m
Fm
Fl
Fl
Fl Fb/
Sh Sb
96
Sm(f)
Fld
106
130m
Fld
122
146m
Fm
Fl
Fm(f)
111
140m
(s)Fm
Fm
(s)Fl
Fl
Fl
(s)Fl
165
135m
Fl
Fl
107
130m
Sm
Fld
109
142m
Fm
Fm
Fl/Sh
80
130m
Fm
Fl
61
108m
Sh
Fl
136
125m
Sm(f)
139
9 m
0m
5
10
15
20
25
0
Sm(f)
Fm
Sbd/Fbd
Dmc
253
98m
Sm
Sh
Sm
Smd
Sm
259
106m
Sm(f)
Fmd
257
111m
Sm
Fb/Sb
Dmc
Sdd
Sbd/Fbd
176
110m
Sm(f)
Fld
Sbd/Fbd
Sm
362
105m
Sm(f)
Dmd
258
10
Sm(f)
Fm
Fm
Fld
Fmd
259
110m
Sm
Sm(f)
Fld
Smd
Fld
273
127m
Fm
Fm
Fl
Dsd
334
128m
Fl
335
115m
Sm(f)
Dsd
Dmd
30
126m
Sm
Fm
Fl
Fm
196
136m
Fm
Fm
Fld
208
144m
Fm
Fm
Fmd
Fld
125
146m
Fm
Fl
135
148m
Fm
Fl
Fm
38
140m
112
100m
Sm(f)
Sm(f)
Fl
Fb
114
110m
Fm
Sm
Fl
Sh
113
103m
Sm(f)
Fm
Fmd
Fm
Fl
82
144m
Fm
Fld
127
127m
Sm
Fm
Sd
Fl
Fd
Fl/Sh

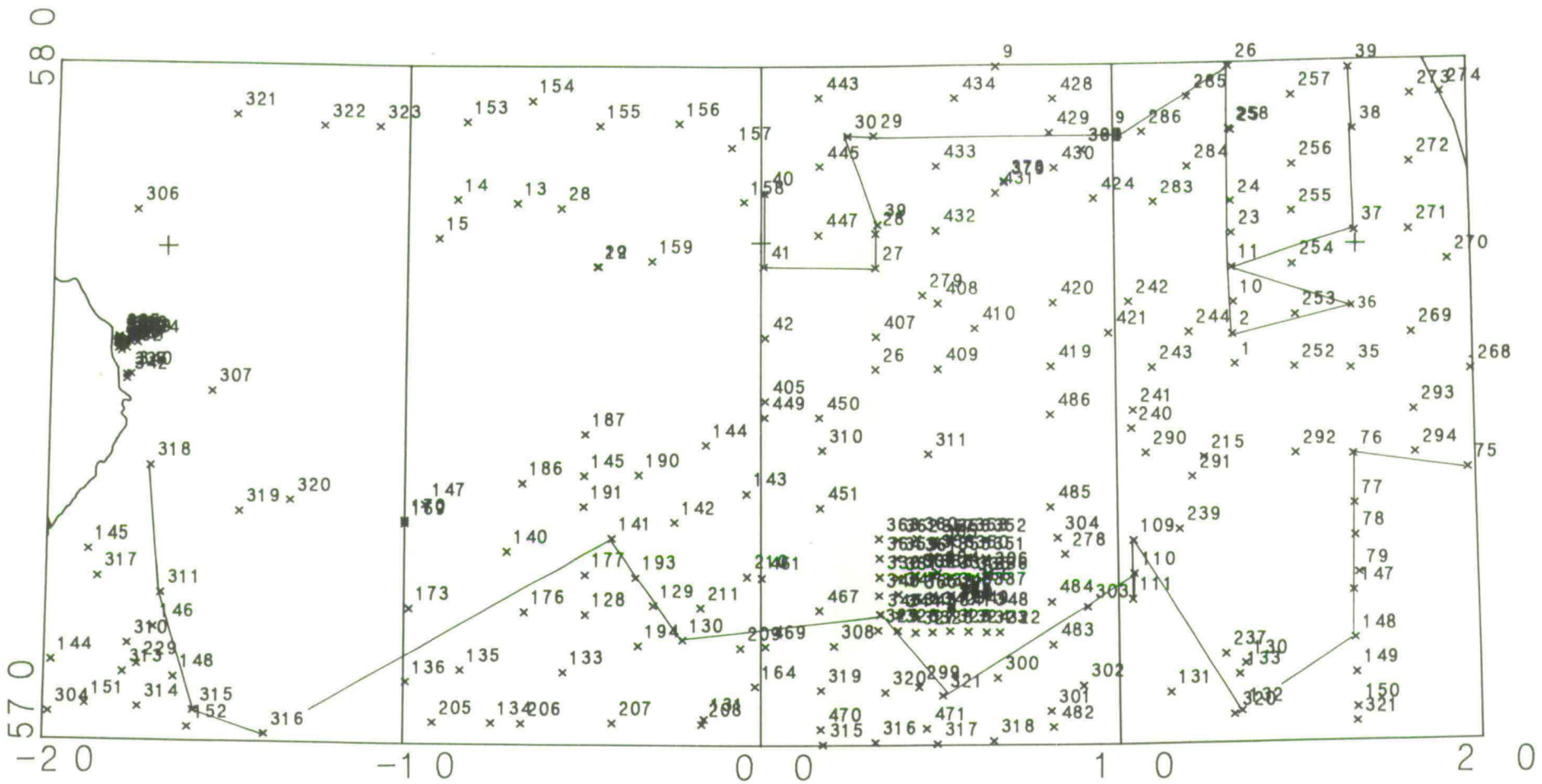

Fig. 4.7. Vibrocore sites in the Peterhead (00 to 02W) and Forties (00 to 02E) areas. The line joins selected vibrocores depicted in Fig. 4.8.

Fig. 4.8. Vibrocore logs from the Peterhead and Forties areas.

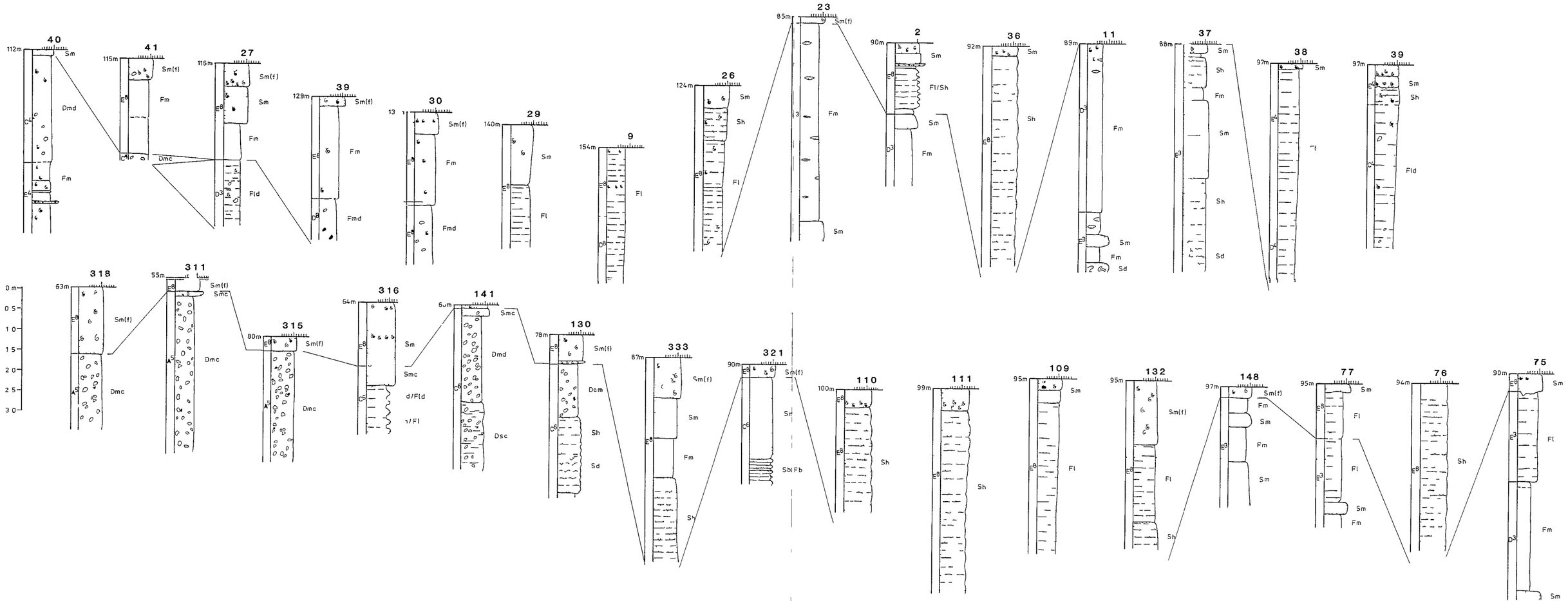
40
112m
Sm
Dmd
Fm
41
115m
Sm(f)
Fm
Dmc
27
116m
Sm(f)
Sm
Fm
Fld
39
129m
Sm(f)
Fm
Fmd
30
13
Sm(f)
Fm
Fmd
29
140m
Sm
Fl
9
154m
Fl
26
124m
Sm
Sh
Fl
23
85m
Sm(f)
Fm
Sm
2
90m
Sm
Fl/Sh
Sm
Fm
36
92m
Sm
Sh
11
89m
Fm
Sm
Fm
Sd
37
88m
Sm
Sh
Fm
Sm
Sh
Sd
38
97m
Sm
39
97m
Sm
Sh
Fld
318
63m
Sm(f)
Dmc
311
55m
Sm(f)
Smc
Dmc
315
80m
Sm(f)
Dmc
316
64m
Sm
Smc
d/Fld
141
64m
Smc
Dmd
Dsc
130
78m
Sm(f)
Dcm
Sh
Sd
333
87m
Sm(f)
Sm
Fm
Sh
321
90m
Sm(f)
Sm
Sbl Fb
110
100m
Sh
111
99m
Sh
109
95m
Sm
Fl
132
95m
Sm(f)
Fl
Sh
148
97m
Fm
Sm(f)
Sm
Fm
Sm
77
95m
Sm
Fl
Fl
Sm
Fm
76
94m
Sh
75
90m
Sm
Fl
Fm
Sm

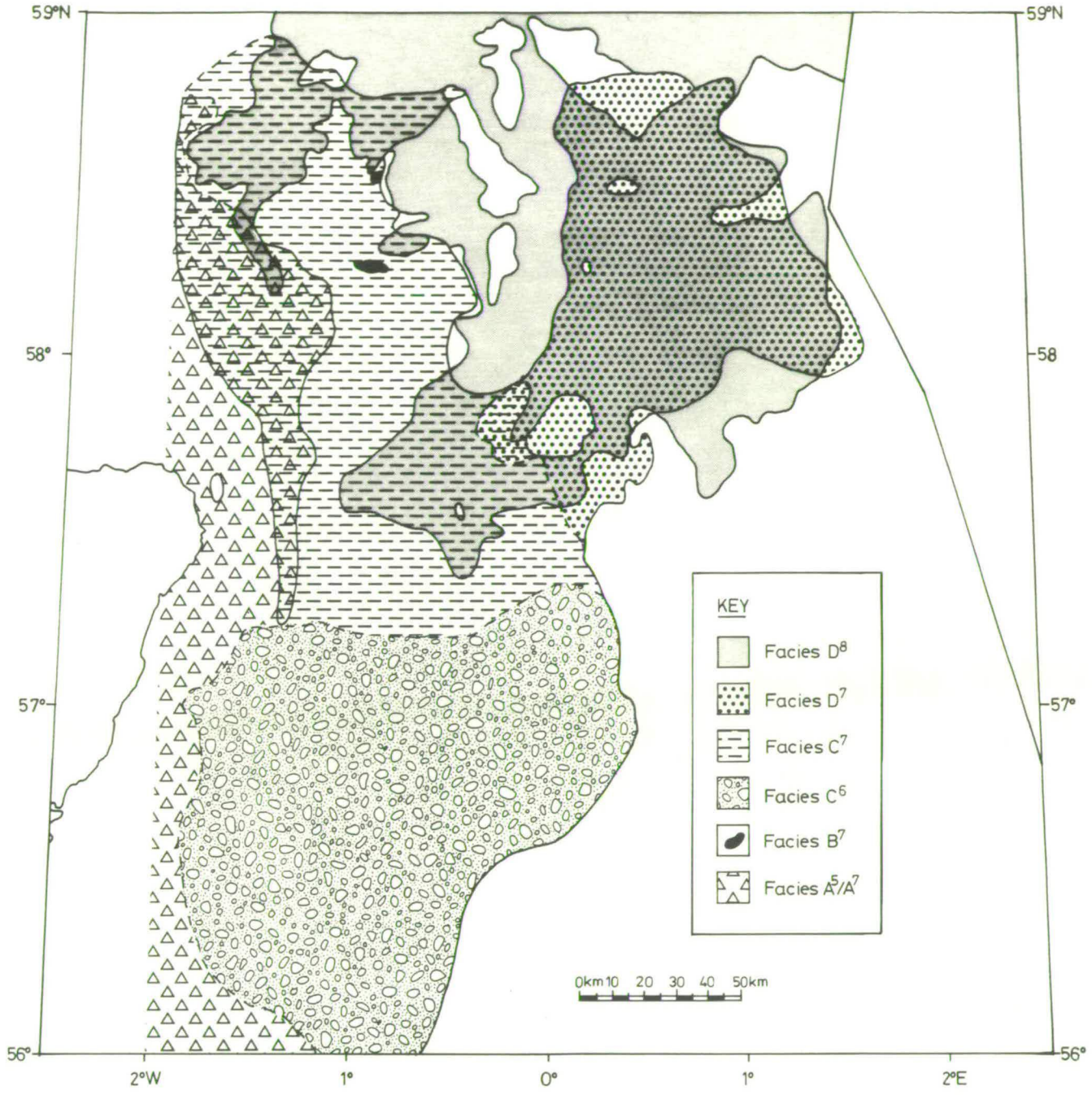

Fig. 4.9. Map showing distribution of late Weichselian sedimentary facies.

Plate 4.1. Facies A^5, massive diamict with abundant clasts. Scale is in centimetres.

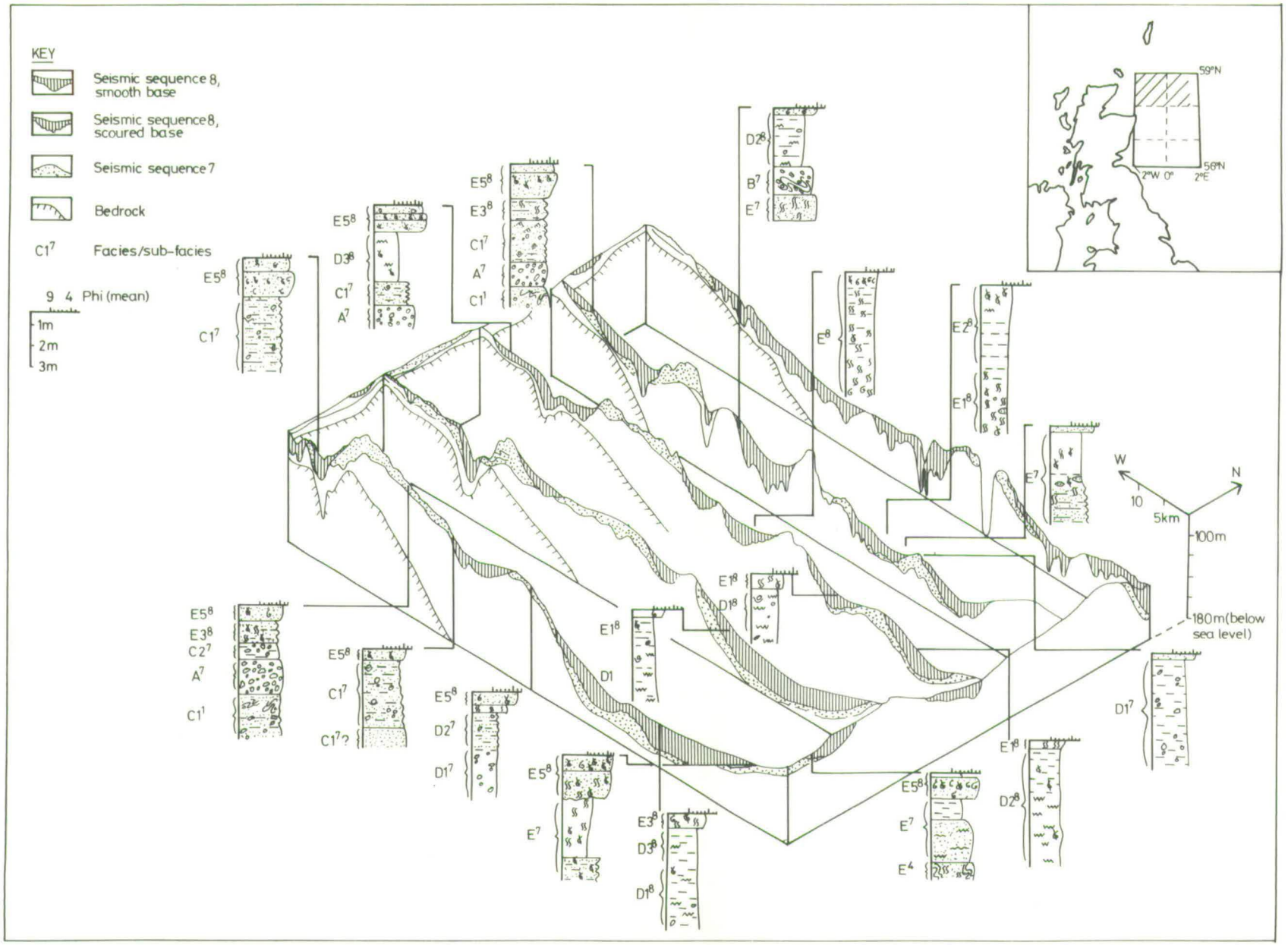

Fig. 4.10. Lithofacies profiles and fence diagram of the late Weichselian sequence in the Bosies Bank and Fladen areas.

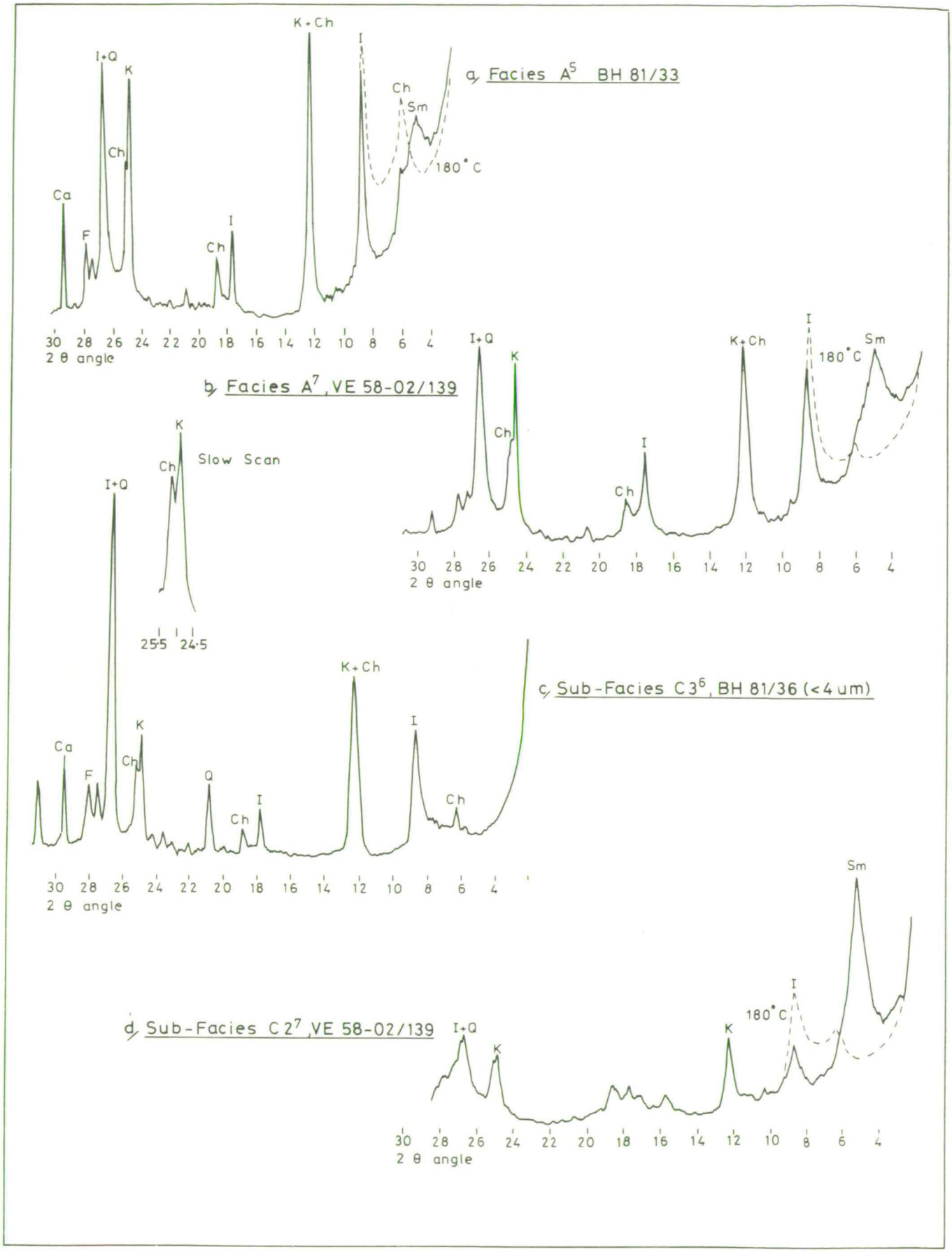

Fig. 4.11. Typical X-ray diffraction (XRD) traces showing the clay mineralogy of late Weichselian facies A – C.

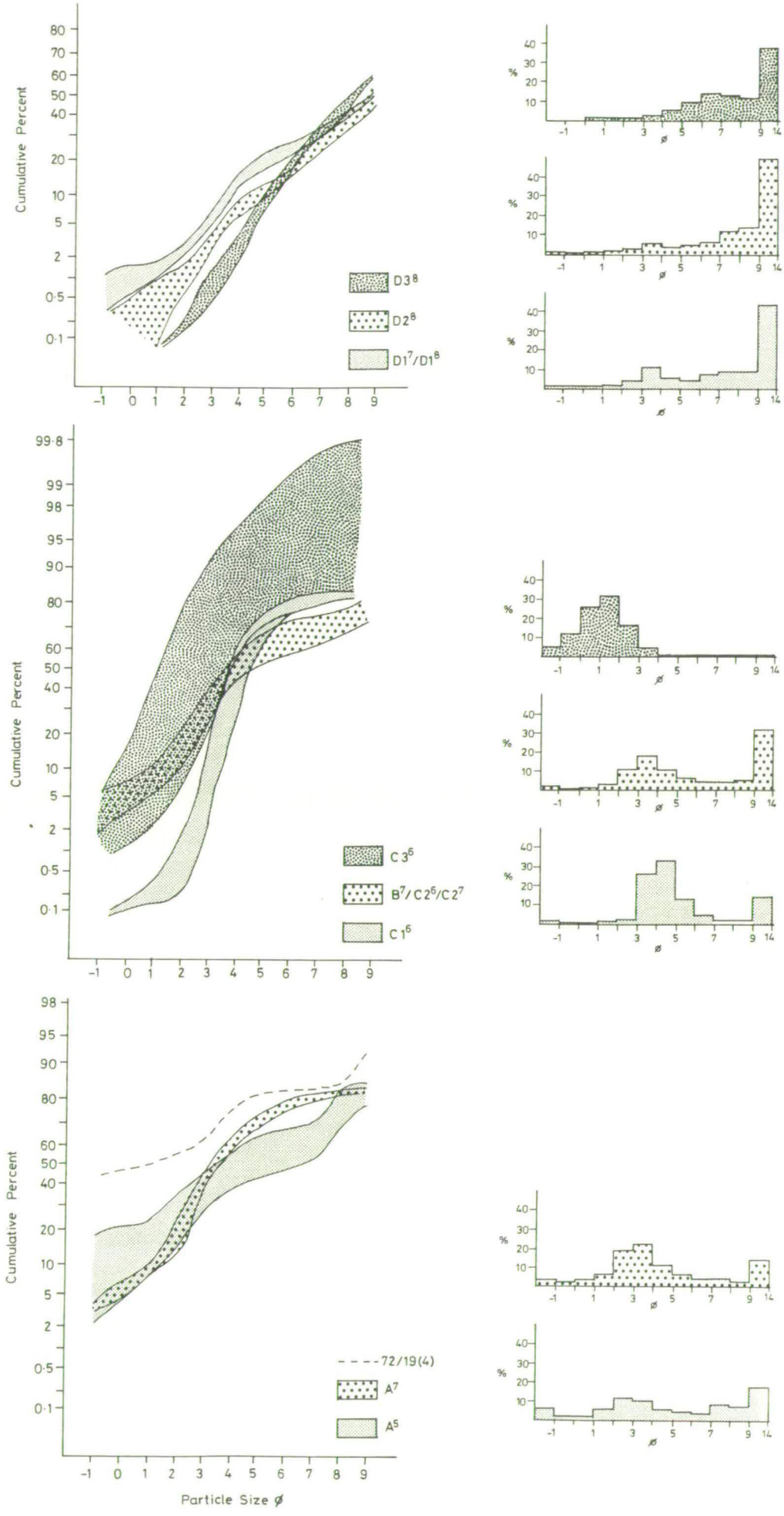

Fig. 4.12. Particle size distributions in sediments from late Weichselian facies A – D.

Plate 4.2. Representative x-radiographs of various sedimentary facies.

(6) Facies D^8, mud with rare clasts.

(5) Vertical alignment of clasts.

(4) Facies $C2^7$, stratified diamict.

(3) Facies A^7, massive diamict.

(2) Facies $C2^1$, stratified diamict.

(1) Facies $C1^1$, bedded sand and gravel.

(A) Artifact.

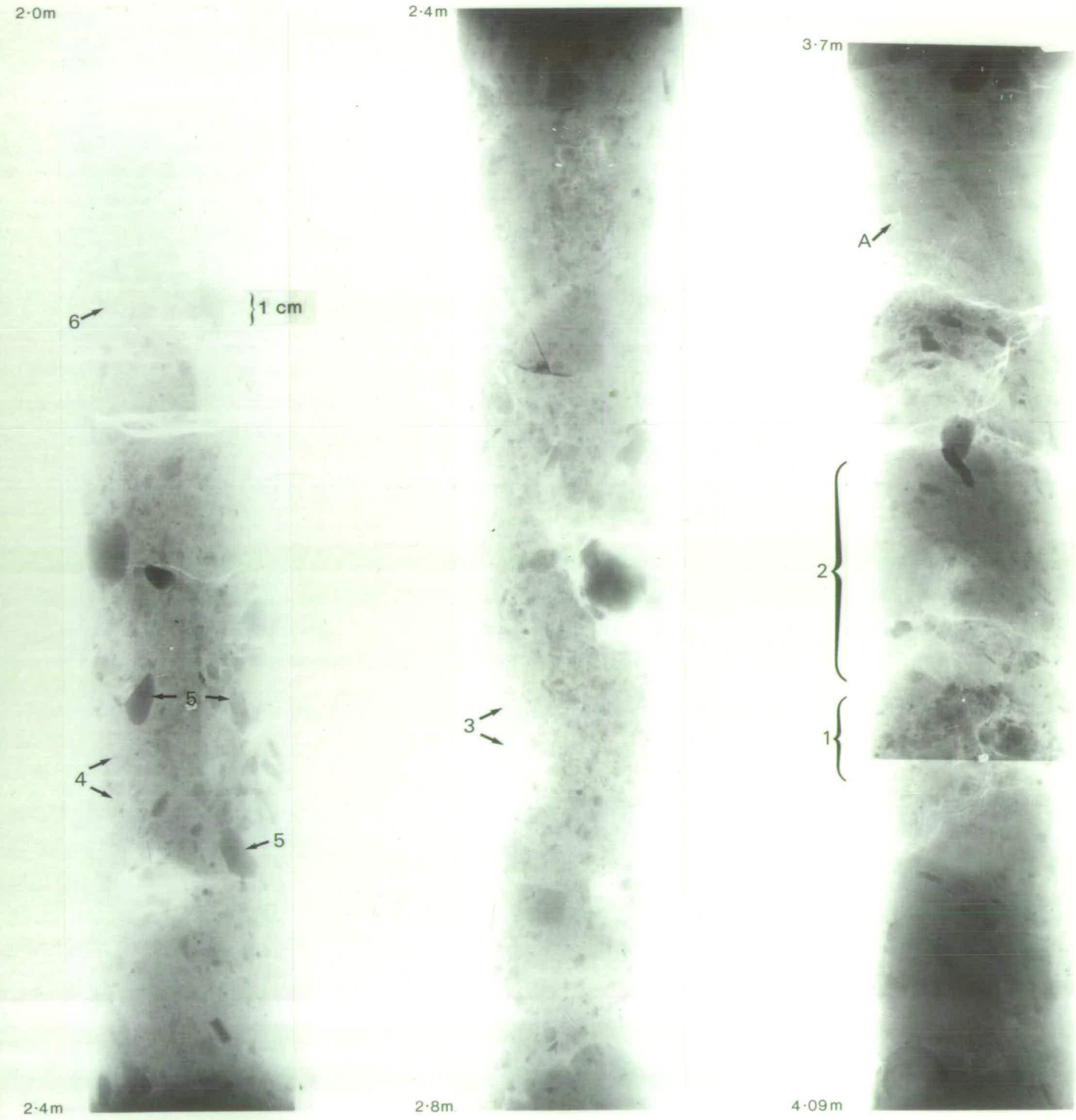
2·0m
6
1 cm
5
4
5
2·4m
2·4m
3
2·8m
3·7m
A
2
1
4·09m

Plate 4.3. Representative x-radiographs of various sedimentary facies.

(6) Facies $D1^{8}$, poorly stratified mud with rare clasts.

(5) Vertical alignment of clasts.

(4) Facies $C2^{7}$, stratified diamict.

(3) Weak horizontal alignment of clasts.

(2) Angular contacts.

(1) Facies B^{7}, complexly stratified diamict.

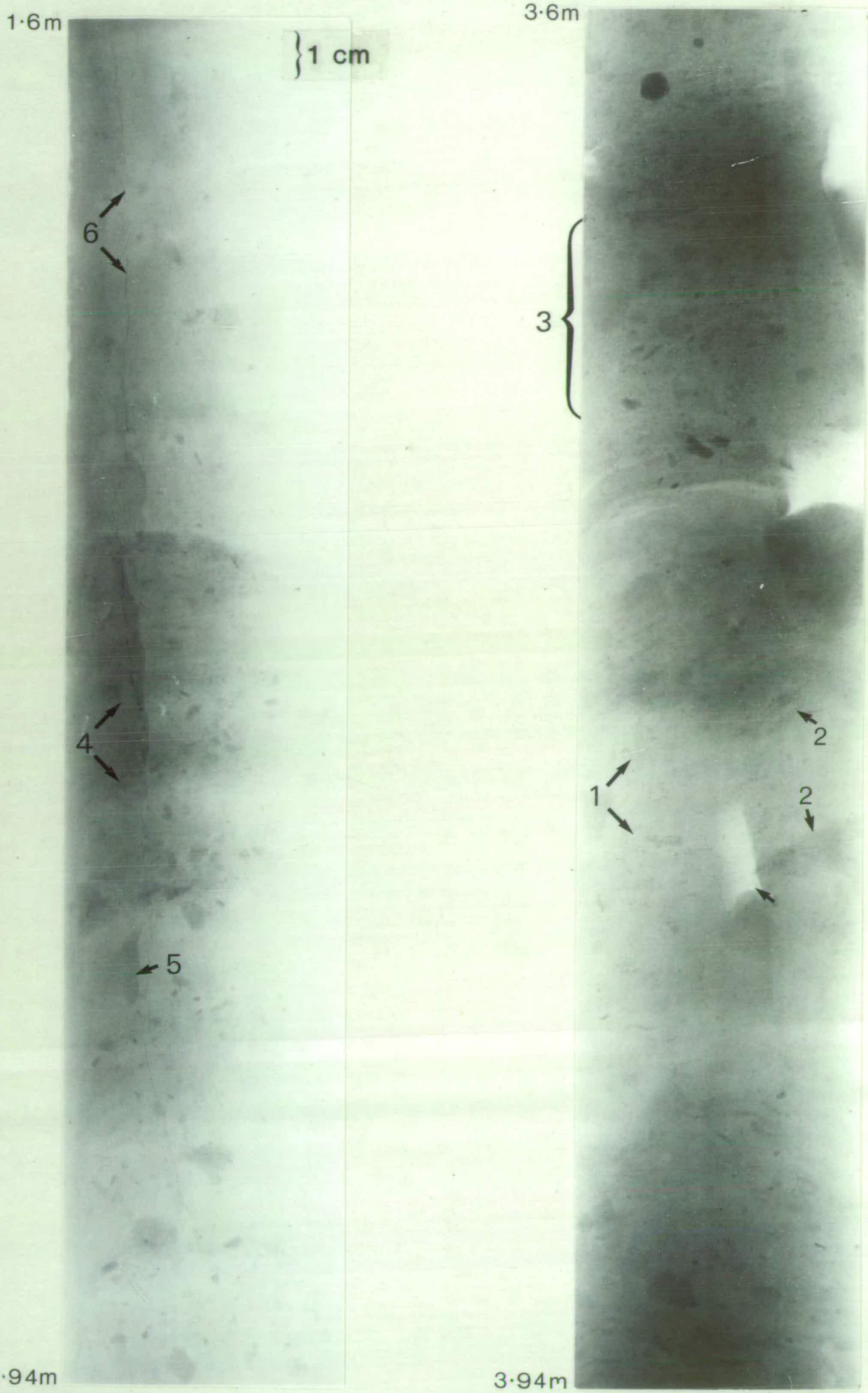
1·6m
1 cm
6
4
5
1·94m
3·6m
3
1
2
2
3·94m

Plates 4.4a. and 4.4b. Facies B^7, complexly stratified diamict. Note that in places the stratification is highlighted by iron staining. Scale is in centimetres.

Plate 4.5. Representative x-radiographs of facies $C1^6$ and $C2^6$.

(4) Facies $C2^6$, massive diamict with gradational base (3).

(2) Facies $C1^6$, laminated mud and sand.

(1) Facies $C1^6$, ripple cross laminated sand with mud drapes.

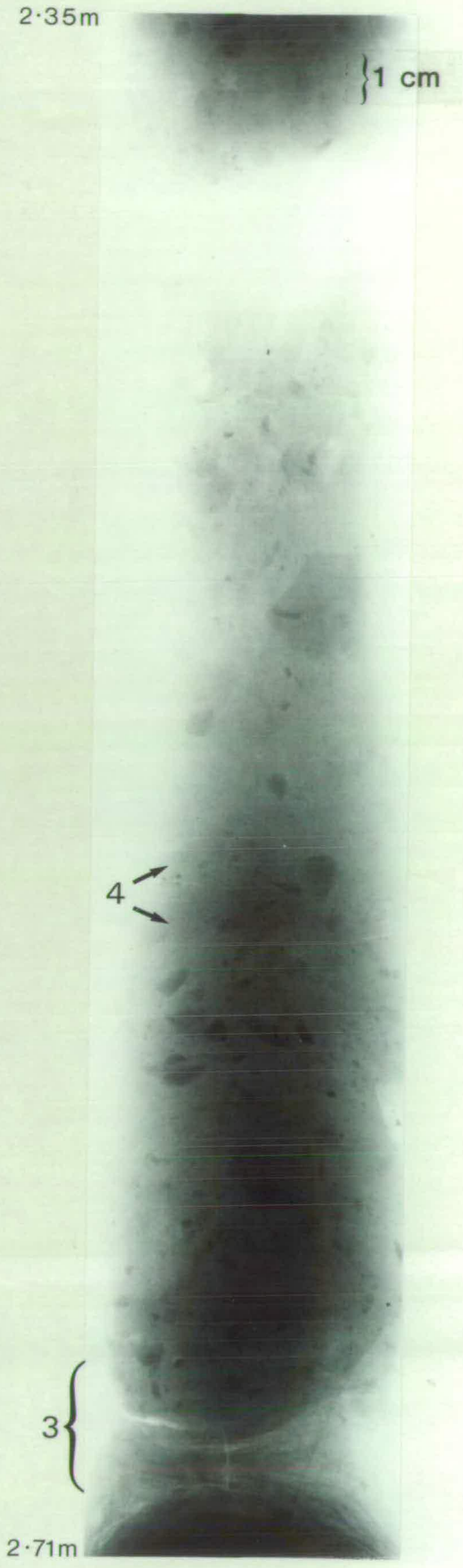
2·35m
1 cm
4
3
2·71m

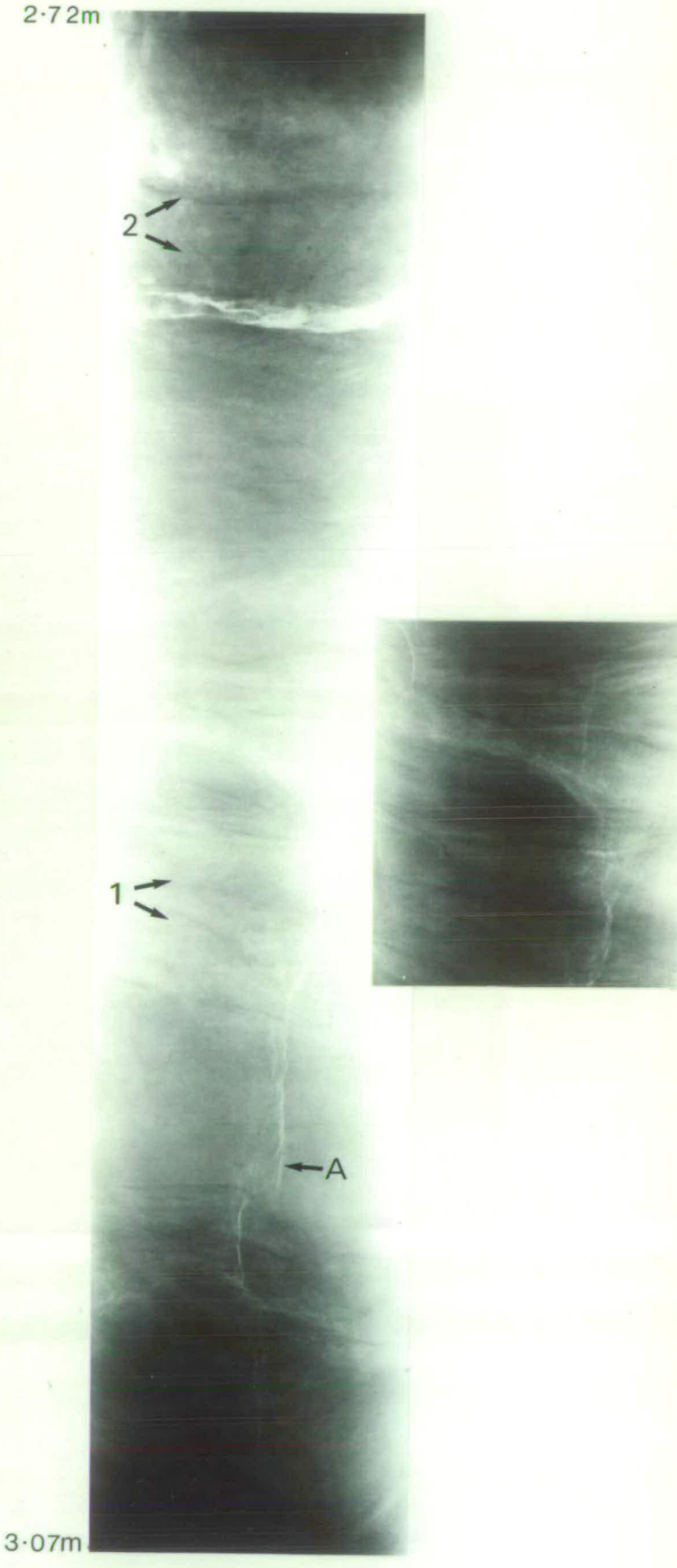
2·72m
2
1
A
3·07m

Plate 4.6. Facies $C1^6$, laminated sands, interbedded with facies $C2^6$, stratified diamict. Note the bands of carbonaceous rich material. Scale is in centimetres.

Plate 4.7. Representative x-radiographs of facies $C1^7$ (2.0-4.2m) consisting of well laminated and bedded sands and muds with clasts, Overlying facies A^7 (4.2-5.8m) consisting of massive diamict. Note the deformation of the laminae underlying a clast at 4.1m (see also Plate 4.8).

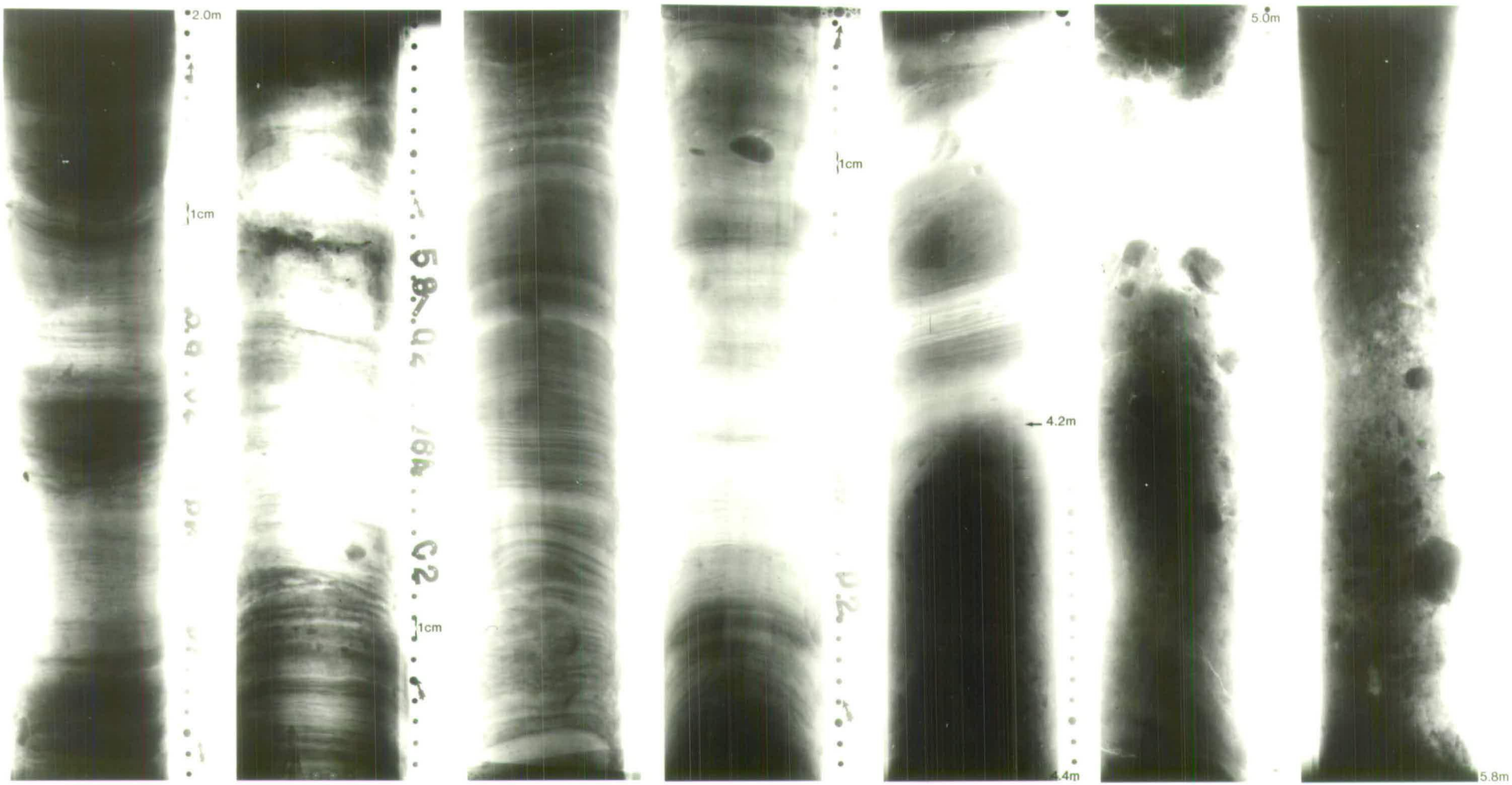
2.0m
1cm
1cm
1cm
4.2m
4.4m
5.0m
5.8m

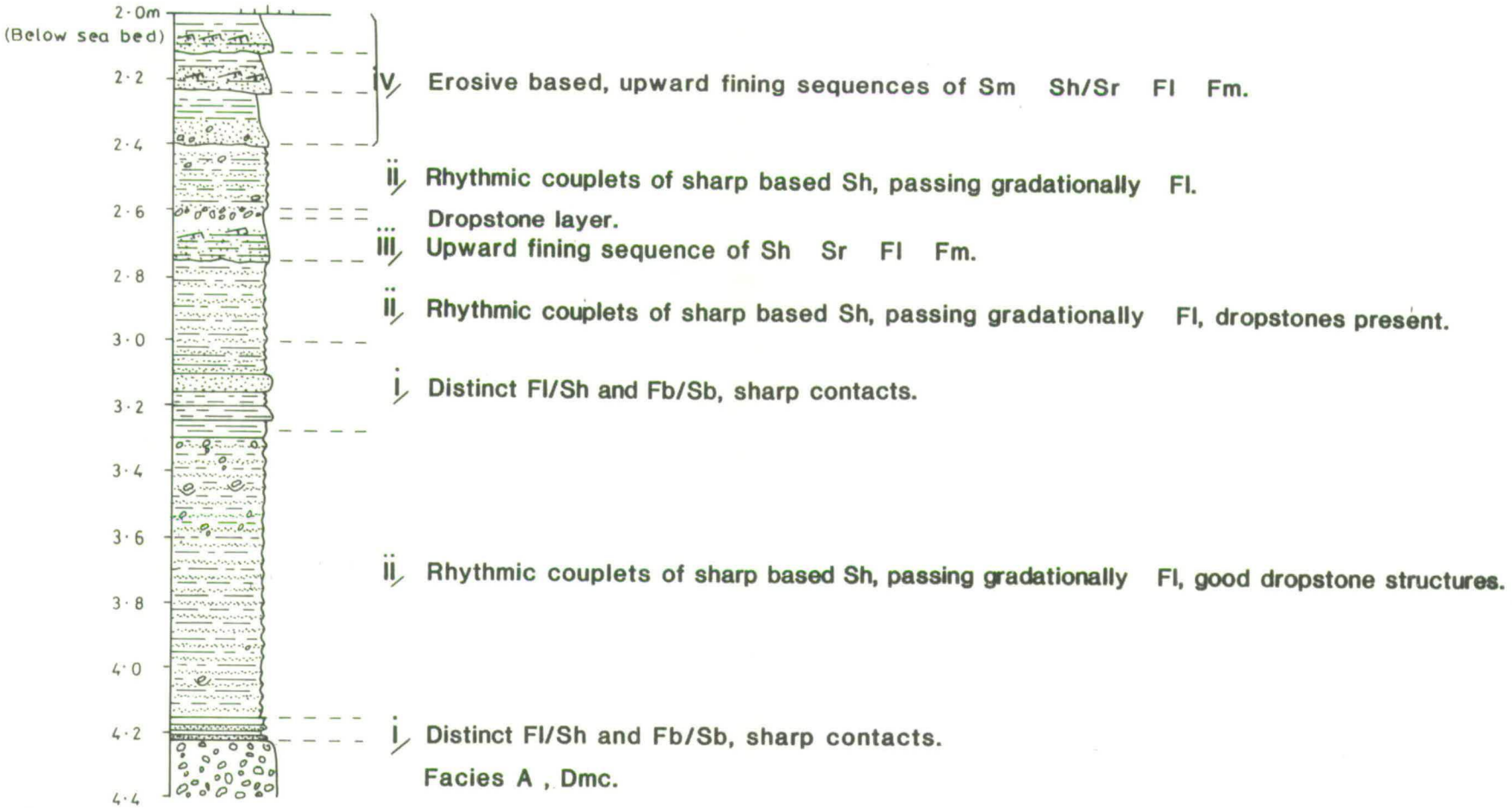

Fig. 4.13. Detailed log showing lithological variations in facies $C1^7$ in a core from the Bosies Bank area.

Plate 4.8a. Representative x-radiograph of facies $C1^7$.

(2) Wispy laminated sands and muds.

(1) Clast layer.

Plate 4.8b. Representative x-radiograph of facies $C1^7$.

(2) Deformation of underlying laminae.

(1) Large clast.

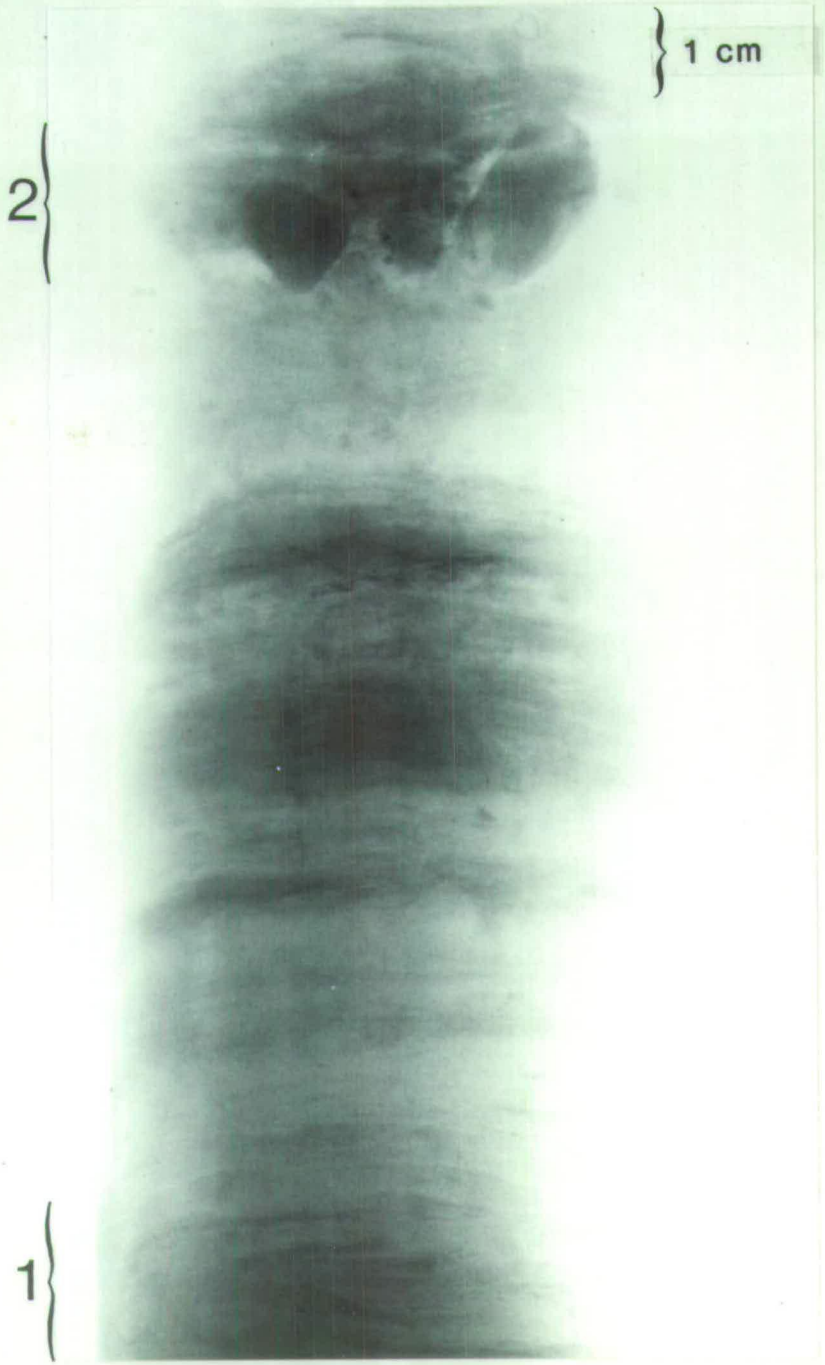
1 cm
2
1

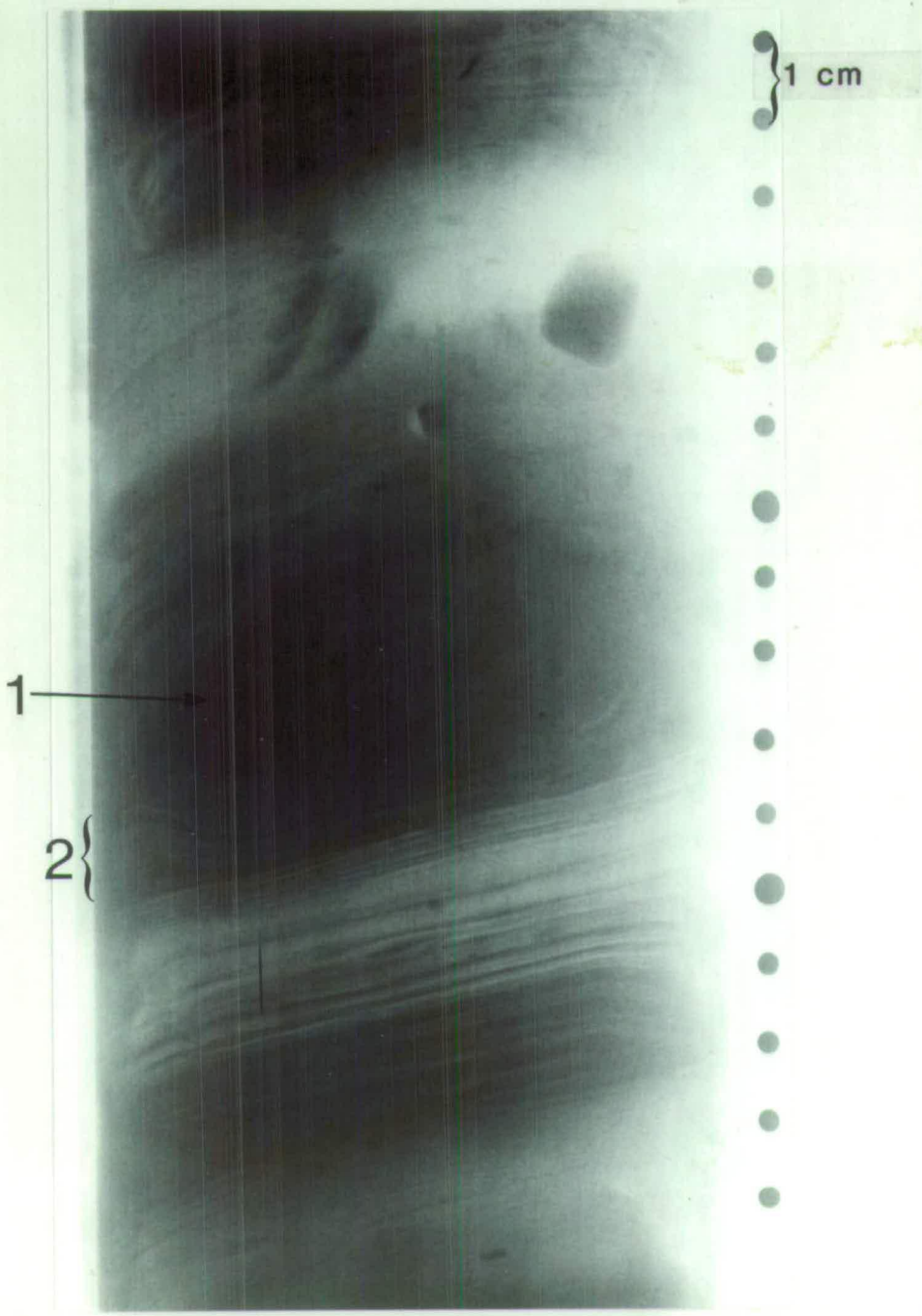
1 cm
1
2

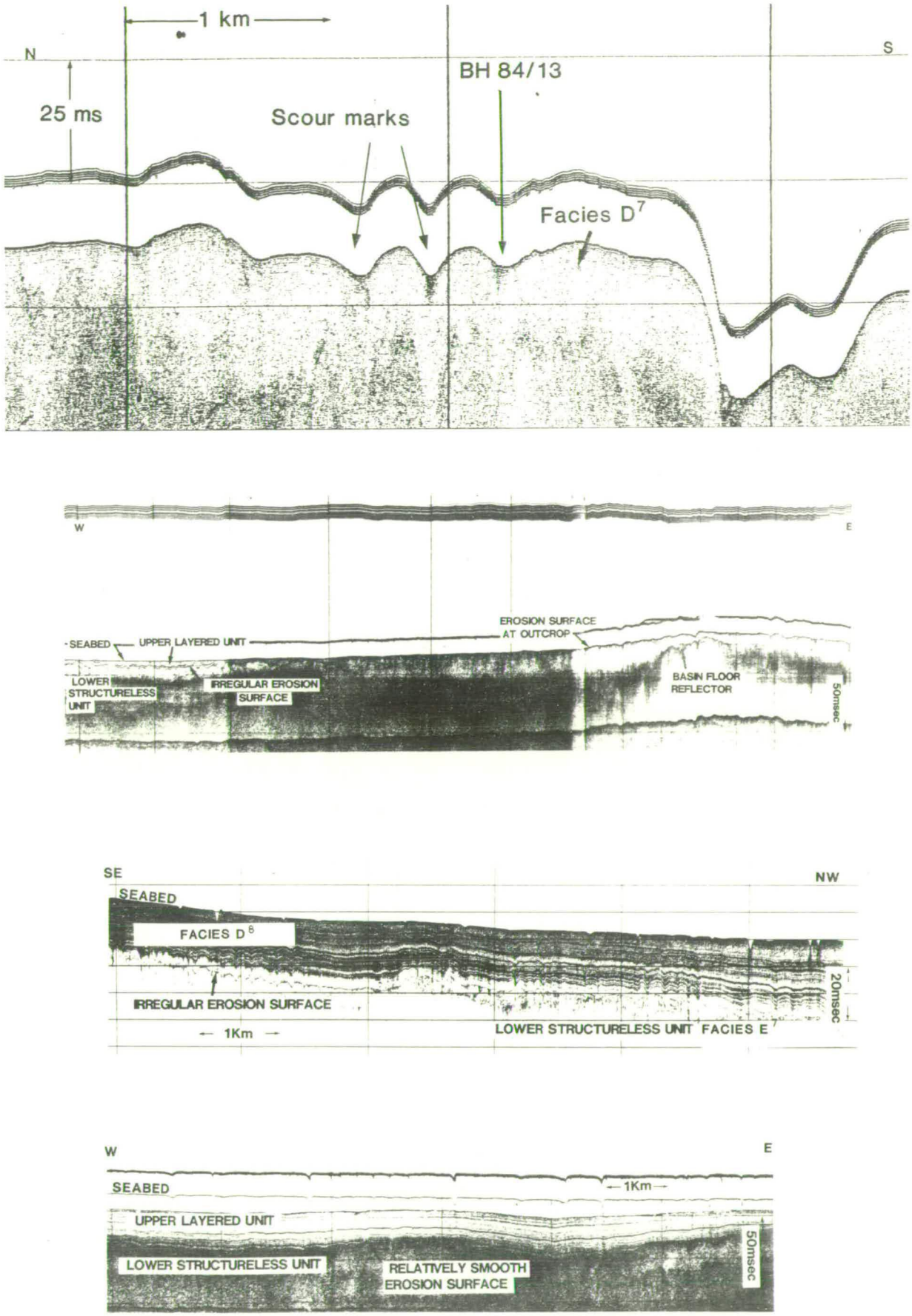

Fig. 4.14. a–d . Sea ice scour marks in the Witch Ground Basin marked by a distinctive irregular erosion surface. Note the absense of scouring in d located in the deepest part of the basin. Figs. b–d are adapted from Stoker and Long (1984).

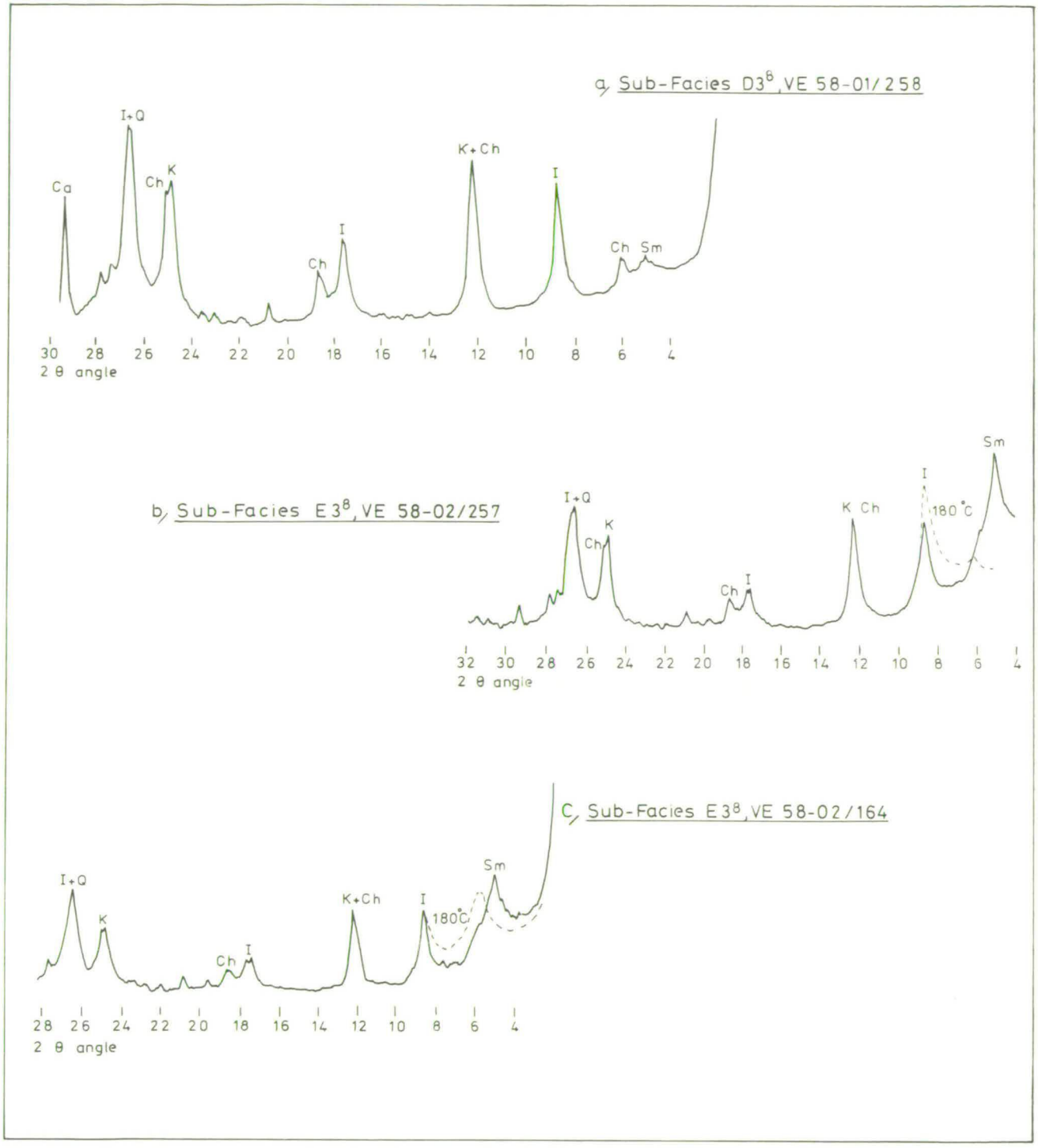

Fig. 4.15. XRD traces showing the clay mineralogy of late Weichselian facies D – E.

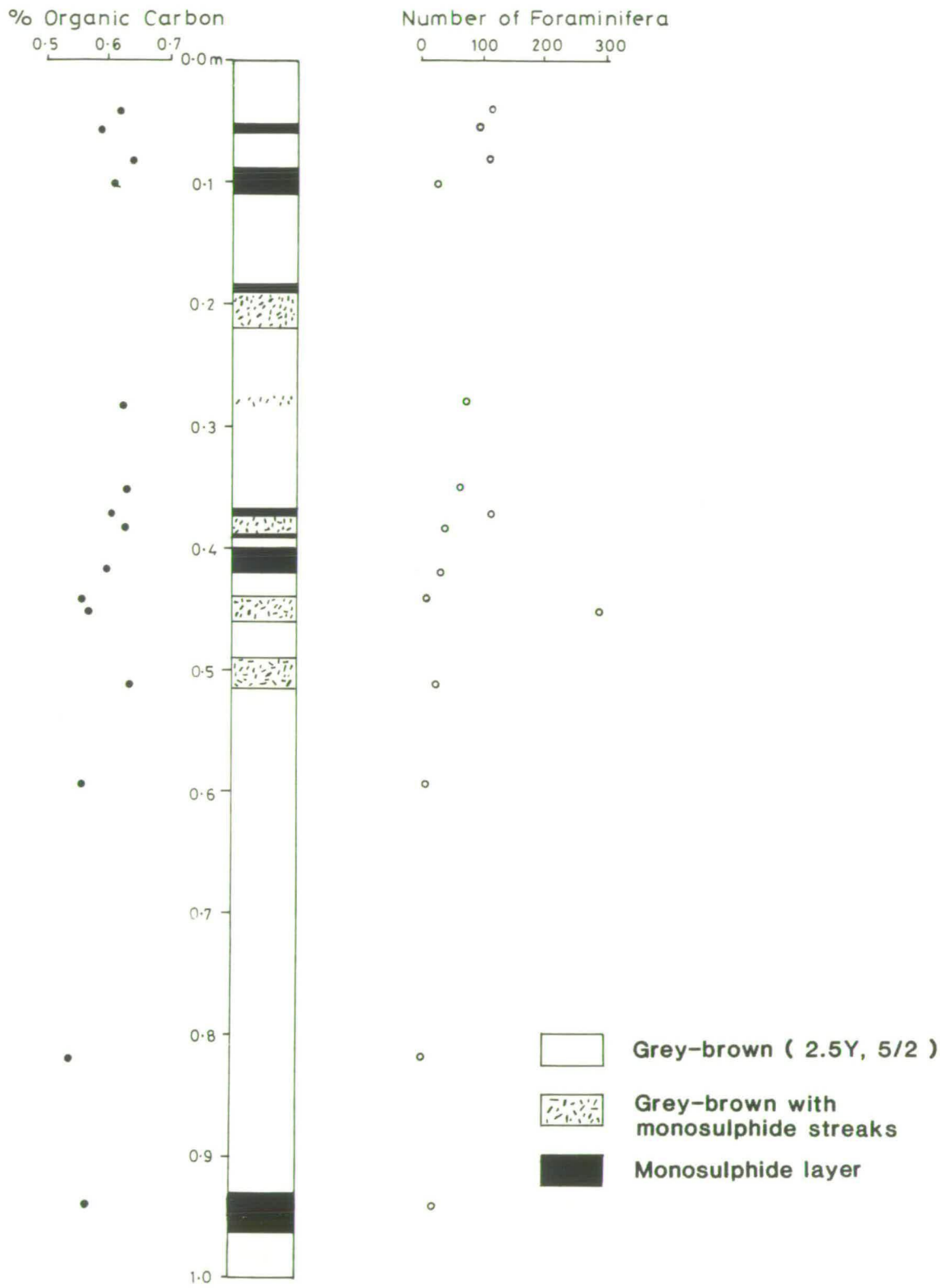

Fig. 4.16. Monosulphide banding and its relationship to the organic carbon content and total number of foraminifera. Taken from BH 84/12, 36.7 - 37.7m.

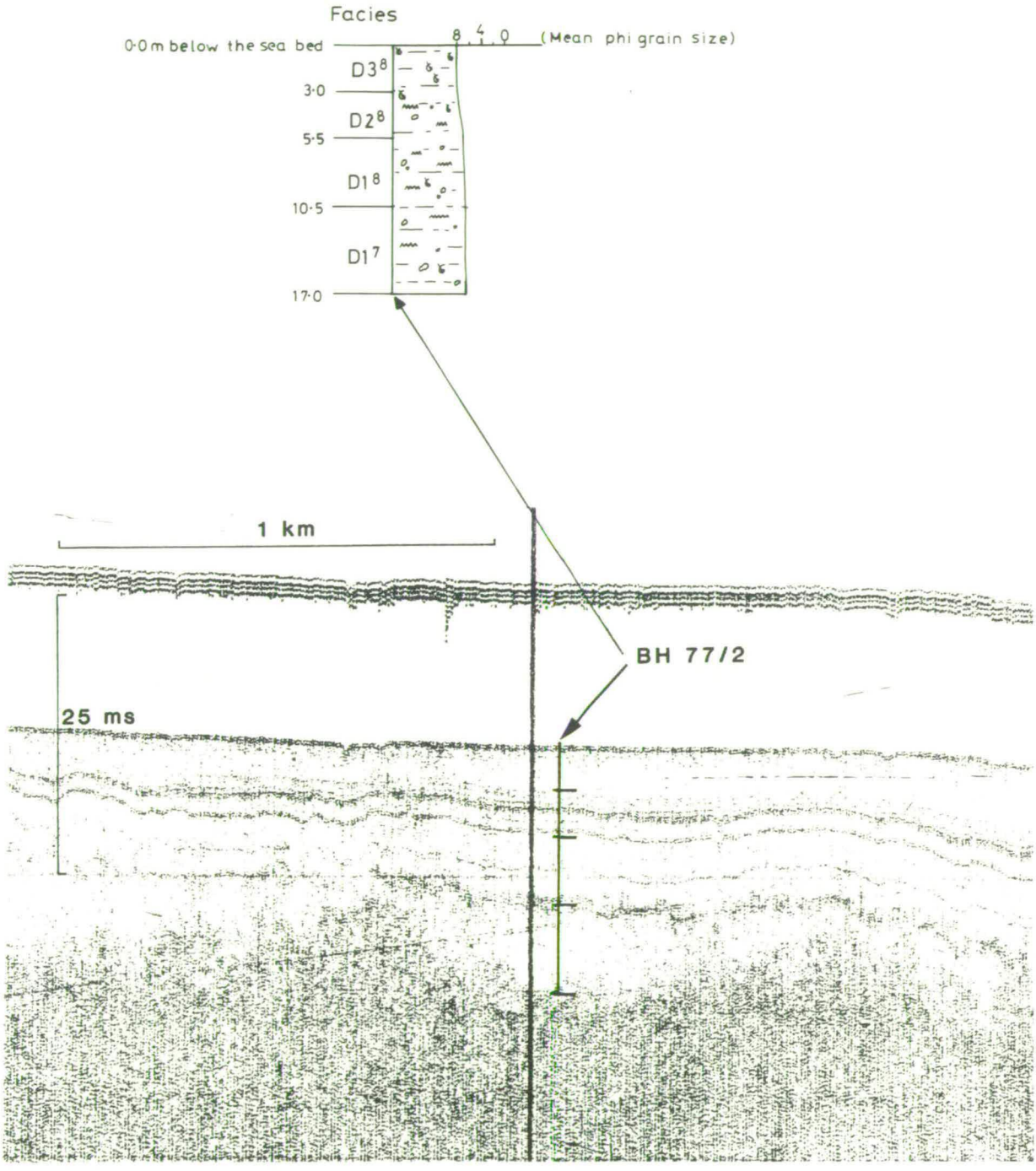

Fig. 4.17. Sub-facies of D^7 and D^8 in BH 77/2, and their relationship to the seismic profile (boomer).

Plate 4.9. Representative x-radiographs of facies E^7, interlaminated and lenticular bedded sands and muds.

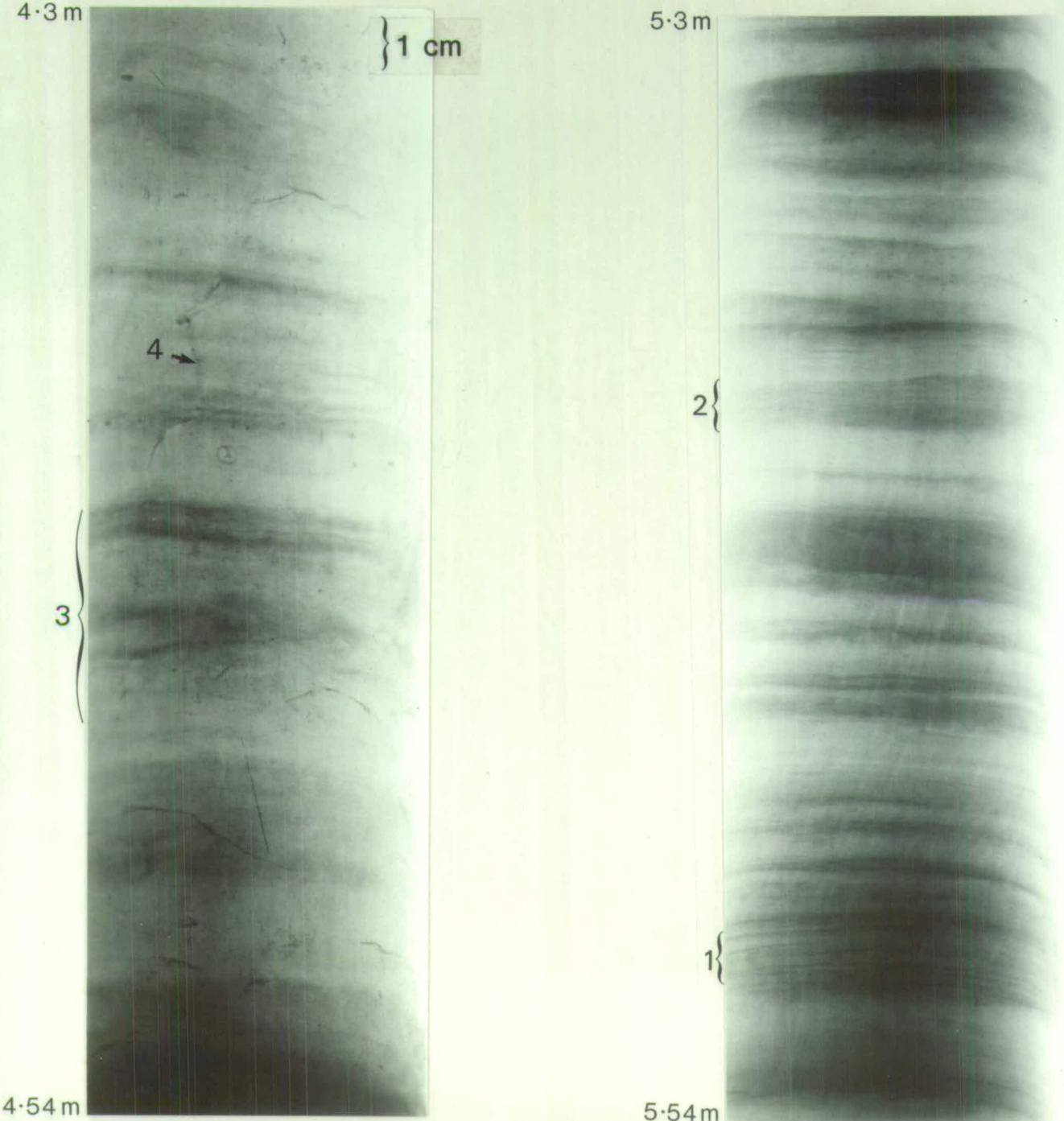
4·3 m
1 cm
4
3
4·54 m
5·3 m
2
1
5·54 m

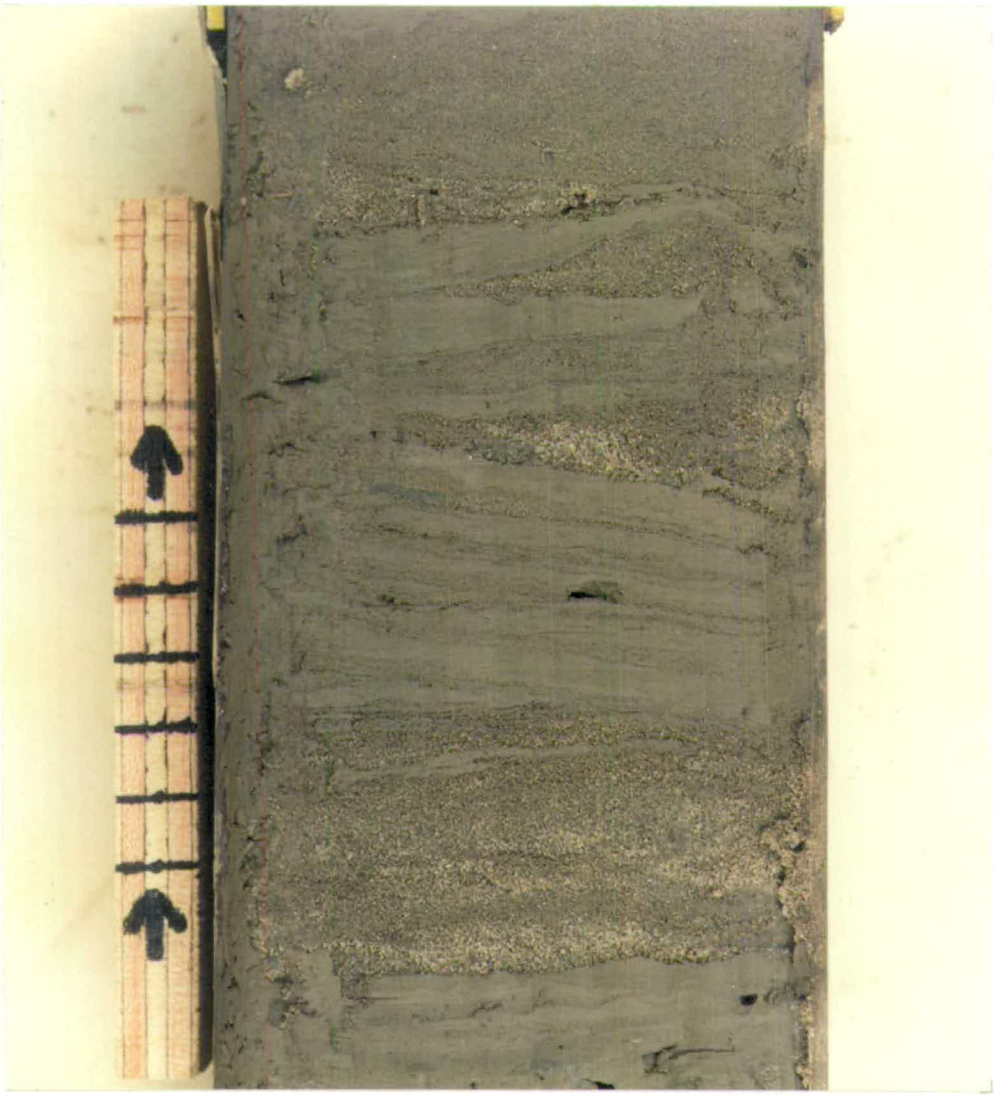

Plate 4.10. Facies E^7, interlaminated and lenticular bedded sands and muds. Note the normal grading of the sand layers. Scale is in centimetres.

Plate 4.11. Facies E^7, mud displaying distinctive blocky texture

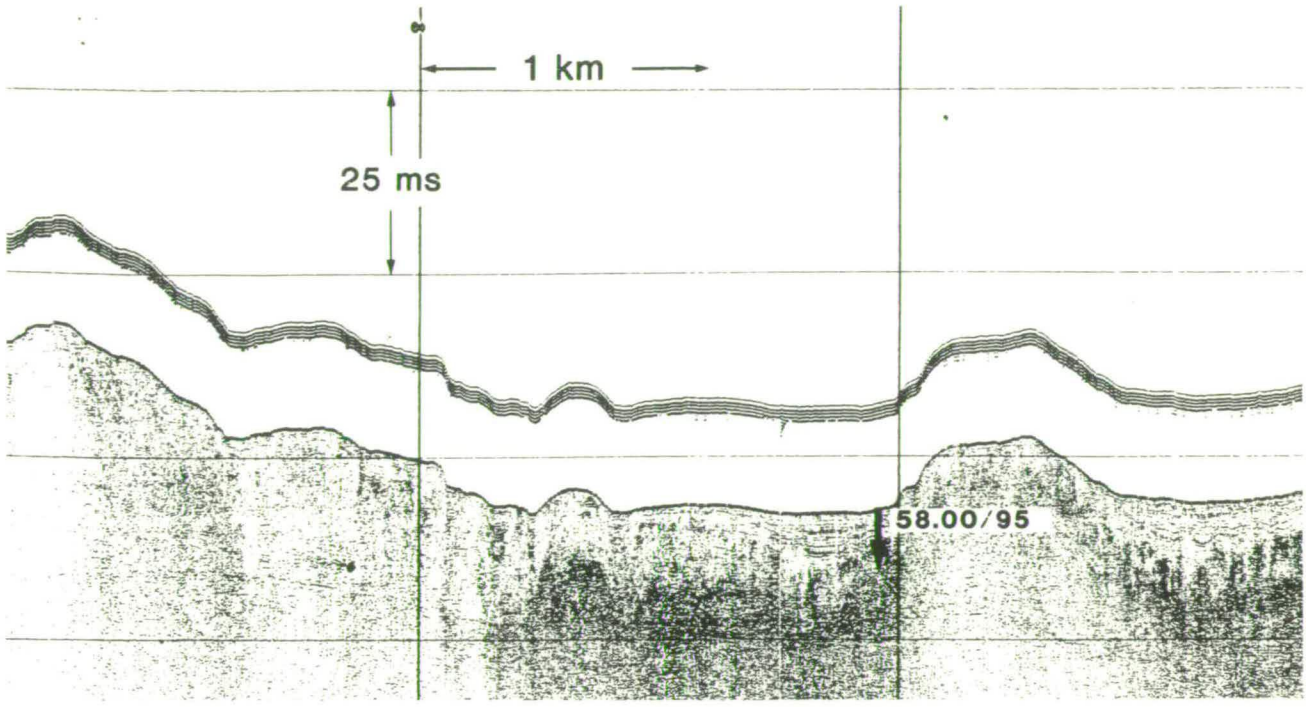

Fig. 4.18.a Boomer profile showing location of VE 58+00/95 which penetrated lower intertidal sediments (facies E^7).

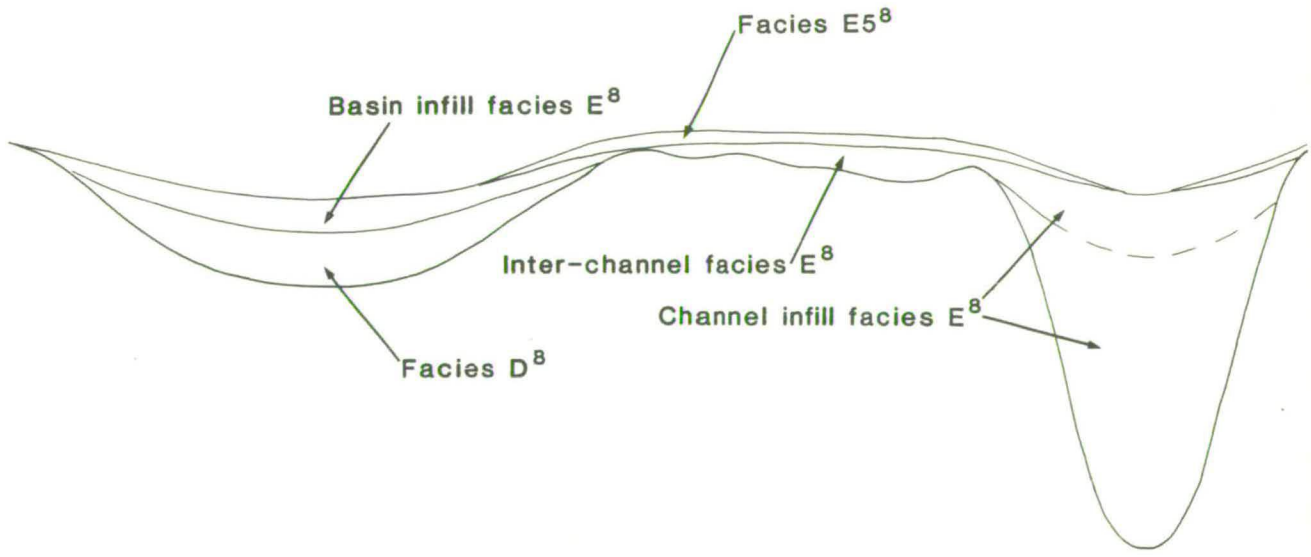

Fig. 4.18.b Schematic diagram showing the relationships between facies D^8 and E^8.

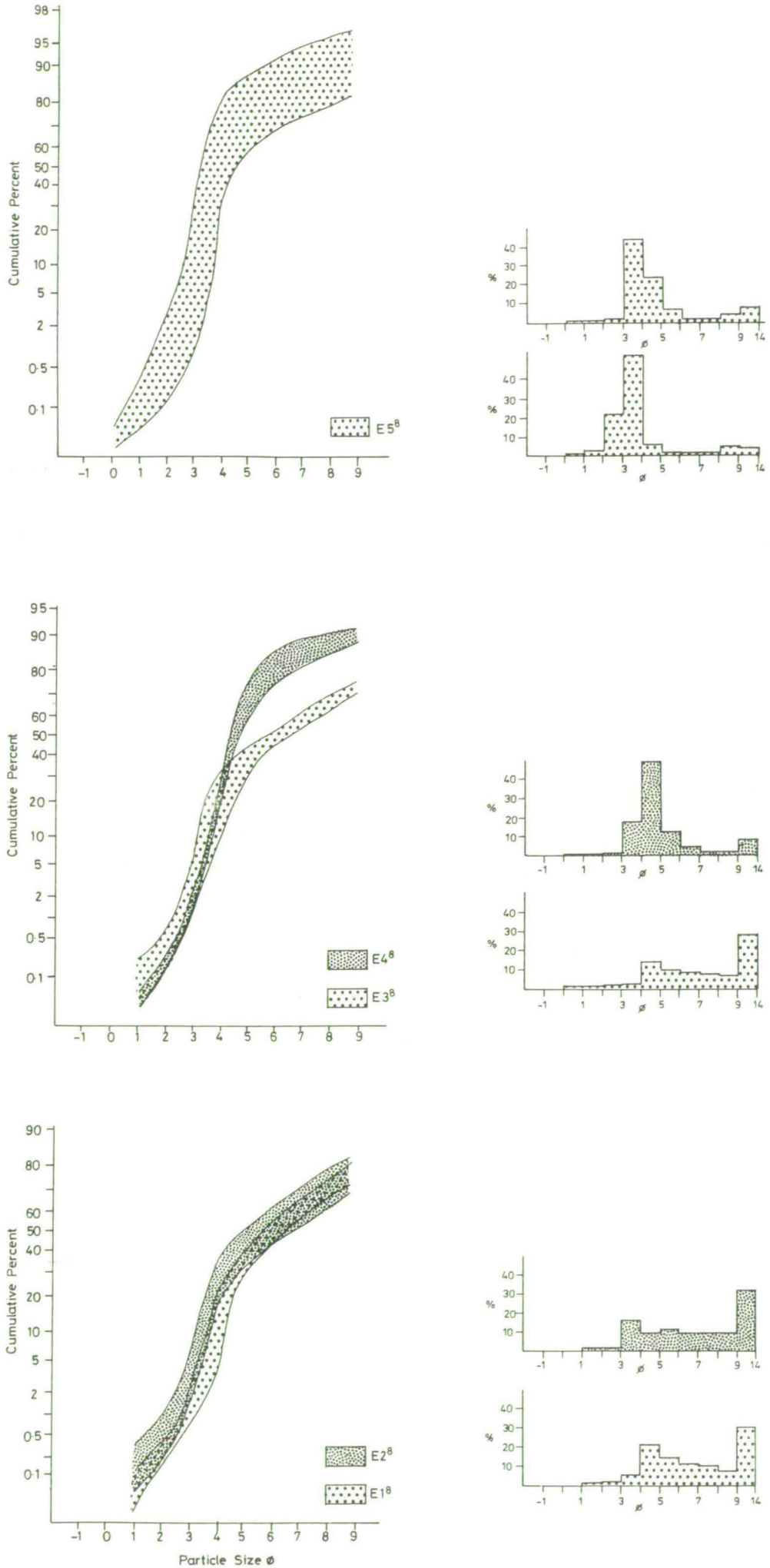

Fig. 4.19. Particle size distributions in sediments from facies E^8.

Plate 4.12. Representative x-radiographs of facies E^8.

(1) Faint stratification.

(M) Myceloid clusters of pyrite threads.

(P) Pyrite tubes.

(C) Chondrites burrows.

(A) Artifact.

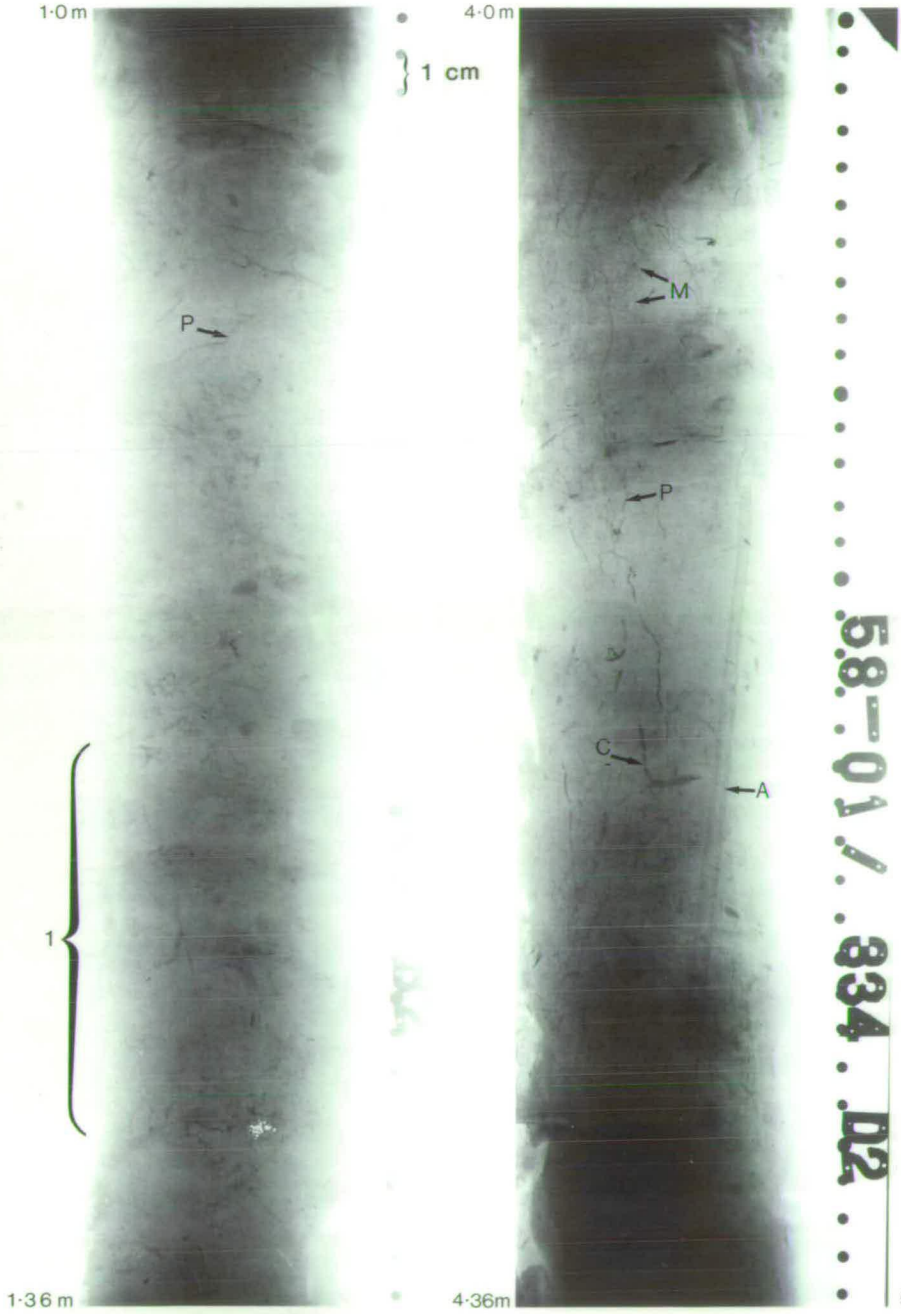
1·0 m
1 cm
P
1
1·36 m
4·0 m
M
P
C
A
4·36m
5·0m
C
C
5·36m

Plate 4.13. Representative x-radiographs of various sedimentary facies.

(7) Burrow.

(6) Diffuse stratification.

(5) Facies E^{8}, faintly laminated mud.

(4) Large clast.

(3) Facies D^{4}, massive mud with rare clasts.

(2) Angular contacts.

(1) Facies B^{4}, complexly stratified diamict.


4·6m
1 cm
5
7
6
4·96m


5·0m
3
4
5·36m


5·4 m
2
1
2
5·76 m

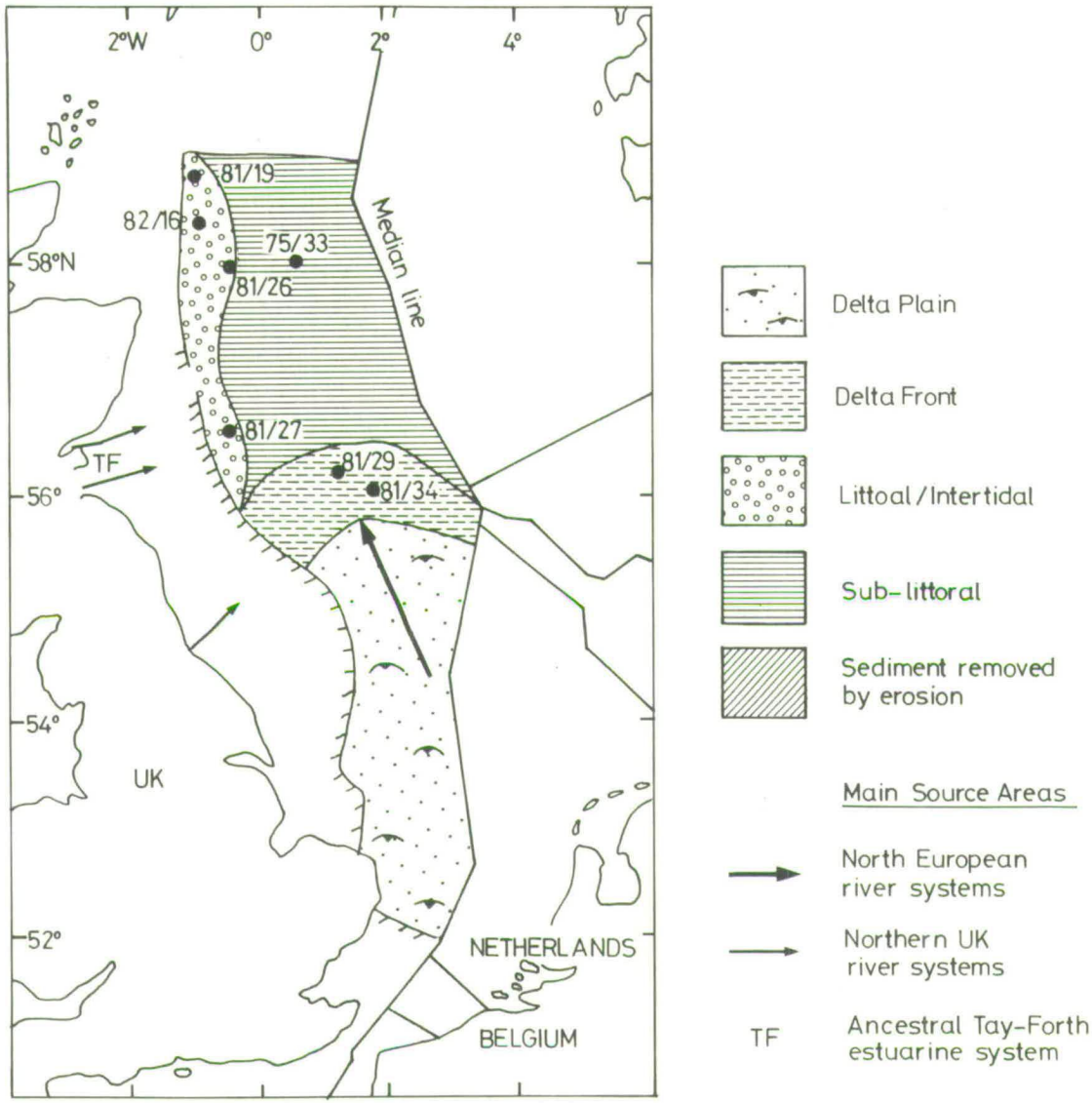

Fig. 5.1. Position of boreholes penetrating Lower Pleistocene marine and deltaic sediments.

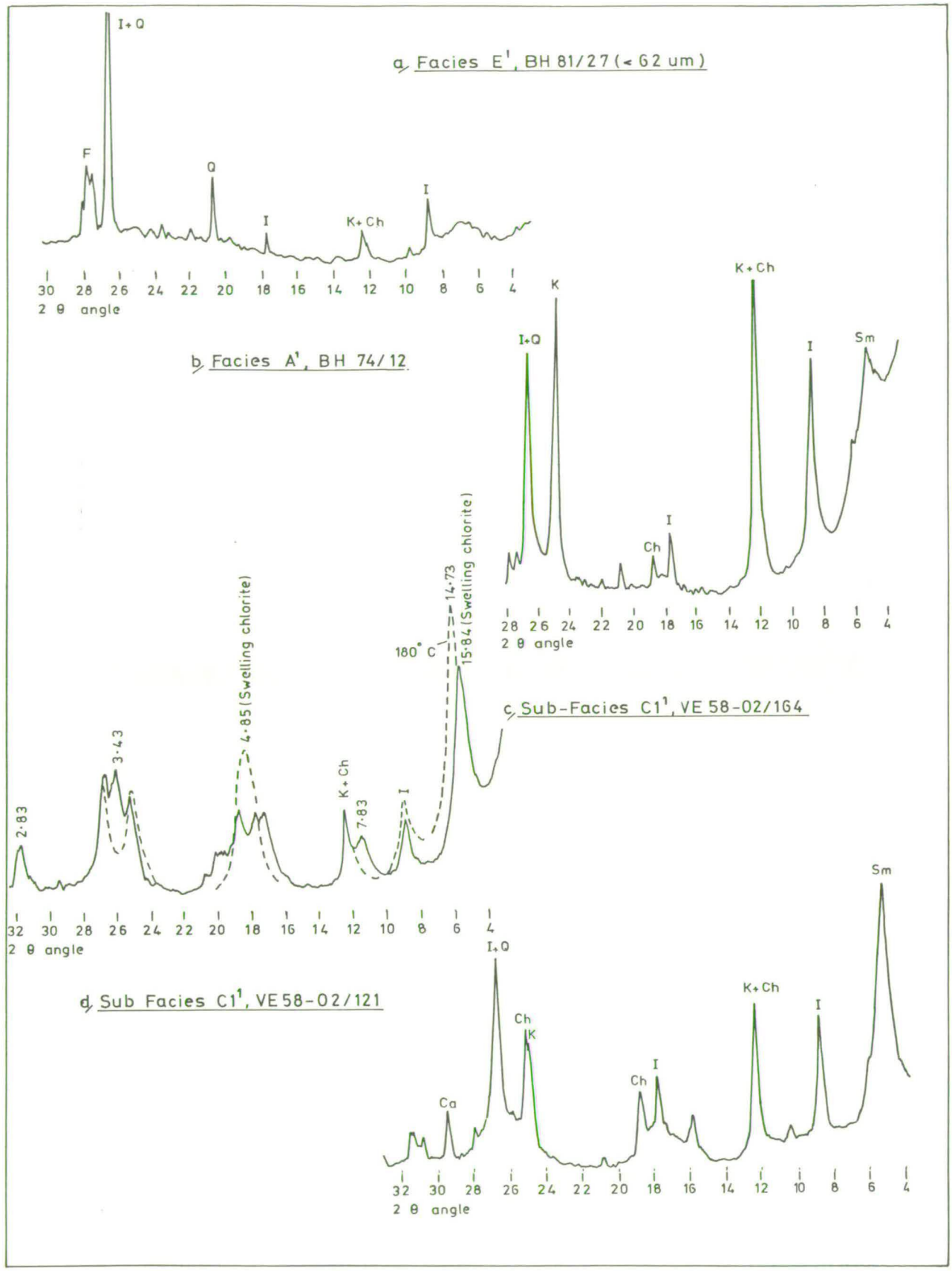

Fig. 5.2. Typical XRD traces showing the clay mineralogy of sediments from facies E , A and C .

Plate 5.1. Facies A^1, massive diamict, overlying facies C^1, laminated sands and muds. Note the deformation of C^1 at the contact. Bar is 1cm.

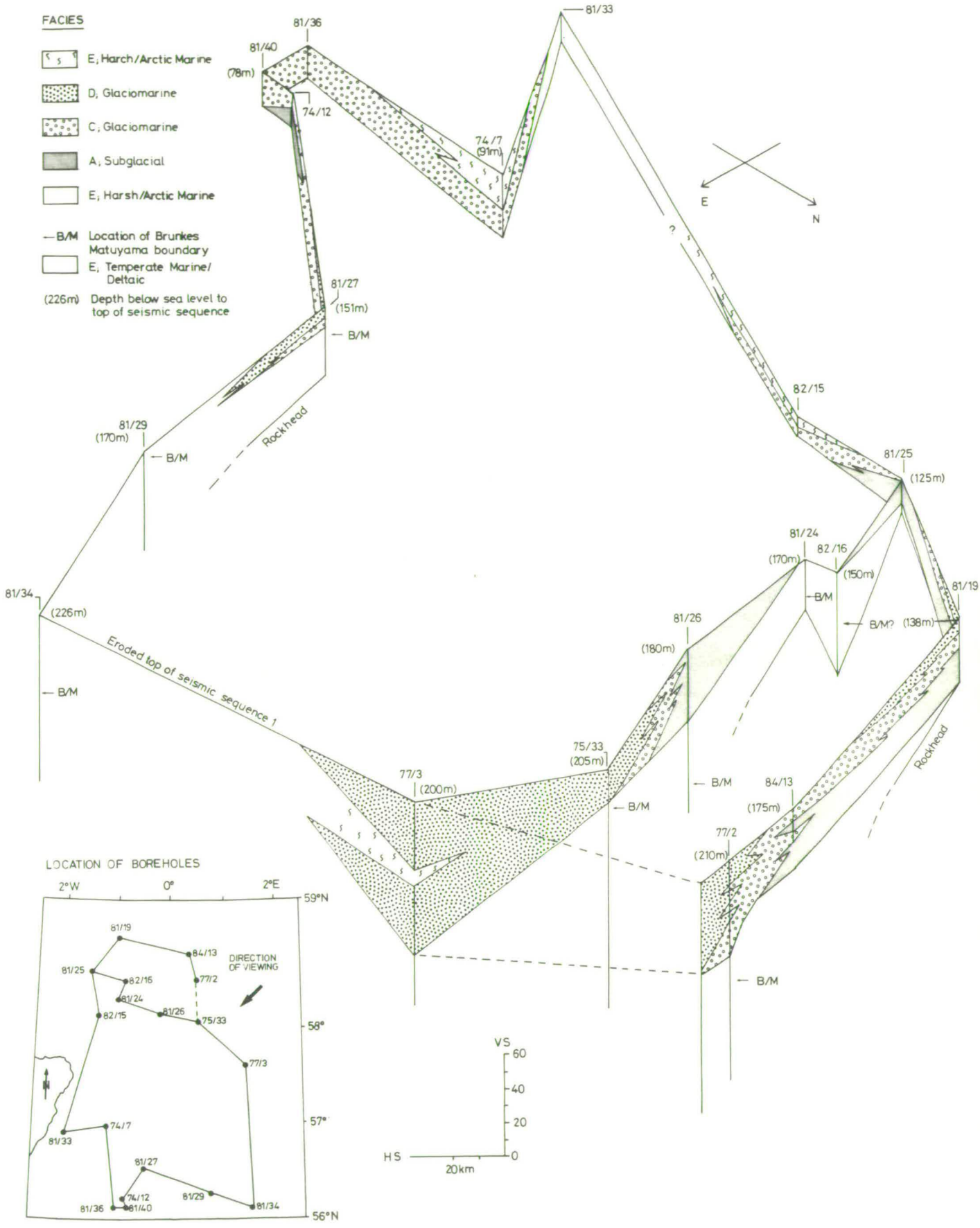

Fig. 5.3. Schematic diagram showing the distribution and relationships of facies A' – E'.

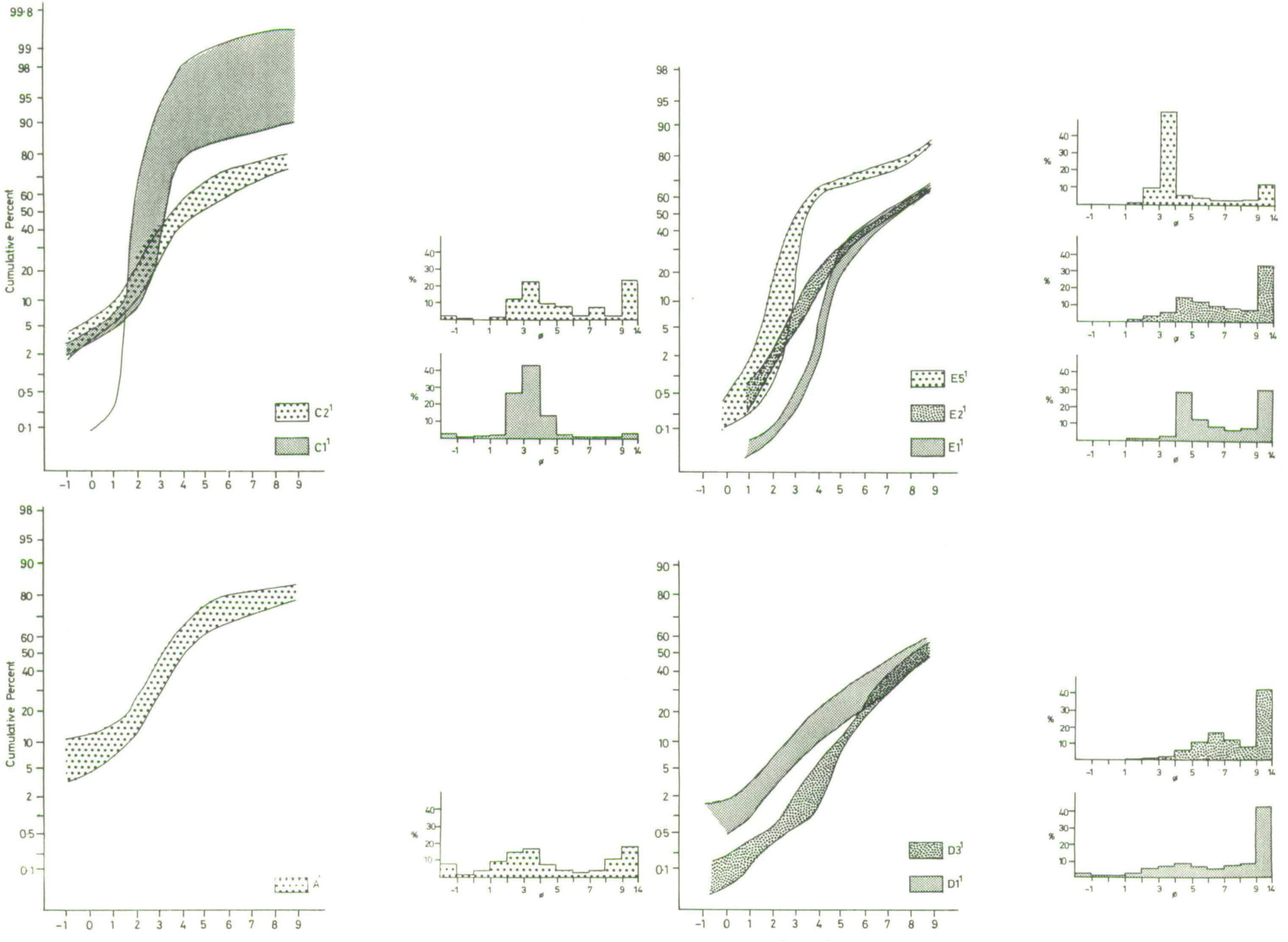

Fig. 5.4. Particle size distributions in sediments from facies A^1– E^1.

Plate 5.2. x-radiograph and core photograph showing the interbedded nature of facies $C1^1$, stratified sands and muds, and facies $C2^1$, stratified diamict.

1 cm

3·7m

4·7m

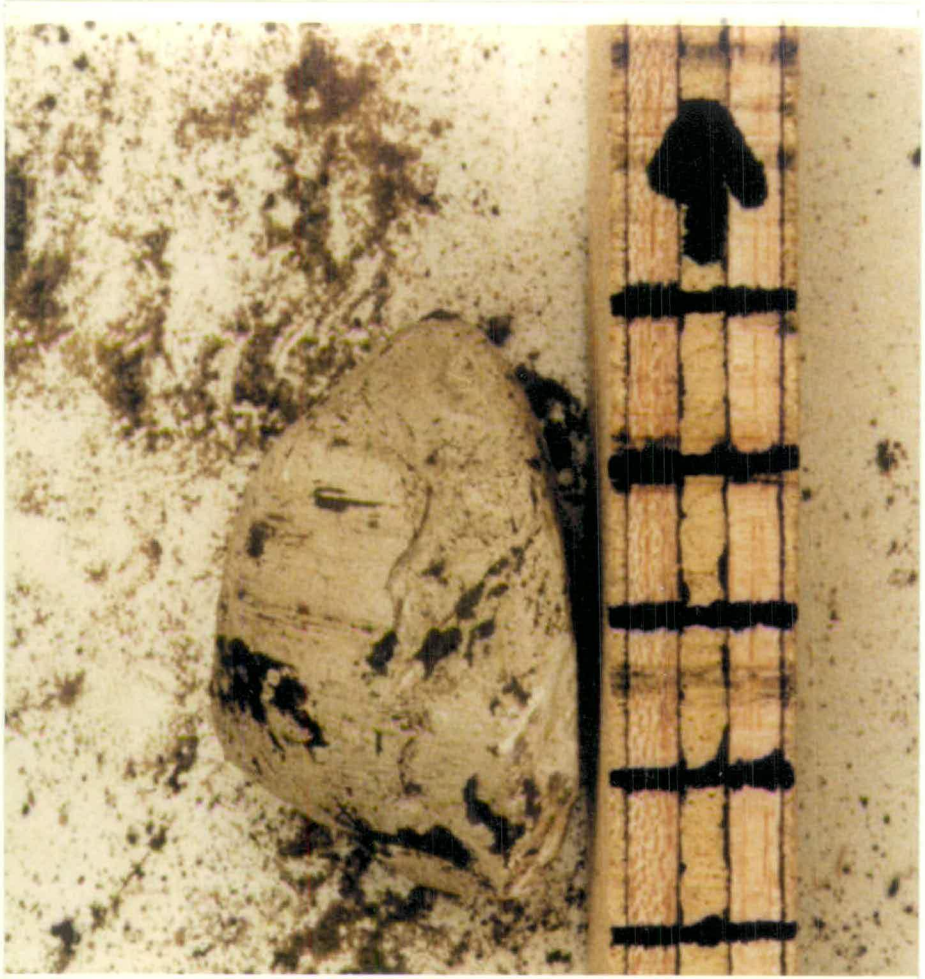

Plate 5.3. Striated chalk clast from facies C^1 . Scale is in centimetres.

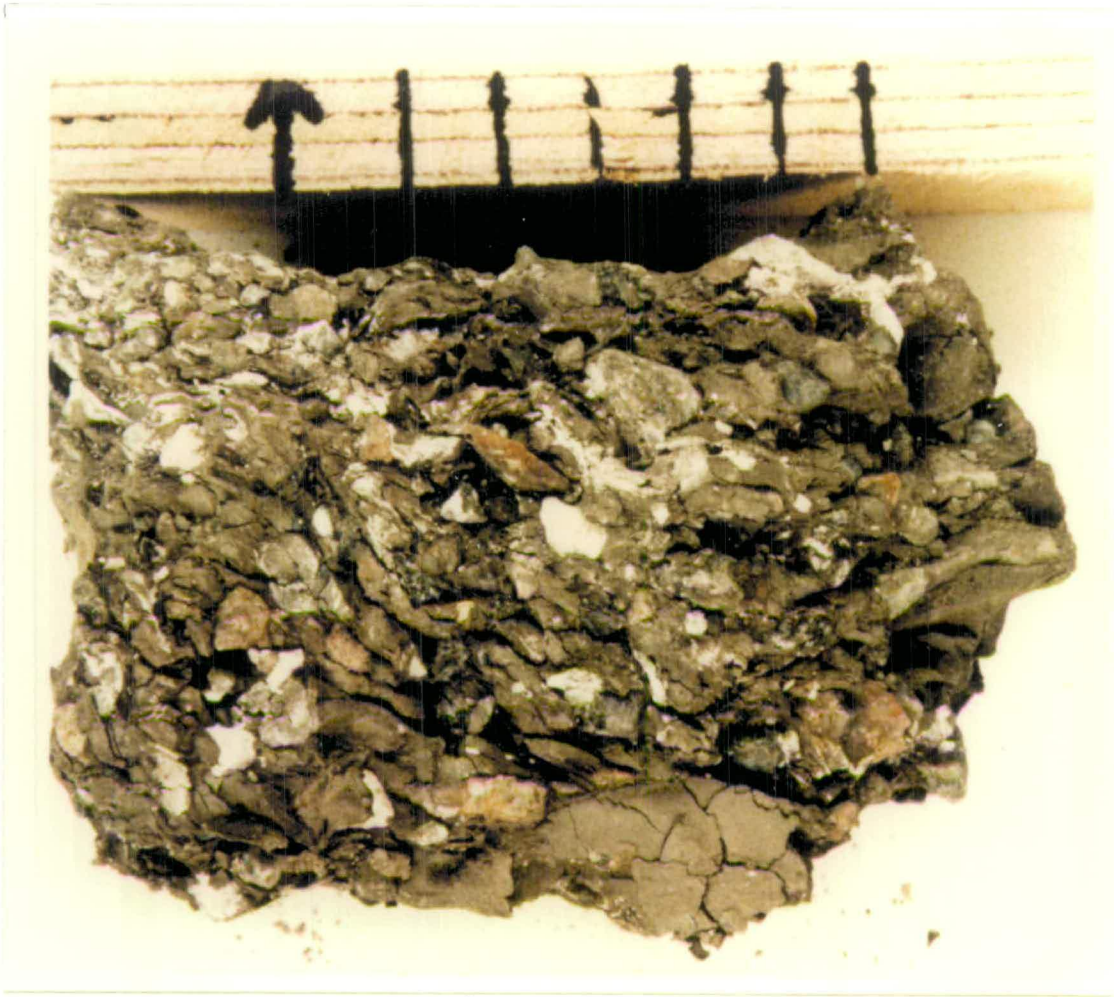

Plate 5.4. Facies $C2^1$, stratified diamict showing distinctive horizontal clast fabric. Scale is in centimetres.

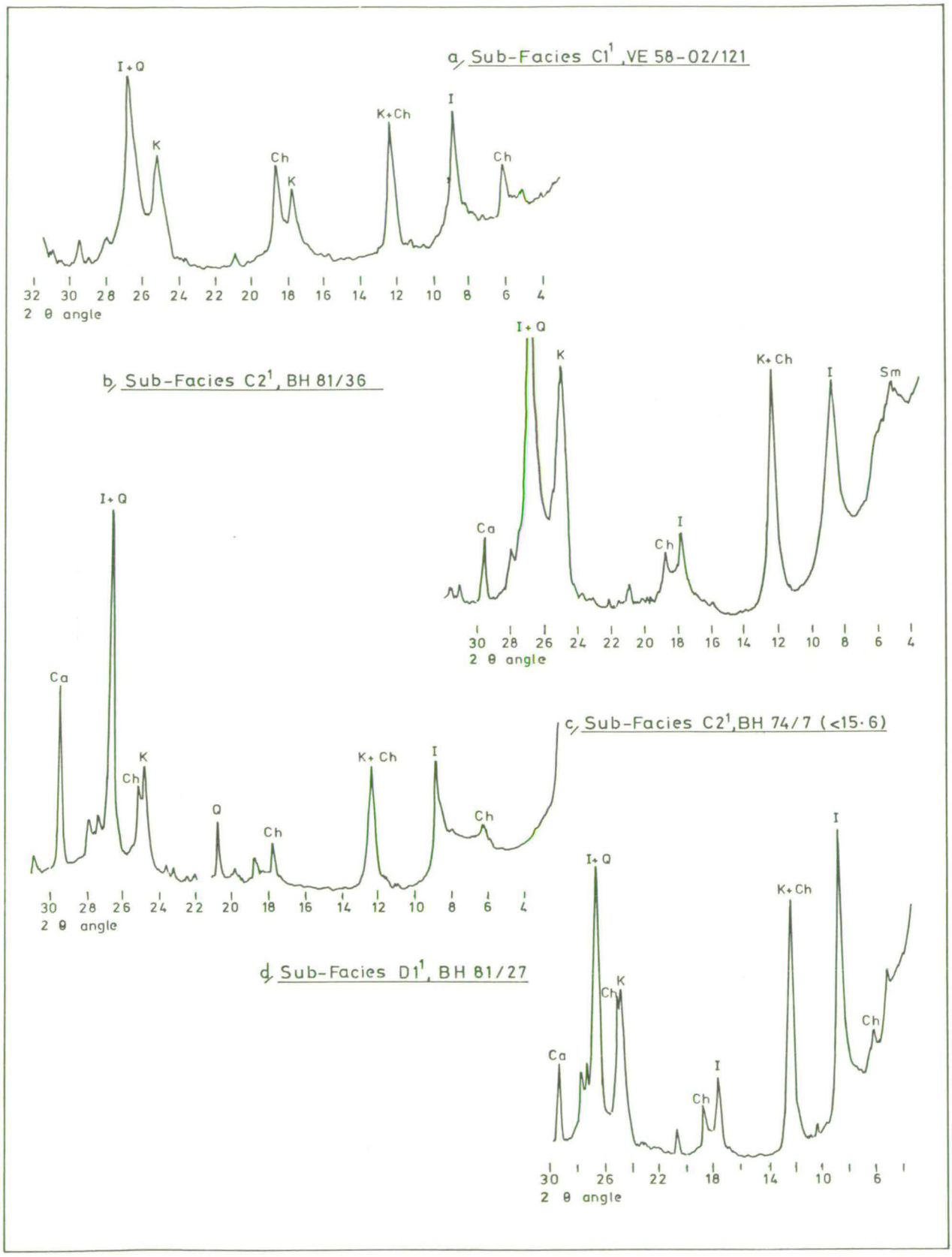

Fig. 5.5. Typical XRD traces showing the clay mineralogy of sediments from facies C^1 an D^1.

Plate 5.5. Representative x-radiograph of facies A^3, massive diamict.

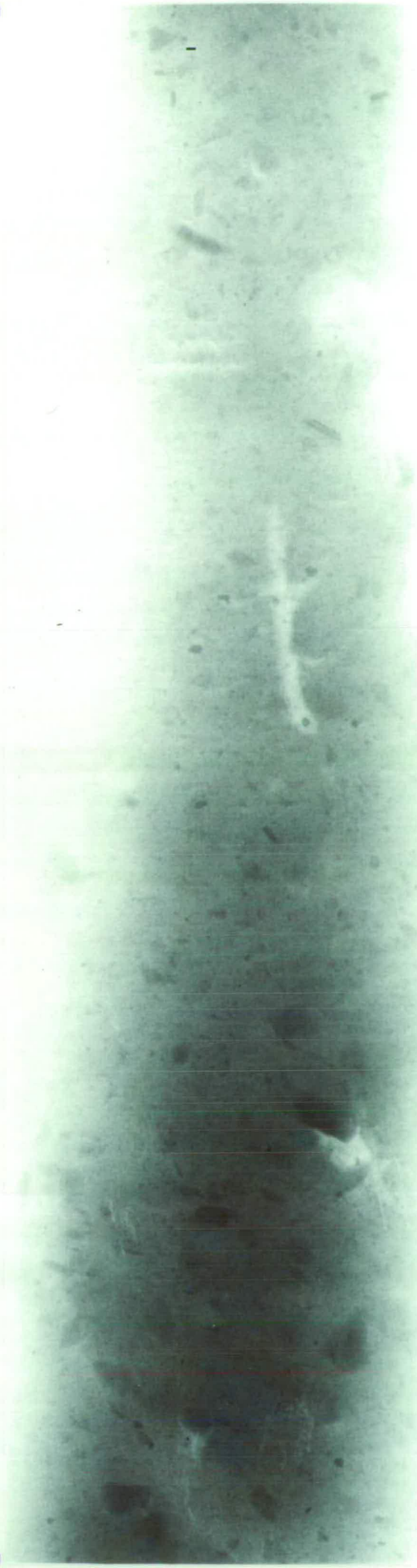
0·3m
0·5 7m

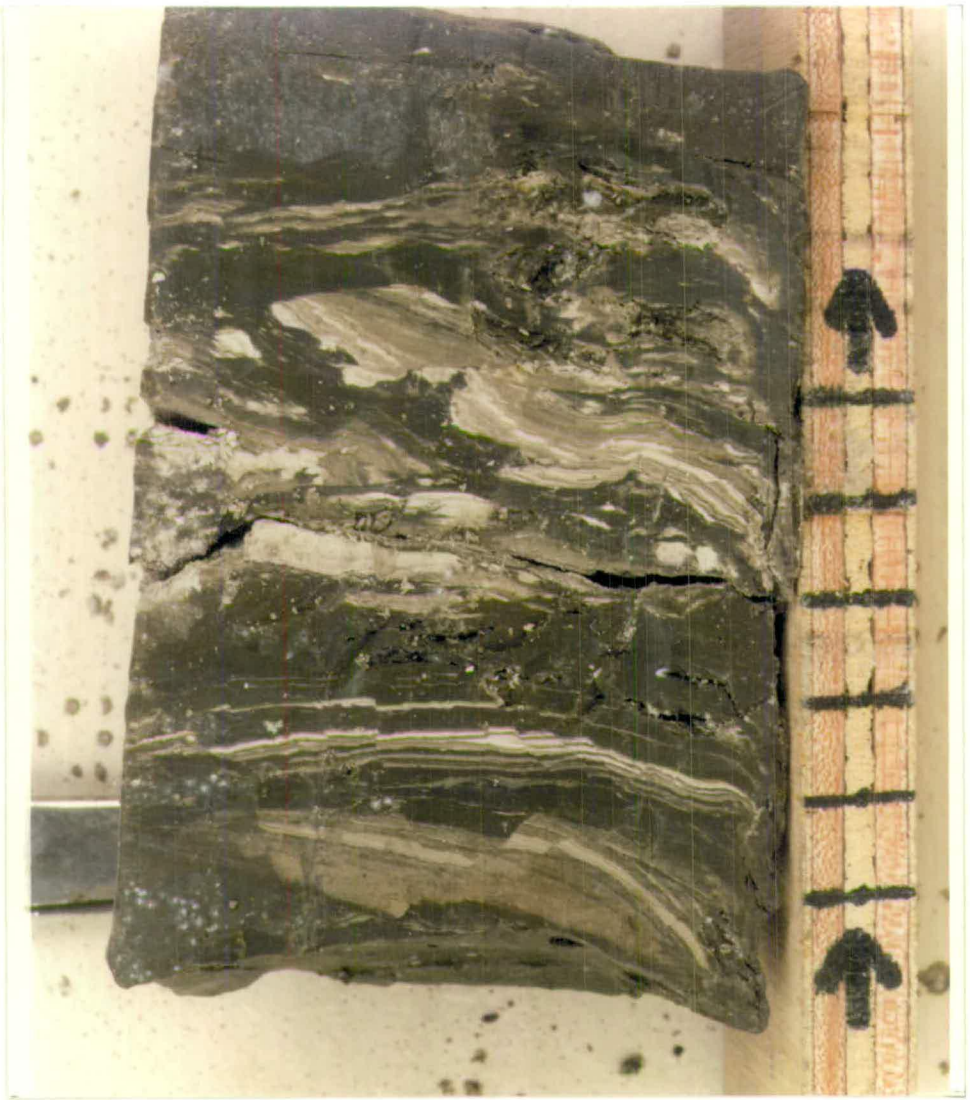

Plate 5.6. Deformation structures in facies B^3.
Scale is in centimetres.

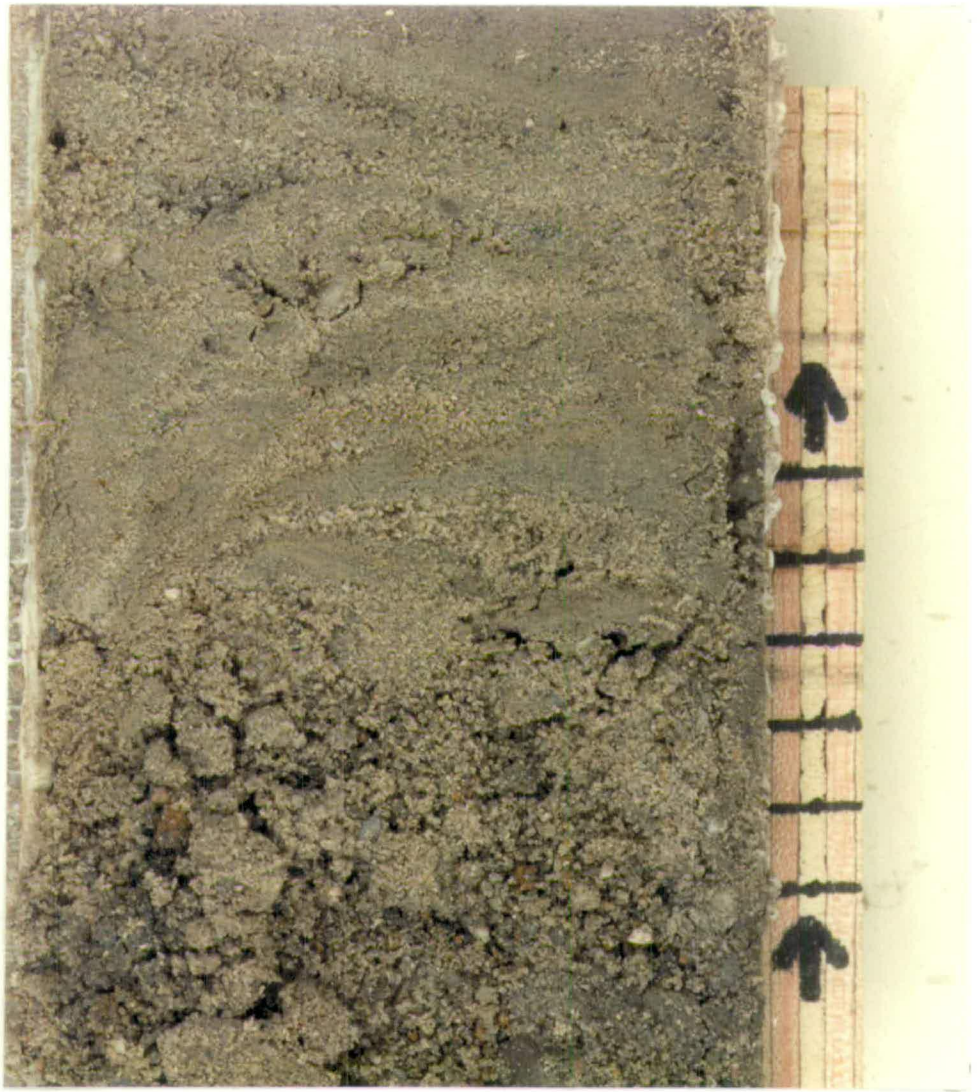

Plate 5.7. Facies $C1^3$, bedded sand and gravel.

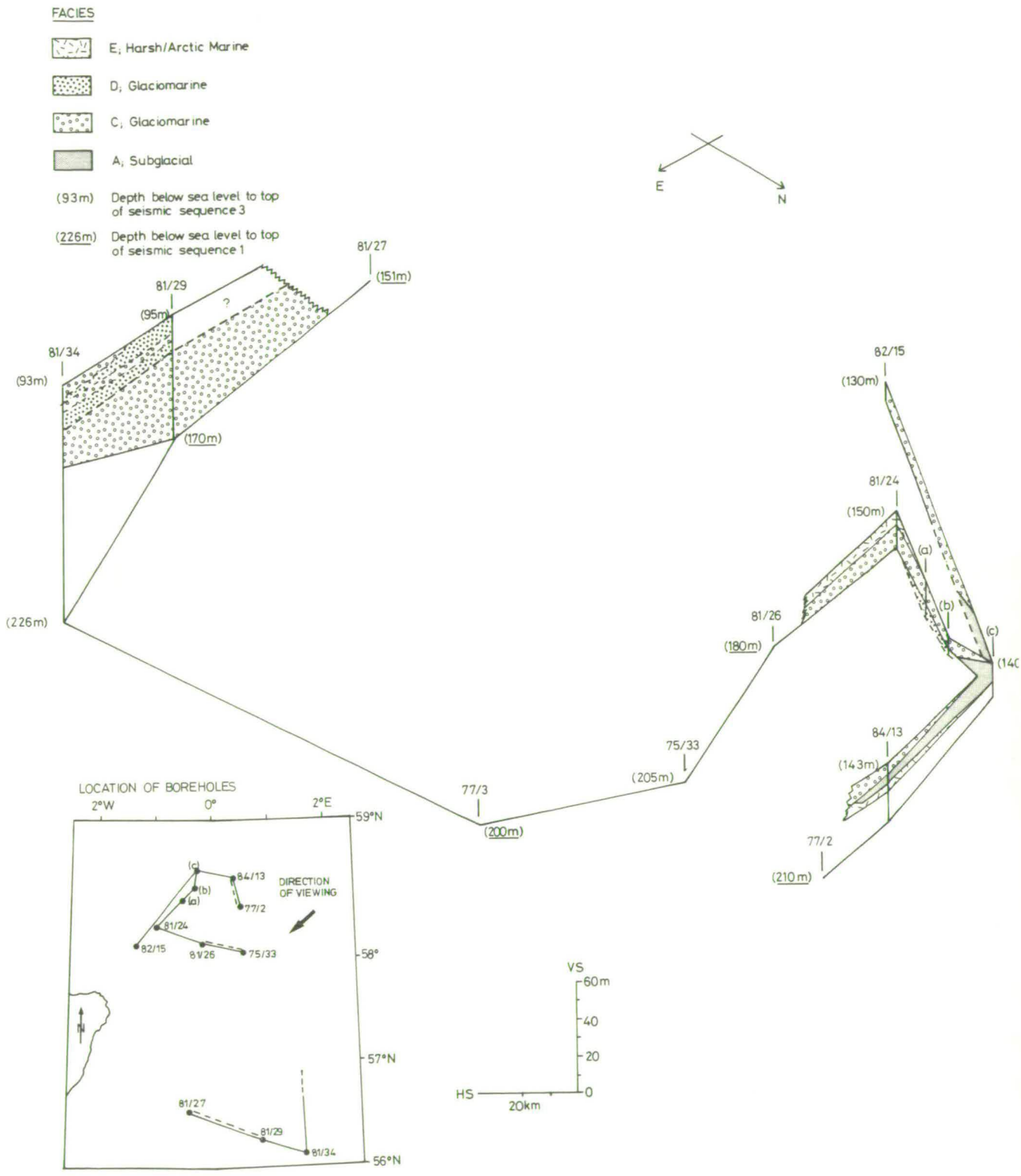

Fig. 5.6. Schematic fence diagram showing the distribution and relationships of facies A^3 – E^3. The top of seismic sequence 1 is marked for reference.

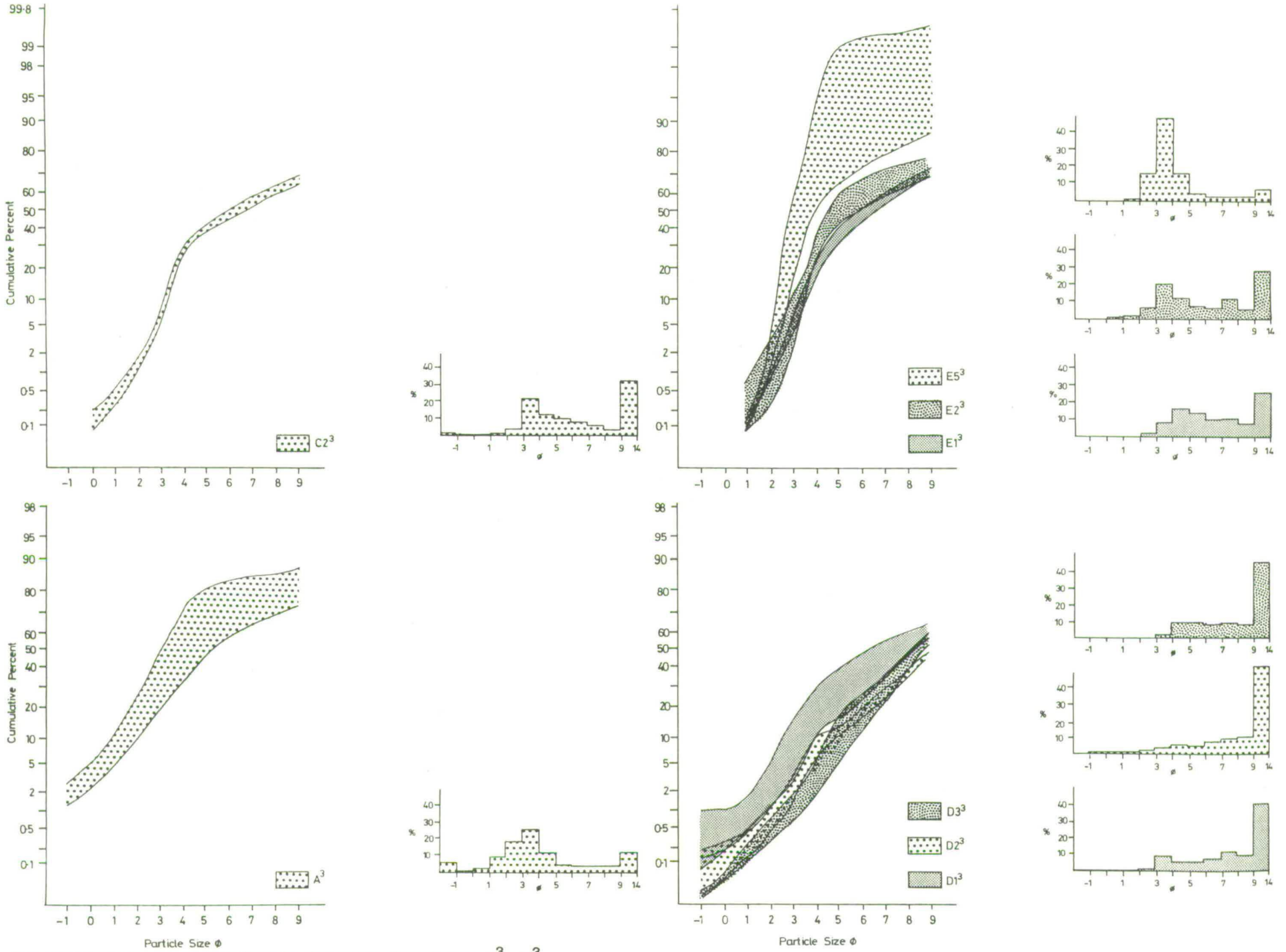

Fig. 5.7. Particle size distributions in sediments from facies A^3– E^3.

Plate 5.8a. X-radiograph showing the upward transition from facies $C2^3$, stratified diamict (1), to facies $C1^3$, planar bedded sand and gravel (3). (2) depicts a clast layer.

Plate 5.8b. Representative x-radiograph of facies $C1^3$. Note the upward coarsening nature of the bedded sand and gravel (1). (2) shows planar and ripple laminated sands.

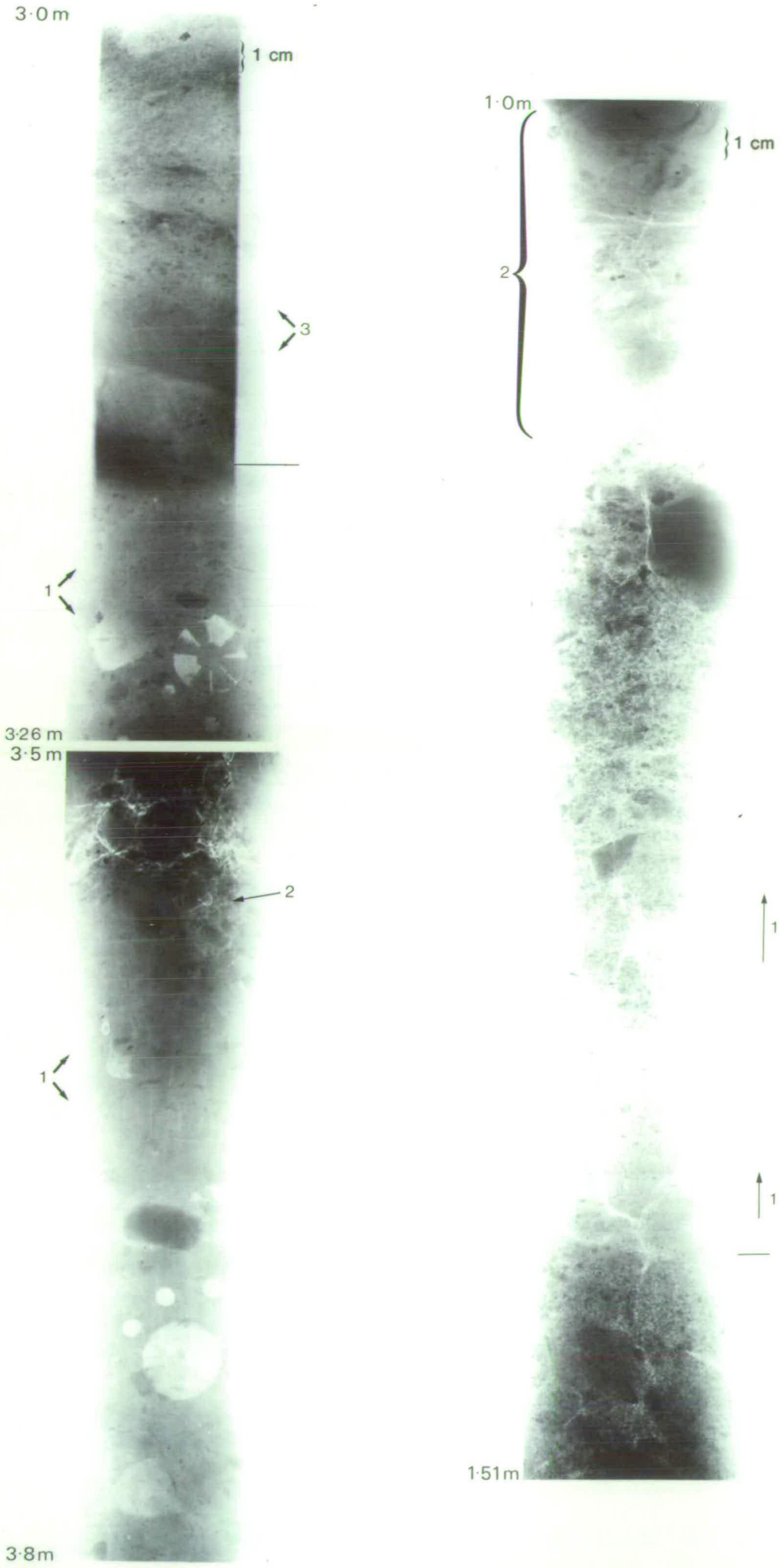
3·0 m
1 cm
3
1
3·26 m
3·5 m
2
1
3·8 m
1·0 m
1 cm
2
1
1
1·51 m

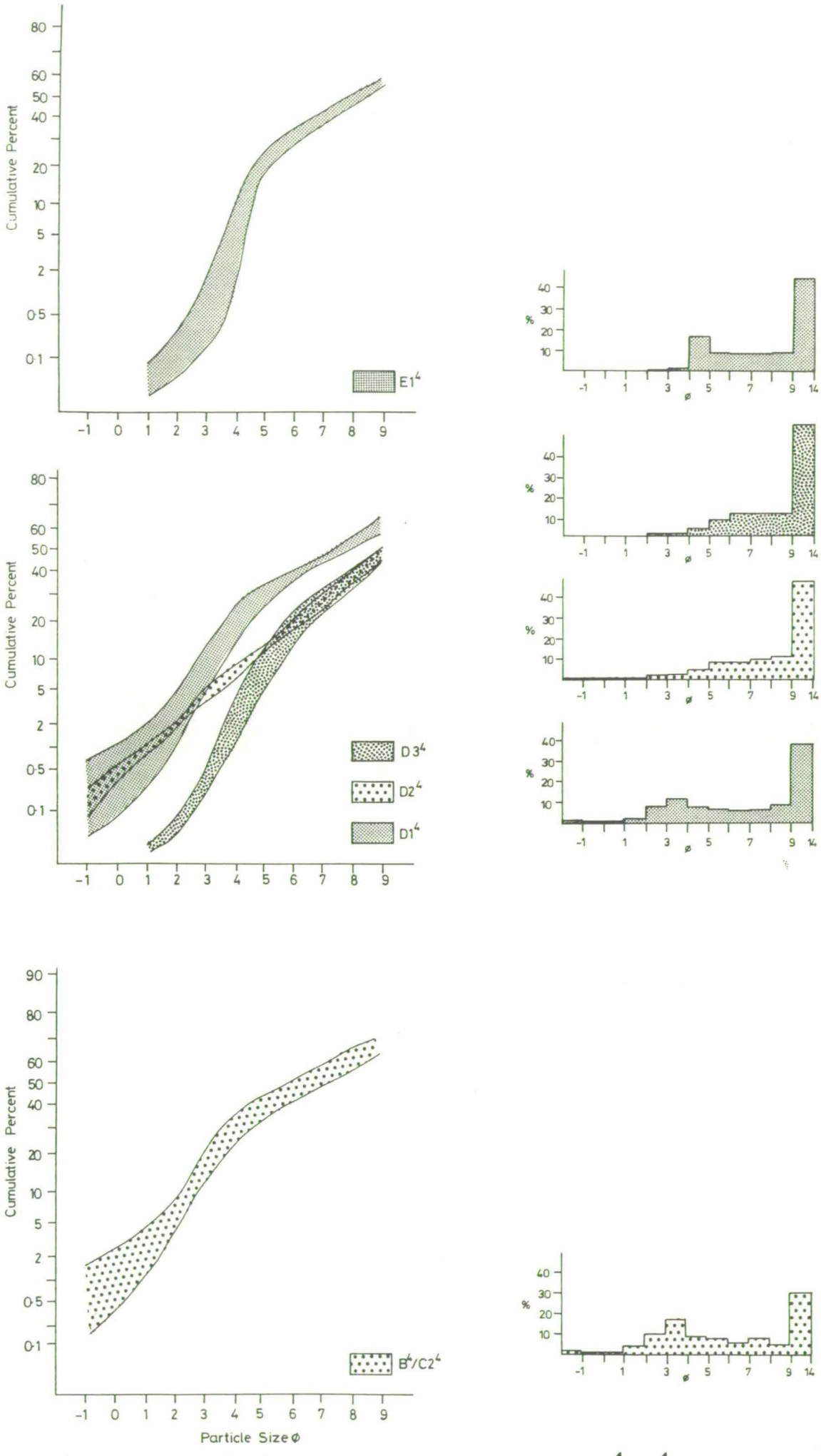

Fig. 5.8. Particle size distributions in sediments from facies B^4– E^4.

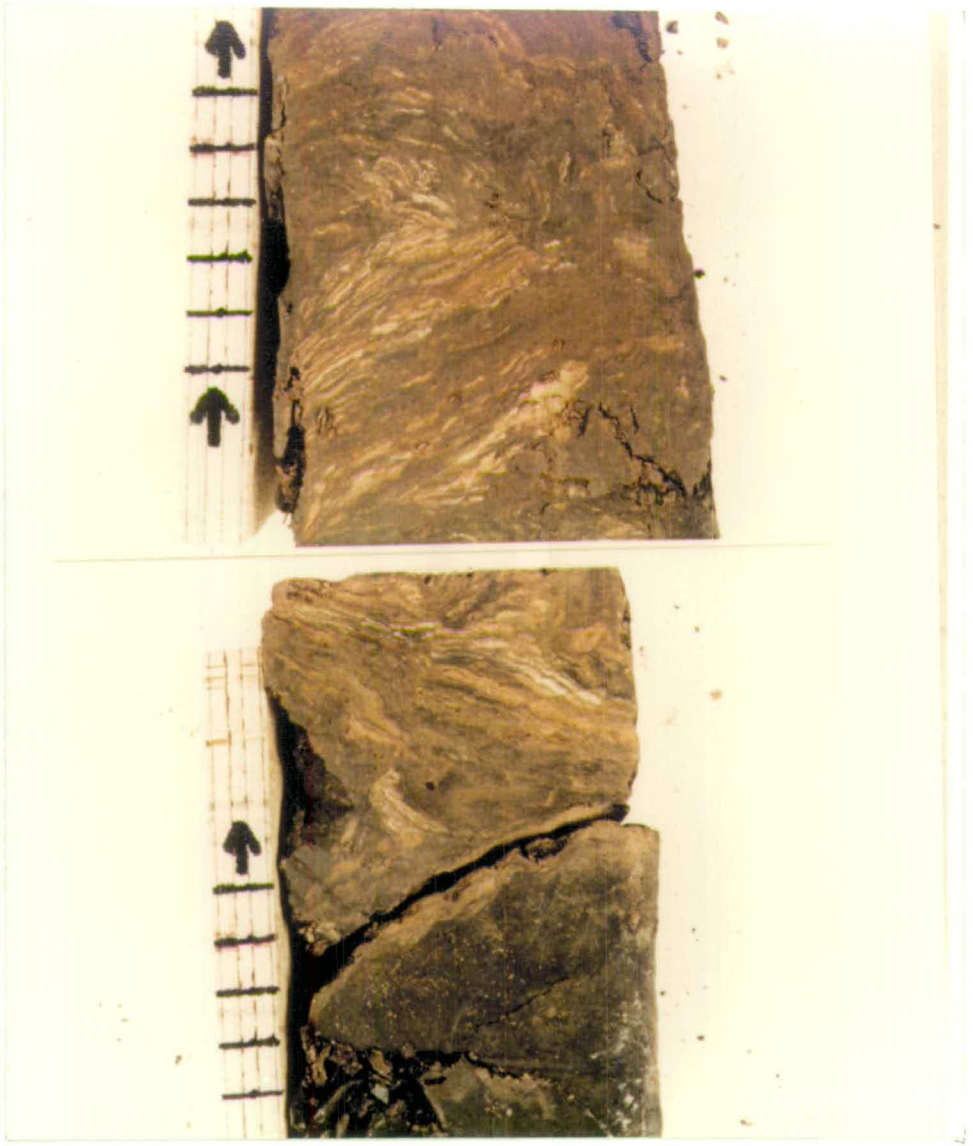

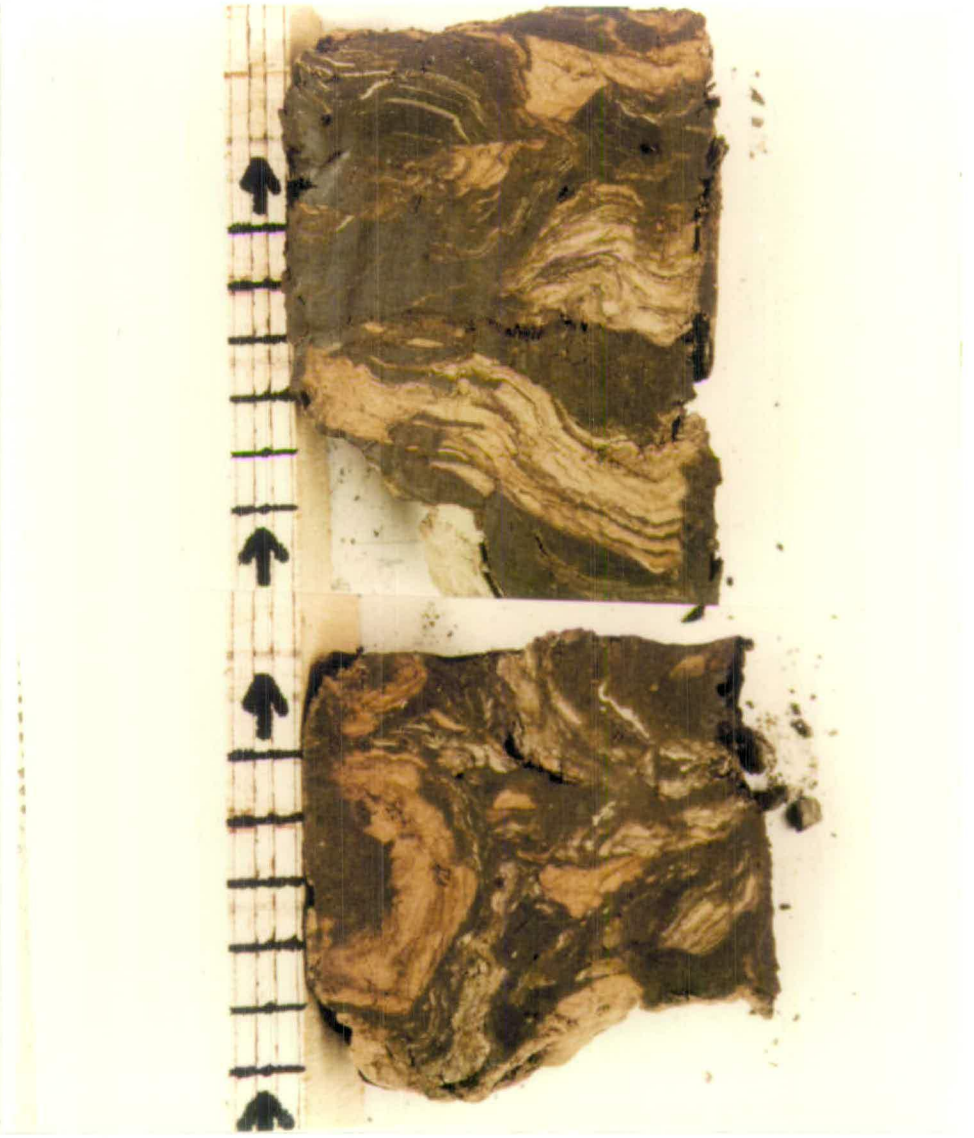

Plates 5.9. and 5.10. Facies B^4, stratified diamict showing distinctive deformation structures. Note the sharp angular basal contact in 5.9. Scale is in centimetres.

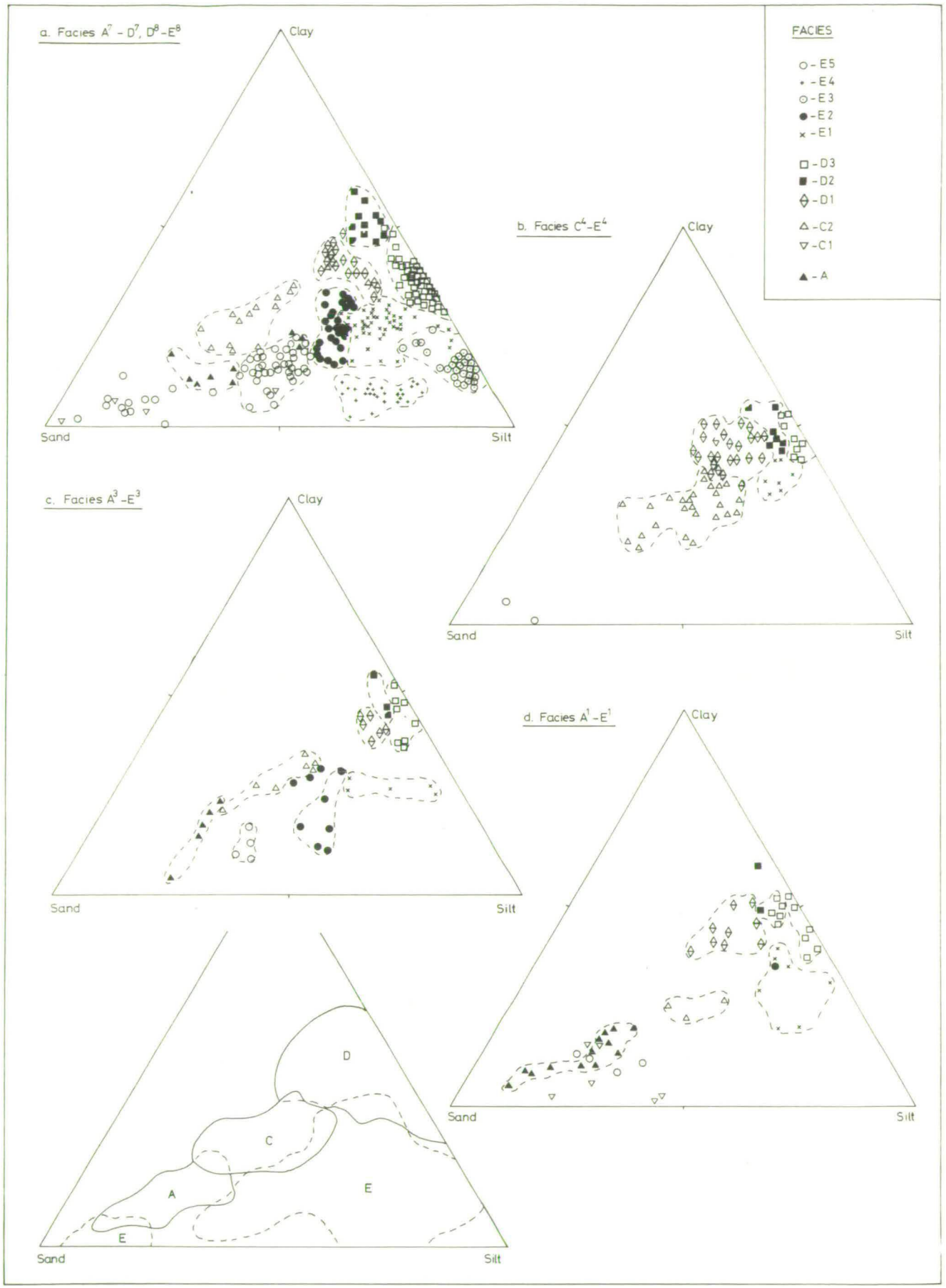

Fig. 5.9. Triangle plots showing the textural variations of the main sedimentary facies.

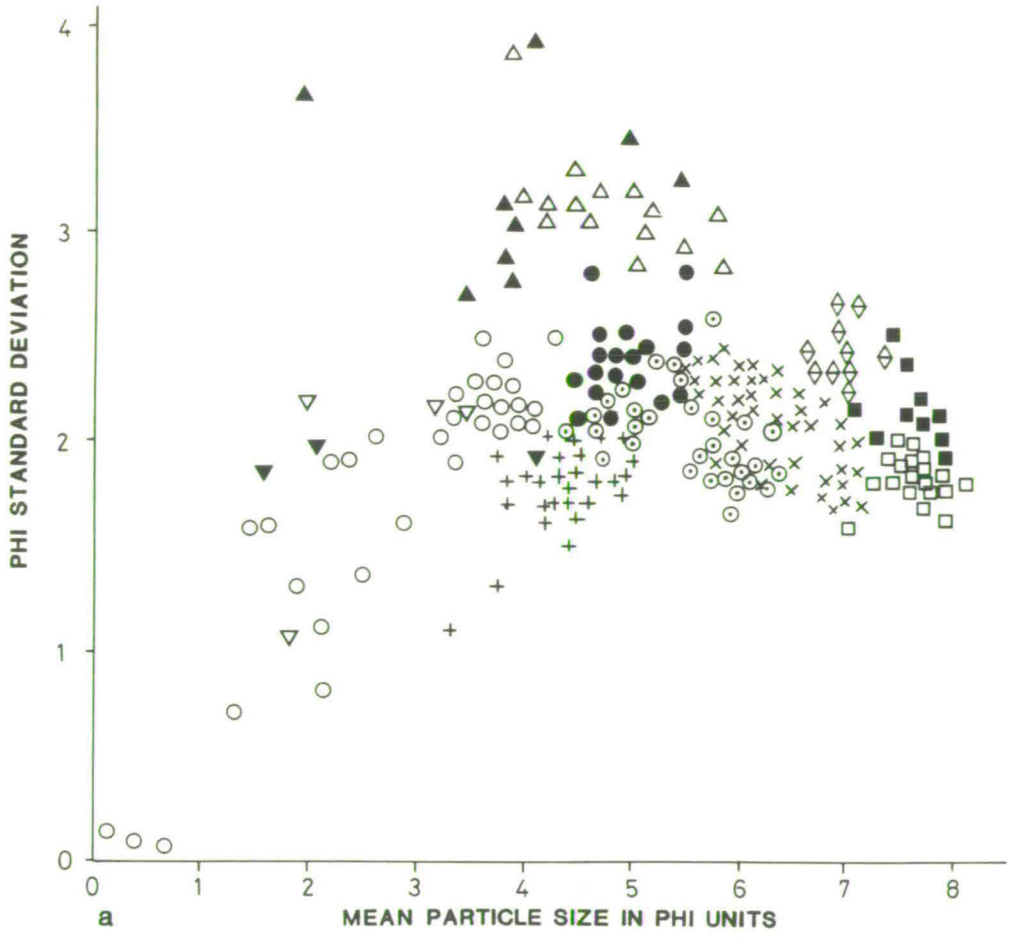

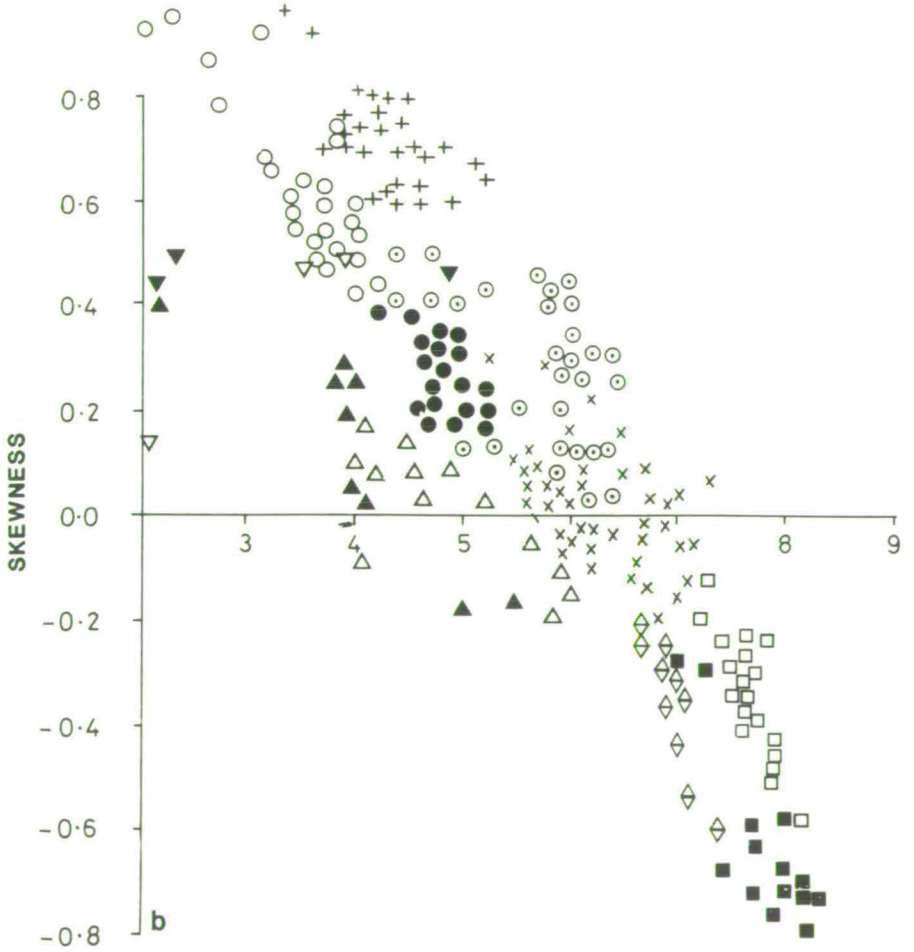

Fig. 5.10. Plots of standard deviation against mean particle size (a) and skewness against mean particle size (b), all samples from late Weichselian facies. See fig. 5.9. for key.

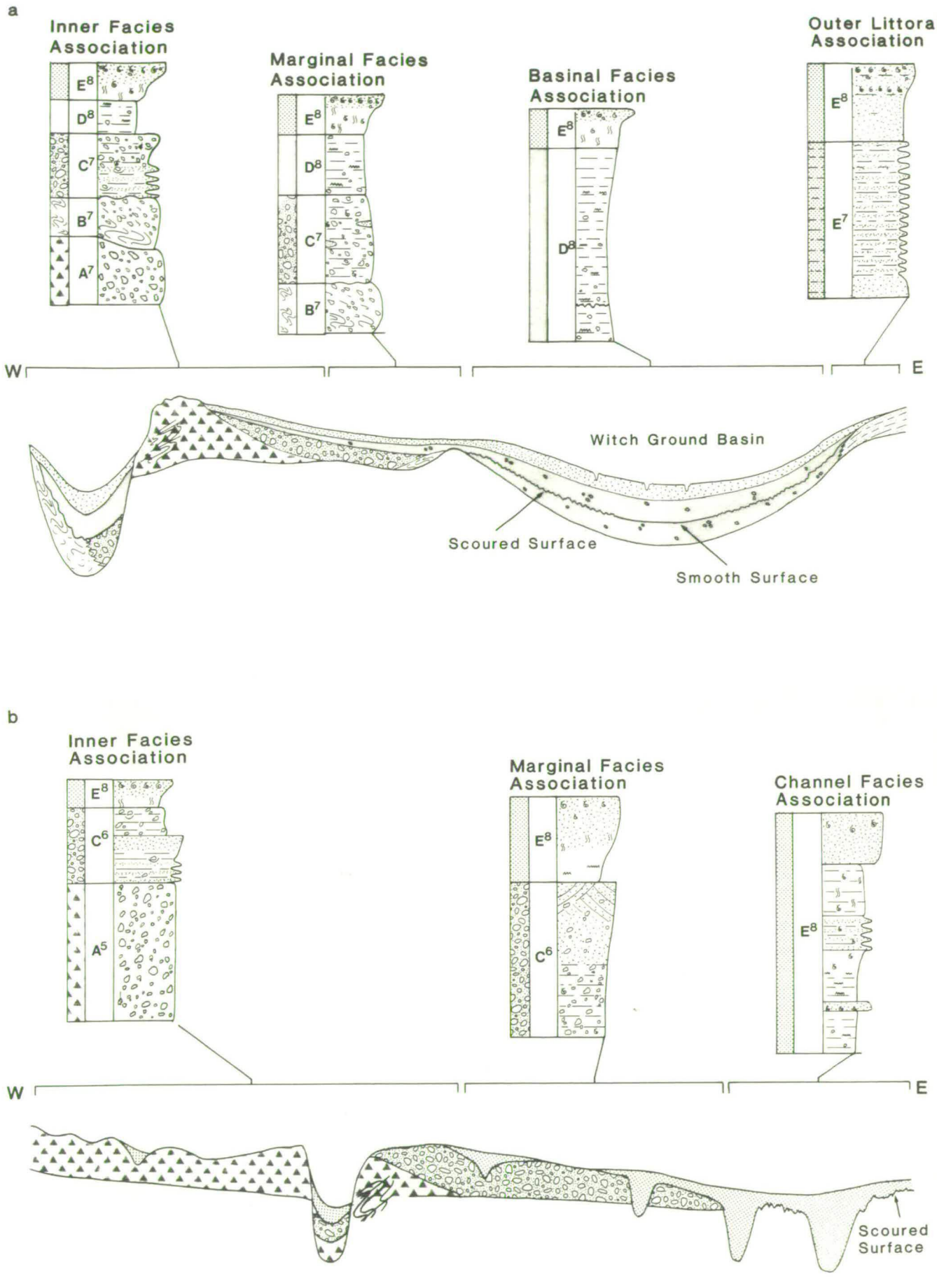

Fig. 6.1. Schematic diagram showing the facies associations in the northern area (a) and southern area (b).

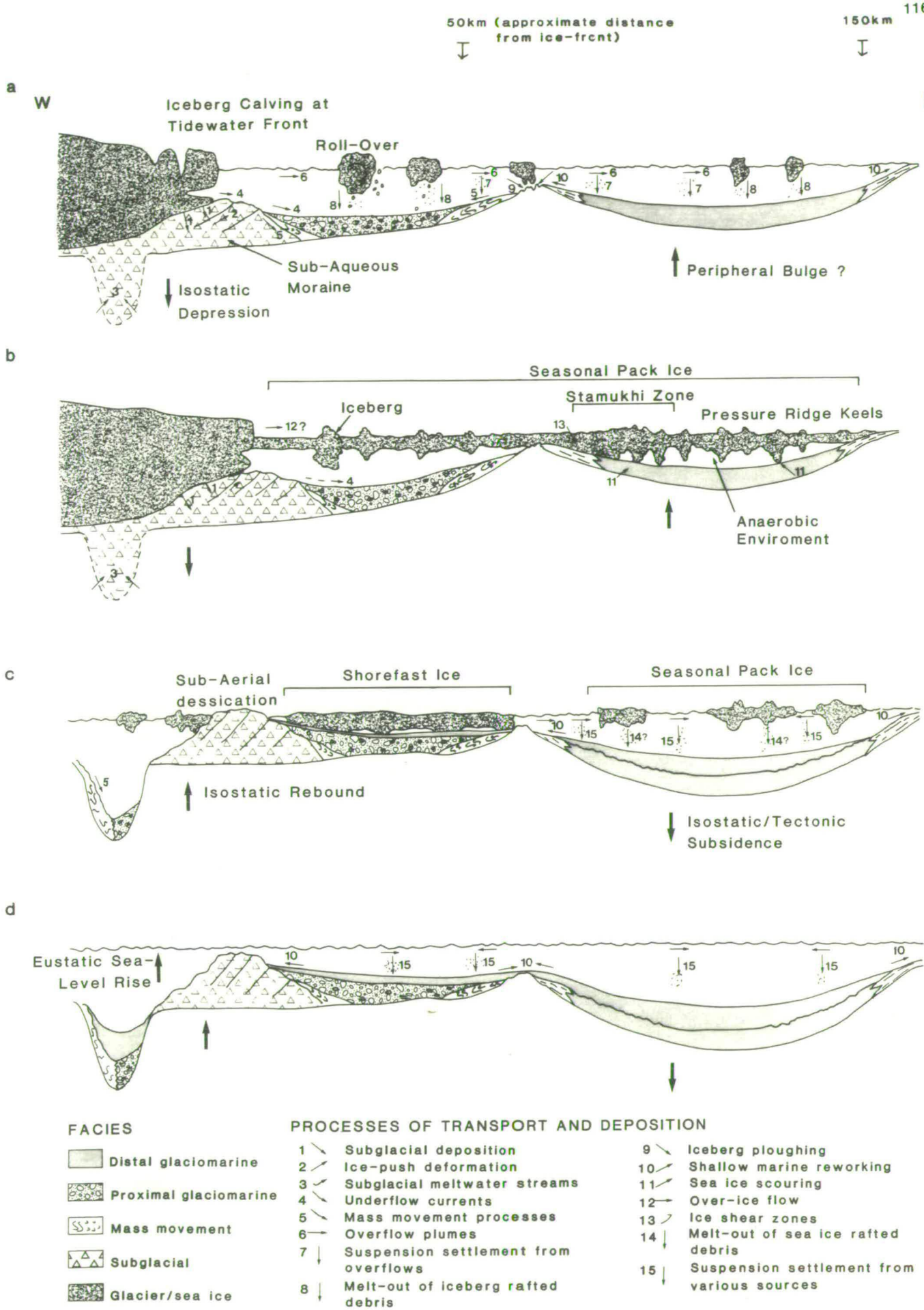

Fig. 6.2a–6.2d Model depicting the development of the facies associations in the northern part of the study area (58° –59° N). See text for details.

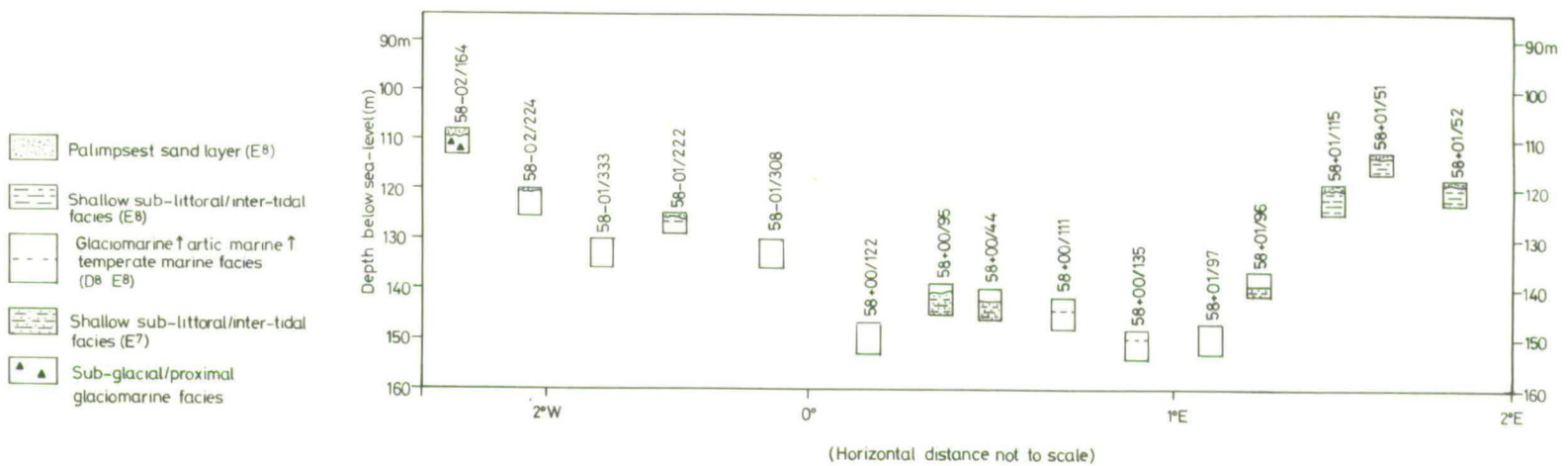

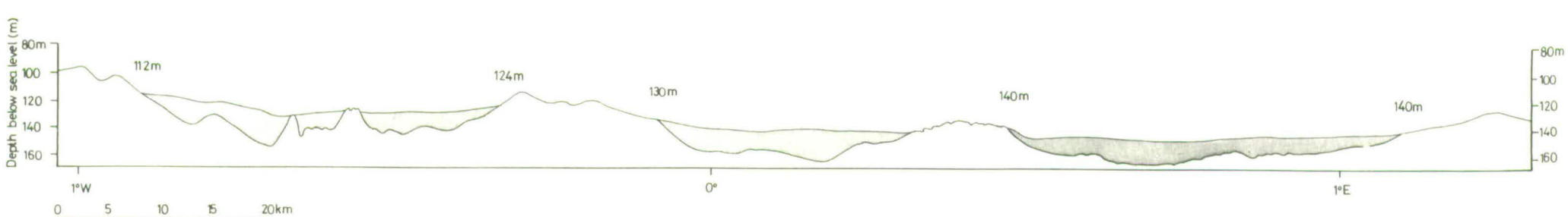

Fig. 6.3. Section across the Bosies Bank and Fladen areas showing the cut-off depth to seismic sequence 8. Inset shows typical depths below present sea level for various late Weichselian facies.

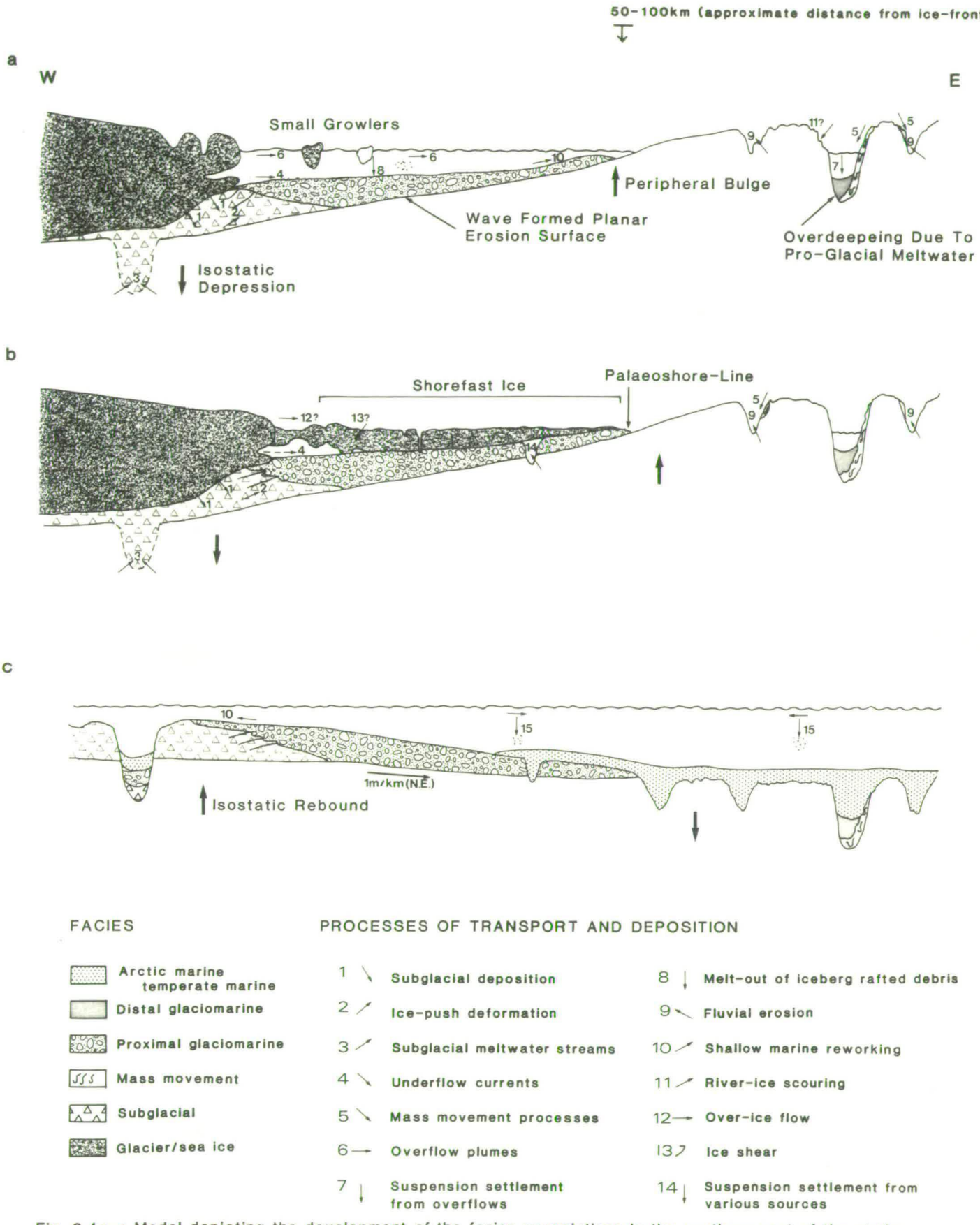

Fig. 6.4a-c Model depicting the development of the facies associations in the southern part of the study area (56° - 58°N). See text for details.

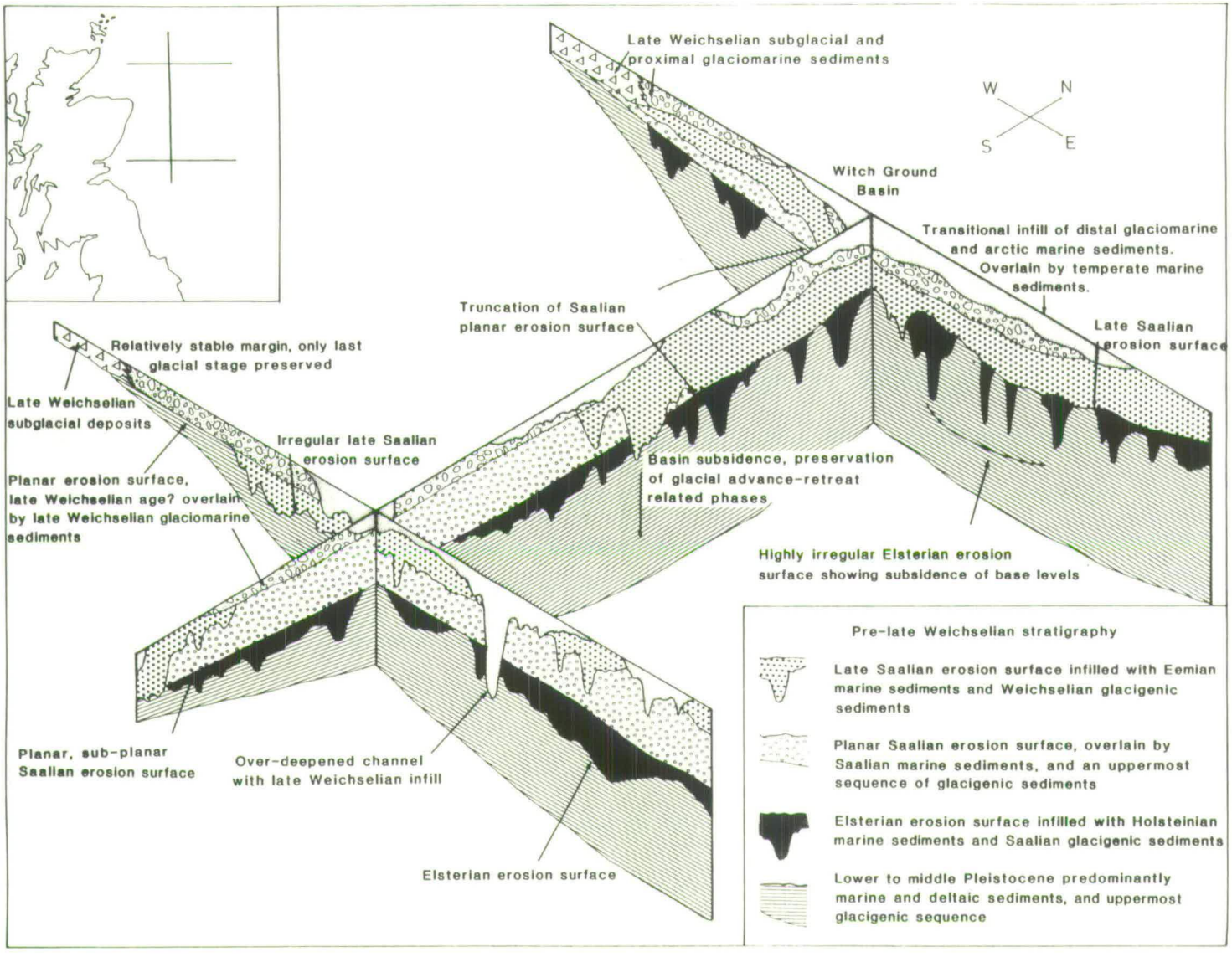

Fig. 6.6. Stratigraphic architecture of the Pleistocene sequence.

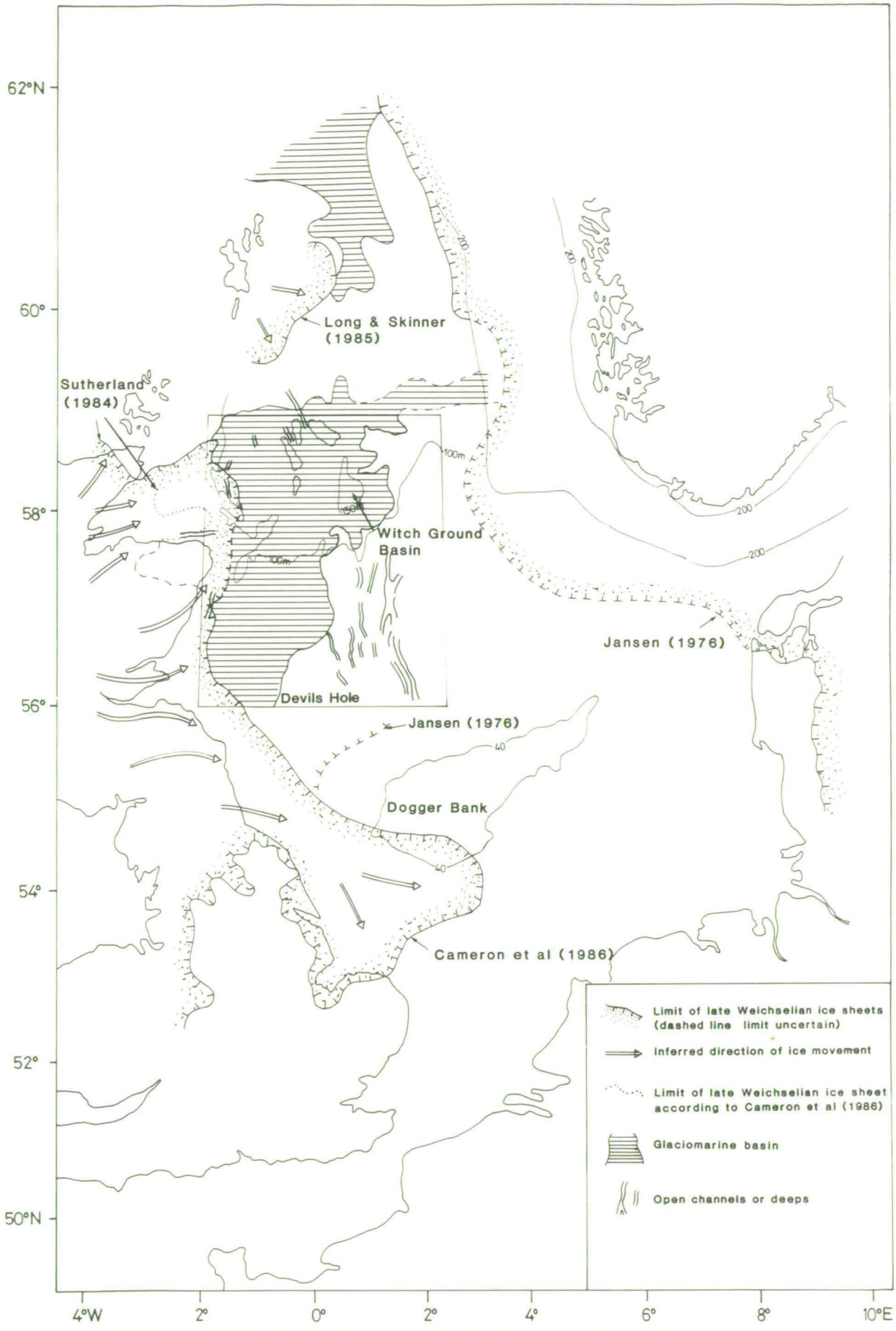

Fig. 6.5 Late Weichselian Palaegeography during the glacial maxima of the Scottish ice sheet. Box shows limits of study area.

APPENDIX 1

SHALLOW GAS AND POCKMARK FEATURES

Acoustic masking, reflector disturbance and eliptical depressions (pockmarks) in the sea floor were all observed on acoustic profiles and sonar records from the study area. Fig. 1 shows the distribution of these features within the Bosies Bank and Fladen areas. The extent of the acoustically well layered, basin infill unit and its thickness are also shown for comparison. It should be noted that the pockmarks are generally restricted to the two above mentioned areas, whilst acoustic masking is observed throughout the study area. A brief description and interpretation of these features is given below.

Pockmarks

Pockmarks were first described as sea-bed features of the Scotian Shelf by King and MacLean (1970) and were subsequently identified in a number of offshore areas including the Norwegian Trench (Hovland, 1981) and the North Sea (McQuillin and Fannin, 1979) and more recently the Barents Sea (Solheim and Elverhoi, 1985). Within the study area they form circular or oval depressions, ranging from 3m-200m in diameter (Fig. 2). On seismic profiles (Boomer and Sparker) they appear as conical depressions some 0.5m-8m deep. The sidewall slopes of these depressions range from 0.5 - 9.5°, and evidence of mass movement was observed on some of the steeper slopes. However, recent work by Hovland et al. (1984) using data collected from a remotely operated vehicle (ROV) suggests that estimates from acoustic profiles may be too low and that depths of 15m and sidewall slopes of 15° are not uncommon.

Within the study area pockmarks are restricted to the acoustically well layered basin infill unit of seismic sequence 8 (Appendix 1, Fig. 1). More specifically they are generally associated with the uppermost temperate marine sediments of Facies E^8, dated as being of late glacial to Holocene in age. Interestingly vibrocores taken from pockmarked areas revealed that the uppermost 0.5m - 2m of sediments commonly contained a significantly high proprotion of coarse silt (Facies $E4^8$, Fig. 4). In chapter 4 it was suggested that this was perhaps related to

pockmark activity (D. Long, pers. com.). Where the pockmarks form large depressions they commonly penetrate down into the arctic marine and glaciomarine muds of facies 8. Other sediment features associated with the pockmarks include the presence of domed shaped reflectors and disruption of the acoustic layering beneath the pockmarks and the occurrence of diffraction hyperbolae below some of the pockmarks (Fig. 2a). As can be seen from Fig. 1 the distribution of pockmarks is not necessarily associated with other gas features, also pockmarks are generally absent from the basin margins where the muds contain a higher proportion of coarse silt and fine sand.

To date, the most favoured theory as to the formation of pockmarks is that they are related to gas seeps (King and Maclean, 1970; McQuillin and Fannin, 1979; Hovland, 1981; Hovland and Sommerville, 1985). Thus, it envisaged that pockmarks are formed by gas escaping through the sea bed which consequently lifts the finer sediment into suspension allowing for a proportion of it to be redistributed by near bottom currents (Hovland et al., 1984). Other possible mechanisms include pore-water escape (Harrington, 1985) and the melting of an underlying permafrost layer (N. Fannin pers. com.).

However, recent work by Hovland and Sommerville (1985) M. Hovland (pers. com. 1984) and A. Judd (pers. com.) appears to confirm that pockmarks in the North Sea and Norwegian trench were formed by gas seeps. This was supported by observations of active pockmarks from an ROV (A. Judd, pers. com.) from which numerous gas seeps were recorded. Similar gas seeps were also observed in areas of acoustic blanking in the Norwegian sector of the North Sea (Hovland and Sommerville, 1984) however in these cases the coarse nature of the sediment cover appears to have precluded the formation of pockmark features. Only one example of a possibly active pockmark was observed on seismic profiles from the study area (Fig. 2b) in which a sediment cloud or gas bubble is evident in the water column immediately above the pockmark. A more recent example from the study area was observed from commercial profiles of a large pockmark feature (Hovland and Sommerville, 1984), above which a distinctive sediment or gas cloud was identified.

Accepting a gas seep mechanism for pockmarks in the study

area it is necessary to identify the source of the gas. In the North Sea area their are two possible sources:-

i. that the gas to biochemically produced by the decay of organic matter.

ii. that the gas was thermogenically produced, allochthonous gas which subsequently migrated up through the sedimentary layers.

Here, the second origin is preferred for three reasons; although it may sometimes be of a mixed origin.

i. An extensive survey of pockmark features in the Forties area by BGS and BP in 1972 provided a wealth of information on the pockmarks. This includes the results of a sniffer cruise (1972) which positively identified the occurrence of heavy hydrocarbons over two pockmark features. This suggests that the gas is of a thermogenic or a mixed thermogenic biogenic source, rather than a purely biogenic origin.

ii. Geochemical analysis of material collected by Hovland and Sommerville (1984) from an area of active gas seepage revealed the presence not only of methance, but also of the heavier hydrocarbons ranging from ethane to hexane; again suggesting a thermogenic source.

iii. The organic carbon content of the sediments associated with pockmark features in the study area is generally less than 1%.

In addition to the occurrence of gas seeps from pockmark features and areas of gas blanking, the use of an ROV also led to the discovery of patches of abundant biological material associated with the active pockmarks (Judd, pers. com.). These patches are up to 30m wide, have sharply defined boundaries and contain a rich faunal variety and abundant bioturbation structures. This led Hovland and Sommerville (1984) to conclude that "hydrocarbon bearing sediments may represent a localised physiochemical environment which stimulates marine life."

On the above basis, pockmark features in the study area are interpreted as follows. Subsequent to the deposition of a transitional unit of soft glaciomarine and arctic marine muds an uppermost layer of temperate marine sediments was deposited. The

latter are characterised by the onset of bioturbation structures and a rich faunal and floral diversity relative to the underlying beds. In total this sequence of glaciomarine, arctic marine and temperate marine muds forms the basin infill unit of seismic sequence 8. The onset of significant indigenous faunal activity and the occurrence of localised gas seeps led to the establishment of niches around the gas vents which were characterised by extremely high faunal activity. Work by Singer and Anderson (1984) has shown that simulated bioturbation (mixing) of the surface sediment can result in the removal of fine material by currents as low as 2.0 cm s^{-1}. Where mixing of the sediment does not occur current velocities greater than 16cm s^{-1} were required to initiate particle movement (the tests were conducted on 'glaciomarine-like' material). It is therefore suggested that pockmark depressions were formed by the preferential removal of fine silt and clay from the biologically active gas seeps leaving a mud rich in coarse silt size particles. Resuspension of material by seeping gas may also have been a contributing factor, although this has not been directly observed (A Judd, pers. com.). Further observations of active pockmarks using ROV's may help prove or disprove this theory. The presence of domed reflectors and disrupted layering are interpreted as the result of raised gas or pore pressures and columnar gas disturbance respectively (Hovland, 1983). The occurrence of diffraction hyperbolae below some pockmarks is thought to be an acoustic phenomenon formed by offset reflectors from strong seabed surface reflectors (Hovland et al., 1984).

Shallow Gas

The occurrence of acoustic masking on seismic profiles was interpreted as indicating the presence of either interstitial gas or gas in free, bubble form. Such masking was not restricted to the soft muds associated with the basin fill unit of seismic sequence 8, but occurred in various sequences and at various depths throughout the study area. The salient features of gas blanking in the study area, and especially in the Witch Ground and Fladen areas (Fig. 1), are listed below:-

i. In the Bosies Bank and Fladen areas, zones of gas

blanking are not necessarily associated with pockmark features at the sea bed. In fact the opposite is the more common occurrence.

ii. Gas blanking is most frequently associated with channel infill features. In some instances the gas was observed to be trapped in synclinal-like features (Fig.2.36).

iii. In some cases the zone of gas blanking formed an almost perfect vertical column, the reasons for this are unknown.

iv. Gas blanking was extensively associated with sediments infilling an irregular Elseterian erosion surface. Coring of these sediments recovered sequences which contained horizons of aerated sand.

The negative correlation of gas blanking and pockmark occurrence was also observed from the Norwegian trench by Hovland (1983) and was attributed to the release of gas through the pockmarks, hence precluding the build up of gas in the underlying sediments. An association of gas blanking with channel infills suggests that these features provide suitable traps for the gas. The actual origin of the gas is attributed to a petrogenic or mixed origin for similar reasons to those discussed previously. Other examples of gas blanking occurring in associated with a deeper hydrocarbon source have been documented from the Guaymas Basin, Gulf of California, (Merewether et al., 1985), the Gulf of Mexico and the Norwegian sector of the North Sea (Hovland and Sommerville, 1984). In the latter, acoustic gas blanking was directly traced to a deep seated diapiric structure.

The more widespread occurrence of gas blanking than pockmark features in the study area is attributed to the association of pockmark features with a soft mud substrate. It was originally thought that this association reflected the need for stable side walls during gas induced resuspension and current transportation (Hovland and Sommerville, 1984). However, in the light of evidence presented here it is possible that the lack of pockmark features over areas of sandy substrate reflects the competency of bottom currents and the possible absence of bioturbation mixing. This would also explain the absence of pockmark features around the margins of the Witch Ground Basin.

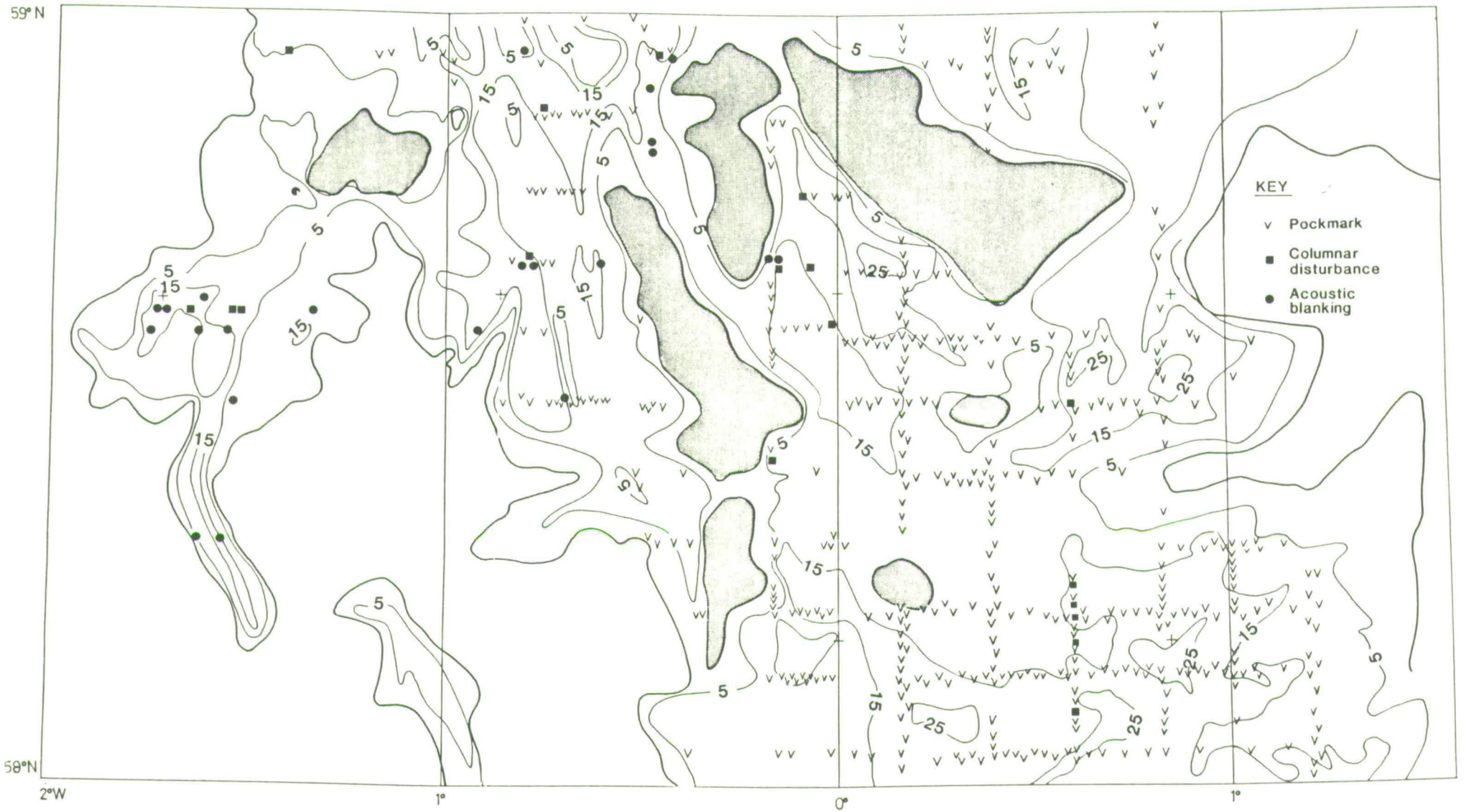

Appendix 1. Fig. 1. Distribution of gas related features in the Bosies Bank and Fladen areas. Contours represent thickness of seismic sequence 8 in 5m intervals.

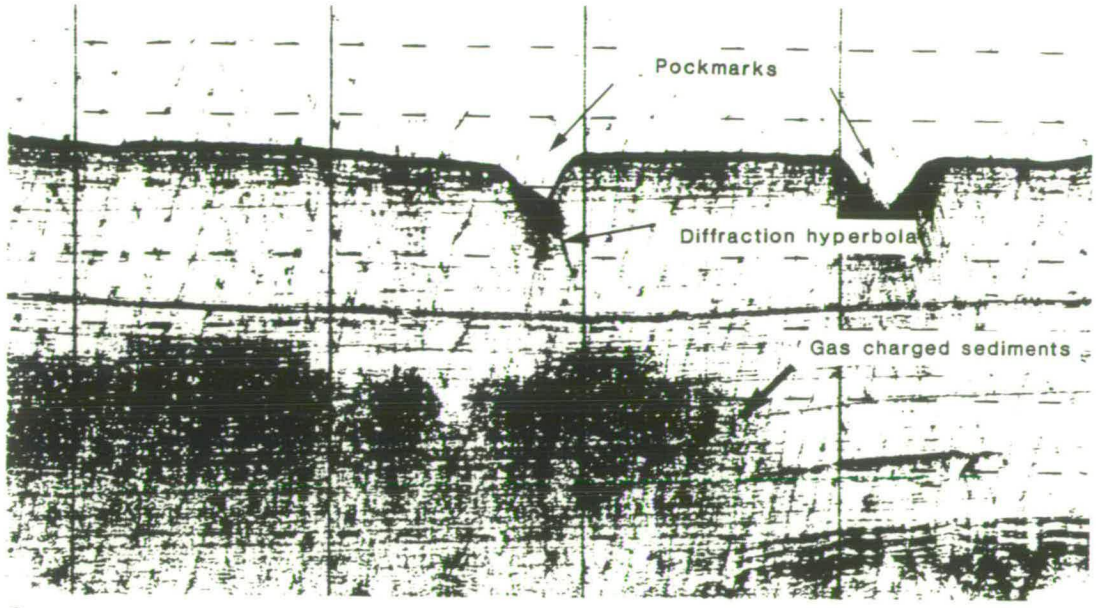

a

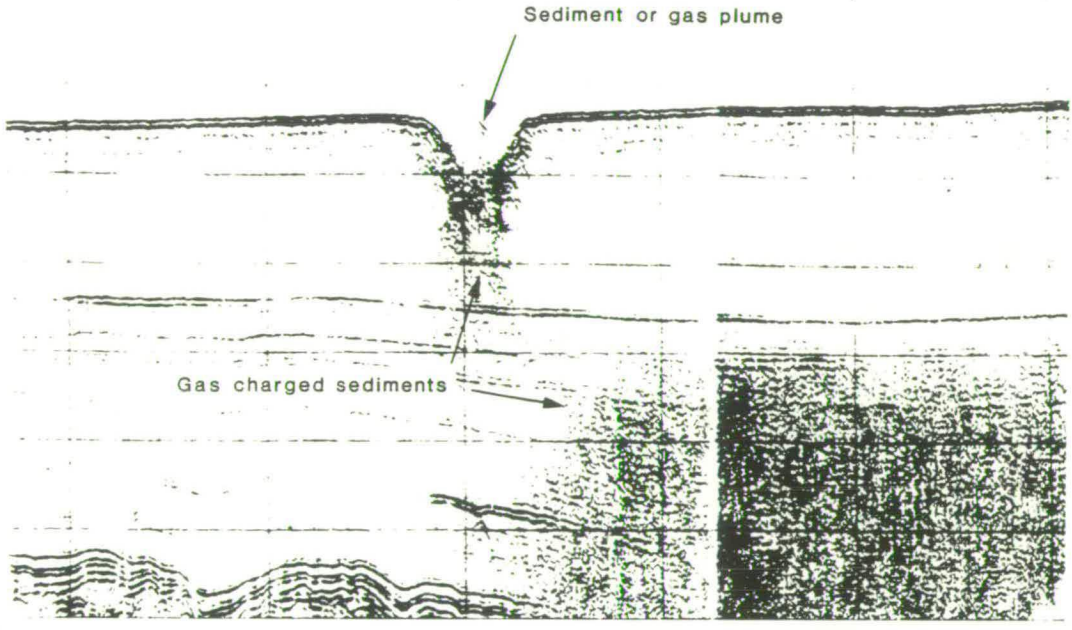

b

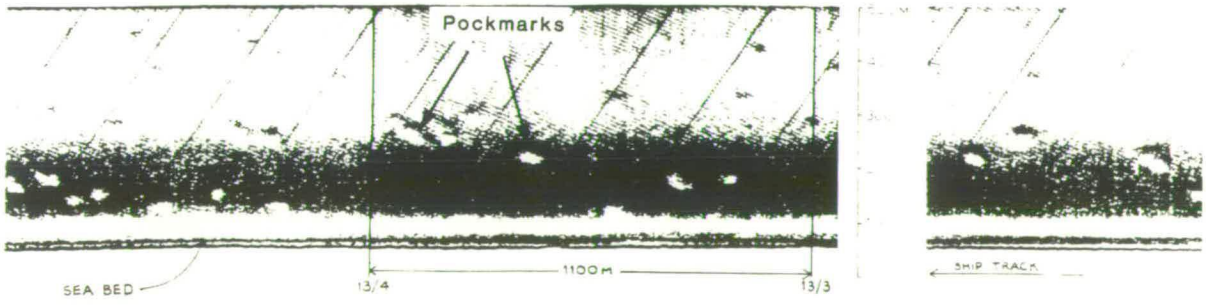

c

Appendix 1. Fig. 2. Gas related features on boomer profiles (a–b) and side-scan sonar record (c).

APPENDIX 2

DINOFLAGELLATE CYST ANALYSIS

Tables 2.1-2.12 were compiled from cyst analyses by Rex Harland (BGS, Keyworth) of samples from various boreholes and vibrocores within the study area. Each table shows the downhole variation in the major dinoflagellate cyst species and the respective dinoflagellate unit and seismic sequence.

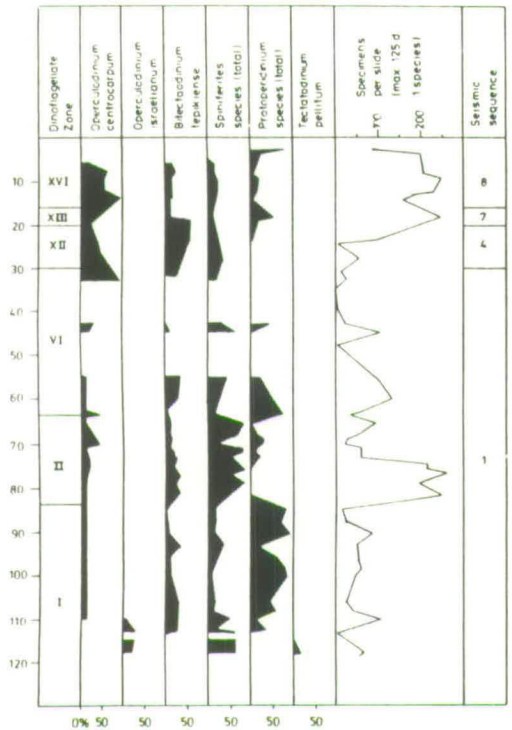

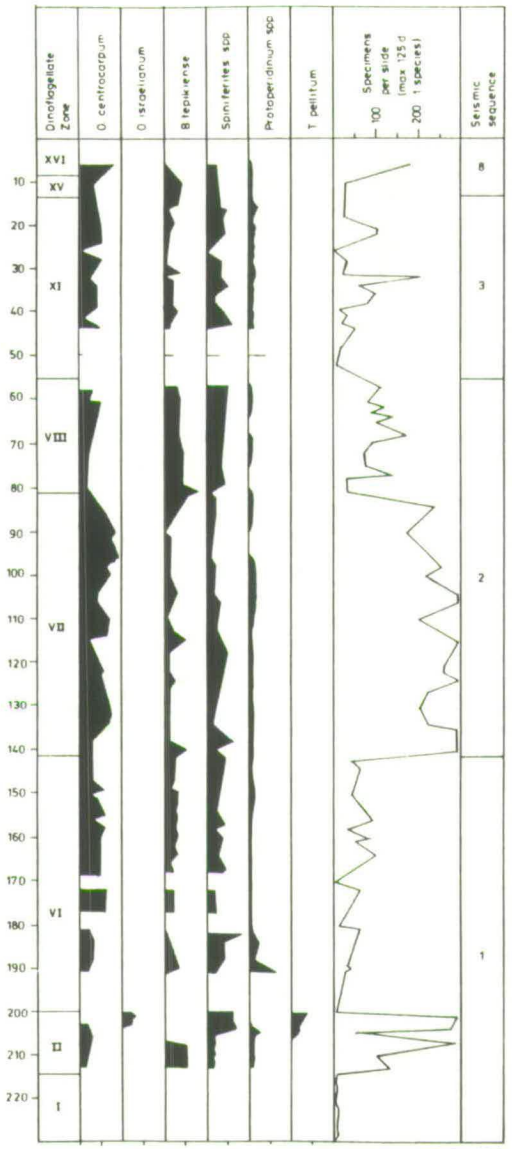

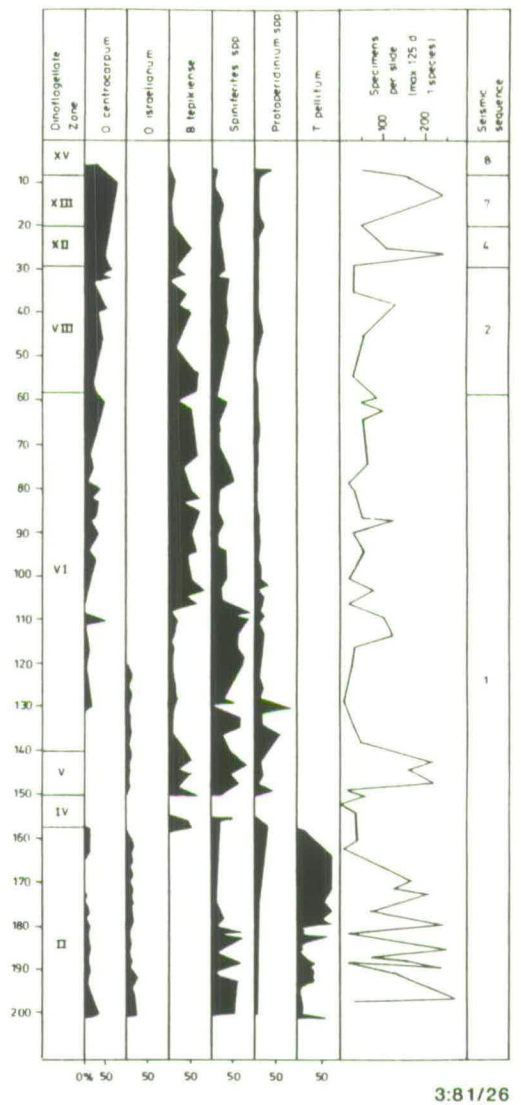

Appendix 2.1 – 2.3

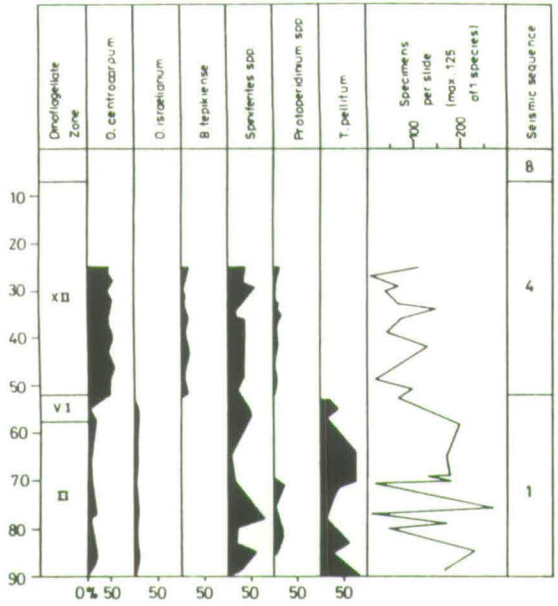

4:81/27

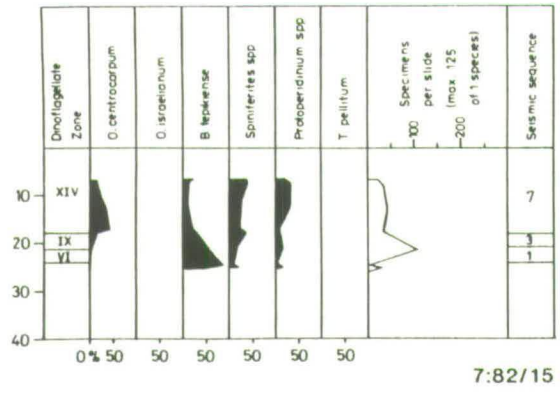

7:82/15

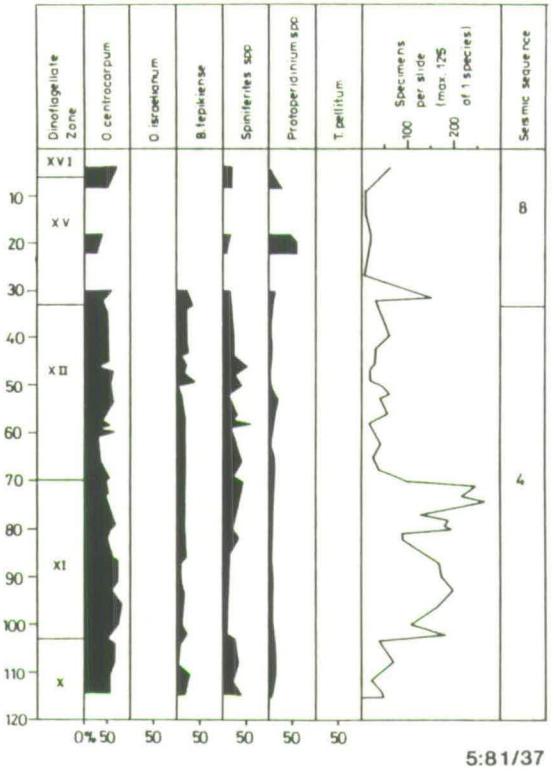

5:81/37

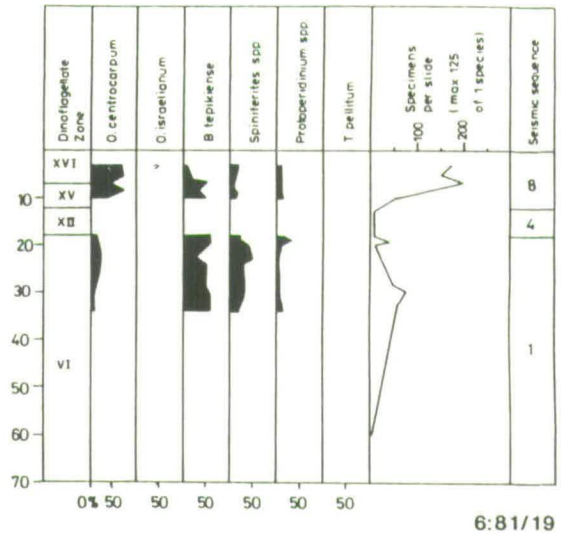

6:81/19

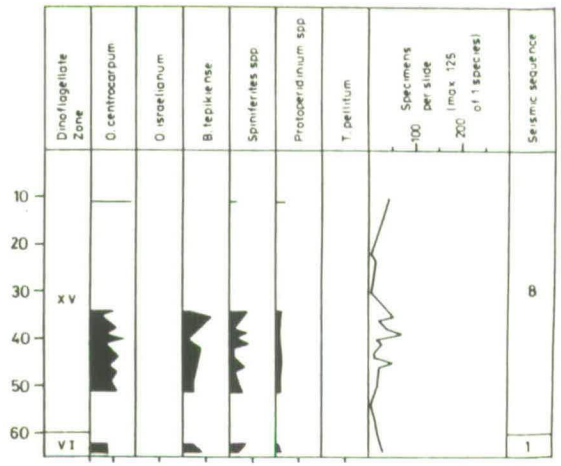

8:81/39

Appendix 2.4 – 2.8

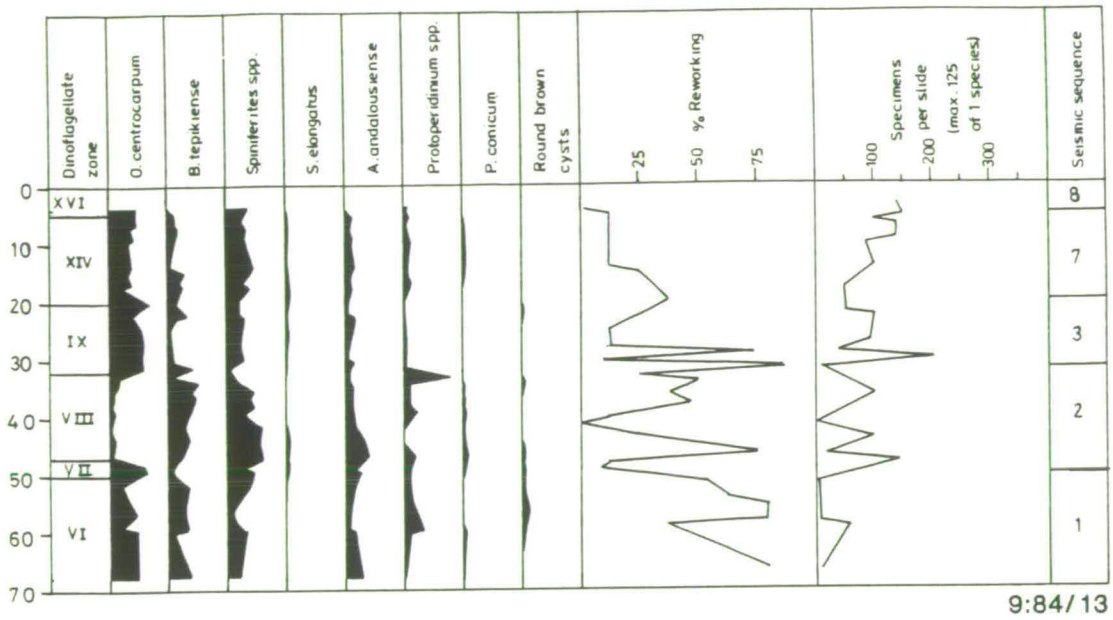

9:84/13

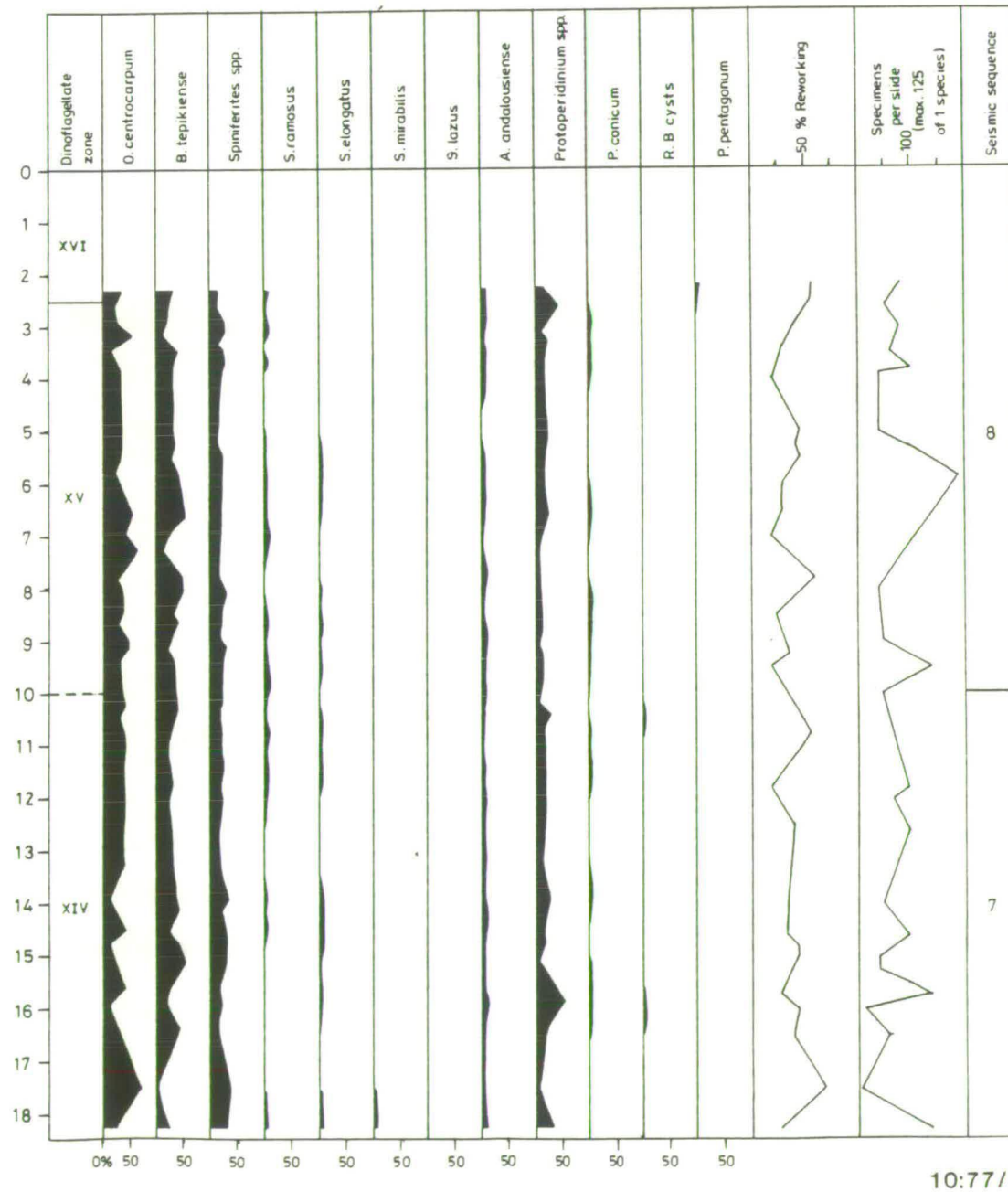

10:77/2

Appendix 2.9 – 2.10

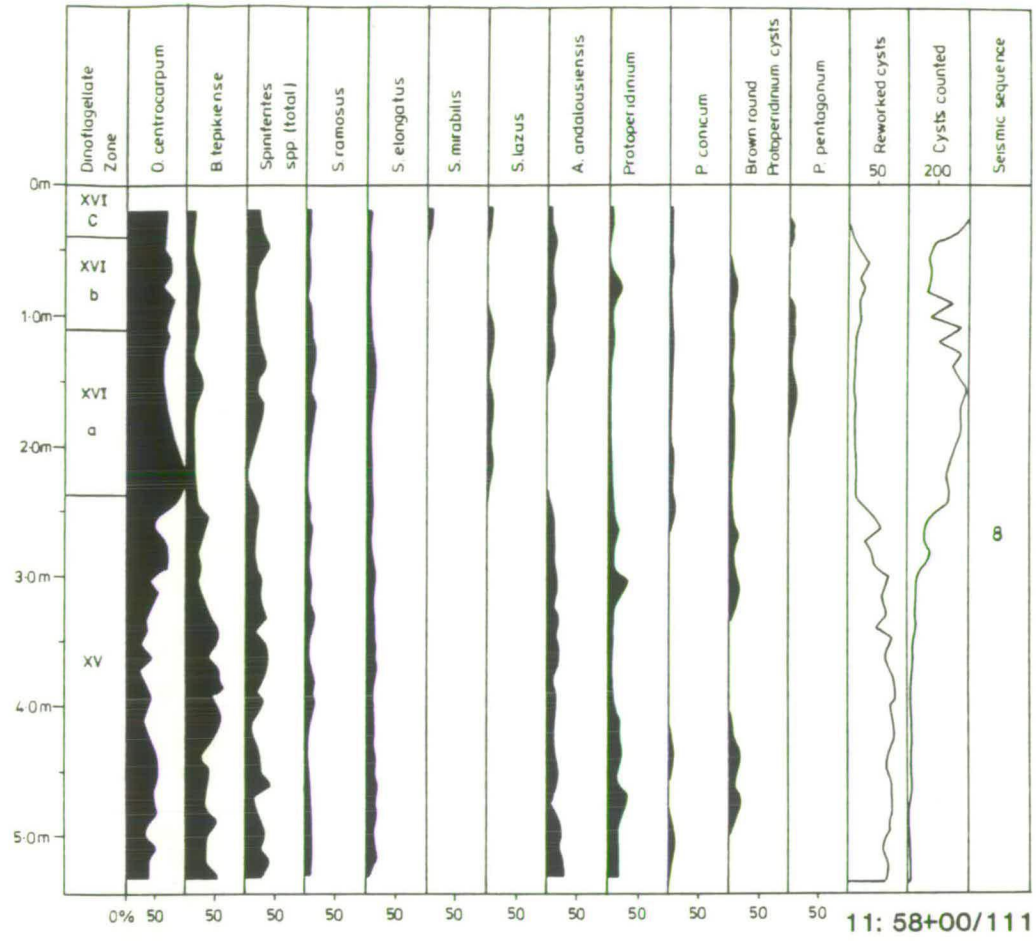

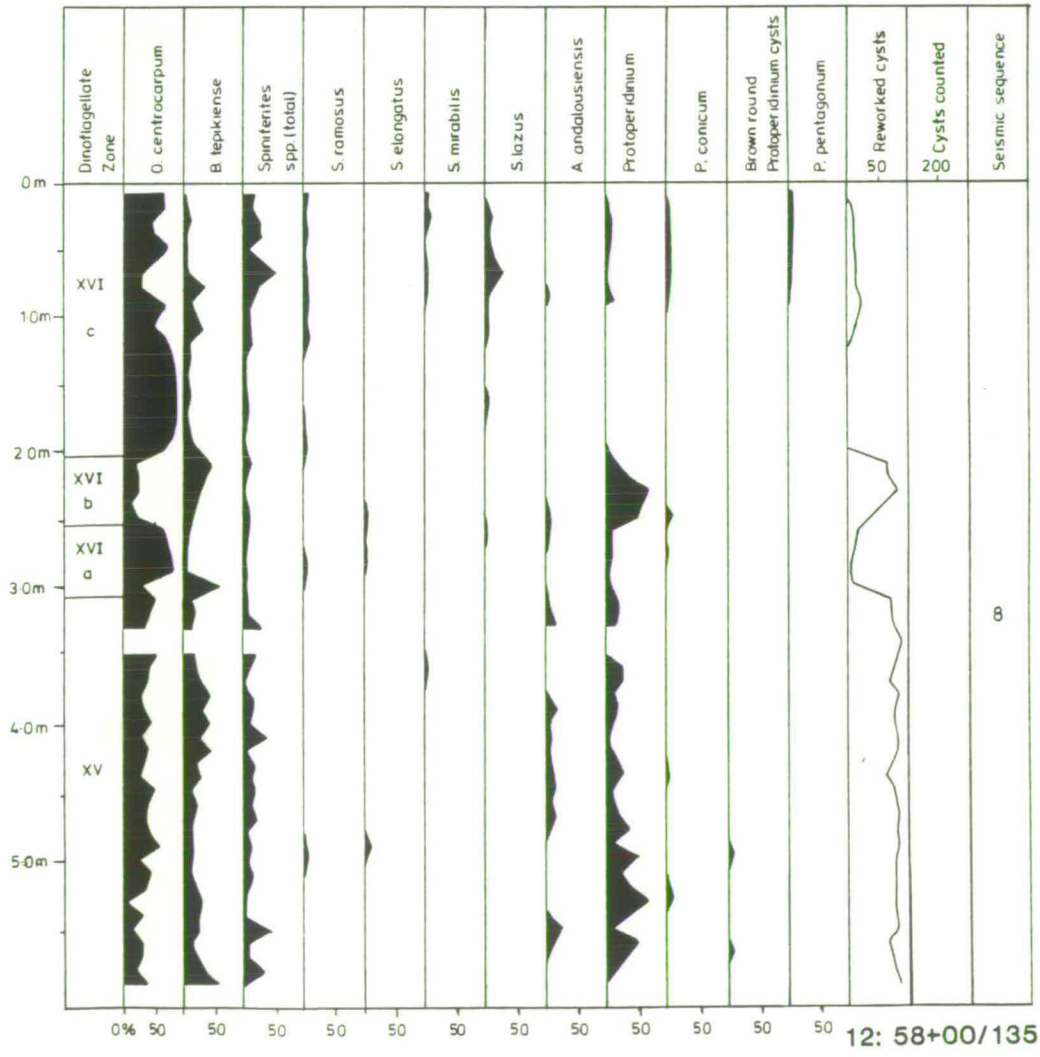

Appendix 2.11 – 2.12

APPENDIX 3

FORAMINIFERA ANALYSIS

Tables 3.1-3.13 were compiled from analyses by Diane Gregory (BGS, Keyworth) fo samples from various boreholes and vibrocores within the study area. Each table shows the downhole variation in the numbers of specimens identified (maximum 300) from each foraminiferal species. It also shows the respective foraminiferal unit, seismic sequence and gross lithology.

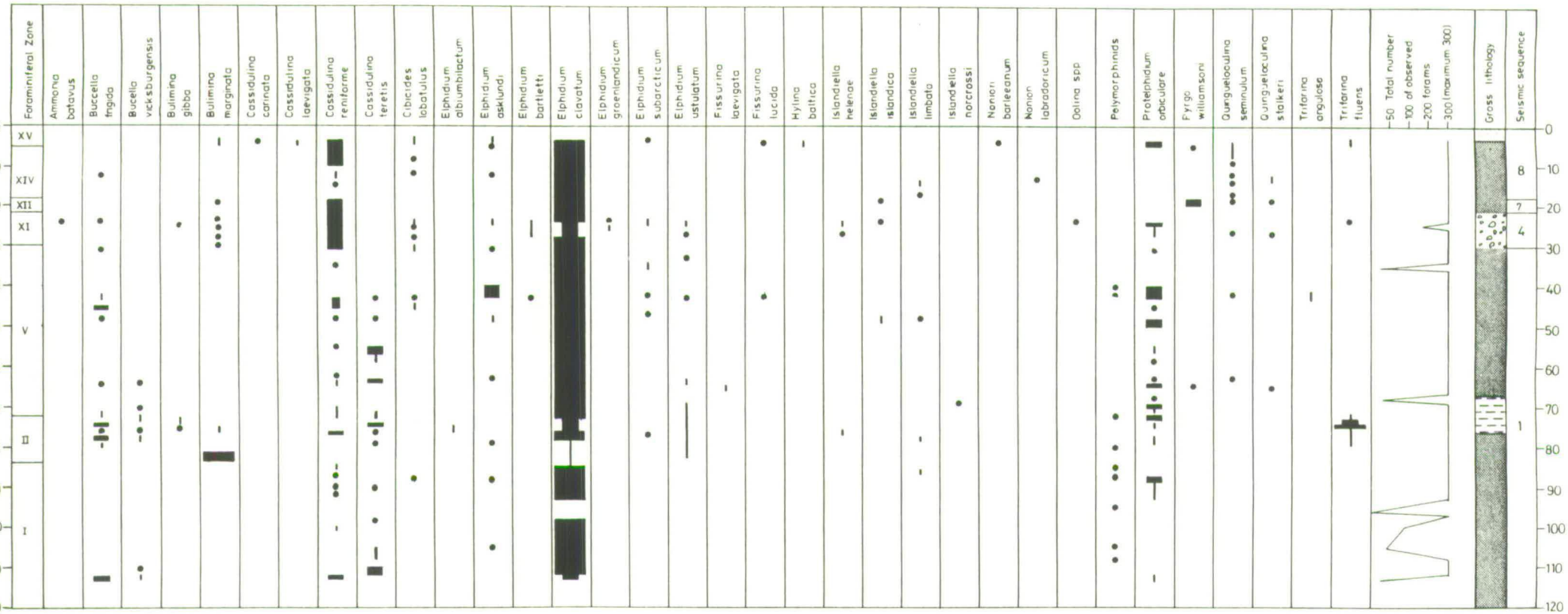

1:82/16

KEY

- ≤ 1%
- 1-5%
- 5-10%
- 10-50%
- > 50%

- Clasts / Diamict
- Sand
- Silt
- Mud

Appendix 3.1

2:81/34

Appendix 3.2

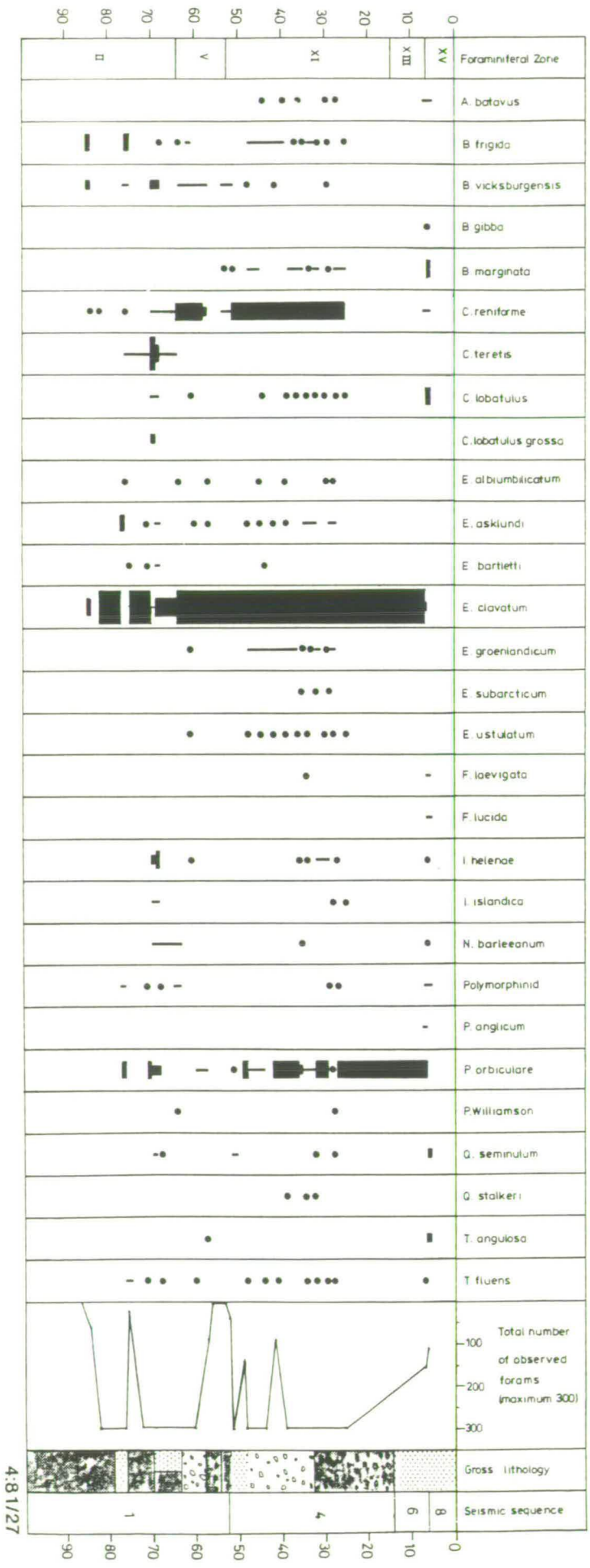
Foraminiferal Zone
A. batavus
B. frigida
B. vicksburgensis
B. gibba
B. marginata
C. reniforme
C. teretis
C. lobatulus
C. lobatulus grossa
E. albiumbilicatum
E. asklundi
E. bartletti
E. clavatum
E. groenlandicum
E. subarcticum
E. ustulatum
F. laevigata
F. lucida
I. helenae
I. islandica
N. barleeanum
Polymorphinid
P. anglicum
P. orbiculare
P.Williamson
Q. seminulum
Q. stalkeri
T. angulosa
T. fluens
Total number of observed forams (maximum 300)
Gross lithology
Seismic sequence
4:81/27

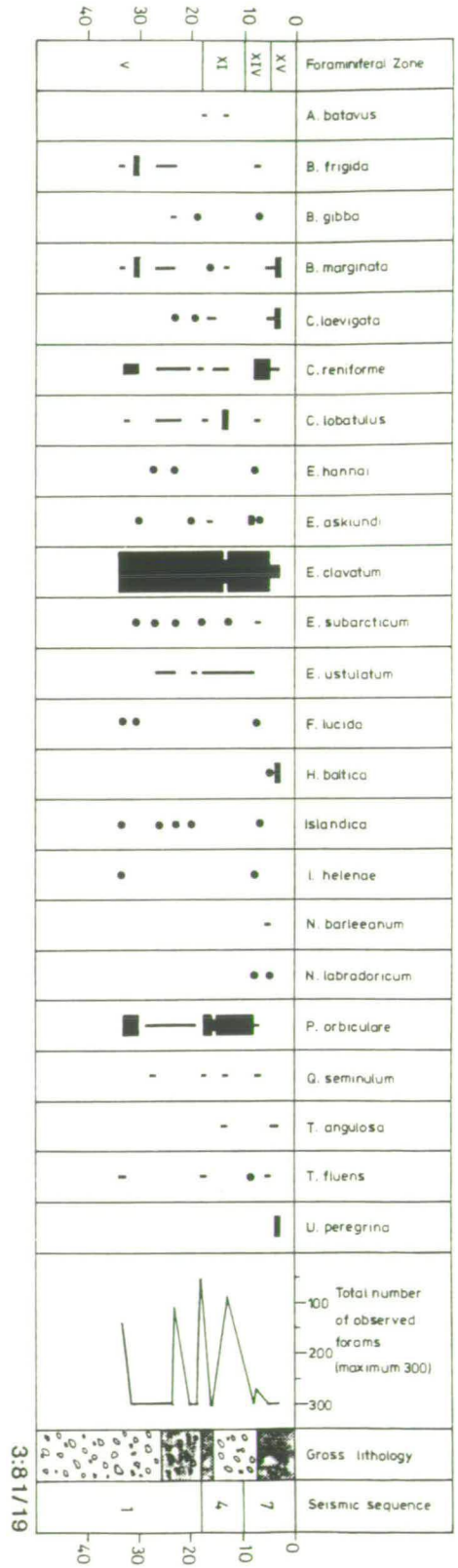
Foraminiferal Zone
A. batavus
B. frigida
B. gibba
B. marginata
C. laevigata
C. reniforme
C. lobatulus
E. hannai
E. asklundi
E. clavatum
E. subarcticum
E. ustulatum
F. lucida
H. baltica
Islandica
I. helenae
N. barleeanum
N. labradoricum
P. orbiculare
Q. seminulum
T. angulosa
T. fluens
U. peregrina
Total number of observed forams (maximum 300)
Gross lithology
Seismic sequence
3:81/19

Appendix 3.5

5:77/2

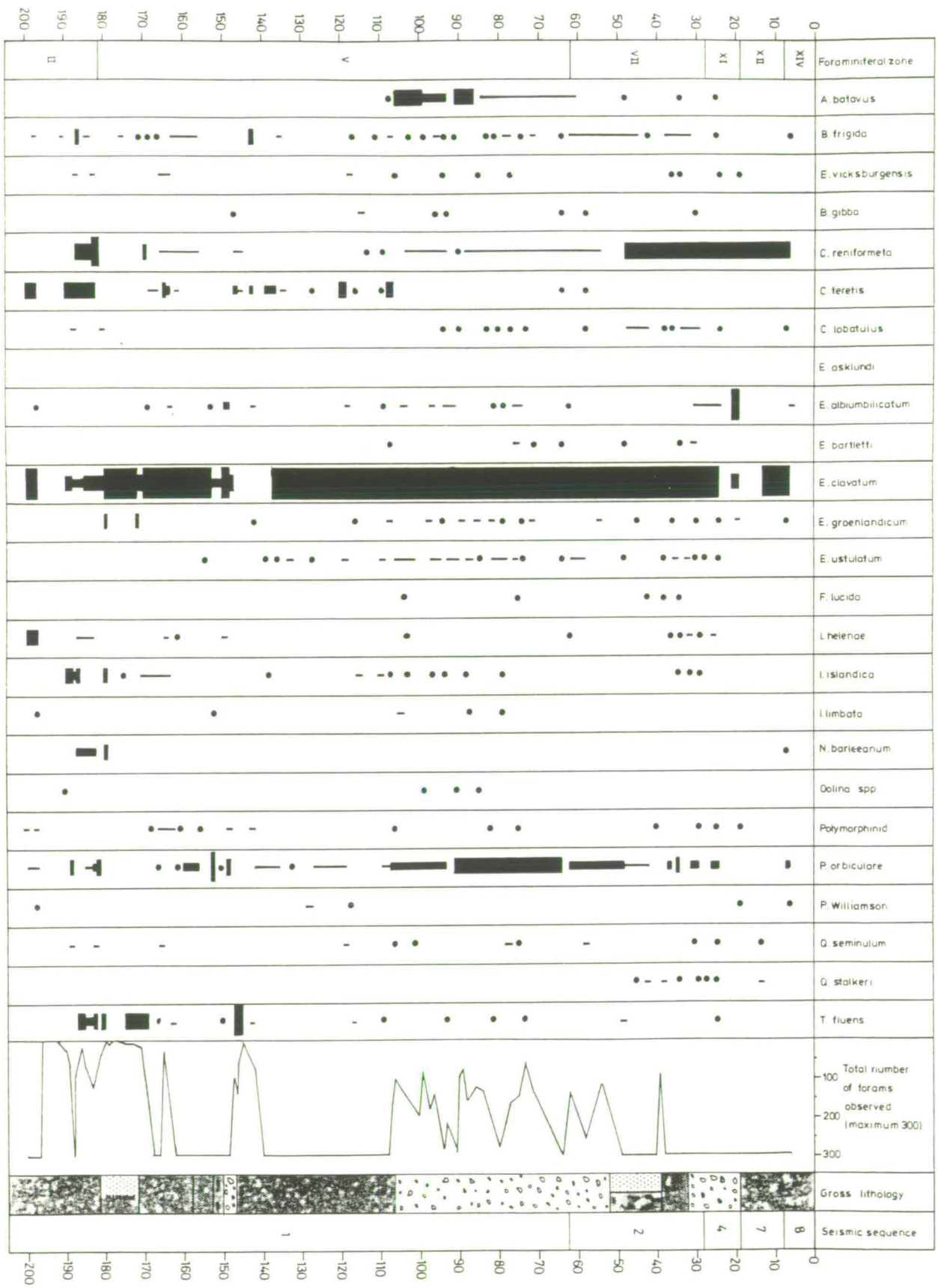
200 190 180 170 160 150 140 130 120 110 100 90 80 70 60 50 40 30 20 10 0
II
V
VII
XI
XII
XIV
Foraminiferal zone
A. batavus
B. frigida
E. vicksburgensis
B. gibba
C. reniformeta
C. teretis
C. lobatulus
E. asklundi
E. albumbilicatum
E. bartletti
E. clavatum
E. groenlandicum
E. ustulatum
F. lucida
L. helenae
L. islandica
L. limbata
N. barleeanum
Oolina spp.
Polymorphinid
P. orbiculare
P. Williamson
Q. seminulum
Q. stalkeri
T. fluens
100
200
300
Total number of forams observed (maximum 300)
Gross lithology
1
2
4
7
8
Seismic sequence

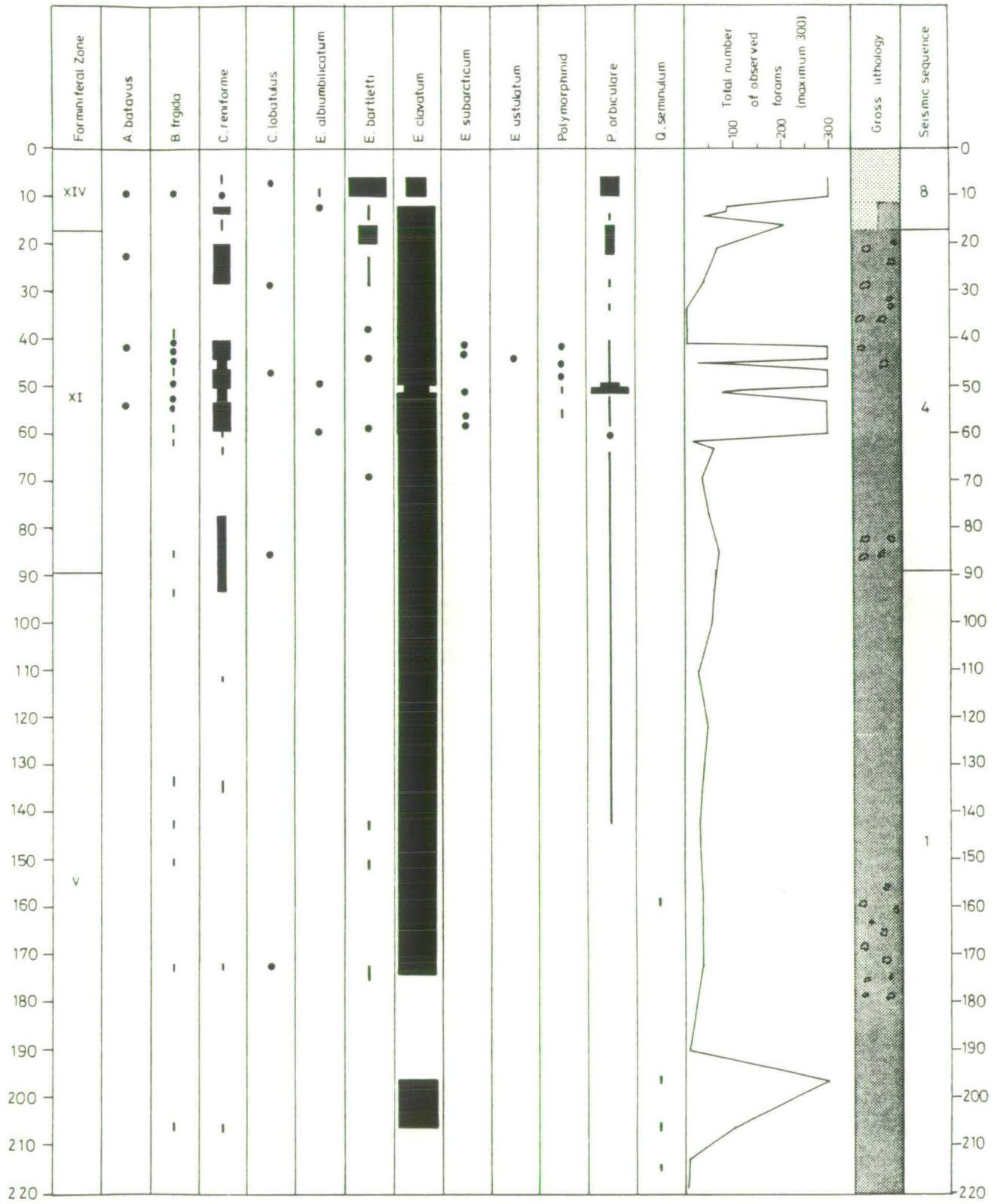

7:77/3

Appendix 3.7

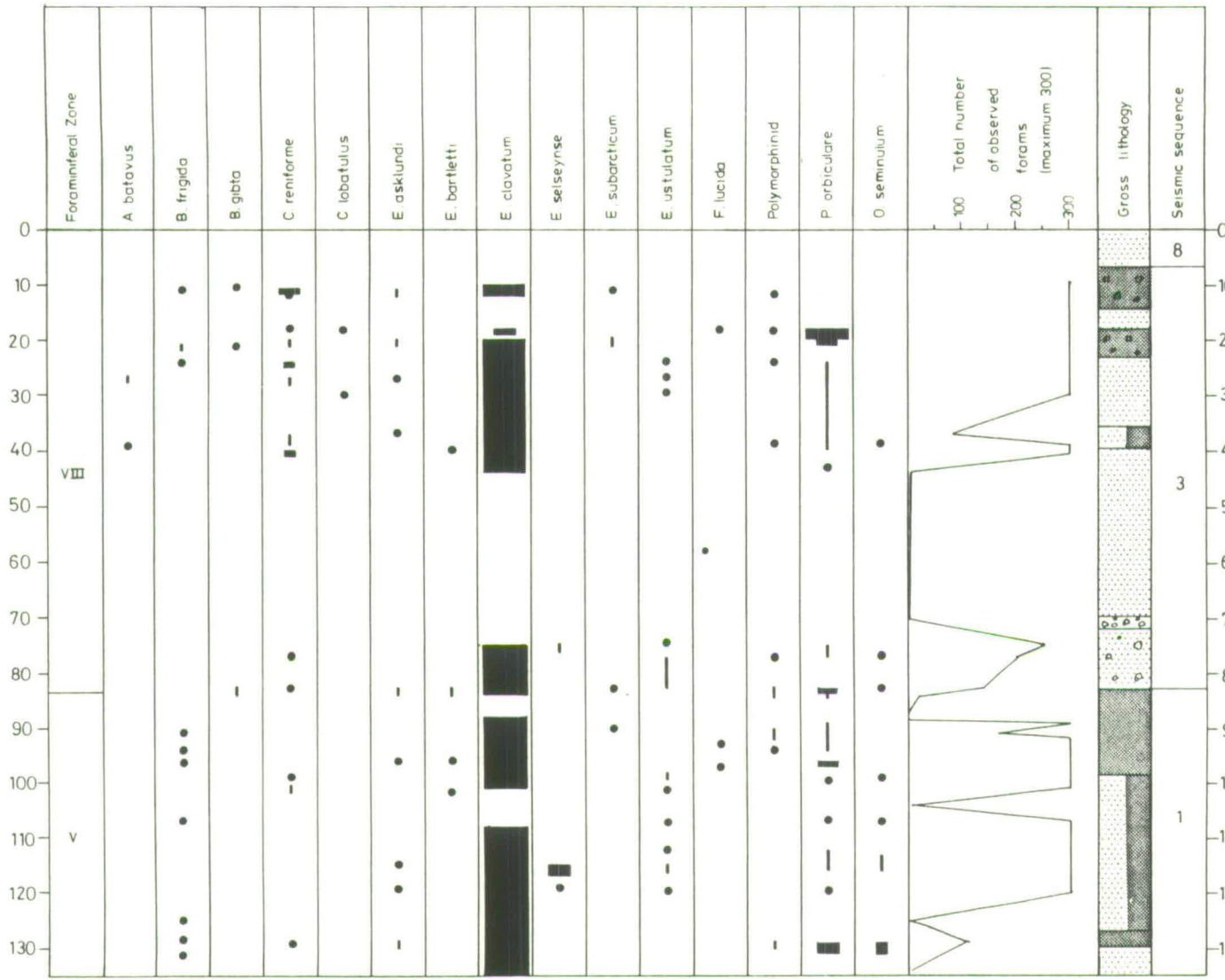

8:81/29

Appendix 3.8

9:82/15

10:84/11

Appendix 3.9 – 3.10

Appendix 3.11 – 3.12

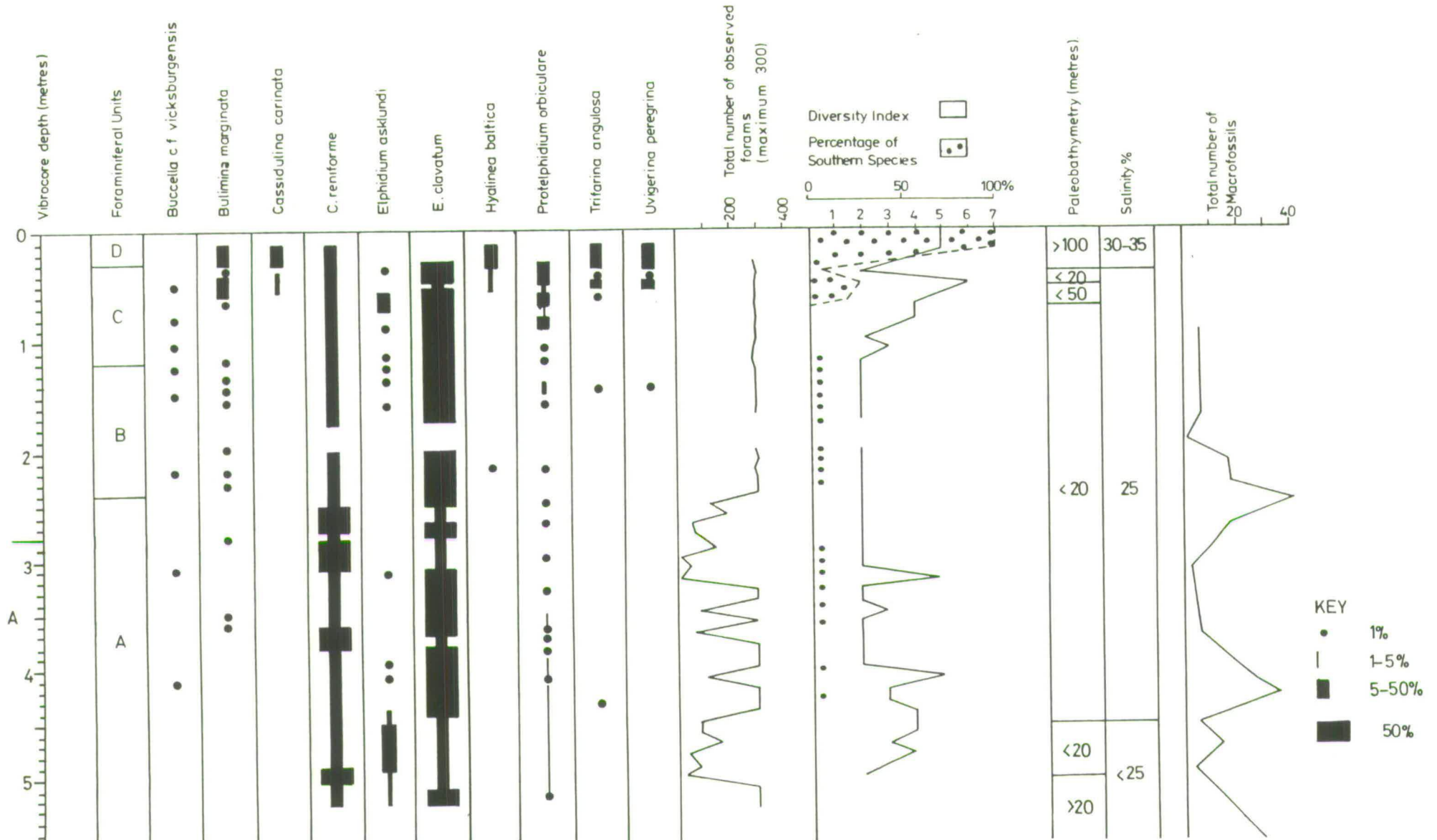

Appendix 3.13 Interpretation of foraminiferal assemblages in V.E 58+00/111 (Long and Bent et. al.,1986).

APPENDIX 4

PARTICLE SIZE ANALYSIS

Tables 1-17 list the results of a large number of particle size analyses of samples from a variety of boreholes and vibrocores collected from the study area. The sample numbers have a prefix which refers to the area from which the core was collected. Thus, 58+01 designates an area between 58°-59°N and 1°-2°E whilst 56-01 designates an area between 56°-57°N and 0°-1°W. For the location of the various boreholes and vibrocores see Fig. 2.8 and Figs. 4.5 and 4.7 respectively. Note that in the text boreholes are referred to by their old numbers, for example BH 81/72, rather than their area number (56-01/171). The old borehole and equivalent new area numbers are therefore listed below:

Acquisition number	Rectangle number
72/18	56-02/6
72/19	7
72/20	8
74/07	19
81/33	303
74/12	56-01/5
81/27	171
81/36	172
81/40	173
75/29	56+00/212
81/29	210
81/39	211
81/34	56+01/230
81/37	231
77/03	57+01/214

81/25	58-02/317
82/15	319
81/19	58-01/373
81/24	374
81/26	375
82/16	376
75/33	58+00/28
77/02	06

CORE	DEPTH	Phi -1	Phi 0	Phi 1	Phi 2	Phi 3	phi 4	Phi 5	Phi 6	Phi 7	Phi 8	Phi 9	>Phi 9	X	SD
56-02/303	5.8	2.09	1.95	2.85	8.2	10.98	10.37	4.9	6.69	4.33	5.29	18.89	23.47	6.2	3.7
56-02/303	6.1	1.16	0.99	2.08	5.54	7.81	19.15	7.59	5.88	4.08	4.01	21.32	20.38	5.9	3.5
56-02/303	8.2	3.55	0.4	0.76	2.34	5.94	31.5	11.7	8.33	4.24	2.56	15.12	13.58	4.7	3.3
56-02/303	9.55	0	.04	0.12	0.57	7.14	34.74	12.05	8.84	3.19	14.76	2.87	15.69	4.8	2.8
56-02/6	22	18.11	2.65	3.31	8.37	12.27	9.94	5.64	4.52	4.33	4.11	10.78	15.97	4.6	4.3
56-02/7	3.4	6.32	1.47	2.82	11.19	14.84	19.16	10.5	5.68	3.27	2.53	9.07	13.14	4.5	3.6
56-02/7	3.9	.08	.03	.03	.08	1.72	26.42	34.17	13.77	4.91	2.33	1.99	14.47	4.8	2.5
56-02/7	7.0	29.3	1.77	0.78	0.71	0.68	5.64	22.46	9.6	2.36	1.12	18.84	6.74	4.4	4.4
56-02/7	12	43.62	3.6	2.28	5.16	6.66	14.05	6.91	2.92	1.38	0.99	6.57	5.87	2.4	4.1
56-01/171	6.6	0	0.16	0.24	0.97	17.62	41.17	10.1	5.05	3.48	2.38	2.04	16.8	4	2.9
56-01/171	24	0	0	.05	0.17	1	14.21	7.52	10.49	11.13	9.12	7.87	38.44	7.1	2.8
56-01/171	55.7	0	.02	.06	0.55	1.44	2.11	1.26	2.4	6.54	8.39	28.12	49.13	8.8	2.1
56-01/171	67.8	0.25	0.28	0.45	0.86	1.5	1.76	3.82	6.5	7.92	.09	.01	76.56	8.9	2.6
56-01/171	69.25	2.56	0.57	0.97	5.59	9.96	9.95	5.93	4.01	4.59	2.27	15.24	38.34	6.8	3.7
56-01/172	16.4	12.17	0.41	0.69	2.6	6.39	18.32	16.28	1.63	9.77	1.63	6.51	23.61	5.1	4
56-01/173	4	0.82	0.5	1.06	4.24	14.59	39.39	15.85	5.56	0.69	2.85	1.35	13.1	3.7	2.9
56-01/173	6.6	2.87	0.48	0.93	4.03	13.32	34.97	14.29	5.17	3.22	2.43	2.36	15.93	4.1	3.2
56-01/173	12	55.3	11.09	2.31	2.25	4.38	7	3.39	2.06	1.55	1.1	1.68	7.9	1.8	4
56-01/5	20	6.65	2.25	3.82	9.11	14.51	17.72	6.84	3.66	3.19	2.97	11.15	18.12	4.8	3.9

CORE	DEPTH	Phi -1	Phi 0	Phi 1	Phi 2	Phi 3	phi 4	Phi 5	Phi 6	Phi 7	Phi 8	Phi 9	>Phi 9	X	SD
57+00/1	1.0	0	0	0	0.2	0.6	40.4	22.3	8.6	5.1	5.5	5.4	11.9	4.3	2.6
57+00/10	1.0	0	0	0	0.4	1.2	43	21.2	7.5	5	4.1	3.5	14.1	4.1	2.6
57+00/11	0.85	0	0	0	0.4	1.4	33	21.2	9.5	7.5	4.5	4	18.5	4.9	2.7
57+00/12	1.0	0	0	0.2	0.4	4.4	21.8	14.6	8.2	8.3	8.2	8.5	25.4	6	2.9
57+00/13	1.0	0	0	0.4	0.4	1.6	24.3	26.7	8	8.7	5.1	4.7	20.1	5.4	2.8
57+00/14	1.0	0	0	1.3	1.3	5	15.3	11.9	8.3	8.5	7.3	6.9	34.2	6.6	3.1
57+00/2	1.0	0	0	0.3	0.6	2.7	24.8	20.7	10.3	8.5	7.1	7.8	17.2	5.4	2.8
57+00/276	0.25	0	0	.06	0.57	5.26	26.95	43.06	8.8	3.3	1.5	1.7	8.8	4.4	2.3
57+00/276	0.5	0	0	0.3	1.42	7.08	33.54	15.76	7.7	6.6	4.5	4.1	19	4.8	2.9
57+00/276	0.75	0	0	0.23	0.35	3.8	22.73	14.29	8.8	9.2	6.8	6.4	27.4	6	2.9
57+00/276	1.25	0	0	.06	0.34	3.84	28.43	13.33	9	8.4	6.7	5.4	24.5	5.5	2.9
57+00/276	1.5	0	0	.07	0.29	1.59	18.45	14.1	10.1	9.6	8.8	7.7	29.3	6.4	2.8
57+00/276	1.75	0	0	.08	0.38	2.43	22.35	20.56	9.7	8.3	7	5.3	23.9	5.8	2.8
57+00/276	2.25	0	0	.04	0.2	1.44	15.56	21.86	11.1	9	7.7	6.4	26.7	6.3	2.8
57+00/276	2.5	0	0	.05	0.15	0.95	13.69	25.76	12.7	9.3	5.9	5.3	26.2	6.3	2.7
57+00/276	2.75	0	0	.02	0.14	0.9	7.76	21.98	14.9	11.2	7.3	6	29.8	6.9	2.7
57+00/276	3.0	0	0	0	0.48	0.52	6.53	18.97	12	12.5	7.8	7.1	34.1	7.2	2.7
57+00/276	3.25	0	0	0.18	0.18	0.9	8.7	15.64	12.7	11.1	9.7	8.7	32.2	7.1	2.7
57+00/28	0.85	0	0	0	0.4	1.5	32.8	24.8	9.8	6.9	4.2	3.9	15.7	4.8	2.7
57+00/29	1.0	0	0	0	0.4	0.6	7.8	34.3	21	7.6	4	4.8	19.5	6.2	2.5
57+00/29	3.0	0	0	0	0.4	0.4	8.3	25.1	17.6	13.7	9	6.4	19.1	6.5	2.5
57+00/3	1.0	0	0	0	0.4	0.4	6.9	28.3	24	12.5	7.9	4.6	15	6.3	2.3
57+00/30	1.0	0	0	0	0.2	0.4	6.7	54.3	15.9	6	4.2	2.3	10	5.6	2.2
57+00/30	3.0	0	0	0.2	0.4	1.3	8.5	15.9	12.1	13.7	11.7	7.7	28.5	7	2.6
57+00/31	1.0	0	0	0	0.4	0.4	21.2	47.3	12.6	5	3.3	1.8	8	4.8	2.1
57+00/36	1.08	0	0	0	0.4	0.8	33.4	26.3	12.5	5.1	5.5	4.3	11.7	4.6	2.5
57+00/37	1.0	0	0	0.8	1.4	16.1	6.2	11.7	6.9	9.6	7.4	8.6	31.3	6.9	3.2
57+00/377	0.25	0	0	.03	0.14	1.24	22.48	50.41	10.8	3.4	1.92	2.31	7.27	4.6	2.1
57+00/377	0.5	0	0	.03	0.24	1.54	19.5	51.19	11.6	3.8	2.46	2.32	7.32	4.8	2.1
57+00/377	0.75	0	0	.02	0	1.49	18.32	48.37	12.8	5.3	2.6	3.24	7.86	4.9	2.2
57+00/377	1.0	0	0	0	0.24	1.23	13.14	46.79	14.7	4.8	4	2.8	12.3	5.4	2.3
57+00/377	1.25	0	0	.03	0.4	2.54	19.6	45.03	9.9	6.9	3.1	2.2	10.3	5	2.3
57+00/377	1.5	0	0	.08	0.58	4.3	17.72	39.82	13.9	6.2	3.1	3	11.3	5.1	2.4
57+00/377	1.75	0	0	0.27	1.46	8.06	20.58	32.33	12.1	5.6	3.7	2.8	13.1	5	2.6

CORE	DEPTH	Phi -1	Phi 0	Phi 1	Phi 2	Phi 3	phi 4	Phi 5	Phi 6	Phi 7	Phi 8	Phi 9	>Phi 9	I	SD
57+00/378	0.25	0	0	.02	.09	0.88	18.68	50.63	10.9	4.3	2.7	3.58	8.22	4.9	2.2
57+00/378	0.5	0	0	.02	0.15	0.99	20.06	48.28	12.3	4.3	2.6	2.5	8.8	4.9	2.2
57+00/378	0.75	0	0	.02	0.16	0.95	18.93	48.84	11.8	4.7	2.5	2.92	9.18	4.9	2.2
57+00/378	1.0	0	0	0	0.24	0.91	13.8	52.55	12.5	3.8	2.3	2.3	11.6	5.3	2.3
57+00/378	1.25	0	0	.03	0.18	1.47	17.41	47.51	13.6	4.8	3.3	2.72	8.98	5	2.2
57+00/378	1.5	0	0	.02	0.18	1.34	17.7	49.06	12.7	5	2.4	2.3	9.3	5	2.2
57+00/378	1.75	0	0	.02	0.27	2.68	21.45	42.58	14	4.4	2.5	3.39	8.71	4.8	2.3
57+00/378	2.0	0	0	0	0.1	1.82	13.78	49.5	13.8	4.4	3.2	2.7	10.7	5.3	2.3
57+00/378	2.25	0	0	.02	0.23	2.8	16.3	50.85	17.5	3.27	1.45	1.8	5.78	4.8	2
57+00/378	2.5	0	0	0.14	0.24	1.85	13.15	45.82	17.3	5.2	3.2	3.69	9.41	5.3	2.2
57+00/378	2.75	0	0	0.24	1.07	4.34	15.15	34.2	18.1	7.2	3.8	3.5	12.4	5.4	2.5
57+00/378	3.0	0	0	0	1.11	1.46	9.49	30.34	12.2	8.6	6.8	4.6	25.4	6.4	2.7
57+00/378	4.0	0	0	0	0.2	0.62	5.88	21.3	13.8	11.2	10.2	7.7	29.1	7.1	2.6
57+00/378	4.5	0	0	.02	0.15	0.74	6.35	13.34	12.5	12.2	10.4	9.8	34.5	7.5	2.6
57+00/379	0.25	0	0	.02	0.5	2.15	23.39	38.54	15	5	3.1	2.3	10	4.8	2.3
57+00/379	0.5	0	0	.08	0.57	4.92	29.24	14.49	8.3	7.6	6.7	5.2	22.9	5.4	2.9
57+00/380	0.25	0	0	.05	0.56	2.75	25.5	44.84	9.8	3.1	2.2	1.71	9.49	4.5	2.3
57+00/380	0.5	0	0	.09	0.3	1.48	21.86	27.67	14.9	8.2	5.9	4	15.6	5.4	2.6
57+00/380	0.75	0	0	.04	0.26	1.79	30.58	22.83	10.1	6.7	5.2	4.8	17.7	5	2.7
57+00/380	1.0	0	0	0	0.51	3.21	35.9	19.38	9.8	6.2	4.8	3.8	16.4	4.6	2.7
57+00/380	1.25	0	0	0.24	0.75	5.4	30.84	13.17	10	6.5	7	4.3	21.8	5.2	2.9
57+00/380	1.5	0	0	.02	0.15	1.37	17.62	9.84	11.5	9.6	9.8	8.8	31.3	6.7	2.8
57+00/380	1.75	0	0	.02	0.16	1.41	20.08	12.03	9.9	9.5	9.3	8.1	29.5	6.4	2.8
57+00/380	2.0	0	0	0	.09	0.38	18.77	16.46	11.2	9.4	10.1	7.8	25.8	6.3	2.7
57+00/380	3.0	0	0	0	0.22	1.31	9.14	24.63	14.1	9	7.8	7.6	26.2	6.7	2.7
57+00/381	0.25	0	0	.02	0.2	1.46	23.45	46.47	11.7	3.9	2.83	2.38	7.59	4.6	2.1
57+00/381	0.5	0	0	.02	0.28	3.56	23.54	44.9	10.7	3.4	2	2.2	9.4	4.6	2.3
57+00/381	0.75	0	0	.07	0.49	3.12	21.28	42.44	13.2	3.9	3	1.7	10.8	4.9	2.3
57+00/381	1.0	0	0	0	0.79	4.95	18.75	44.71	13.1	2.1	3	2.7	9.9	4.9	2.3
57+00/381	1.25	0	0	0.12	0.88	7.99	22.37	26.64	10.1	6.2	4.5	3.5	17.7	5.2	2.8
57+00/381	1.5	0	0	.04	0.18	2.26	18.59	18.83	10.8	8.4	7.2	6.4	27.3	6.2	2.8
57+00/381	1.75	0	0	.02	0.11	1.04	10.64	13.59	12	10.2	10.1	7.5	34.8	7.1	2.7
57+00/381	2.0	0	0	0	0.44	2.17	15.38	23.51	8.3	7.8	7.6	6.6	28.2	6.4	2.8
57+00/381	3.0	0	0	0	0.12	0.96	6.19	20.63	9.5	11	9.5	8.4	33.7	7.3	2.6

CORE	DEPTH	Phi -1	Phi 0	Phi 1	Phi 2	Phi 3	phi 4	Phi 5	Phi 6	Phi 7	Phi 8	Phi 9	>Phi 9	I	SD
57+00/382	0.25	0	0	0.18	0.72	3.94	26.98	43.38	9	3.5	1.8	1.9	8.6	4.4	2.3
57+00/382	0.5	0	0	0.1	0.39	2.33	30	21.38	11	7.1	5.4	4.1	18.2	5.1	2.7
57+00/382	0.75	0	0	.07	0.48	4.32	35.8	19.33	10.1	6.1	4.6	3.4	15.8	4.6	2.7
57+00/382	1.0	0	0	0	1.03	5.89	39.3	20.38	8.1	4.1	4.1	2.4	14.7	4.2	2.7
57+00/382	1.5	0	0	.04	0.1	1.4	17.27	11.19	10	10.4	9.6	8.6	31.4	6.7	2.8
57+00/382	1.75	0	0	.04	0.13	2.02	21.25	18.16	9	9.4	7.9	6.4	25.7	6	2.8
57+00/382	2.0	0	0	0	0.1	1.17	14.46	19.07	10.2	7.4	11.3	8.4	27.9	6.6	2.8
57+00/382	3.0	0	0	0	0.22	1.15	10.46	18.87	12.5	9	10.3	8.4	29.1	6.9	2.7
57+00/382	4.0	0	0	0	0.22	0.83	5.62	15.73	13.2	11	10.2	9.3	33.9	7.4	2.6
57+00/383	0.25	0	0	0.14	0.57	2.33	23.29	39.37	14.4	4.8	3.3	2.4	9.4	4.8	2.3
57+00/383	0.5	0	0	0.15	0.89	6.03	41.94	18.69	7.2	4.9	3.7	2.7	13.8	4.1	2.7
57+00/384	0.25	0	0	.07	0.58	2.76	26.7	44.49	10.4	3.3	2.2	2.1	7.4	4.4	2.2
57+00/384	0.5	0	0	.03	0.7	2.65	24.92	33.4	14.3	5.8	2.4	3	12.8	4.9	2.5
57+00/384	0.75	0	0	0.24	0.82	5.41	41.69	17.84	7.4	5.1	4.1	3.2	14.2	4.1	2.7
57+00/384	1.0	0	0	0	0.96	5.66	32.2	17.18	7.6	6.4	6.2	3.7	20.1	5	2.9
57+00/384	1.25	0	0	.06	0.14	1.81	22.71	13.68	9.1	9.1	8.3	7.2	27.9	6.1	2.9
57+00/384	1.5	0	0	.05	0.13	1.71	18.44	14.77	9.3	9	8.1	7.8	30.7	6.5	2.9
57+00/384	1.75	0	0	.07	0.26	2.54	18.2	13.83	9.9	8.9	8.6	7.8	29.9	6.4	2.9
57+00/384	2.0	0	0	0	.09	1.67	17.66	22.58	7.6	11.8	8	6.1	24.5	6.2	2.8
57+00/384	2.25	0	0	.02	0.1	1.35	11.05	15.48	10.4	10.2	9.6	9.5	32.3	7	2.7
57+00/384	2.50	0	0	0.14	0.21	2.11	11.58	20.06	12.6	9.7	7.9	7.1	28.6	6.7	2.8
7+00/384	2.75	0	0	.03	.07	1.03	13.88	23.09	12.5	9.2	6.6	7.4	26.2	6.4	2.7
57+00/384	3.0	0	0	0	0.16	0.76	4.71	18.17	10.4	11	12.2	9.7	32.9	7.5	2.6
57+00/385	0.25	0	0	.03	0.24	1.85	23.58	48	10.8	2.4	1.7	2.1	9.3	4.6	2.2
57+00/385	0.5	0	0	.07	0.57	4.67	25.23	38.46	10.6	3.7	2.6	2.5	11.6	4.7	2.4
57+00/385	0.75	0	0	.09	0.19	2.21	24.44	20.67	9.9	7.7	6.2	6.4	22.2	5.6	2.8
57+00/385	1.0	0	0	0	0.22	1.71	14.67	16.8	10.6	10	10	8.4	27.6	6.6	2.8
57+00/385	1.25	0	0	.02	.08	0.99	10.82	10.09	10	13.4	9.4	9.2	36	7.3	2.7
57+00/385	1.5	0	0	.02	0.14	1.71	19.31	20.42	10.6	8.6	7.6	5.8	25.8	6.1	2.8
57+00/385	1.75	0	0	.02	0.11	2.13	18.29	19.45	9.8	9.7	7.6	5.8	27.1	6.2	2.8
57+00/385	2.0	0	0	0	0.26	1.34	10.68	17.82	12.6	11.7	8.6	11.6	25.4	6.8	2.7
57+00/385	2.25	0	0	0.1	0.16	1.72	20.1	21.12	9.3	9.4	6.9	6.3	24.9	6	2.8
57+00/385	2.5	0	0	0.1	0.15	1.33	17.72	21.4	11.3	8.9	6.8	6.3	26	6.2	2.8
57+00/385	2.75	0	0	.02	0.11	1.86	10.3	22.71	13.5	10	7.4	4.9	29.2	6.7	2.7

CORE	DEPTH	Phi -1	Phi 0	Phi 1	Phi 2	Phi 3	phi 4	Phi 5	Phi 6	Phi 7	Phi 8	Phi 9	>Phi 9	I	SD
57+00/386	0.25	0	0	0.12	0.67	7.35	32.21	34.85	7.8	3.6	1.6	2	9.8	4.2	2.4
57+00/386	0.5	0	0	0.51	0.93	6.69	41.71	17.36	7.4	5	2.9	2.9	14.6	4.1	2.7
57+00/386	1.0	0	0	0	0.38	2.99	21.95	16.18	9.5	8.7	8.3	6.5	25.5	6	2.9
57+00/388	0.25	0	0	.03	0.54	2.48	26.72	44.53	9.1	3.4	1.9	1.6	9.7	4.5	2.3
57+00/388	0.5	0	0	.04	0.18	1.45	20.74	20.69	13	8.8	6.7	5	23.4	5.9	2.8
57+00/388	0.75	0	0	.02	0.17	1.95	29.96	19.9	9.5	7.8	5.9	4.1	20.7	5.2	2.8
57+00/388	1.0	0	0	0	1.03	5.89	44.7	19.98	6.8	3.6	3	2.5	12.5	3.8	2.6
57+00/388	1.25	0	0	0.29	0.21	2.22	21	12.18	9.5	9.9	7.8	7.5	29.4	6.3	2.9
57+00/388	1.5	0	0	.04	0.1	1.14	17.51	12.91	9.9	9.8	9.2	7.7	31.7	6.6	2.8
57+00/388	1.75	0	0	.06	0.14	1.33	17.61	13.66	10	9.8	8.7	8.7	30	6.5	2.8
57+00/388	2.0	0	0	0	0.18	1	14.43	22.89	5.3	9.6	9.2	8.8	28.6	6.6	2.8
57+00/388	3.0	0	0	0	1.23	1.98	14.04	20.75	10.5	8.9	7.5	7.5	27.6	6.5	2.8
57+00/39	1.0	0	0	0.2	1.1	4.3	10.9	20.1	14.1	13.9	9.1	9.1	17.2	6.3	2.7
57+00/39	3.0	0	0	0	0.3	1	4.2	11.8	11.9	15.1	12.7	9.3	33.7	7.6	2.5
57+00/390	1.0	0	0	0	0.18	1.09	39.34	26.29	7.7	4.8	3.6	3.2	13.8	4.3	2.6
57+00/390	2.0	0	0	0	0.22	1.34	21.54	21.2	9.5	7.7	8.5	5	25	5.9	2.8
57+00/390	3.0	0	0	0	0.2	1.54	15.29	30.97	8.9	9.8	5.1	5.4	22.8	6	2.7
57+00/391	1.0	0	0	0	0.14	0.63	36.22	24.21	7.8	7.6	4.1	4.4	14.9	4.6	2.6
57+00/391	2.0	0	0	0	0.7	4.59	25.7	19.11	8.8	7.4	6.3	5.6	21.8	5.5	2.9
57+00/391	3.0	0	0	0	0.26	1.48	11.69	20.87	10.7	7.7	10.4	8.6	28.3	6.7	2.7
57+00/392	1.0	0	0	0	0.16	0.81	37.78	26.65	5.7	6.7	4	4.2	14	4.4	2.6
57+00/392	2.0	0	0	0	0.56	4.7	33.19	19.35	8.4	6.3	4.3	4.3	18.9	4.9	2.8
57+00/392	3.0	0	0	0	0.18	1.08	17.5	20.84	9.9	7.9	8.3	7.3	27	6.3	2.8
57+00/392	4.0	0	0	0	0.14	1.35	17.53	24.98	10.6	7.8	6.8	6.6	24.2	6.1	2.8
57+00/393	1.0	0	0	0	0.58	3.36	42.35	21.01	7	3.9	4.9	2.2	14.7	4.1	2.7
57+00/393	2.0	0	0	0	0.38	3.07	30.98	19.57	7.4	7.2	6.3	4.3	20.8	5.1	2.8
57+00/393	3.0	0	0	0	0.32	3.52	23.5	22.66	10	6.8	6.1	5	22.1	5.6	2.8
57+00/394	1.0	0	0	0	0.14	0.46	29.44	26.86	10	7.9	4.7	4.1	16.4	5	2.6
57+00/394	2.0	0	0	0	0.64	4.9	35.14	18.32	6.7	7.5	3.4	5.2	18.2	4.7	2.8
57+00/394	3.0	0	0	0	0.26	1.09	13.91	19.94	8.9	10.5	7.2	8.4	29.8	6.6	2.8
57+00/394	4.0	0	0	0	.02	1.69	11.61	24.68	10.8	9	8.3	7	26.9	6.6	2.7
57+00/395	1.0	0	0	0	0.23	1.46	46.94	23.77	6	4.1	3.1	2.6	11.8	3.7	2.5
57+00/395	2.0	0	0	0	0.82	3.98	35.93	15.57	9.7	5.4	5	3.9	19.7	4.8	2.9
57+00/395	3.0	0	0	0	0.31	1.51	15.07	19.11	6	13	8.6	8.8	27.6	6.6	2.8
57+00/395	4.0	0	0	0	0.26	1.23	11.08	27.63	10.6	9.7	6.1	7.4	26	6.5	2.7

CORE	DEPTH	Phi -1	Phi 0	Phi 1	Phi 2	Phi 3	phi 4	Phi 5	Phi 6	Phi 7	Phi 8	Phi 9	Phi 9	X	SD
57+00/396	1.0	0	0	0	0.65	5.5	31.53	20.72	8.1	5.9	5.1	4.5	18	4.9	2.8
57+00/396	2.0	0	0	0	0.15	1.35	22.36	19.24	9.5	8.2	7.5	4.9	26.8	5.9	2.8
57+00/396	3.0	0	0	0	0.28	1.19	15.22	19.71	9.8	8.8	8.6	6.2	30.2	6.5	2.8
57+00/396	4.0	0	0	0	0.24	2.04	10.84	20.28	11.6	8.5	8.5	6.1	31.9	6.8	2.8
57+00/40	1.0	0	0	2.6	2.8	9.9	18	12	6.6	7.7	5.8	5.7	28.9	6	3.3
57+00/40	3.0	0	0	1.1	1.6	6.4	13.3	11.7	7.3	9	9.2	8	32.4	6.7	3.1
57+00/400	1.0	0	0	0	0.26	0.57	1.64	40.83	19.2	12.5	5.2	4.7	15.1	6.4	2.3
57+00/400	2.0	0	0	0	0.24	0.5	1.94	32.62	28.5	12.6	6	5.1	12.5	6.4	2.2
57+00/401	1.0	0	0	0	0.58	0.87	1.66	39.79	25.3	12.1	6.1	2.5	11.1	6.2	2.2
57+00/401	2.0	0	0	0	0.14	0.22	0.62	11.02	14	18.9	13.3	10.2	31.6	7.8	2.3
57+00/43	1.0	0	0	0.2	0.6	3.8	29.3	15.7	9.8	8.9	7	6.9	17.8	5.2	2.8
57+00/47	1.0	0	0	0	0	0	1.3	13.4	12	23.3	15	16.5	18.5	7.5	2.1
57+00/48	1.0	0	0	0	0	0.2	5.4	28.4	31.1	10.3	5.2	5.9	13.5	6.3	2.3
57+00/50	0.75	0	0	0	0.6	2.1	38.6	20.7	9.2	6.2	4.5	4.4	13.7	4.4	2.6
57+00/52	1.0	0	0	0	0	0.6	3.8	26.8	25.5	15.1	7.7	6.3	14.2	6.5	2.3
57+00/524	1.0	0	0	0	0.2	0.44	2	34.86	28.5	11.4	5.5	4.4	12.7	6.3	2.2
57+00/524	2.0	0	0	0	0.17	0.33	0.97	31.03	25.3	16	6.4	4.6	15.2	6.6	2.2
57+00/53	1.0	0	0	0	0	0.8	1.9	22.6	30.4	15.2	8.4	5.7	14	6.6	2.2
57+00/54	1.0	0	0	0	0	0.6	2.4	31.7	26.4	13.1	6.6	5.8	13.4	6.5	2.2
57+00/55	1.0	0	0	0	0	0.5	3.8	42.1	24.9	8	4.7	5	10	6	2.2
57+00/6	1.0	0	0	0	0.3	0.6	2.5	23	17.4	16.3	12.1	10.4	17.4	7	2.3
57+00/7	1.0	0	0	0	0.2	0.4	2.5	25.2	26.4	14.8	9.2	7	14.3	6.7	2.2
57+00/8	1.0	0	0	0.2	0.9	1.6	10.5	32.9	18.2	7.9	2.7	2	23.1	6.1	2.7
57+01/1	0.75	0	0	0.6	2.2	7	19.4	12.9	8.1	7.2	8	5.6	29	6.1	3.1
57+01/10	1.0	0	0	0	0	1.9	5.1	5.9	6.8	10.4	14.9	17.2	37.8	8	2.4
57+01/10	3.0	0	0	0	0	1.7	5.2	7.1	8.4	11.2	16.4	18	37	8	2.4
57+01/10	5.0	0	0	0	0	1.3	5.1	6.9	7.1	9.4	14	11.5	44.7	8.1	2.4
57+01/109	1.0	0	0	0	0.2	0.4	15.6	36.2	19.7	7.9	2.6	1.9	11.5	5.1	2.3
57+01/109	3.0	0	0	0	0.2	0.4	8.2	31.1	17.5	11.6	4.7	3.4	22.9	6.4	2.6
57+01/11	1.0	0	0	0	0	2.2	7.5	7.7	4.5	8.4	15.2	14.2	40.3	7.8	2.6
57+01/11	3.0	0	0	0	0	2.5	6.4	8	7.3	12	10.3	12.9	40.6	7.8	2.6
57+01/11	5.0	0	0	0	0	3.7	26.2	18.6	9.9	7	5.9	5.5	23.6	5.6	2.9

CORE	DEPTH	Phi -1	Phi 0	Phi 1	Phi 2	Phi 3	phi 4	Phi 5	Phi 6	Phi 7	Phi 8	Phi 9	Phi 9	X	SD
57+01/110	1.0	0	0	0	0.2	0.8	52.7	32.6	6.2	1.9	0.4	0.6	4.6	2.9	1.9
57+01/110	3.0	0	0	0	0.1	1	47.1	31.3	8.6	2.9	2.2	1.3	5.5	3.4	2
57+01/111	1.0	0	0	0	0.2	2.3	71.4	21.5	3.1	0.7	0.4	0.2	0.2	1.8	1.2
57+01/111	3.0	0	0	0	0.2	0.5	26.8	52.1	10.3	4	1.5	0.9	3.7	4.2	1.8
57+01/111	5.05	0	0	0	0.2	0.4	32.8	50.8	9.1	2.4	1.1	0.5	2.7	3.8	1.6
57+01/130	1.0	0	0	0	0.2	1	24.6	25.4	14.4	9.1	4.8	3.2	17.3	5.3	2.6
57+01/130	3.0	0	0	0	0	0.7	20.9	21.4	14.9	10.4	6.1	5.8	19.8	5.8	2.7
57+01/130	4.64	0	0	0	0.6	1.2	13.7	19.3	11.8	10.6	9.8	5.4	27.6	6.5	2.7
57+01/133	1.0	0	0	0	0	0	0.5	4.3	2.5	10.3	17.9	16.7	47.8	8.8	1.9
57+01/133	3.0	0	0	0	0	0	1.2	5.5	7.4	10.9	15.4	16.6	43	8.5	2.1
57+01/133	4.95	0	0	0	0	0.2	6.4	23.8	20.8	9.5	8.1	6.5	24.7	6.8	2.5
57+01/147	1.0	0	0	0	0.3	0.9	3.3	3.7	5.7	7	17.2	14.8	47.1	8.4	2.2
57+01/147	3.0	0	0	0	0	1.1	5.3	11.8	14.7	10.9	15.6	13.3	27.3	7.4	2.4
57+01/149	1.0	0	0	1.4	2	9.6	15.7	10.9	7.2	8.3	5.6	5.6	33.7	6.4	3.2
57+01/149	3.0	0	0	0	0.5	2.4	7.4	7.2	5.2	7.6	11.3	13.4	45	7.9	2.6
57+01/149	4.88	0	0	0	1	6.8	19.7	6.9	4.9	7	10.4	11.4	31.9	6.5	3.1
57+01/2	1.0	0	0	0	0.4	6.1	26.1	17.7	10.2	6.7	3.5	4.1	15.2	4.5	2.7
57+01/2	3.0	0	0	0	0.9	3.1	9.2	7.4	5.5	8.8	13.5	14	37.6	7.6	2.7
57+01/214a	6.0	0	0	0	0.17	1.96	17.41	25.36	19.7	8.7	5.3	4.3	17.1	5.7	2.6
57+01/214a	8.1	0	0	0	.09	1.55	15.67	18.69	11.7	8.7	7.7	7.5	28.4	6.5	2.8
57+01/214a	10.0	0	0	0	0.18	1.7	16.44	21.48	13.9	9.3	5.5	5	26.5	6.2	2.8
57+01/214a	11.9	0	0	0	0	0.17	0.93	18.1	15.3	14.7	5.9	4.9	40	7.7	2.5
57+01/214a	13.9	0	0	0	0	0.36	11.72	23.52	15.4	11.3	5.6	4.4	27.7	6.5	2.7
57+01/214a	15.9	.06	.05	.05	0.13	0.89	14.68	21.24	16.9	9.6	6.6	5	24.8	6.3	2.7
57+01/214a	17.9	0	0	0.24	0.64	2.77	6.43	7.72	4.6	8.5	10.6	10.3	48.2	8	2.7
57+01/214a	20.0	0	0	0.26	0.57	2.48	6.54	7.65	7.4	8.3	10.7	9.3	46.8	7.9	2.7
57+01/214a	28	0.51	0.49	0.5	1.15	2.94	6.85	7.26	5.9	7.6	10.6	8.9	47.3	7.8	2.9
57+01/214a	29.5	0	0	0.11	0.35	-0.25	6.23	11.16	4	9.5	9.5	9.9	49.5	8	2.5
57+01/214a	33.0	0	0	0.34	0.72	.05	9.95	11.04	3.2	8.5	8.1	7.7	50.4	7.8	2.8
57+01/214a	35.0	0	0	0	0.18	0.7	2.46	7.26	5.8	8	12.6	8.4	54.6	8.5	2.3
57+01/214a	36.0	0	0	0	0.28	1.83	7.12	3.27	12.5	9	10.7	10.1	45.2	7.9	2.6
57+01/214a	37	0.13	0.32	.02	.08	0.72	1.98	6.05	6.3	10.8	10.4	10	53.2	8.5	2.4
57+01/214a	38.0	0	0	0	0	0.53	2.28	8.39	9	12.2	10	10.8	46.9	8.2	2.3

CORE	DEPTH	Phi -1	Phi 0	Phi 1	Phi 2	Phi 3	ohi 4	Phi 5	Phi 6	Phi 7	Phi 8	Phi 9	>Phi 9	I	SD
57+01/214b	41.0	0	0	0	0	0.64	2.29	3.67	4.9	10.6	10.7	9.9	57.3	8.7	2.2
57+01/214b	43.0	0	0	0	0	1.66	7.44	5.7	6.8	8.5	12	10.2	47.7	8	2.5
57+01/214b	45	0	0	0	0	1.13	4.68	8.29	5.6	6.9	13.1	14.2	46.1	8.2	2.4
57+01/214b	47.0	0	0	0	0	1.28	4.82	7.3	5.8	9.4	11.8	10.8	48.8	8.2	2.4
57+01/214b	51.0	0	0	0	0	1.05	4.45	7.5	4.6	10.7	12.8	12.5	46.4	8.2	2.4
57+01/214b	56.15	0	0	0	0	1.1	4.54	8.36	7.1	9.5	12.5	12.3	44.6	8.1	2.4
57+01/214b	57.9	0	0	0	0	2.28	9.76	10.76	5.4	8.9	10.6	10.6	41.7	7.5	2.7
57+01/214b	59.9	0	0	0	0	1.73	7.09	8.38	6.7	8.9	12.6	10.9	43.7	7.9	2.6
57+01/214b	69.9	0	0	0	0	1.3	5.37	8.03	5.1	11.2	11.7	11.2	46.1	8.1	2.5
57+01/214b	85.0	0	0	0	0	0.48	2.14	7.08	6.9	9.6	12.6	11.6	49.6	8.4	2.3
57+01/214b	92.1	0	0	0	0	0.38	1.69	5.33	7.2	10.2	11.3	12.3	51.6	8.6	2.2
57+01/214b	94.9	0	0	0	0	0.13	1.04	2.83	6.7	11.1	11.2	11.5	55.5	8.8	2
57+01/214b	102.8	0	0	0	0	0.67	2.84	5.19	7.1	12.2	8.8	11.2	52	8.4	2.3
57+01/214b	107.5	0	0	0	0	0.73	4.11	12.16	13.2	12	11.3	10	36.5	7.7	2.5
57+01/214b	116.1	0	0	0	0	0.47	5.38	10.25	6.7	8.4	10.6	10.9	47.3	8.1	2.5
57+01/214b	121.1	0	0	0	0	0.46	5.99	11.25	6.5	8	9.7	9.7	48.3	8	2.5
57+01/214b	121.9	0	0	0	0	0.48	9.59	9.53	5.8	8.4	8.5	8.8	48.9	7.8	2.7
57+01/214b	133.1	0	0	0	0	0.6	3.35	5.35	3.5	6.9	10.2	10.1	60	8.7	2.2
57+01/214b	144.7	0	0	0.32	0.32	1.52	16.79	20.45	11.7	9	6.6	5	28.3	6.3	2.8
57+01/214b	151.0	0	0	0	0	0.88	8.35	16.67	7.8	13.2	6.8	5.3	41	7.4	2.7
57+01/23	1.0	0	0	0	0.7	3.4	17.9	16.8	9.2	8.8	7.7	6.9	28.6	6.3	2.9
57+01/23	3.0	0	0	0	0.5	2.7	20.5	16.8	12.6	7.2	6	7.9	25.8	6	2.9
57+01/23	5.0	0	0	0	0	0.6	38.2	22.1	6.5	5.5	5.2	4.7	17.2	4.6	2.7
57+01/26	1.0	0	0	0	0.6	3.9	63.6	14.7	2.7	1.8	2.1	1.1	9.5	2.7	2.4
57+01/26	3.0	0	0	0	0.4	2.1	12.4	20.5	9.7	11.2	9	9.8	24.9	6.6	2.7
57+01/27	0.91	0	0	1.3	0.8	2.9	6.9	5.2	4.9	9.6	12.2	12	44.2	7.9	2.8
57+01/32	0.57	0	0	0	0.2	3.4	29.2	24.1	9.7	7.2	4.2	5.7	16.3	5	2.7
57+01/34	0.59	0	0	0	1.6	7.1	16.7	13.9	12.3	8.7	7	5.3	27.4	6.2	3
57+01/35	1.0	0	0	0	0.3	1.2	1.8	4.4	5.5	9.9	14.2	14.5	48.2	8.5	2.2
57+01/35	3.0	0	0	0	0	0.3	1	3.1	3.5	10.9	14.7	13.2	53.3	8.8	2
57+01/37	1.0	0	0	0	0.4	3.1	26.9	20.4	5.2	3.9	4	3.3	17.9	4.5	2.8
57+01/37	3.0	0	0	0	0.2	10.6	26.9	29	8.4	3.7	1.4	1.6	8.2	3.9	2.3
57+01/37	5.0	0	0	0	0.4	8.1	36.8	20.4	5.2	3.9	4	3.3	17.9	4.5	2.8

CORE	DEPTH	Phi -1	Phi 0	Phi 1	Phi 2	Phi 3	phi 4	Phi 5	Phi 6	Phi 7	Phi 8	Phi 9	>Phi 9	M	SD
58-02/121	1.9	3.11	1.73	1.81	7.97	40.97	23.93	5.93	2.28	2.05	2.14	1.48	6.61	3.5	2.8
58-02/121	2.4	25.02	4.5	3.93	6.76	12.09	14.46	10.35	6.19	4.77	3.56	2.73	5.65	3.2	3.8
58-02/139	2.5	0	0	.07	0.52	1.31	1.9	7.21	14.15	14.21	13.16	11.82	35.65	7.9	2.4
58-02/139	4.1	3.69	1.4	1.56	5.25	15.6	21.55	9.75	5.76	4.48	5.01	5.93	20.03	5	3.6
58-02/139	4.5	3.01	1.29	3.43	13.12	21.99	19.8	9.14	4.92	3.63	3.72	3.82	12.14	4.3	3.3
58-02/139	5.45	3.68	1.07	2.57	11.22	24.95	20.1	7.33	3.75	2.39	2.02	2.15	18.78	4.4	3.5
58-02/164	1.7	0	0	0	.05	0.11	5.38	27.93	17.46	10.24	6.04	5.18	27.61	6.9	2.6
58-02/164	2.7	0	0	0	0	0	0.47	4.99	15.05	15.24	12.76	10.32	41.17	8.2	2.2
58-02/164	4.5	3.15	2.5	2.62	2.93	22.41	28.37	11.96	5.44	3.37	2.98	2.61	11.65	4	3.2
58-02/164	5.1	3.43	2.72	3.02	6.28	19.73	22.32	11.16	5.63	4.42	4.49	3.48	13.31	4.3	3.4
58-02/164	5.4	3.37	0.44	0.61	1.98	26.8	44.36	13.9	2.51	1.08	0.99	0.64	3.31	2.7	2.2
58-02/176	0.5	0	0	0.48	5.03	18.16	49.56	14.32	2.37	0.99	1.13	0.95	7.01	2.9	2.3
58-02/176	1.4	0	0	2.22	7.34	15.15	20.02	7.53	5.51	4.28	5.29	5.22	27.44	5.6	3.5
58-02/176	3.2	0	1.12	1.86	7.31	12.94	19.12	8.66	5.33	5.58	3.51	5.65	28.91	5.7	3.5
58-02/231	1.7	0	0	.08	0.13	0.55	9.05	30.73	16.28	9.78	5.86	5.39	22.17	6.4	2.6
58-02/231	3.2	19.35	1.96	2.48	9.28	24.4	21.09	5.22	2.37	1.79	2.18	0.74	9.15	3.1	3.5
58-02/231	4.0	8.04	0.84	2.04	10.7	28.98	27.32	7.88	2.02	2.35	1.19	0.7	7.95	3.2	3
58-02/257	1.0	0	0	.09	0.87	3.56	20.22	15.17	8.57	7.08	3.61	9.76	31.07	6.3	3
58-02/257	1.5	0	0	0.9	5.97	11.94	15.83	10.54	6.63	6.24	4.84	5.91	31.2	6.1	3.4
58-02/257	1.8	4.48	1.35	1.98	7.76	17.87	20.33	6.44	4.01	2.79	4.3	3.24	25.46	5	3.8
58-02/257	1.85	1.88	1.63	2.32	9.4	18.98	20.3	6.92	4.16	3.66	3.83	6.72	20.2	4.9	3.6
58-02/257	4.15	2.1	0.9	2.99	11.38	18.86	25.15	14.19	6.51	3.52	2.01	1.58	10.8	4	3
58-02/259	0.4	1.26	2.12	2.78	5.03	18.05	45.37	12.41	3.76	0.13	0.99	1.25	6.87	2.9	2.6
58-02/259	0.7	1.72	0.34	1.09	3.61	7.86	14.05	10.92	4.96	5.87	6.38	7.52	35.67	6.5	3.5
58-02/295	1.5	18.24	1.26	1.34	5.67	30.47	27.79	5.82	1.91	0.76	1.24	0.66	4.85	2.6	3.1
b58-01/373	3.2	0	0	0	0.21	0.62	31.36	33.39	8.02	3.58	2.69	2.43	17.71	4.7	2.7
b58-01/373	4.5	0	0	0	0.13	0.36	20.54	37.99	10.48	5.98	4.88	2.7	16.95	5.3	2.6
b58-01/373	7.9	5.42	1.88	3	6.06	12.35	21.91	10.51	5.47	4.1	4.32	3.77	21.21	4.8	3.7
b58-01/373	13	3.39	0.83	1.69	6.14	12.12	18.66	10.7	6.32	5.29	5.26	4.74	24.86	5.4	3.6
b58-01/373	15.4	0	0	0	.08	0.42	6.96	19.75	12.27	7.98	8.37	6.42	37.75	7.3	2.7
b58-01/373	18.7	0	0.42	0.31	1.35	2.71	3.75	5.23	6.19	6.42	10.73	11.35	51.54	8.2	2.7
b58-01/373	19.5	1.37	0.11	0.57	2.46	4.58	5.44	5.22	4.65	6.37	9.32	9.98	49.92	7.9	3.1

CORE	DEPTH	Phi -1	Phi 0	Phi 1	Phi 2	Phi 3	phi 4	Phi 5	Phi 6	Phi 7	Phi 8	Phi 9	>Phi 9	I	SD
58-01/200	0.8	1.34	1.62	2.57	9.18	22.01	21.94	8.31	4.47	3.29	3.62	3.38	18.27	4.6	3.4
58-01/200	1.5	0.67	1.46	2.22	7.87	17.15	23.88	9.16	4.02	3.25	3.78	3.67	22.89	4.9	3.5
58-01/200	2.5	2.08	1.36	2.59	8.9	19.09	27.23	10.59	4.29	3.11	3.07	2.92	14.78	4.2	3.3
58-01/200	4.5	1.41	2.03	3.16	10.18	22.46	33.65	11.46	3.74	3.36	2.76	1.96	3.84	3.2	2.6
58-01/207	0.5	0	0.76	1.31	3.31	9.33	19	10.45	6.41	6.15	6.52	5.84	30.93	6	3.3
58-01/207	1.5	1.85	0.86	1.22	3.78	9.67	17.09	9.3	7.69	5.75	7.97	4.61	30.22	6	3.5
58-01/207	2.4	0.88	0.92	1.33	5.3	9.03	14.46	7.39	8.27	6.09	7.3	6.2	32.83	6.3	3.5
58-01/207	4.5	0.54	0.73	1.44	3.35	9.45	19.17	9.19	6.69	5.87	6.25	6.51	30.81	6	3.4
58-01/208	1.9	0	0.15	0.73	1.31	3.21	9.77	20.06	11.08	9.5	8.57	7.17	28.45	6.7	2.9
58-01/208	1.9	0	.04	0.2	0.36	0.89	2.71	5.83	5.7	8.2	9.82	11.7	54.54	8.5	2.4
58-01/222	1.8	0.29	0.57	0.19	0.67	1.43	2.57	5.41	8.07	13.32	11.27	8.83	47.39	8.2	2.6
58-01/222	3.3	0.79	0.84	2.05	4.52	12.55	21.92	10.67	5.67	4.65	5.28	4.57	26.49	5.4	3.4
58-01/222	3.7	2.2	1.13	1.61	4.8	19.28	26.01	8.74	3.8	3.77	2.88	4.21	21.55	4.7	3.5
58-01/222	4.0	0	.05	.09	0.23	0.41	3.31	10.53	10.55	8.57	9.92	9.59	46.85	8.1	2.5
58-01/224	1.5	1.41	0.5	0.41	0.83	3.64	4.71	4.86	7.27	10.41	10.61	8.5	46.85	7.9	3
58-01/224	3.5	3.84	1.74	2.79	5.48	12.81	23.32	12.24	5.32	4.62	4.5	4.07	19.27	4.7	3.5
58-01/224	4.5	0	.03	0.11	8.3	54.32	20.48	2.64	1.8	1.88	1.43	1.69	7.31	3.8	2.6
58-01/258	0.8	0	0	0	0	0	5.32	6.75	12.59	10.34	12.83	10.34	41.84	7.9	2.4
58-01/258	2.0	1.15	0	.04	0.44	1.55	3.54	4.64	5.63	8.47	10.07	13.75	50.73	8.3	2.6
58-01/335	0.6	0	0.4	0.55	1.94	7.02	15.93	10.02	7.87	6.59	7.89	7.37	34.42	6.6	3.2
58-01/335	1.5	1.74	0.49	0.58	1.79	6.34	15.81	10.7	5.16	8.56	7.54	6.58	34.7	6.5	3.3
58-01/335	2.9	0.92	0.44	0.61	1.75	5.69	13.82	10.55	7.71	7.28	7.31	7.36	36.56	6.7	3.2
58-01/335	3.9	0.78	0.26	0.68	2.11	7.04	15.73	11.4	7.06	6.76	7.09	7.16	33.94	6.5	3.3
58-01/350	0.5	0	0.46	0.54	1.55	5.18	11.22	12.78	8.7	9.1	6.93	8.17	35.35	6.9	3
58-01/350	1.5	0	0	0	0.16	0.4	1.91	4.65	6.21	7.67	12.03	9.49	57.49	8.7	2.2
58-01/350	2.5	0	0.53	1.07	4.11	8.89	14.93	10.43	7.44	5.59	6.55	8.74	31.93	6.4	3.3
58-01/350	3.5	0.21	0.33	0.5	1.25	3.09	7.01	6.29	4.34	5.24	9.43	11.02	51.29	8	2.9
58-01/362	0.7	0	0.23	0.57	3.33	8.78	14.23	10.46	5.19	7	6.47	7.11	36.63	6.6	3.3
58-01/362	2.4	0	1.12	1.23	6.61	14.23	18.32	9.9	5.22	4.32	5.11	4.26	29.69	5.7	3.5
58-01/362	4.5	0	0.81	1.29	6.44	16.26	22.43	11.64	5.99	4.55	3.24	6.42	20.93	5.1	3.3

CORE	DEPTH	Phi -1	Phi 0	Phi 1	Phi 2	Phi 3	phi 4	Phi 5	Phi 6	Phi 7	Phi 8	Phi 9	>Phi 9	X	SD
b58-01/373	21.2	1.26	0.27	0.72	2.84	5.91	7.67	8.51	7.05	6.3	7.88	8.89	42.69	7.3	3.3
b58-01/373	24.9	0.51	0.34	1.2	3.64	7.07	10.54	8.34	6.8	6.27	7.59	7.93	39.75	7	3.3
b58-01/373	30.2	7.89	1.48	2.75	9.54	14.37	20.47	12.07	5.36	3.57	3.43	4.78	14.3	4.3	3.6
b58-01/373	31.6	3.27	0.86	1.85	7	15.21	24.4	8.66	5.39	3.63	4.94	3.29	21.49	4.8	3.5
b58-01/373	32.5	4.92	1.31	5.01	16.08	19.06	19.78	9.47	4.58	3.14	2.96	2.53	11.16	4	3.3
b58-01/373	32.7	1.43	1.4	3.07	9.85	16.79	26.01	11.13	4.41	3.35	3.18	2.37	17	4.3	3.3
b58-01/373	35.7	6.98	1.91	6.66	14.07	19.54	24.45	8.89	2.82	1.71	1.75	1.09	10.12	3.4	3.3
b58-01/373	41.2	4.19	1.56	2.41	8.53	14.94	23.36	9.34	5	4.3	3.91	2.55	19.92	4.6	3.6
b58-01/373	52.7	2.15	1.23	2.75	9.86	16.38	24.94	10.34	4.07	3.64	2.95	5.07	16.61	4.5	3.4
b58-01/373	55	1.3	1.45	3.76	12.87	18.91	25.03	9.97	4.38	2.82	2.49	3.2	13.83	4.1	3.3
b58-01/376	0.4	0	0	0	0	0.23	15.83	39.43	12.91	6.21	4.02	1.56	19.81	5.7	2.6
b58-01/376	3.5	0	0	0	0	0.2	3.84	20.25	16.36	9.12	5.41	6.89	37.93	7.5	2.6
b58-01/376	13.5	0	0	0	0.11	0.21	3.2	20.97	15.34	9.59	7.18	7.01	36.39	7.5	2.6
b58-01/376	19.5	0	0	0	0	0.24	0.95	12.34	17.14	8.33	9.15	7.83	44.03	8	2.4
b58-01/376	19.8	0	0	0	0.3	0.37	0.44	1.98	4.34	7.56	10.08	10.52	64.41	9.1	1.9
b58-01/376	23.4	0.7	0.47	0.78	2.06	5.39	12.73	12.04	7.64	6.55	7.82	5.29	38.55	6.8	3.2
b58-01/376	24.4	1.03	0.74	1.37	2.96	8.13	18.77	14.16	6.53	5.37	5.57	5.47	29.89	5.9	3.4
b58-01/376	24.5	0	0.21	0.15	5.58	39.77	36.41	6.8	1.62	1.29	1.02	1.58	5.58	3.2	2.3
b58-01/376	28	0.57	0.88	1.41	5.37	14.84	27.13	11.85	5.27	3.84	4.39	4.14	20.3	4.8	3.3
b58-01/376	30.2	0.78	0.85	1.56	6.94	16.95	20.24	9.79	6.31	4.33	5.67	4.07	22.51	5.2	3.4
b58-01/376	30.5	0	0	.07	0.28	1.31	3.11	5.41	7.76	11.8	10.12	10.38	49.75	8.3	2.4
b58-02/317	13.5	0	0	.08	0.13	0.38	14.81	29.94	13.59	7.19	5.57	3.83	24.49	6.1	2.7
b58-02/317	18	11.11	1.65	1.87	5.3	16.38	21.37	10.96	4.46	3.34	3.34	2.96	18.15	4.3	3.8
b58-02/317	19	0	0	0	0.21	1.13	29.16	25.17	7.44	5.22	5.17	5	21.5	5.2	2.8
b58-02/319	7.5	0	0.23	0.9	2.99	8.74	16.8	11.3	6.88	4.08	6.29	6.22	35.57	6.4	3.3
b58-02/319	12	0.77	0.36	0.98	3.14	10.7	18.11	11.75	6.55	4.92	4.82	5.29	32.61	6	3.4
b58-02/319	12.7	3.43	0.52	1.22	4.65	11.59	20.63	9.41	5.84	4.33	5.05	5.4	27.93	5.5	3.6
b58-02/319	12.9	1.84	1.47	2.13	8.3	17.38	23.68	10.22	3.66	4.48	3.78	4.24	18.81	4.7	3.4
b58-02/319	16.5	0.27	0.22	0.33	1.36	4.56	11.17	11.15	7.85	7.81	8.13	7.07	40.09	7.1	3
b58-02/319	17.6	0	0	0.33	1.1	4.34	22.02	13.09	9.73	7.51	5.65	4.6	31.62	6.1	3
b58-02/319	20.1	9.88	0.81	0.85	2.37	4.49	19.21	12.09	5.92	5.51	1.78	9.36	27.73	5.4	4
b58-02/319	20.7	0	0	0.47	1.4	4.11	22.79	13.13	9.6	5.55	5.44	5.51	32	6	3.1
b58-02/319	20.9	0	0	0.45	1.04	3.48	21.71	12.86	9.32	6.76	6.28	5.35	32.75	6.2	3.1

CORE	DEPTH	Phi -1	Phi 0	Phi 1	Phi 2	Phi 3	phi 4	Phi 5	Phi 6	Phi 7	Phi 8	Phi 9	>Phi 9	I	SD
58+01/09	1.3	0.41	0.32	0.46	0.18	5.79	12.77	7.32	5.35	7.04	7.92	6.42	46.02	7.3	3.1
58+01/112	0.5	0	.04	0.32	3.16	22.26	53.64	5.97	2.02	1.65	1.16	5.51	4.26	2.8	2.3
58+01/112	0.9	0	0	0.24	2.31	27.1	48.87	5.26	2.17	1.6	1.91	4.19	6.35	3	2.5
58+01/112	2.5	0	0	0.21	0.42	1.61	45.42	24.83	7.58	3.85	2.65	5.08	8.35	3.7	2.4
58+01/112	4.3	0	0	0	0	0.26	5.27	7.74	8.19	11.52	9.6	14.45	42.96	8	2.4
58+01/112	5.65	0	0	0	0	.07	2.76	10.29	8.44	9.77	7.56	3.75	57.36	8.3	2.4
58+01/113	0.5	0	0.28	0.31	3.69	22.79	55.72	6.61	1.5	1.29	0.27	0.72	6.82	2.5	2.3
58+01/113	1.6	0	.09	0.19	0.8	3.38	18.17	12.06	7.59	6.2	6.03	6.29	39.21	6.7	3.1
58+01/113	2.5	0	0	0.16	0.87	3.21	10.68	10.68	9.04	9.15	7.47	6.3	42.44	7.3	2.9
58+01/114	0.09	0	0	0.4	0.58	3.86	19.55	11.83	12.27	11	5.37	11.9	23.23	6.1	2.9
58+01/114	0.5	0	0	0	0.4	7.03	73.97	8.02	1.55	0.64	0.36	3.77	4.26	1.9	2
58+01/114	1.5	0	0	0	.06	0.95	10.48	15.47	12.7	8.13	8.36	12.78	31.07	7.1	2.7
58+01/114	3.5	0	0	0.19	0.24	1.33	46.22	11.03	5.69	5.76	3.79	8.58	17.18	4.3	2.9
58+01/114	4.3	0	0	0	0.2	0.98	51	12.94	4.07	4.27	2.25	1.96	22.33	4	2.9
58+01/127	0.5	.06	0.1	0.29	1.37	12.36	32.82	22.64	6.32	4.08	3.1	1.95	14.91	4.4	2.8
58+01/127	0.9	0	0	0	1.28	6.07	17.27	19.16	8.19	7.34	5.27	4.63	30.8	6.2	3
58+01/136	5.5	0	0	0	.09	1.12	58.21	17.62	4.69	2.42	1.89	2.14	11.83	3.1	2.5
58+01/61	0.5	0.59	0.43	0.72	5	60.45	16.83	5.18	1.5	1.16	0.62	1.05	6.48	3.8	2.4
58+01/61	0.9	0	.06	0.15	4.6	76.22	11.18	3.81	0.32	0.25	.06	0.41	2.95	3.8	1.8
58+01/61	2.2	0	0.21	0.26	1.2	13.52	26.18	11.45	6.28	5.2	5.08	3.91	26.7	5.4	3.2
58+01/82	0.25	0	0	0.29	1.89	11.49	19.44	27.52	11.99	4.35	3.21	7.96	11.86	5.1	2.7
58+01/82	0.45	0	0	0	0	0	3.08	6.07	10.91	11.17	10.49	19.58	38.7	8.2	2.2
58+01/82	0.75	0	0	0.52	1.19	5.69	12.71	9.43	6.49	7.04	8.36	13.18	35.41	7	3
58+01/82	1.5	0	0.15	0.26	0.56	2.87	10.75	13	9.71	8.91	8.17	12.39	33.23	7.1	2.8
58+01/82	5.2	0	0.55	0.67	1.22	5.9	13.56	8.81	6.72	7.01	5.18	2.51	47.88	7.1	3.2
b58+00/28a	0.5	0	0	0.14	.09	0.23	0.43	7.81	14.3	15.7	14	13.7	33.6	8	2.2
b58+00/28a	1.3	0	0	.06	0.59	.01	1.46	7.48	11.7	15.1	12.6	13.4	37.6	8.1	2.3
b58+00/28a	3.8	0	0	0.14	0.64	4.02	7.39	8.21	9.7	11.9	10.3	10.7	37	7.5	2.7
b58+00/28a	4.4	0	0	.06	0.39	0.48	2.07	7.8	11.3	15.1	12.9	10.7	39.2	8	2.3
b58+00/28a	5.4	0	0	.06	0.12	1.22	2.44	6.36	10.4	14.4	12.8	12.3	39.9	8.1	2.3
b58+00/28a	6.15	0	0	.08	0.1	0.44	1.25	6.93	13.2	14.2	13.1	12	38.7	8.1	2.3
b58+00/28a	6.8	0	0	.06	0.12	0.75	1.86	4.71	9.9	12.4	12	12	46.2	8.4	2.3
b58+00/28a	7.8	0	0	0.17	.04	1.03	2.83	5.53	6.2	11	12.6	12.8	47.8	8.4	2.3

CORE	DEPTH	Phi -1	Phi 0	Phi 1	Phi 2	Phi 3	phi 4	Phi 5	Phi 6	Phi 7	Phi 8	Phi 9	>Phi 9	I	SD
b58+00/28a	8.42	0	0	.06	.06	0.9	2.28	2.2	5.7	9.4	13.2	12.7	53.5	8.7	2.1
b58+00/28a	9.9	0	0	0.12	0.14	0.5	1.62	3.12	4.3	10.2	12.7	13.2	54.1	8.7	2.1
b58+00/28a	10.7	0	0	.09	0.5	1.59	5.04	3.78	5	6.5	10.4	12.7	54.4	8.4	2.4
b58+00/28a	13.47	0.27	0.15	0.21	1.01	1.48	4.2	4.68	4.9	7.2	11.6	13.7	50.6	8.3	2.6
b58+00/28a	13.77	0.6	0.18	0.48	1.46	6.7	11.76	8.32	6	7.5	8.2	10	38.8	7.1	3.2
b58+00/28a	14.62	0.1	0.32	0.56	1.47	5.58	9.47	7.1	4.9	8.1	9.7	11.3	41.4	7.4	3
b58+00/28a	17.3	0.59	0.47	0.62	1.56	5.08	8.86	4.52	6	5.7	10.6	11.6	44.4	7.6	3.1
b58+00/28a	17.95	0.23	0.25	0.43	1.42	5.21	8.37	4.59	5.7	6.4	10.2	11.6	45.6	7.7	3
b58+00/28a	18.7	0.19	0.3	0.38	1.36	5.22	8	4.35	5.2	7	10.3	12.3	45.4	7.7	2.9
b58+00/28a	19.38	0.2	0.34	0.48	1.43	5.45	9.44	5.66	5	7.5	10.2	12.1	42.2	7.5	3
b58+00/28a	20.16	0.14	0.26	0.52	1.32	5.51	9.5	7.15	5.4	7.7	8.7	11	42.8	7.5	3
b58+00/28b	27.0	0.36	0.38	0.56	1.31	5.86	10.66	10.17	6.9	8	7.3	9.7	38.8	7.1	3.1
b58+00/28b	27.35	1.41	1.07	1.08	1.61	12.78	18.61	8.04	5.4	5.7	6.3	6.2	31.8	6	3.5
b58+00/28b	32.3	0.81	0.72	0.75	1.49	7.99	14.21	6.43	7.2	7.4	7	7	39	6.8	3.3
b58+00/28b	33.36	1.13	0.56	0.94	2.45	10.89	22.02	14.51	6.1	6.4	6.1	6.5	22.4	5.4	3.3
b58+00/28b	36.9	.07	0.32	0.55	1.53	7.6	14.86	10.67	6.9	7	7.4	7.7	35.4	6.7	3.2
b58+00/28b	38.10	0.53	0.5	0.74	2	7.41	13.47	7.35	6	7	6.8	8	40.2	6.9	3.3
b58+00/28b	43.4	0.31	0.69	0.47	2.12	8.05	12.2	6.66	6.9	7.1	7.3	8	40.2	7	3.3
b58+00/28b	46.1	0.72	0.64	0.82	2.36	8.29	11.84	7.33	7	6	6.8	8.8	39.4	6.9	3.3
b58+00/28b	52.49	.05	0.38	0.26	1.12	3.05	3.87	4.07	5.4	6.5	9.3	11.5	54.5	8.3	2.7
b58+00/28b	54.5	0.34	0.32	0.34	0.38	2.45	2.56	5.41	9.4	9.3	10.1	10.8	48.6	8.2	2.6
b58+00/28b	59.4	0	0	0.19	.07	0.24	0.62	5.58	9	14.2	14.1	11.9	44.1	8.4	2.2
b58+00/28b	72.6	0	0	0.27	0.27	0.66	1.87	5.93	11.2	16.9	12.1	8.5	42.3	8.1	2.3
b58+00/28b	74.8	0	0	.02	0.14	0.56	3.6	8.88	8	10.4	11.8	13.7	42.9	8.1	2.4
b58+00/28b	79.30	0	0	0.36	0.22	0.32	0.5	7.6	18.5	16.5	9.2	7.9	38.9	8	2.4
b58+00/28b	82.5	0	0	0.19	0.86	3.6	5.78	15.27	12.6	10.1	8.9	8.1	34.6	7.3	2.8
b58+00/28b	85.3	0.37	.08	0.32	0.8	2.22	5.76	14.95	10.2	10.1	8	8	39.2	7.4	2.8
b58+00/28b	102.2	0	0	.02	.04	0.1	0.26	1.18	3.4	9.5	14.9	15	55.6	9	1.8
b58+00/28b	111.7	0	0	.08	0.22	0.59	2.29	6.82	8.5	10.5	9.4	10.3	51.3	8.4	2.3
b58+00/28b	115	0	0	0.18	0.12	0.3	1.05	3.95	3.2	8.7	10.6	13.5	58.4	8.9	2
b58+00/28b	119.2	0	0	.02	.06	0.3	0.93	4.69	4.5	10.2	10.8	15.7	52.8	8.7	2
b58+00/28b	151.9	0	0	.03	.03	0.51	2.6	28.83	13.4	8.9	6.5	8	31.2	7.2	2.6

CORE	DEPTH	Phi -1	Phi 0	Phi 1	Phi 2	Phi 3	phi 4	Phi 5	Phi 6	Phi 7	Phi 8	Phi 9	>Phi 9	I	SD
b58+00/6	2.7	0	0	0	0	0.4	1.12	4.88	6.2	14.2	17	17.5	38.7	8.4	2.1
b58+00/6	3.36	0	0	.04	0.87	2.06	5.04	4.39	6	10.2	10.5	12.4	48.5	8.2	2.5
b58+00/6	4.95	0	0	0.8	0.72	2.41	5.74	4.83	4.6	9.2	11.3	11.2	49.2	8.1	2.7
b58+00/6	6.7	0.74	0.26	0.25	0.92	2.76	7.33	5.54	5.7	9.2	9.6	8.8	48.9	7.8	2.9
b58+00/6	8.3	1.16	0.34	0.27	1.09	3.47	9.19	7.08	4.4	8	11.6	7.4	46	7.5	3.1
b58+00/6	9	0	0	0.73	1.39	4.6	10.97	7.61	5.8	7.2	9.6	9	43.1	7.4	3
b58+00/6	10.4	0.25	0.35	0.39	1.28	4.25	10.98	5.7	5.5	8.8	9.2	9.2	44.1	7.4	3
b58+00/6	12.05	0.11	0.39	0.35	1.38	4.25	10.68	6.34	5.1	8.8	11.1	9.2	42.3	7.4	3
b58+00/6	28.62	0.24	0.26	0.26	0.87	3.08	8	9.39	4.3	10.2	11.2	10.5	41.7	7.6	2.8
b58+00/6	15.75	0.13	0.37	0.18	1.1	3.7	9.6	7.82	5.7	7.5	11	11	41.9	7.5	2.9
b58+00/6	17.05	0	0	.07	0.15	0.51	2.06	9.31	6.9	13.8	9.1	10	48.1	8.3	2.4
b58+00/6	18.35	0	0	.03	0.13	1.73	6.6	7.51	8.6	10.1	10.7	10.1	44.5	7.9	2.6
b58+00/6	19.65	0	0	0.24	0.7	4.13	17.59	18.14	9.7	7	5.9	6.7	29.9	6.3	3
b58+00/6	20.8	0	0	0	.08	0.32	5.2	16.8	10.3	8.2	9.2	8.5	41.4	7.7	2.6
b58+00/6	22.1	0	0	0.1	0.18	1.13	7.83	17.26	7.8	8.2	6.7	7.8	43	7.5	2.8
b58+00/6	23.1	0	0	0.1	0.26	1.18	6.55	15.11	9.9	7.8	8.6	7.8	42.7	7.6	2.7
b58+00/6	24.35	0.35	0.45	0.28	1.44	6.31	17.56	17.41	4.9	7.7	7.2	7	29.4	6.2	3.1
b58+00/6	25.8	0	0	0.37	0.81	5.49	19.42	18.51	10	5.6	5.8	.8	28.2	6	3
b58+00/6	26.9	0	0	0	0	0.12	1.48	11.1	11.1	10.5	9.7	10.2	45.8	8.2	2.4
b58+00/6	28.75	0	0	0	0	0.11	2.72	16.77	9.3	8.5	8.5	8.9	45.2	8	2.5
b58+00/6	30.25	0	0	0	0	0.14	3.67	18.59	10.6	9.1	7.1	8.5	42.3	7.7	2.6
b58+00/6	32.2	0	0	0	0	0.21	4.68	18.81	10.8	7.9	9	8.3	40.3	7.6	2.6
b58+00/6	33.5	0	0	0	0	0.16	4.86	17.38	10	8.4	8	7.7	43.5	7.7	2.6
b58+00/6	35.35	0	0	0	0	0.34	3.66	11.1	9	9	8.5	8.6	49.8	8.1	2.5
b58+00/6	40.00	0	0	0	0	0.21	0.66	3.93	8	10.9	10.9	10.9	54.5	8.7	2.1
b58+00/6	41.25	0	0	0	0	0.19	6.1	20.41	19	11.8	3.8	5	33.7	7.1	2.6
b58+00/6	55.55	0	0	0	0	0.16	2.04	10.7	12.1	13.4	9.4	6.7	45.5	8.1	2.4
b58+00/6	63.55	0	0	0	0	0.25	1.15	4	7.4	12.9	10	10.7	53.6	8.6	2.1

CORE	DEPTH	Phi -1	Phi 0	Phi 1	Phi 2	Phi 3	phi 4	Phi 5	Phi 6	Phi 7	Phi 8	Phi 9	>Phi 9	X	SD
58+00/107	0.5	0	0	.05	0.15	0.34	5.83	17.89	10.21	9.13	7.11	28.22	21.09	7.4	2.5
58+00/107	1.5	0	0	.06	0.18	0.63	4.76	15.75	9.53	10.08	8.35	8.33	42.33	7.7	2.6
58+00/122	5.5	0	0	.08	0.36	2.64	7.91	12.07	10.59	10.8	8.51	13.46	33.58	7.4	2.7
58+00/125	1.5	0	0	.08	0.5	4.07	11.22	10.89	10.29	8.39	9.87	7.01	37.68	7.1	2.9
58+00/135	0.45	0	.06	.06	0.42	3.19	8.66	13.53	7.89	3.61	17.02	3.1	42.45	7.4	2.8
58+00/135	0.75	0	0.16	0.55	2.04	9.27	17.98	5.62	3.14	8.67	6.38	6.03	40.17	6.6	3.3
58+00/135	2.75	0	0	0.1	0.29	0.52	2.24	4.95	10.41	11.82	10.52	8.62	50.54	8.4	2.3
58+00/135	3.65	0	0	0	0.13	0.46	3.07	5.07	7.34	9.82	9.53	7.99	56.61	8.5	2.3
58+00/135	4.5	0	0	0.1	0.1	0.29	1.19	6.35	10.4	12.48	10.36	9.58	49.16	8.4	2.3
58+00/165	2.5	0	0	0	0.12	0.19	0.62	1.1	4.82	8.86	10.23	11.33	62.73	9	1.9
58+00/165	5.5	0.32	.06	0.22	0.35	1.12	3.25	2.42	3.71	8.05	9.3	11.7	59.48	8.7	2.3
58+00/35	0.25	0	0	.01	0.32	1.95	2.29	28.93	27.5	10.7	3.9	8.5	15.9	6.6	2.4
58+00/35	0.5	0	0	.02	0.21	0.39	0.49	6.19	21	18.2	14.8	9.1	29.6	7.8	2.2
58+00/35	1.0	0	0	0	0.22	1.42	2.36	5.1	11	14.8	15.1	11.3	38.7	8.1	2.3
58+00/35	3.0	0	0	0	0.43	1.76	3.7	11.01	9.7	12.1	14.3	13.4	33.6	7.7	2.5
58+00/36	0.25	0	0	.04	0.21	1.3	2.32	31.13	27	10.4	5.7	5.6	16.3	6.5	2.4
58+00/36	0.5	0	0	.03	0.18	0.38	0.61	6.4	22.1	17	12.8	11.2	29.3	7.8	2.2
58+00/36	0.75	0	0	.03	.09	0.51	0.48	1.99	13.7	17.3	16	13.3	36.6	8.2	2.1
58+00/36	1.0	0	0	0	0.18	0.53	0.86	8.03	9.7	16.1	15.8	14.8	34	8.1	2.2
58+00/36	1.25	0	0	.03	.06	0.18	0.5	2.63	14.1	15.6	14.6	13.7	38.6	8.3	2.1
58+00/36	1.5	0	0	.08	.06	.06	0.28	5.92	14.1	16.7	15.3	13	34.5	8.1	2.1
58+00/36	1.75	0	0	.07	.04	.04	0.34	5.91	15.6	16.8	14.3	13.2	33.7	8.1	2.2
58+00/36	2.0	0	0	0	0.13	0.25	0.78	6.64	13.4	16.7	13	14.4	34.7	8.1	2.2
58+00/36	3.0	0	0	0	0.68	3.48	6.64	9.4	13	11.2	12.2	10.6	32.8	7.4	2.7
58+00/37	0.25	0	0	.04	0.49	2.53	3.02	29.82	27.4	11.3	6.1	5.4	13.9	6.4	2.3
58+00/37	0.5	0	0	.01	0.25	0.54	0.71	4.79	12.9	16.3	15.4	14.2	34.9	8.1	2.2
58+00/37	0.75	0	0	.02	0.11	0.19	0.4	7.48	11	13.9	16.5	15.1	35.3	8.2	2.2
58+00/37	1.0	0	0	0	0.61	.01	1.26	7.22	11	11.7	16.5	14	37.7	8.2	2.2
58+00/37	1.25	0	0	.05	.04	.07	0.35	10.99	11.7	16.8	13.8	15.1	31.1	8	2.2
58+00/37	1.5	0	0	.05	.04	.07	0.27	9.97	14	15.1	12.7	12.5	35.3	8	2.2
58+00/37	1.75	0	0	0	0	.05	0.24	11.01	12.1	15.8	11.9	11	37.9	8.1	2.3
58+00/37	2.0	0	0	0	.08	0.39	1	8.53	13.2	14.1	14.6	13.1	35	8	2.3
58+00/37	2.25	0	0	0	.04	0.19	0.33	7.54	14.9	16.2	10.9	12	37.9	8.1	2.2
58+00/37	2.5	0	0	0	0	0.13	0.25	8.42	12.8	15.1	13	12	38.3	8.2	2.2

CORE	DEPTH	Phi -1	Phi 0	Phi 1	Phi 2	Phi 3	phi 4	Phi 5	Phi 6	Phi 7	Phi 8	Phi 9	>Phi 9	I	SD
58+00/38	0.25	0	0	.02	0.14	0.93	3.71	38	25.7	9.2	6.1	5.3	10.9	6.2	2.2
58+00/38	0.5	0	0	.04	0.1	0.73	2.29	32.24	27.5	10.3	6.9	6.5	13.4	6.5	2.3
58+00/38	0.75	0	0	0.1	0.22	0.86	1.49	28.33	25.6	15.6	8	6.3	13.5	6.6	2.2
58+00/38	1.0	0	0	0	0.67	2.19	1.84	29.7	30.8	9.9	6	5.8	13.1	6.4	2.3
58+00/38	1.25	0	0	.05	0.14	0.37	0.49	9.15	13.4	16.1	15.7	13.1	31.5	7.9	2.2
58+00/38	1.5	0	0	.04	.08	0	0.35	10.93	13.8	15	14.1	12.7	33	8	2.2
58+00/38	1.75	0	0	.02	.04	.04	0.21	10.09	14	15.3	14.2	13	33.1	8	2.2
58+00/38	2.0	0	0	0	0.13	0.3	0.86	7.51	13.5	15.6	13.9	13.3	34.9	8	2.2
58+00/38	2.25	0	0	.03	.06	0.16	0.28	10.57	12.6	15.4	13.2	11.2	36.5	8	2.3
58+00/38	2.5	0	0	.08	.08	.06	0.11	6.57	13.6	15.5	14.8	11.6	37.6	8.2	2.2
58+00/38	2.75	0	0	0.38	0.3	1.39	2.63	12.1	10.5	14.4	11.1	9.6	37.6	7.8	2.5
58+00/38	3.0	0	0	0	0.52	2.03	3.43	6.02	12.8	15	13.9	11.1	35.2	7.8	2.4
58+00/38	3.25	0	0	0.18	0.49	3.91	7.77	8.85	11.8	12	10.6	8.3	36.1	7.4	2.7
58+00/38	3.5	0	0	1.17	0.67	3.76	6.71	7.69	10.6	13.2	10	10.6	35.6	7.4	2.8
58+00/39	0.25	0	0	.02	0.29	1.73	2.88	38.38	25.5	8.1	4.3	4	14.8	6.2	2.3
58+00/39	0.5	0	0	.08	0.41	0.85	0.66	10.7	22.2	18.5	11.2	9.9	25.5	7.5	2.3
58+00/39	1.0	0	0	0	0.25	0.98	1.49	6.98	9.1	13.3	15.8	13.4	38.7	8.2	2.3
58+00/39	2.0	0	0	0	0.25	0.95	1.63	8.37	12.3	15.8	14.9	12.9	32.9	7.9	2.3
58+00/39	3.0	0	0	0	0.47	1.4	2.67	7.66	9.9	12.9	12.3	11.5	41.2	8.1	2.4
58+00/41	0.25	0	0	0.24	1.05	3.81	2.69	21.01	18.3	12.3	8.7	8.3	23.6	7	2.6
58+00/41	0.5	0	0	.06	.06	0.12	0.24	4.32	14.8	16.5	14.1	15.5	34.3	8.2	2.1
58+00/41	1.0	0	0	0	0.17	0.38	1.04	6.71	11.4	14.1	14.2	14.5	37.5	8.2	2.2
58+00/41	2.0	0	0	0	1.08	4.4	7.14	9.58	9	8.3	12.9	9	38.6	7.5	2.8
58+00/41	3.0	0	0	0	0.41	1.09	2.42	9.88	9.3	15.2	13.6	10.3	37.8	7.9	2.4
58+00/42	0.25	0	0	.02	.08	0.55	0.22	36.83	26.6	11	5.4	4.5	14.8	6.5	2.2
58+00/42	0.5	0	0	.02	.04	0.35	2.59	31.1	26.8	10.3	8.6	6.1	14.1	6.5	2.3
58+00/42	0.75	0	0	.02	.06	0.51	2.64	28.87	29	11.7	6.7	7	13.5	6.5	2.2
58+00/42	1.0	0	0	0	0.12	0.22	1	30.76	32	11.8	6.1	5.4	12.6	6.5	2.2
58+00/42	1.25	0	0	.02	.09	0.71	3.62	25.16	29.2	12	8.7	6	14.5	6.5	2.3
58+00/42	1.5	0	0	.02	.08	0.53	2.49	24.88	30.3	12.9	7.2	6	15.6	6.6	2.3
58+00/42	1.75	0	0	.02	.08	0.36	2.6	21.94	29.6	14	8.5	8.4	14.5	6.7	2.2

CORE	DEPTH	Phi -1	Phi 0	Phi 1	Phi 2	Phi 3	phi 4	Phi 5	Phi 6	Phi 7	Phi 8	Phi 9	>Phi 9	I	SD
58+00/43	1.0	0	0	0	0.1	0.22	1.07	31.41	30.6	10.9	7.2	3.1	15.4	6.5	2.2
58+00/43	1.25	0	0	.06	.06	0.22	0.67	24.89	27.9	12.5	8.5	6.6	18.6	6.9	2.3
58+00/43	1.5	0	0	.04	.06	0.22	0.87	27.81	27.8	12.2	7.1	6.5	17.4	6.8	2.3
58+00/43	1.75	0	0	.08	0.1	0.4	0.93	27.59	29.5	11.7	6.9	5.5	17.3	6.7	2.3
58+00/43	2.0	0	0	0	0.19	0.47	1	29.14	25.6	12.1	8.9	6.6	16	6.7	2.3
58+00/43	2.25	0	0	.04	.08	0.12	0.58	21.28	31.1	13.5	9	6.4	17.9	6.9	2.2
58+00/43	2.45	0	0	.04	.04	.04	0.26	10.72	27.9	18.6	9.8	9.6	23	7.4	2.2
58+00/43	2.65	0	0	0.12	0.51	2.45	3.85	13.97	22.9	12.1	8.9	7.2	28	7.2	2.6
58+00/46	0.25	0	0	.02	0.39	1.49	1.73	21.67	29.7	14.9	8.8	6.4	14.9	6.7	2.3
58+00/46	0.5	0	0	.02	0.48	1.21	1.08	11.91	24.9	18.6	12.2	8.8	20.8	7.3	2.3
58+00/46	1.0	0	0	0	0.14	0.55	0.53	4.28	12	13.3	16.7	13.6	38.9	8.3	2.1
58+00/46	2.0	0	0	0	0.14	0.45	1.17	7.44	12.2	16	13.3	13.2	36.1	8.1	2.2
58+00/46	4.0	0	0	0	0.28	1.43	2.14	6.15	10.5	14.4	15.1	12.6	37.4	8.1	2.3
58+00/47	0.25	0	0	.06	0.67	2.96	1.75	26.96	28.1	12	8	5.9	13.6	6.5	2.3
58+00/47	0.5	0	0	.02	.06	0.49	0.62	7.31	19.8	19.4	13.7	13.4	25.2	7.7	2.2
58+00/47	1.0	0	0	0	0.15	0.39	0.46	9	12	13.2	14.2	12.8	37.8	8.1	2.3
58+00/47	2.0	0	0	0	.09	0.11	0.38	7.02	13.2	17.2	15.8	13.1	33.1	8.1	2.2
58+00/47	3.0	0	0	0	1	4.53	8.25	10.22	11.7	10.6	12.3	9.4	32	7.2	2.8
58+00/48	0.25	0	0	.02	0.17	1.35	2.4	31.76	27.6	11.8	6.7	6.6	11.6	6.4	2.2
58+00/48	0.5	0	0	.02	0.24	1.15	1.34	15.45	31.1	15.7	10.4	8.5	16.1	7	2.2
58+00/48	0.75	0	0	.02	0.17	0.66	0.7	13.45	27.4	16.5	13.7	9.5	17.9	7.2	2.2
58+00/48	1.0	0	0	0	0.24	0.39	0.44	11.33	20.9	22.1	13.2	8.4	23	7.5	2.2
58+00/48	1.25	0	0	.02	0.23	0.72	0.9	9.73	23.5	20.6	12.9	11.9	19.5	7.4	2.2
58+00/48	1.5	0	0	.02	0.6	1.2	1.01	8.67	20.8	18.2	13	10.5	26	7.6	2.3
58+00/48	1.75	0	0	.07	0.13	0.16	0.47	7.57	14.4	15.1	14.1	13.8	34.2	8.1	2.2
58+00/48	2.0	0	0	0	0.19	0.18	0.28	9.15	13.4	16.6	14.2	12	34	8	2.2
58+00/48	2.25	0	0	0.26	0.44	2.25	3.8	7.65	12.1	14.7	13.6	12.3	32.9	7.7	2.5
58+00/48	2.5	0	0	0.43	0.81	4.66	8.44	4.96	10	10.7	10.7	10.3	39	7.5	2.8
58+00/48	3.0	0	0	0	0.23	1.5	2.61	8.66	9.2	14.3	13	12.9	37.6	8	2.4
58+00/95	0.15	0	0	0.17	0.49	5.16	53.21	12.17	8.83	3.92	1.2	6.16	8.69	3.4	2.5
58+00/95	5.2	0	0.2	0.25	0.84	2.58	8.02	15.74	12.98	13.59	5.11	18.94	21.75	6.9	2.7
58+00/96	0.4	19.88	8.45	7.38	10.36	22.84	7.91	2.56	2.33	1.91	2.24	0.38	13.77	3.4	4
58+00/96	5.4	0	0.25	0.31	0.74	3.55	14.21	10.69	8.05	7.5	5.97	8.84	39.89	7	3

APPENDIX 5

X-RADIOGRAPHY

X-radiographs of a large number of whole and split cores using a SCANRAY x-ray machine (Plate 1). The cores were placed in specially built silica moulds to improve the resolution at the edges of the core. Kodak industrial x-ray film and developer was used for the negatives.

Generally, only the split cores allowed for the detailed resolution and study of sedimentary structures although it was possible to discern clast content and fabric in the whole cores. Typical machine settings are given below:

½ core	soft mud	80 KV	5 MA	2.5 minutes
½ core	compact sand	85 KV	5 MA	2.5 minutes
whole core	compact mud	95 KV	5 MA	2.75 minutes

Plate 1.

APPENDIX 6

CLAY MINERALOGY AND GEOCHEMISTRY

Introduction

This appendix describes the principal clay minerals identified in Pleistocene sediments from the North Sea. It outlines the principles behind their identification, and tabulates the results in order to provide a data set from which to refer when discussing sedimentological features in chapters 4 and 5. The results of a limited number of geochmical analyses (Tables 10-12) are briefly discussed at the end of the appendix.

Clay Minerals

Clay minerals, also known as hydrous-layer silicates belong to the larger family of phyllosilicates. Their principal building blocks are tetrahedral and octahedral sheets of which there are two principal arrangements. First, a 1:1 layer formed by linking one tetrahedral sheet with one octahedral sheet. The uppermost unshared plane of anions in the octahedral sheet then consists entirely of OH groups. Second, a 2:1 layer in which two tetrahedral sheets are linked with one octahedral sheet. The upper tetrahedral sheet is inverted so that the apical oxygen points down. If the 1:1 or 2:1 layers are not electrostatically neutral, the excess layer change is neutralised by various interlayer minerals, including individual cations, hydrated cations and hydroxide octahedral groups and sheets.

Layer silicates can be classified, on the basis of layer type, layer change, and type of interlayer, into eight major groups. This study, however, is only concerned with the following four:

Kaolin (1:1)
Smectite (2:1)
Illite (2:1)
Chlorite (2:1)

Sample Preparation

Samples for clay mineral analysis by x-ray diffraction (X.R.D) were generally collected as part of the grain size analysis procedure. Samples were primarily taken from the clay fraction, defined here as material with a particle size less than 2 μm, although occasional samples of the < 63 μm, < 15.6 μm and <4 μm fractions were also taken. The samples had been previously dispersed for grain size analysis using 4% calgon and ultrasonic vibration.

The method of thin section preparation can have a critical effect on the end results and Gibbs (1965) has shown that the pipette on glass technique, and all techniques which involve gravitational settling or centrifugation of clay particles, gave rise to size segregated specimens which are unsuitable for quantitative analysis. It was therefore decided to use the smear-on-glass slide technique (Theisen & Harward, 1962) which basically involves centrifuging and washing the sample twice prior to smearing it on a petrographic slide with a microspatula. Where cation saturation analysis was required the sample was treated with a 1n solution of the relevant cation. Several treatments were generally necessary for complete saturation, and after each treatment the clay was centrifuged and the supernatant solution removed before adding fresh chloride solution.

The Major Clay Minerals and their X-Ray Identification

Illite

The term illite was first proposed by Grim, Bray and Bradley (1937) as a group name for the clay size micaceous components in argillaceous sediments. Its identification was based primarily on the presence of a strong (001) reflection at 10Å (Fig. 1a & 1b), more accurate resolution of the 001 peak can be used to identify the actual illite polytype as shown below:-

Polytype	2M	1M	1Md (broad)
Å	10.014	10.077	10.077

Accurate identification of the illite polytype is useful because they act as a provenance indicator. For example the 1Md polytype is common in sediments and soils, the 1M type in

sediments, low grade metamorphic rocks and alteration zones, and the 2M polytypes in igneous and high grade metamorphic rocks (Caroll, 1970).

Sediments from the study area generally include both 1Md and 2M polytypes in various porportions, and display a high 10Å to 5Å ratio (Fig. 1a) which suggests an Fe-rich variety with low crystallinity (Moriarty, 1977). A number of samples, especially from the finer glaciomarine and marine sediments displayed a distinct scattering on the low angle side of the 001 reflection (Fig. 1b) which suggests that the illite forms mixed layers with other clay minerals (Thorez, 1976). Illite crystallinity indices were calculated according to Robert & Maillot (1983) and are included in Table 1-9. High values of crystallinity index often occur in association with high smectite percentages and are thought to indicate an increase in the hydrolozing capacity of the weathering environment, producing an open illite structure (Singer, 1984).

Chlorite

Well crystallised varieties can be identified by an integral series of basal reflections (Fig. 1a) at: 14Å (001), 7Å (002), 4.7Å (003), 3.5Å (004) and 2.8Å (005). Further characteristics of chlorites include the stability of the d spacings after glycolation, the enhancement of the (001) reflection after heating to 500°c (Starkey et al., 1984).

Chlorite was initially identified on the basis of the d spacings. However, reduction or even total collapse of the 14Å peak after heating the sample to 450°c suggests that the type of chlorite present in the majority of samples was of a poorly crystallised nature and probably a soil chlorite (Lucas, 1963; Starkey et al., 1984). Further to this, the weak nature of the 001 and 003 peaks in most of the sediments analysed suggests that the chlorite was generally an Fe-rich variety (Carroll, 1970).

Kaolinite

Kaolinite was distinguished by a series of reflections: 7.15Å (001), 3.58Å (002), 2.35Å (003), and 1.79Å (004). The presence of disordered kaolinite is shown by broad (001) and (002)

reflections. Further diagnostic features of most kaolinites include the stability of the (001) reflection upon glycolation and its supression after heating to 500°c (Starkey et al., 1984).

In the majority of samples analysed both kaolin and chlorite were found to be present although differentiation of the two was often difficult due to the overlapping nature of the 7Å and 3.5Å reflections. Identification using thermal treatments was generally of no use due to the fact that some poorly crystallised sedimentary chlorites collapsed at 450°c.

Identification and differentiation of kaolinite and chlorite was therefore based on resolving the 3.5Å peak by running the sample at a slow scanning speed ($(\frac{1}{2}-\frac{1}{4}°)$ per minute). From this it was possible to identify the kaolinite (002) reflection at 3.58Å and the chlorite (004) reflection at 3.53Å (Biscaye, 1964) as shown in Fig. 1c. These results were corroborated by heating certain samples in warm (80°c) HCL (Starkey et al., 1984) resulting in the preferential dissolution of chlorite and the collapse of the 3.54Å peak (Fig. 1b and Table 8).

Smectite

Identification of smectite-type minerals, probably montmorillonite, was based primarily upon the presence of a reflection at 17Å after treating the sample with ethylene glycol (Fig. 2a). Subsequent heating of the sample to 180°c provoked a collapse of the first order, the mineral becoming anhydrous with a value of d spacing equal to 9.6Å - 10.0Å (Fig. 2a).

The degree of crystallinity of the smectite varies greatly between samples and was calculated using Biscaye's (1965) valley/peak ratio. A further refinement of this is given by Thorez (1976), who provides a comprehensive guide to variations in smectite crystallinity. The smectite/illite ratio referred to in Table 1-9 is calculated by comparing the height of the 17Å and 10Å peaks after treating the sample with ethylene glycol.

Further analysis of the smectite related minerals was carried out by saturating certain samples with KCL and then treating them with ethylene glycol. Where such samples showed an absence or marked reduction of the 17Å peak it is suggested that some of the

expanding silicate layers had been rendered non-expanding by the uptake of K+ cations (Thorez, 1976) as shown in Fig. 2c. This would indicate that either the smectite forms a mixed layer with other clay minerals such as illite, or alternatively that it originated by the weathering of mica (Thorez, 1976).

Where the smectite still expanded after KCL saturation and ethylene glycol treatment then it is suggested that the mineral is authigenic or neoformed (Jonas, 1975). This is typical, for example, of montmorillonite which has formed authigenically from volcanic ash.

Quantitative Analysis

A variety of methods exist for calculating the various proportions of clay minerals in any one sample. Unfortunately, the final results vary markedly depending on which method is chosen and it appears that any attempt to correlate results from various sources is highly dubious unless identical parameters were used.

A single sample was therefore taken and calculated using three different methods; the results are shown below (sample 58+00/96, 0.4m).

i. Griffin (1971):-	illite	= 48%
	chlorite	= 10%
	kaolinite	= 11%
	smectite	= 31%
ii. Johns et al. (1954):-	illite	= 63%
	chlorite	= 8%
	kaolinite	= 14%
	smectite	= 16%
iii. Robert & Maillot (1983):-	illite	= 32%
	chlorite	= 27%
	kaolinite	= 13%
	smectite	= 27%

From the above, and similar calculations for other samples, it was decided to use the method outlined by Griffin (1971), which is based on the height of peaks on the ethylene glycol and 180°c treated diffractograms. The method of Johns et al. (1954),

although widely used, proved particularly unsuitable here because it assumed that any loss at the 3.5Å and 7Å peaks was related to chlorite, whilst evaluations based on Robert and Maillot's method (1983) proved inconsistent. However, it should be stressed that Griffin's method (1971) occasionally produced dubious results and reference should always be made to the smectite/illite ratio (S.I.) and the valley/peak ratio (v.p.).

From the results of the quantitative analysis (Tables 1-9) it is obvious that, with the exception of 3 samples, illite was the prominent clay mineral in all the sediments analysed, and in the majority it forms over 50% of the total clay mineral assemblage. Subordinate proportions of kaolin, chlorite and smectite vary substantially between facies types.

Kaolin generally forms between 12-18% of the total clay fraction, although higher proportions occur consistently in sub-glacial sediments from the Marr Bank area (Facies A^5 and A^1) and in sub-facies $C2^3$ from the Bosies Bank area.

Chlorite was consistently present in all the samples analysed and the proportion of chlorite showed little variation beween facies types, generally forming about 10-15% of the total clay fraction.

Conversely the proportion of smectite and its degree of crystallinity displayed distinctive differences between certain facies and sub-facies. However, as will be discussed, it is thought that such variations purely reflect changes in provenance.

Interpretation of Clay Minerals

In most modern marine sediments the clay minerals can be split into two categories (Monkin, 1970). First, primary stage or neoformation clay minerals. Second, those clay minerals which result from a change of previously existing clay minerals, known as N+1 minerals. This distinction is critical as in situ neo-formed clays will contain a direct imprint of the environment of formation (Singer, 1984). However, these minerals may be re-cycled through a series of depositional and reworking stages in which no change of the clay minerals take place. In this case the clay minerals will represent the environment of the source rock and not the host sediment.

The presence of kaolinite, in what is essentially a glacigenic suit of sediments, may therefore be simply explained by the fact that the mineral was derived from ancient sediments which may well have existed under conditions more favourable for the formation of kaolinite. High proportions of kaolinite in facies A^1 and A^5 (Table 1) are therefore thought to relate to the reworking of surrounding Mesozoic strata in the Marr Bank area (Stoker, 1984). Similar examples of the presence of kaolin in high latitude marine sediments are recorded by Elverhoi (1975), Darby (1975) and Bjorlykke et al. (1977). In both cases the kaolin is derived from Mesozoic sediments.

N+1 clay minerals in marine environments include degraded and mixed layer minerals. However, it is now the general opinion that the majority of clay minerals in recent marine sediments are of a detrital nature (Jonas, 1975; Elverhoi & Lauritzen, 1984) although subtle changes may take place when the minerals are introduced into the marine environment. As an example of this, degraded types of smectite appear to take up K^+ or Mg^{2+} on returning to sea water, but montmorillonite of a framework silicate derivation (volcanic) is relatively stable (Mankin, 1970). Thus, the varying nature of smectite in the sediments probably relates to post-depositional processes acting on smectites derived from different sources.

Over much of the eastern half of the Bosies Bank area the primary source of smectite is from Palaeogene sediments and volcanics, which often contain between 80-100% smectite in the < 2um fraction (Fig. 4a). This is interpreted as a result of halmyrolytic transformation of volcanic glass (Karlsson, et al., 1978), and Fig. 4a shows that this smectite is relatively well crystallised and of a framework silicate derivation. KCL saturation of such material has no effect on the swelling characteristics of the mineral (P Condon, pers. com.). An additional source of smectite, although this is likely to be of a more degraded nature, is from cretaceous and Danian chalk to the west and north of the area respectively (Chesher and Lawson, 1983).

Sediments with a source in the above mentioned area, especially facies A^7 and facies C^7 therefore contain relatively high proportions (30-90%) of moderately well crystallised smectite. Chalk clasts are ubiquitous throughout these facies and

reworking of chalk material rich in smectite (Scholle, , 1977) would have acted as an additional source. Facies C^1 from the same area contains similarly high amounts of smectite, whilst facies E^8 contains progressively smaller amounts of smectite with increasing distance from the main smectite source along the western edges of the study area. Thus, in the Fladen area the clay fraction in facies E^8, and indeed in the majority of other facies, is dominated by illite with less than 10% smectite, most of the material having been supplied by the erosion of surrounding Pleistocene sediments similarly lacking in smectite. This eastward transition may partly reflect the offlapping nature of the Tertiary in the area (Fig. 4) and the change from smectite dominated Palaeogene sediments along the western edge of the area to illite and chlorite dominated Neogene sediments further east (Karlsson et al., 1978).

The suggestion that the clay mineralogy primarily reflects the geology of the source area is corroborated by the fact that facies A^7, C^7 and A^1 and C^1 from the north-western corner of the Bosies Bank area contain less than 10% smectite (58-02/164, 121, 231 and 295), and yet these same samples commonly display high smectite/illite ratios (0.8-2.5). This discrepancy can only be explained by the fact that smectite from these sources is engaged in a mixture with illite and therefore does not collapse to 10Å on heating to 180°C so precluding quantitative analysis by the method outlined previously (Thorez, 1976). The source of this material is probably the local Permo-Triass and Devonian strata which form the Caithness Ridge (Skinner, in press) and consist primarily of poorly sorted red and green sandstones, and less frequently siltstones. Analysis of the red sandstone, probably of Devonian age, showed it to be devoid of crystalline smectite (Fig. 4b). A pre-Tertiary source for mixed illite-smectite species is supported by an apparent lack of such phases in North Sea Tertiary sediments (Karlsson, 1978).

It should be noted that the majority of sediments analysed displayed a relatively constant and monotonous clay mineralogy dominated by illite, with subordinate chlorite, kaolinite and smectite. This is due to two factors. First, over most of the study area the bedrock immediately underlying the Pleistocene succession consists of Neogene silts and sands whose clay

mineralogy consists primarily of illite. Second, many of the Pleistocene sediments contain material partly derived from surrounding older Pleistocene sediments. As discussed previously, the exceptions to this occur along the western edge of the study were Palaeozoic, Mesozoic and Palaeogene strata outcrop as a result of the easterly younging nature of the succession described in chapter 1.

Further factors which must be taken into account when interpreting clay minerals include the affects of flocculation, size sorting and the degree of crystallinity (Singer, 1984). Edzwald and O'Melia (1975) determined the stability against the flocculation of clay minerals and found that illite is more stable than kaolin which in turn is more stable than smectite. Thus distal or proximal changes in clay mineral proportions may relate to flocculation. With regards to the crystallinity of clay minerals, size sorting may lead to only the finest grains being transported and as such these would display relatively poor crystallinity.

Conclusion

Of special interest to many workers studying Caenozoic marine sediments is the possibility of down core variations in the clay mineralogy delimiting cold and warm phases. The dominance of illite and chlorite in sediments of Pliocene and Pleistocene age is taken to suggest a cooling of climate, but may also relate to greater rapidity of exchange of material with northerly latitudes and to ice rafting (Singer, 1984). Subtle variations in the smectite/illite ratio have been used to distinguish between glacials and interglacials (Grousset et al., 1982), based on the assumption that smectites often dominate in sediments where chemical weathering prevails in the source area. Conversely a mineral assemblage containing illite and chlorite in the clay fraction with micas, quartz and amphiboles in the silt fraction, are interpreted as the result of cold climate mechanical weathering.

On this basis, it is obvious that the overall clay mineralogy of Pleistocene sediments from the North Sea is dominated by stable detrital material produced by mechanical weathering under high

latitude climatic conditions (Biscaye, 1965; Jacobs, 1970). The presence of significant amounts of smectite and kaolinite in certain sediments does not indicate on amelioration in climatic conditions, but rather reflects the geology of the source area (Fig. 4). Also it was not possible to link the variations in clay mineralogy to specific transport processes, for example ice-rafting and bottom currents, and their affects on dispersal pathways; although such effects have apparently been identified in the North Atlantic (Singer, 1984).

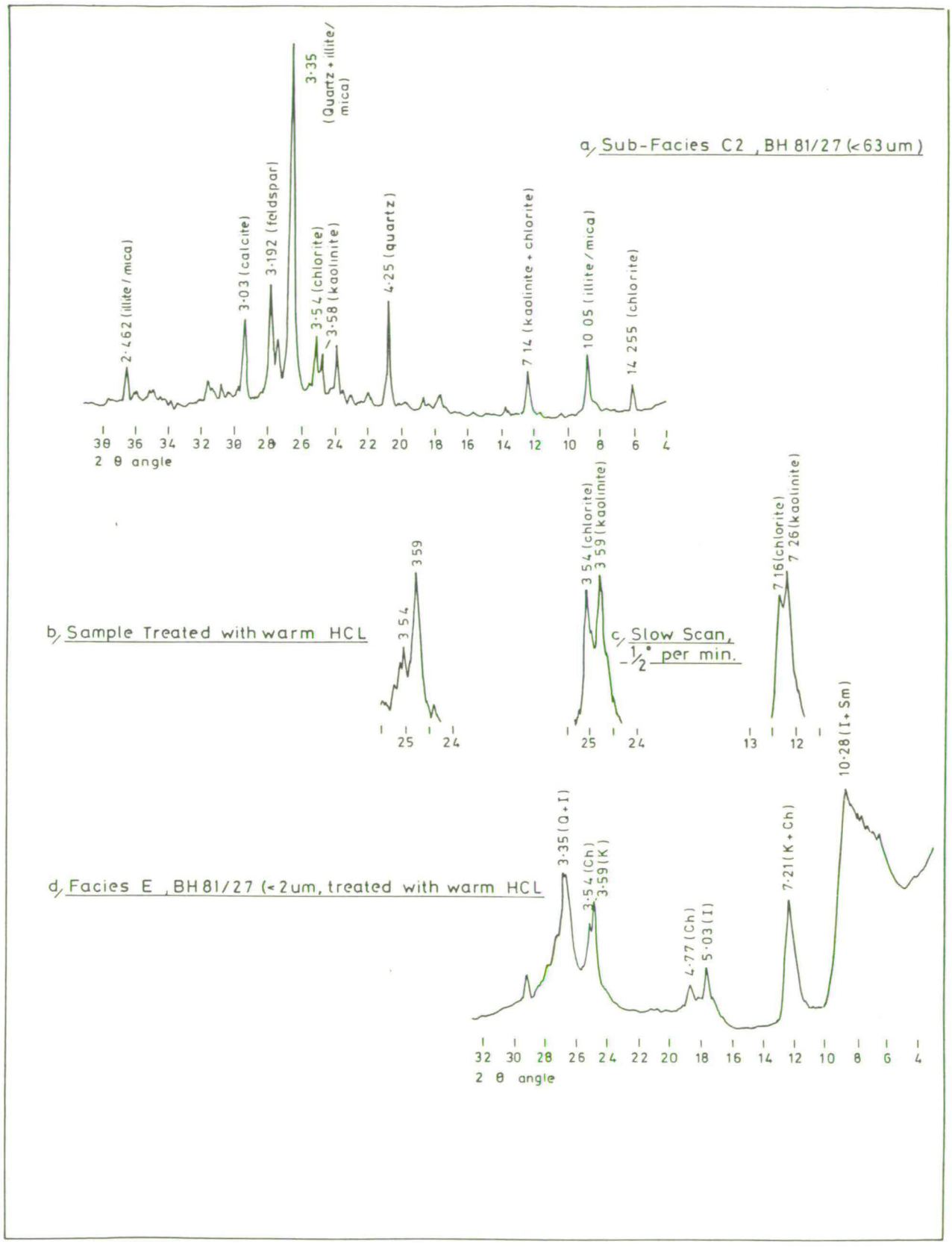

Appendix 6. Figs. 1a–c. XRD traces showing some of the criteria used to distinguish different clay minerals.

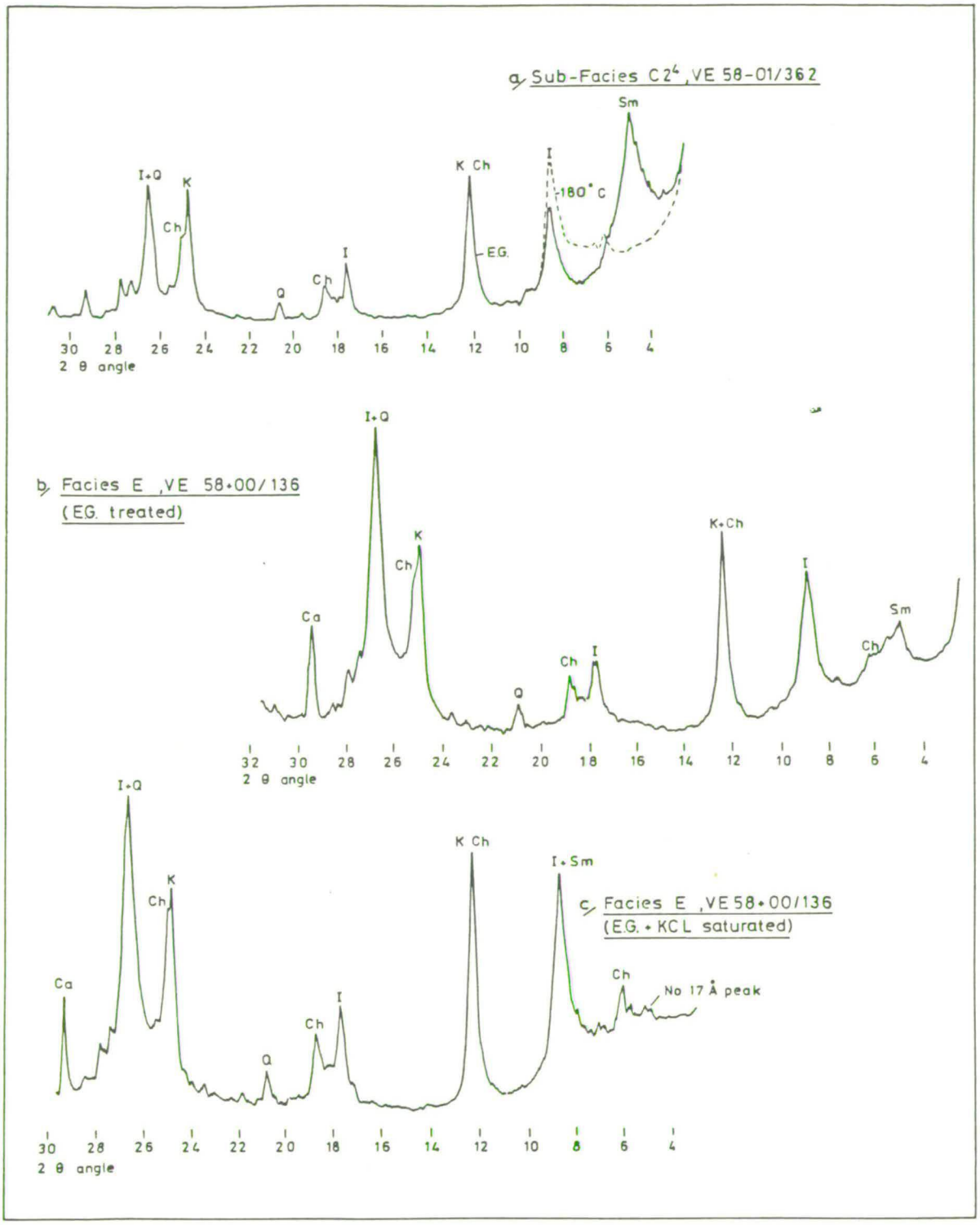

Appendix 6. Figs. 2a–c. XRD traces.

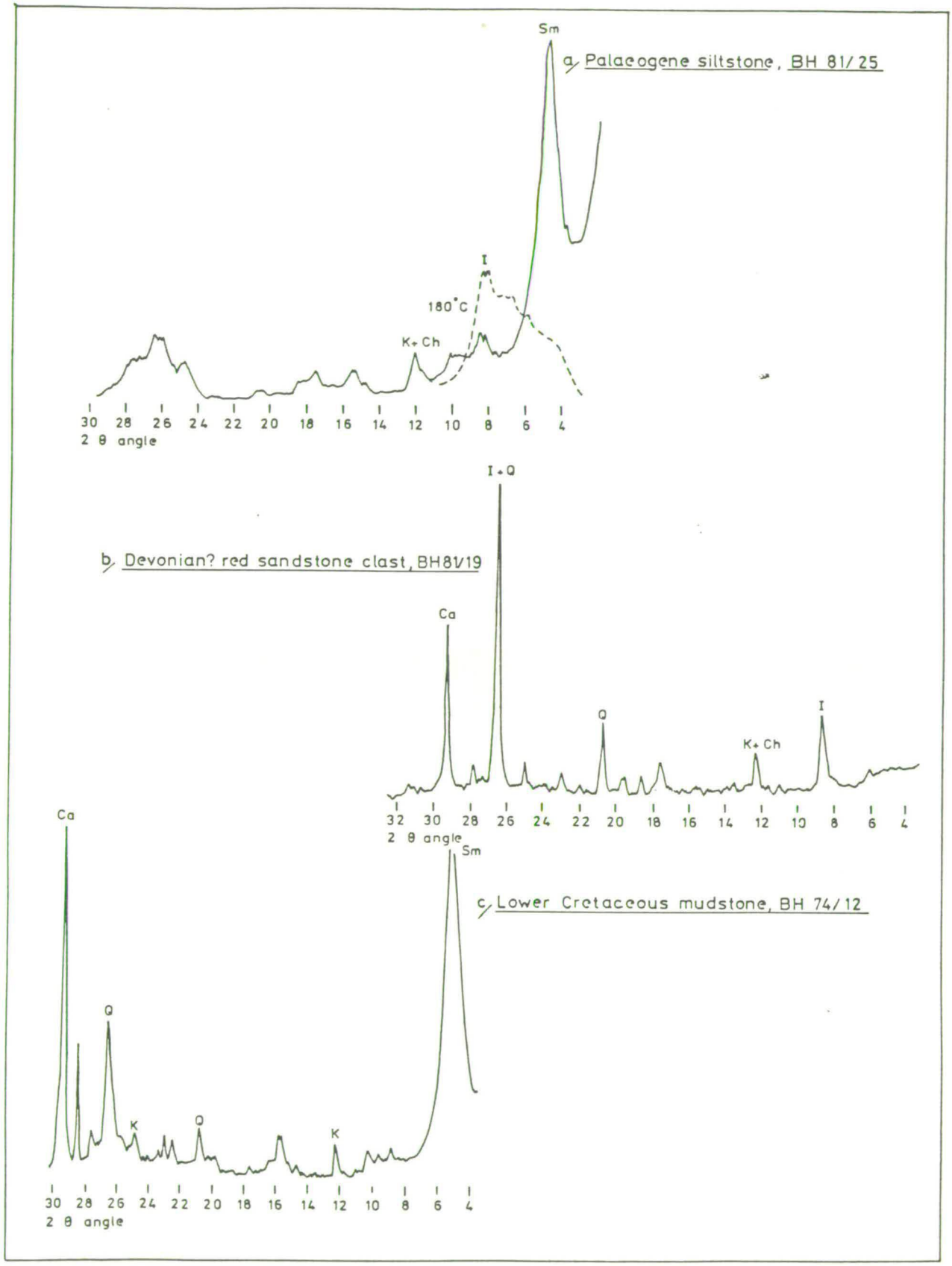

Appendix 6. Figs. 3a–c. XRD traces from selected sub-Pleistocene samples.

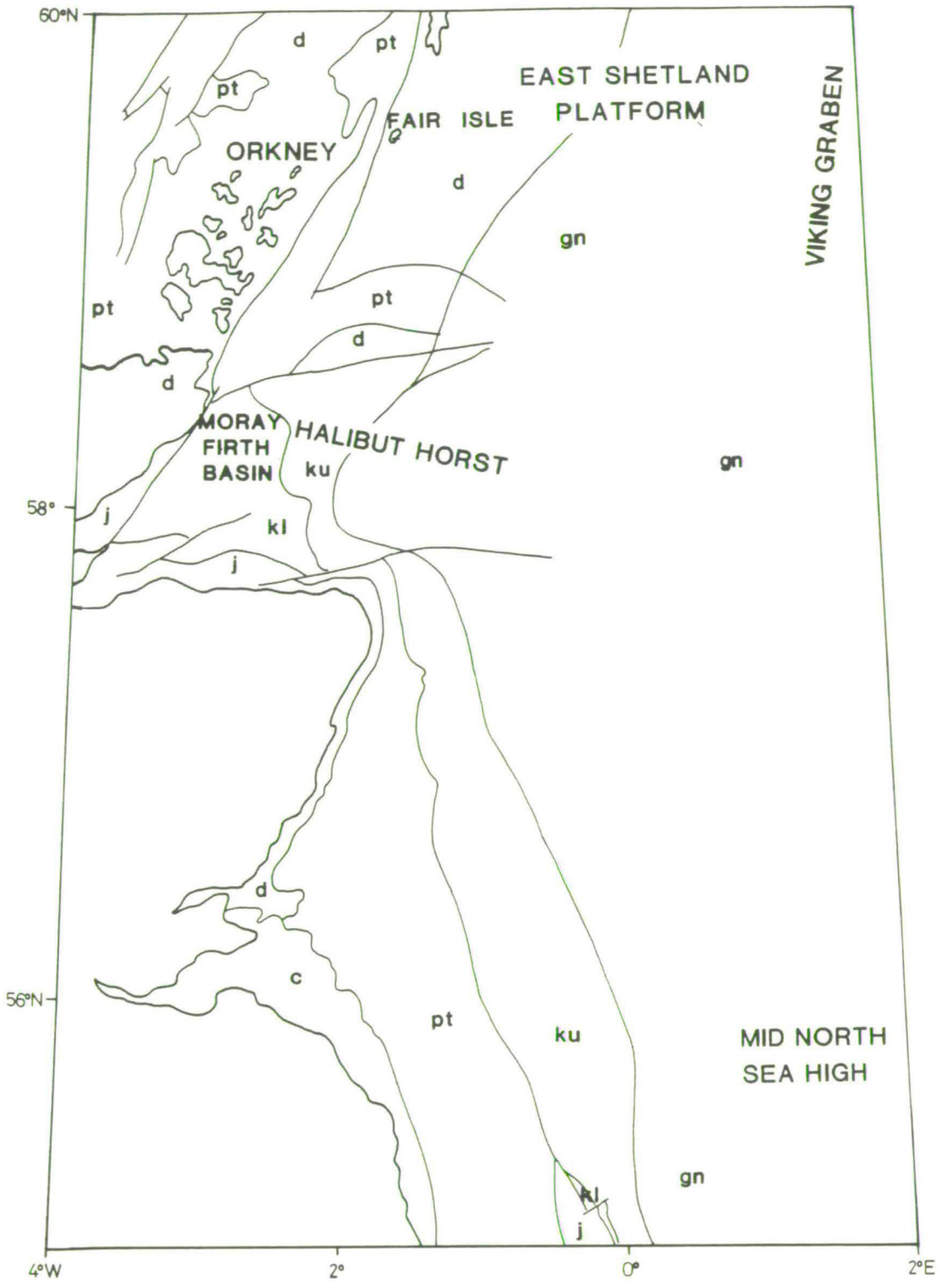

KEY

gn	Tertiary	pt	Permo – Trassic
ku	Upper Cretaceous	c	Carboniferous
kl	Lower Cretaceous	d	Devonian and Old Red Sandstone
j	Jurrassic		

Appendix 6. Fig. 4. Sub-Pleistocene geology of the study area.

Tables 1-9. Clay mineralogy data showing the height of significant peaks in mm and the approximate proportions of the main clay minerals calculated after Griffin 1971). The illite ratio and valley/peak ratio of smectite, both indicators of the degree of crystallinity were calculated after Robert and Maillot (1983) and Biscaye (1965) respectively.

Core Number.	Depth (M)	10 Å Peak (E.G.)	7 Å Peak (E.G.)	10 Å Peak (180°)	7 Å Peak (180°)	3.58 Å Peak (180°)	3.54 Å Peak (180°)	illete Ratio (1.R.)	smectite/illite (S.I.)	valley/Peak (V.P.)	% illite	% chlorite	% kaolinite	% smectite	Bedrock	Facies.	Mean ($\bar{X}$)	% Clay
56-02/6	22	60	186	110	220	185	80	0.2	0.8	0.6	35	16	28	19		A^5	4.1	16
56-02/7	3.4	100	120	-	-	-	-	0.06	0.6	0.5	-	-	-	-	(Triassic, red mst.	C^6	4.0	13
	12	90	131	120	120	80	70	0.06	0.8	0.5	54	15	16	15		A^5	1.9	6
(Rockhead)	16	122	114	145	137	65	114	0.03	0.1	-	73	17	10	0	-	-	-	-
56-02/8	30	50	230	61	225	160	80	0.14	0.2	0.4	32	20	40	8	-	A^5	4.0	11
56-02/19	52	55	78	-	-	-	-	0.05	0.5	0.6	-	-	-	-	(Upper Cretaceous chalk.	C^1	4.9	35
56-02/303	5.8	145	200	190	210	160	95	0.02	0.4	0.3	58	12	19	11	(Permian gypsum -anhydrite	A^5	5.7	24
	6	140	130	180	136	80	70	0.02	0.4	0.2	63	11	12	13		A^5	5.4	20
	8.2	153	140	172	146	80	70	0.02	0.1	-	56	12	13	19		A^5	4.3	14
	9.5	124	167	172	171	100	80	0.03	0.2	-	52	12	16	20		E^1	4.3	16
56-01/5	20	120	210	180	220	200	85	0.03	0.5	0.3	43	10	26	21	(Lower Cretaceous mst.	A^1	4.4	18
56-01/171	30	105	111	149	130	69	53	0.04	0.3	-	61	11	15	13	(Palaeogene sist.	D^4	6.6	48
	33	110	120	138	117	53	61	0.04	0.4	-	73	12	14	2		D^4	7.2	51
	42	90	76	-	-	-	-	0.05	0.3	0.4	-	-	-	-		D^4	6.6	50
1.	45	125	118	155	117	47	56	0.03	0.4	-	61	11	13	15		C^4	6.7	40

Core Number	Depth (M)	10 Å	7 Å	10 Å	7 Å	3.58 Å	3.54 Å	I.R.	S.I.	V.P.	ill.	Chl.	Kao.	Sme.	Bedrock	Facies	$\bar{X}$	% Clay
56-01/171	55	72	66	93	80			0.11	0.4	0.1	54	12	16	19		E^1		
(< 0.5um)	56	128	137	210	135	105	62	0.14	1.0	0.4	48	8	13	32		E^1	8.4	49
	58	60	54	170	124	47	75	0.13	0.1	-	68	12	12	6		D^1	6.4	38
	60	111	111	153	131	66	75	0.5	0.2	-	64	12	14	11		D^2	6.8	45
	64	64	73	100	80	71	50	0.1	0.4	0.2	53	10	14	23		E^2	7.8	49
	66	124	136	153	123	123	106	0.11	0.4	0.3	55	11	13	20		E^1	8.4	60
56-01/172	16.4	114	143	164	180	150	107	0.1	0.5	0.3	60	12	18	10	Lower Cretaceous mst.	C^1	5.0	
	19.2	65	103	-	-	-	-	0.1	0.5	0.1	-	-	-	-		C^1	5.1	
56-01/173	4	72	117	70	105	82	57	0.1	0.2	-	57	13	24	6	Upper Cretaceous Chalk	C^6	3.2	13
	6.6	106	132	147	142	80	60	0.04	0.2	-	56	16	26	16		C^1	3.6	16
	12	100	140	87	106	66	53	0.1	0.4	0.2	64	15	18	3.5		C^1	1.3	8
56+01/210	3	50	44	110	80	55	52	012	0.3	0.3	64	11	12	13		E^1		
58-02/121	1.9	70	88	88	91	66	78	0.06	1.8	0.9	57	16	14	13	Devonian red Sst.	C^1	2.0	6.6
	2.4	74	76	79	84	64	64	0.06	-	-	73	15	12	0		C^1	2.7	5.7
58-02/139	2.5	55	72	66	84	49	50	0.08	0.7	07	64	17	17	2	Palaeocene	D^8	7.5	36
2.	4.1	30	46	59	45	28	37	0.23	3.3	08	38	10	13	39	Siltstone	C^7	4.5	20

Core No.	Depth (M)	10 Å	7 Å	10 Å	7 Å	3.58 Å	3.54 Å	I.R.	S.I.	V.P.	ill.	Chl.	Kao.	Sme.	Bedrock	Facies	$\bar{X}$	% Clay
58-02/139	4.5	36	44	61	44	27	23	0.19	3.4	0.8	45	10	12	32		A^7	3.8	12
	5.5	75	98	99	99	85	35	0.07	0.7	0.5	7	1	2	90		A^7	3.9	19
58-02/164	1.7	32	40	45	45	30	20	0.19	1.1	0.6	57	11	17	14	Permo-Triass Sst.	E^8	6.4	28
	2.7	78	99	92	109	60	80	0.06	0.4	0.7	63	18	14	5		D^8	7.8	41
	4.5	69	83	78	79	60	71	0.04	0.8	0.7	60	15	13	11		A^7	3.5	12
	5.1	70	79	74	85	48	60	0.06	0.9	0.8	50	17	14	0		A^7	3.8	13
	5.4	35	49	42	44	62	66	0.14	2.5	0.8	56	16	15	13		C^2	2.3	3
58-02/176	0.5	39	51	41	51	35	30	0.09	0.2	0.4	63	18	15	4	Palaeocene	E^8	2.4	7
	1.4	40	46	55	47	27	37	0.18	1.4	0.7	55	11	15	19		C^7	5.1	27
	3.2	29	35	49	36	30	23	0.31	1.7	0.7	47	9	12	30		C^7	5.2	29
58-02/231	1.7	64	92	80	99	71	77	0.06	0.3	0.8	57	17	16	10	Devonian	E^8	5.9	22
	3.2	89	90	115	96	72	87	0.06	0.3	0.4	62	14	11	13		A^1	2.6	9
	4.0	46	51	66	58	40	52	0.13	0.8	0.4	59	15	11	15		A^1	2.8	8
58-02/257	1.0	43	52	65	55	37	45	0.15	1.2	0.7	52	11	13	22	Palaeocene	E^8	5.8	31
	1.5	48	59	72	58	49	34	0.17	1.4	0.7	50	10	14	26		E^8	5.6	31
3.	1.8	54	52	66	51	46	27	0.11	0.5	0.4	61	9	15	15		C^8	4.5	26

Core No.	Depth (M)	10Å	7Å	10Å	7Å	3.58Å	3.54Å	I.R.	S.I.	V.P.	ill.	Chl.	Kao.	Sme.	Bedrock	Facies	$\bar{X}$	% Clay
58-02/257	1.9	27	34	47	37	28	21	0.32	1.4	0.7	48	10	14	29		C^7	4.5	20
	4.2	29	18	53	18	16	13	0.31	2.3	0.7	48	5	7	40		C^1	3.5	11
58-02/259	0.4	20	22	25	19	12	15	0.55	1.5	0.5	53	13	10	24		E^8	2.4	7
	0.7	25	31	51	34	24	18	0.36	4.5	0.8	42	9	12	37		C^7	6.0	36
58-02/295	1.5	29	34	52	52	33	27	0.26	1.7	0.7	61	13	16	11	Permo-Triass	A^2	2.2	5
58-02/317 (Bedrock)	19	20	21	65	25	15	10	1.2	7.8	1.4	26	5	8	61	Tertiary sist.	-	-	-
58-02/319	7.5	39	49	47	59	42	25	0.14	0.8	0.7	67	12	21	0	Palaeocene tuffs & sist.	C^7	5.9	36
	12	30	39	35	40	27	22	0.18	0.8	0.6	60	14	17	8		C^7	5.6	33
	12.6	30	34	44	38	22	12	0.18	1.2	0.6	57	9	17	18		C^7	5.0	28
	12.9	38	48	44	50	30	24	0.12	1.1	0.6	62	14	17	7		C^7	4.2	19
	16.5	44	55	40	48	40	27	0.1	0.6	0.6	65	13	19	3		E^7	6.7	40
	17.6	36	52	47	71	60	40	0.2	0.4	0.2	62	15	22.8	0		C^3	5.6	32
	20	63	101	40	65	54	23	0.08	0.3	0.6	65	15	20	0		C^3	5.0	28
	20.7	60	90	71	97	88	48	017	0.3	0.4	61	12	27	0		C^3	5.6	32
	21	57	81	67	79	70	27	0.09	0.3	0.4	59	12	23	6		C3	5.7	33

Core No.	Depth (M)	10 Å	7 Å	10 Å	7 Å	3.58 Å	3.54 Å	I.R.	S.I.	V.P.	ill.	Chl.	Kao.	Sme.	Bedrock	Facies	$\bar{X}$	% Clay
58-01/200	0.8	54	52	69	50	37	20	0.13	0.5	0.3	59	8	14	19		A^3	4.6	18
	1.5	37	44	51	51	34	17	0.16	0.4	0.3	60	10	19	11		A^3	4.0	23
	2.5	60	70	56	75	40	39	0.11	0.4	0.1	60	17	18	5		A^3	4.0	15
58-01/208	1.9	30	35	31	35	17	15	0.33	0.7	0.5	67	15	17	2		C^3	6.6	29
58-01/224	1.5	29	33	37	36	27	25	0.22	0.9	0.5	62	13	15	10		D^8	7.4	47
	3.5	40	44	47	51	30	22	0.11	0.4	0.4	69	13	17	1		C^7	4.2	19
58-01/258	0.8	53	68	60	77	59	53	0.07	0.2	0.3	66	16	18	0	Eocene	D^8	7.5	42
58-01/335	0.6	30	49	56	52	36	34	0.2	0.5	0.1	40	15	15	30		C^4	6.5	34
	1.5	39	49	54	46	35	28	0.18	0.5	0.1	51	11	14	24		C^4	6.6	36
58-01/350	0.5	24	30	46	47	49	40	0.63	0.6	0.3	58	13	16	12		E^8	6.4	35
	1.5	27	29	29	60	52	20	0.26	0.9	0.4	45	12	33	10		D^8	8.2	58
	2.5	42	47	48	48	21	36	0.14	0.4	0.6	64	18	11	8		D^4	5.9	32
58-01/362	0.7	29	38	44	43	35	22	0.21	0.9	0.5	54	11	17	18	Palaeocene	C	6.2	37
	3.4	39	59	55	64	41	32	0.13	1.0	0.6	52	14	18	16		C^4	5.2	30
5.	4.5	41	64	63	68	57	34	0.13	1.6	0.6	48	11	19	22		C4	4.6	21

Core No.	Depth (M)	10 Å	7 Å	10 Å	7 Å	3.58 Å	3.54 Å	I.R.	S.I.	V.P.	ill.	Chl.	Kao.	Sme.	Bedrock	Facies	$\bar{X}$	% Clay
58-01/373	3.2	50	46	59	49	30	10	0.2	0.8	0.6	68	6	19	7	Palaeogene mst. & sist.	E^8	4.3	18
	4.5	33	26	40	30	20	10	0.27	1.1	0.6	73	7	15	5		E^8	4.9	17
	7.9	25	30	40	35	20	11	0.44	-	-	54	9	17	20		C^4	4.3	21
	13.0	38	39	48	46	21	6	0.13	0.5	0.6	68	6	22	5		C^4	4.9	25
	15.4	29	28	38	32	22	3	0.21	0.6	0.7	65	3	22	10		E^4	6.9	38
	18.7	40	44	51	56	28	20	0.11	0.15	0.8	69	13	18	0		D^1	7.8	52
	19.5	52	61	60	65	33	20	0.09	0.2	0.1	64	11	19	5		D^1	7.4	50
	21.7	24	26	31	28	15	8	0.25	1.3	1.0	61	9	17	12		D^1	6.9	43
	24.9	22	25	46	38	23	14	0.32	1.1	1.1	52	4	15	23		D^1	6.5	40
	30.2	34	30	39	34	20	14	0.15	0.5	0.9	73	11	15	1		A^1	3.8	14
	31.6	25	26	45	33	18	14	0.27	0.7	0.7	55	10	13	23		A^1	4.3	22
	32.5	52	58	56	59	35	15	0.08	0.21	0.7	66	9	21	4		A^1	3.5	11
	32.7	60	76	73	79	61	46	0.08	0.22	0.5	60	13	17	10		A^1	3.9	17
	35.7	81	88	87	89	55	35	0.1	0.2	0.4	67	11	18	4		A^1	3.0	10
	41.2	30	30	34	34	6	20	0.33	0.4	0.3	71	22	7	0		A^1	4.1	20
	52.7	51	57	58	68	38	16	0.09	0.16	0.4	71	9	22	0		A^1	4.0	17

Core No.	Depth (M)	10Å	7Å	10Å	7Å	3.58Å	3.54Å	I.R.	S.I	V.P.	ill.	Chl.	Kao.	Sme.	Bedrock	Facies	$\bar{X}$	% Clay
58-01/373	55	38	38	48	46	39	14	0.16	0.4	0.2	69	7	20	3		A^{1}	3.7	14
58-01/376	0.4	38	46	34	44	30	33	0.12	0.6	0.5	63	17	16	4	Tertiary	E^{8}	5.2	20
	0.9	48	60	64	71	50	47	0.09	0.6	0.4	61	15	16	8		E^{8}	7.0	38
	13.5	26	25	30	34	21	8	0.21	0.1	-	68	8	22	2		E^{8}	7.0	36
	19.4	25	27	35	29	17	10	0.24	0.8	0.5	58	9	16	17		E^{8}	7.6	44
	19.6	22	18	28	19	10	5	0.27	1.4	0.7	6	7	14	73		E^{7}	8.6	64
	23.5	30	33	35	24	20	7	0.23	0.7	0.5	49	6	16	30		D^{4}	6.3	39
	24.4							0.28	0.6	0.6						C^{4}	5.5	29
	24.5	43	45	46	41	43	50	0.16	0.7	0.4	63	14	12	11		C^{4}	2.8	6
	28	44	41	60	46	31	0	0.16	0.3	0.2	63	0	23	13		C^{4}	4.4	20
	30.2	37	35	50	41	31	0	0.19	0.3	0.3	65	0	25	10		C^{4}	4.8	23
	30.5	62	75	110	99	72	65	0.09	0.3	0.4	55	9	16	19		E^{1}	7.8	50
58+00/96	0.4	135	150	225	152	110	117	0.04	0.5	0.4	48	11	10	31		E^{8}	2.9	14
58+00/122	5.5	142	185	178	180	130	127	0.03	0.3	0.4	55	14	15	16		D^{8}	6.9	13.4
58+00/125	1.5	48	132	140	145	98	102	0.04	0.3	0.6	54	15	14	16		D^{8}	7.1	38
58+00/165	2.5	113	155	168	180	141	140	0.04	0.2	0.1	55	15	15	15		D^{8}	9	63

Core No.	Depth (M)	10Å	7Å 10Å	7Å	3.58Å	3.54Å	I.R.	S.I.	V.P.	ill.	Chl.	Kao.	Sme.	Bedrock	Facies	$\bar{X}$	% Clay
58+00/165	5.5	139	185	157	175	140	132	0.04	0.14	0.2	58	15	15	11	D^8	8.6	62
58+00/135	0.5	150	195	186	210	144	164	0.02	0.2	0.4	60	17	14	9	E^8	7	42
	0.75	170	240	220	240	160	150	0.03	0.2	0.4	54	15	16	16	E^8	6.6	40
	2.75	87	130	115	135	120	95	0.05	0.2	0.6	53	14	18	15	E^8	51	8.3
	3.65	146	202	210	240	160	150	0.03	0.2	0.6	56	16	16	12	D^8	57	8.5
<15.6 UM	3.65	95	106	110	102	82	85	0.04	0.2	0.5	60	14	13	12	D^8	57	8.5
<15.6 (Acid)	3.65	60	50	75	60	06	25	0.06	0.5	-	73	6	18	3	D^8	57	8.5
58+00/136	0.7	58	82	74	75	55	61	0.1	0.3	0.4	51	15	14	20	E^8	-	-
(KCL)	0.7	87	108	-	-	-	-	0.06	-	-	-	-	-	-	E^8	-	-
	1.8	140	205	165	196	158	135	0.04	0.2	0.6	51	15	18	16	D^8	-	-
	2.6	86	99	113	102	84	83	0.07	0.3	0.6	55	14	15	16	D^8	-	-
<15.6 UM (Acid#Kcl)	2.6	62	44	65	39	38	24	0.05	-	-	68	7	12	12	D^8	-	-
58+01/09	1	139	189	151	188	139	127	0.04	0.1	0.7	61	16	17	6	D^4	6.8	4.6
58+01/61	0.5	47	61	70	60	54	43	0.09	0.4	0.3	49	11	14	25	E^8	3.4	6.5
	0.9	56	80	80	67	52	42				43	11	14	31	E^8	3.3	3
8.	2.2	44	55	70	48	54	46	0.05	0.3	0.4	43	10	12	35		5.0	27

Core No.	Depth (m)	10 A	7 A	10 A	7 A	3.58 A	3.54 A	I.R.	S.I.	V.P.	ill.	Chl.	Kao.	Sme.	Bedrock	Facies	X	% Clay
58+01/82	0.25	48	58	-	-	-	-	0.13	0.3	0.3	-	-	-	-		E^8	5.0	12
58+01/112	0.5	165	215	205	215	158	132	0.02	0.2	0.5	57	13	16	14		E^8	2.3	4
	0.9	134	187	173	196	155	131	0.04	0.3	0.6	56	14	17	13		E^8	2.6	6
	2.5	124	175	175	180	145	120	0.04	0.3	0.3	52	13	16	19		E^8	3.2	8
	4.3	92	125	105	113	88	75	0.05	0.3	0.6	56	15	17	12		D^8	7.6	43
58+01/113	0.5	122	168	140	161	123	110	0.03	0.2	0.4	57	15	17	11		E^8	2.1	7
	1.6	65	78	75	72	43	40	0.18	0.3	0.4	58	13	14	15		D^4	6.2	32

Geochemistry

The bulk geochemistry of some 70 samples from a variety of sediment types was determined using x-ray fluorescence spectrometry. The analytical procedure is outlined in Chapter 1 and the results listed in Tables 10-12. Additional samples were sent to the BGS Geochemical Directorate for trace element analysis.

It was hoped that the results might provide a further means of identifying glaciomarine sediments from those deposited in other marine environments. For example, Angino (1960, 1968) suggested that it is possible to distinguish between glaciomarine sediments, and pelagic and continental shelf marine sediments. Certain elements, including Fe, Ti and Mn are cited as being especially useful in highlighting glacial input. Similar work by Elverhoi and Roaldset (1983) showed that glaciomarine sediments from the Weddell Sea plotted in a restricted field on a Al, Si, Ca triangle. Comparison of sediments from the North Sea to those from the Weddell Sea (Fig. 5a) shows that the apparent similarity between the two sets of data, only subglacial and proximal glaciomarine sediments from the North Sea differ significantly. Similarly a plot of Fe, Al, Mn and Ti ratios (Appendix 6, Fig. 5b) shows the close relationship of glaciomarine, arctic marine and temperate marine sediments in the North Sea to glaciomarine sediments from the Berring Sea (Angino, 1960), and the difference between these sediments and the pelagic muds from the Pacific (Goldberg and Arrhenius, 1958).

However, Table 10 lists the average geochemical composition of sediments from a variety of marine environments, including the Antarctic glaciomarine muds analysed by Angino (1966). Three points of special interest can be observed from this table

i. The average geochemical composition of glaciomarine sediments from the North Sea is very similar to the average of 43 samples of typical continental shelf muds, compiled by Matsumoto and Iljima (1983).

ii. Glaciomarine sediments do not differ significantly from the average crustal abundance (Taylor, 1964).

iii. Deep sea clays are easily identified from other marine sediments on account of their low content of silica and

relatively high abundance of trace elements.

In fact Table 10 shows that it would be presumptious to ascribe a glaciomarine origin to any sediment purely on the basis of bulk geochemical analysis. However, it would be reasonable to distinguish between a continental shelf and a deep sea environment on the basis of trace element analysis.

A detailed analysis of the bulk geochemistry of VE 58+00/111 was carried out to see if the results could instead be used to aid interpretation as to the environment of depositon. The down core chemical variations are presented in Long et al. (Appendix 8) Fig. 5.

The indices S* and D* permit the recognition of detrital paticles (Bostrom and Peterson, 1969), and 5* shows a strong negative correlation with the percentage of clay.

The most notable feature of Fig. 5 is the variation in the Mn:Al ratio which changes markedly down core. As this variation does not directly correlate with the clay content it is possible that higher Mn values may be representative of slower rates of deposition which would have increased the chance of Mn being absorbed onto the sediment surface (Arrhenius, 1963). The Fe:Al ratio shows a slight increase with depth to a maximum of 4.45m. The occurrence of distinct monosulphide bands in the lower part of the core probably account for these slightly higher concentrations of iron. Overall, however, most variations are controlled by a negative correlation with SiO_2 and were of little use in further elucidating the environment of deposition. This agrees with Johnson and Elkins (1979) who noted that coarse grained superficial sediments from the northern North Sea consistently showed higher Si/Al values than did the finer grained sediments. Also reference to Fig. 5b shows that there is no discernible difference between temperate marine and glaciomarine sediments in the North Sea. The one exception to this was the geochemical composition of an indurated layer in lower Pleistocene marine sediments from boreholes 81/27 and 75/33, described in Chapter 5. Analysis of these layers showed them to be atypical continental shelf sediments (Table 5.1), especialy with regard to their high P_2O content. Although the P_2O content of these layers it too low for them to be termed phosphorites, their mode of formation is obviously different

from the bulk of the Pleistocene sediments and is further discussed in Chapter 5.

In conclusion, when compared with the work of Hirst (1962), Cronan (1976) and Matsumoto and Iljima (1983), it is clear that glaciomarine sediments from the North Sea represent a typical continental shelf marine clay assemblage, irrespective of latitude. Trace elements displayed none of the extremes in composition associated with deep sea clays, and generally the concentrations are very close to crustal abundance.

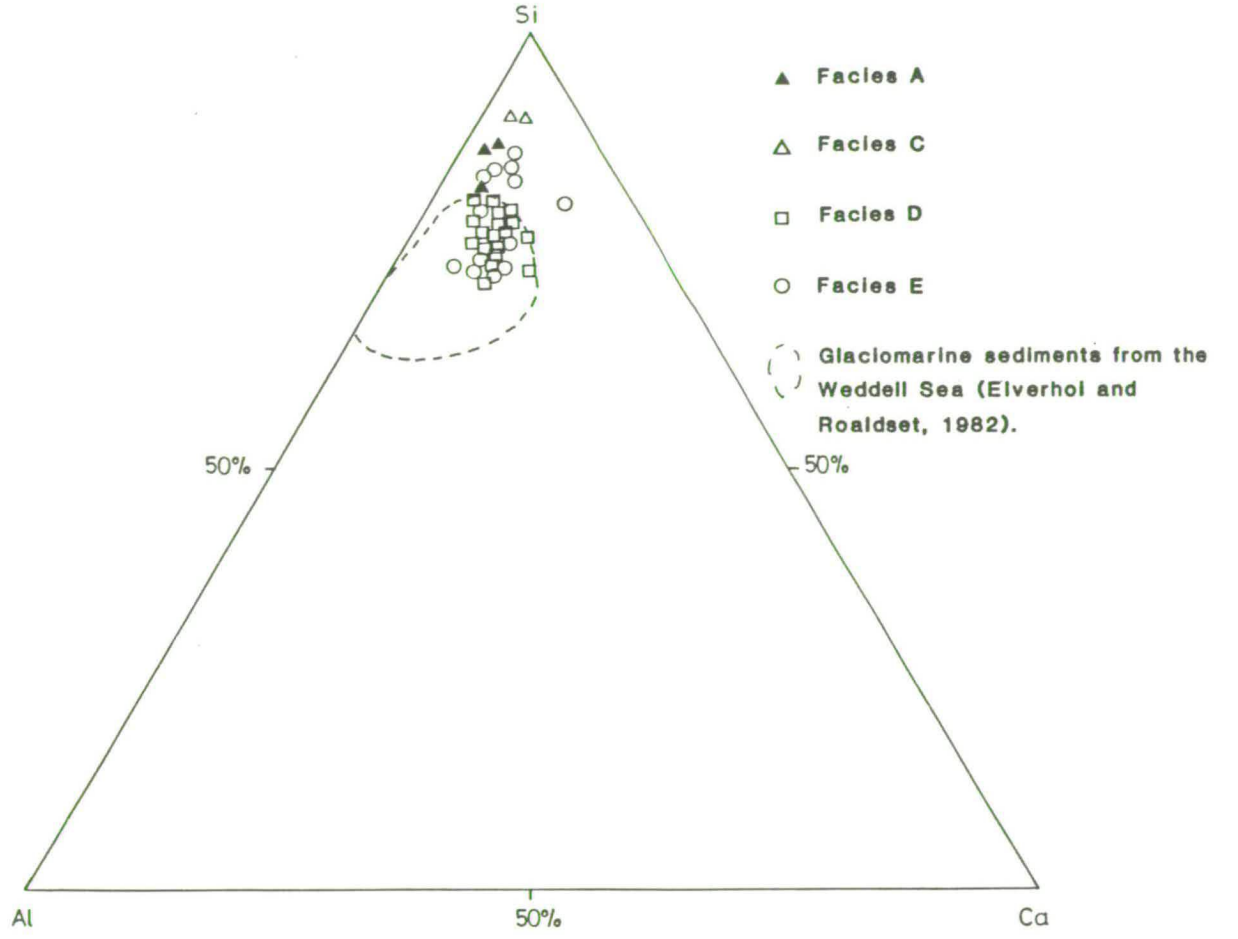

Appendix 6. Fig. 5a. Al-Si-Ca triangular plot for late Weichselian sediments.

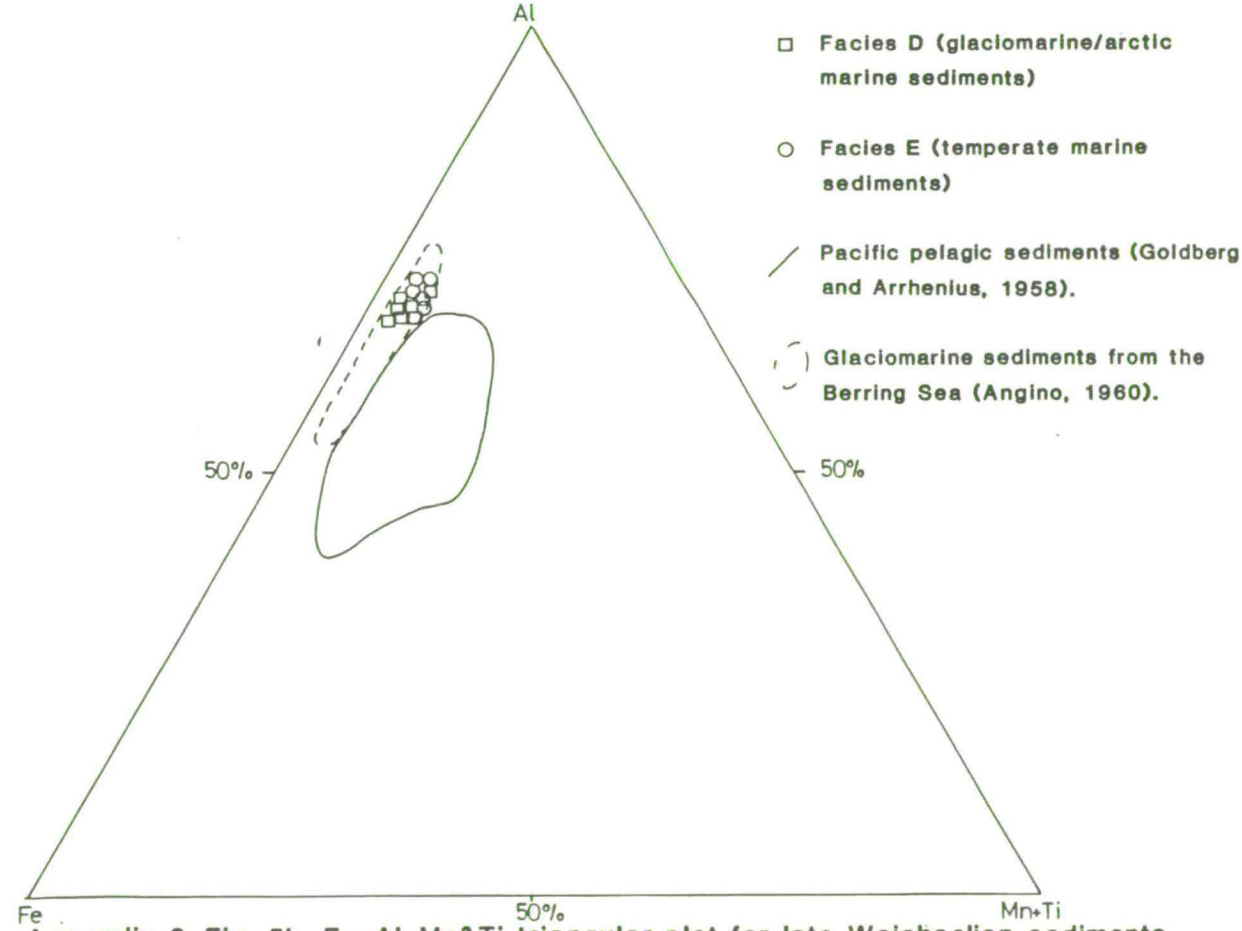

Appendix 6. Fig. 5b. Fe-Al-Mn&Ti triangular plot for late Weichselian sediments from VE 58+00/111.

Tables 10-12. Geochemical data listing the major element components (oxides) of each sample.

CORE No.	DEPTH (m)	Si02	Al203	Fe203	MgO	CaO	Na20	K20	Ti02	MnO	P205
56-02/303	5.8%	71.4	12.0	4.7	2.2	3.9	1.9	2.7	0.67	0.07	0.13
	6.0	79.4	8.8	2.9	1.4	2.8	1.6	2.3	0.49	0.05	0.06
	8.2	79.7	8.4	2.7	1.3	2.9	1.6	2.6	0.46	0.05	0.09
	9.6	79.6	8.4	2.6	1.3	3.4	1.4	2.2	0.49	0.05	0.09
56-02/172	16.4	68.8	12.5	5.0	2.6	5.3	1.5	3.0	0.71	0.07	0.14
	26.0	74.7	10.1	3.9	2.0	4.4	1.3	2.5	0.59	0.06	0.13
173	6.6	82.7	7.1	2.5	1.2	2.6	1.3	1.9	0.44	0.04	0.08
171	6.5	83.8	6.5	2.0	1.0	2.7	1.1	1.9	0.39	0.03	0.07
	54.0	60.5	17.4	6.9	3.4	4.9	1.6	3.7	0.94	0.08	0.17
	58.0	68.9	12.9	4.9	2.2	5.0	1.7	3.2	0.64	0.07	0.15
	68.6	67.7	6.2	17.3	0.8	3.6	1.2	1.6	0.34	0.08	0.33
	69.0	52.5	10.4	9.5	2.0	9.2					3.3
58+00/95	0.5	73.4	11.2	4.1	2.8	3.2	1.8	2.8	0.64	0.04	0.12
	1.8	68.4	12.2	4.9	2.5	5.5	1.9	3.0	0.68	0.06	0.14
	3.8	60.7	15.6	6.4	2.9	6.9	2.1	3.4	0.85	0.08	0.17
	5.2	65.3	13.7	5.4	2.6	6.3	1.8	3.2	0.73	0.06	0.16
96	0.4	80.7	6.7	2.2	1.1	6.2	1.2	1.8	0.32	0.03	0.07
	5.4	69.4	12.3	4.8	2.2	5.5	1.6	3.0	0.66	0.06	0.14
106	0.5	72.8	10.5	4.0	2.1	5.2	1.6	2.5	0.58	0.05	0.12
107	0.8	65.4	13.2	5.4	2.7	6.8	1.6	3.2	0.72	0.07	0.16
	1.5	63.3	13.9	6.0	3.2	6.6	2.0	3.2	0.77	0.07	0.17
109	5.2	74.4	9.9	3.4	1.9	5.4	1.5	2.5	0.57	0.05	0.12
111	0.34	75.7	9.6	3.4	1.7	4.8	1.7	2.4	0.55	0.05	0.12
	1.4	67.0	12.9	5.1	2.8	6.0	2.0	3.0	0.71	0.06	0.15
	2.2	64.8	14.0	5.5	3.0	6.1	2.1	3.1	0.76	0.06	0.16

CORE No.	Depth(m)	Si02	Al203	Fe203	MgO	CaO	Na20	K20	Ti02	MnO	P205
58+00/111	3.1%	63.7	13.7	5.5	2.8	7.7	1.9	3.2	0.72	0.07	0.16
	3.5	63.8	13.9	5.5	2.8	7.1	2.0	3.2	0.74	0.08	0.16
	3.6	60.0	15.5	6.4	3.1	7.6	2.2	3.4	0.82	0.09	0.18
	3.8	68.5	13.4	5.5	2.9	3.3	2.3	3.1	0.73	0.06	0.13
		59.0	16.2	7.0	3.3	7.7	2.0	3.6	0.84	0.09	0.18
	5.3	73.6	10.2	3.8	1.8	4.9	1.6	2.6	0.60	0.05	0.12
122	4.5	65.6	14.1	5.8	3.1	4.0	2.2	3.2	0.79	0.06	0.16
125	1.5	66.7	12.7	5.0	2.8	6.1	1.9	3.0	0.69	0.06	0.14
	5.5	62.0	14.4	6.1	3.0	7.3	1.8	3.3	0.77	0.08	0.17
135	0.5	62.2	12.2	5.0	2.7	7.5	2.0	2.7	0.69	0.05	0.14
	0.8	73.4	10.7	4.2	2.2	3.7	1.8	2.6	0.62	0.04	0.11
	1.5	61.6	14.9	6.2	3.3	6.6	2.2	3.4	0.80	0.07	0.16
	2.8	60.8	14.9	6.2	3.2	7.6	2.0	3.4	0.80	0.08	0.16
	3.0	68.6	11.9	4.5	2.5	6.4	1.7	2.9	0.65	0.06	0.14
	3.7	61.9	14.3	6.0	3.1	7.2	1.9	3.4	0.78	0.08	0.16
	4.5	61.9	14.6	5.9	3.1	7.3	1.9	3.4	0.77	0.08	0.17
136	0.7	61.1	14.7	6.1	3.2	7.5	2.0	3.3	0.78	0.08	0.17
	1.8	62.2	14.2	6.2	3.1	7.1	1.9	3.2	0.77	0.07	0.16
	2.6	63.9	13.9	5.9	2.7	6.7	1.8	3.4	0.74	0.08	0.16
160	4.6	62.4	14.3	5.9	3.2	6.7	2.1	3.3	0.77	0.07	0.16
	4.8	62.0	14.7	5.9	3.3	6.7	2.2	3.3	0.79	0.07	0.17
	4.9	60.7	15.2	6.2	3.4	6.9	2.1	3.4	0.80	0.08	0.17
	5.4	60.3	15.8	6.3	3.4	6.8	2.0	3.6	0.81	0.08	0.17
58+00/165	0.3	78.2	8.9	3.2	1.5	4.0	1.3	2.3	0.52	0.04	0.10
	2.5	57.3	16.6	7.1	3.4	7.8	1.9	3.9	0.85	0.09	0.18
	5.5	57.9	15.8	7.4	3.4	7.8	2.1	3.4	1.0	0.10	0.20
166	5.5	64.7	13.9	5.4	2.8	6.9	1.7	3.4	0.73	0.08	0.15

Middle Pleistocene glacial and glaciomarine sedimentation in the west central North Sea

MARTYN S. STOKER AND ALISTAIR BENT

BOREAS

Stoker, Martyn S. & Bent, Alistair 1985 12 01: Middle Pleistocene glacial and glaciomarine sedimentation in the west central North Sea. *Boreas*, Vol. 14, pp. 325–332. Oslo. ISSN 0300-9483.

A sequence of Middle Pleistocene (approximately early 'Cromerian Complex') sediments has been subdivided into subglacial, proximal glaciomarine, distal glaciomarine and marine facies. The subglacial facies represents lodgement till deposited during the final stages of ice-sheet advance. At the onset of ice-sheet retreat, streams deposited their load into a shallow-water glaciomarine environment; gravelly sediments immediately in front of the ice-grounding line and finer material, in suspension, to more distal areas. Ice-rafting, slumping and traction currents were also active within the glaciomarine environment. The lithofacies characteristics of this sequence are consistent with deposition from a grounded tidewater ice-sheet. The glacigenic succession is restricted to the Forth Approaches area, which implies that the ice-sheet had a limited offshore extent.

Martyn S. Stoker, British Geological Survey, Murchison House, West Mains Road, Edinburgh, EH9 3LA, Scotland; Alistair Bent, Grant Institute of Geology, University of Edinburgh, Kings Buildings, West Mains Road, Edinburgh, Scotland; *1st October, 1984 (revised 6th February, 1985).*

The possible existence of pre-Weichselian Quaternary sediments in the central North Sea was first suggested by Jansen (1976). This was disputed by Holmes (1977) who, on the basis of radiocarbon age dates, assigned the bulk of the Quaternary sequence to the Weichselian glacial stage. However, more recent detailed stratigraphic work by Jansen *et al.* (1979), Jansen & Hensey (1981) and Stoker *et al.* (1983; in press a, b) has confirmed the original conclusion that a more extensive Pleistocene sequence exists in the central North Sea.

In the western part of the central North Sea, the Forth Approaches area (Fig. 1), the only previously recorded glacial and glaciomarine sediments are of late Weichselian age (Thomson & Eden 1977). In this paper we present stratigraphic and sedimentological evidence for an early Middle Pleistocene ice-sheet in the vicinity of the Forth Approaches. This combines regional stratigraphic data (Stoker *et al.* in press b) with a sedimentological analysis and facies interpretation of nine boreholes. In view of their age and spatial setting, these sediments enable us to compare the offshore extent of this ice-sheet with the Late Weichselian ice-sheet.

Stratigraphic setting

The sediments described in this paper belong to the Aberdeen Ground Formation, previously called the Aberdeen Ground Beds (Holmes 1977), which is the oldest proven Quaternary unit in the central North Sea (Fig. 2). This formation occurs mostly at subcrop below younger Quaternary formations and forms an easterly thickening wedge-shaped unit, at least 130 m thick in the eastern part of the central North Sea. Its areal extent and western subcrop limit are shown in Fig. 1.

In the west, the base of the formation rests with angular unconformity on rocks of Palaeozoic, Mesozoic and Tertiary age. To the east, as the sequence thickens, the base becomes obscured on seismic records by multiple reflections and cannot be identified at present. The top of the formation is marked by a distinct irregular erosion surface, and is unconformably overlain by the Ling Bank Formation (formerly Lower Channel Deposits of Holmes (1977)), although younger formations come on to the west.

A Lower to Middle Pleistocene age for the Aberdeen Ground Formation was suggested by a palaeomagnetic study which identified the Brunhes/Matuyama palaeomagnetic boundary in this unit (Stoker *et al.* 1983). This has generally been taken to mark the Lower/Middle Pleistocene boundary (Butzer & Isaac 1975) and has been placed towards the base of the 'Cromerian Complex' (Zagwijn 1979). Estimates of the age of this boundary vary from 0.73 Ma (Mankinen & Dalrymple 1979) to 0.79 Ma (Johnson 1982). The existence of Lower and Middle Pleistocene

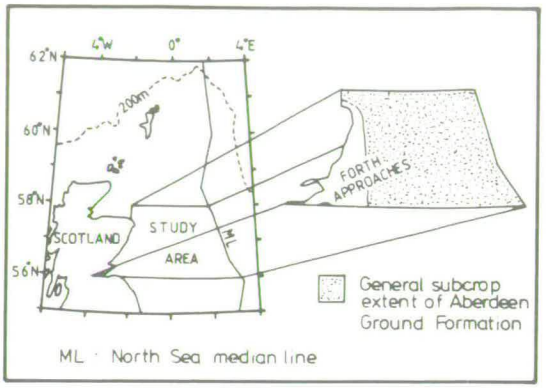

Fig. 1. Location of study area and subcrop extent of the Aberdeen Ground Formation in the central North Sea.

strata has subsequently been confirmed by amino-acid geochronology (Brigham-Grette & Sejrup 1984), and micropalaeontological data which have identified sediments as old as Tiglian in age (Stoker *et al.* in press b). The overlying Ling Bank Formation includes a rich interglacial marine fauna and flora (Stoker *et al.* in press b) and macrofossils of the freshwater plants *Potamogeton* sp. and *Azolla filiculoides* (Griffin 1984). *A. filiculoides* has not been recorded in sediments younger than Holsteinian in age in Britain or north-west Europe (Godwin 1975). The interglacial has thus been correlated with the Holsteinian and the erosion surface at the top of the Aberdeen Ground Formation is most probably of late Elsterian age.

The Lower Pleistocene part of the Aberdeen Ground Formation consists predominantly of bioturbated marine muds with occasional interbedded sands which were deposited in a temperate to boreal, inner to middle shelf environment. Just above the Brunhes/Matuyama boundary the sediments and microfossils in the upper part of the Aberdeen Ground Formation contain the earliest indications of fully glacial climatic conditions in the central North Sea. In the study area, a thin wedge of glacigenic sediments, in the west, pass eastwards into argillaceous marine sediments. It is the description and stratigraphic setting of these sediments which form the basis of our study.

Facies

Subdivision of the glacigenic sequence has been made predominantly on the basis of sediment core description, grainsize analysis of the $< 2\,\mu m$ fraction and clast content. Sediment terminology is after Folk (1954). Palaeontological data have been included where available.

Three main facies have been identified within the glacigenic sequence and these are described separately below. A brief summary of the more normal marine facies, which forms the bulk of the Aberdeen Ground Formation, is also included as it is relevant to the general stratigraphic setting and overall facies model. The lithofacies relationships are shown in Fig. 3, which also indicates the position of the Brunhes/Matuyama palaeomagnetic boundary in boreholes 81/27 and 81/34 and provides a baseline for temporal correlation.

Subglacial facies

This facies occurs at the base of boreholes 74/10 and 74/12 and appears to form a localised mounded unit, 2 to 3 m in thickness (Fig. 3). In borehole 74/12 the base of the facies rests sharply on pyritous Lower Cretaceous shales, and may

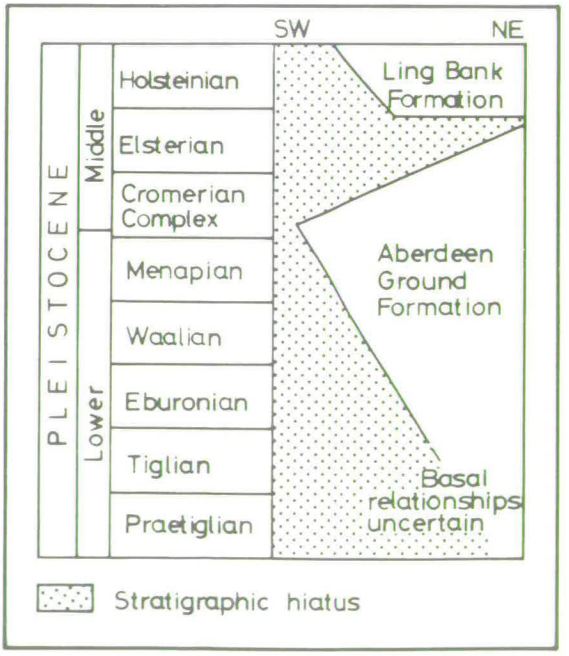

Fig. 2. Stratigraphic column of Lower, and part of Middle Pleistocene succession in the central North Sea, using British Geological Survey recommended terminology (after Stoker *et al.* in press a). Subdivision of the Pleistocene is based on the Dutch stratigraphic classification (Zagwijn 1979).

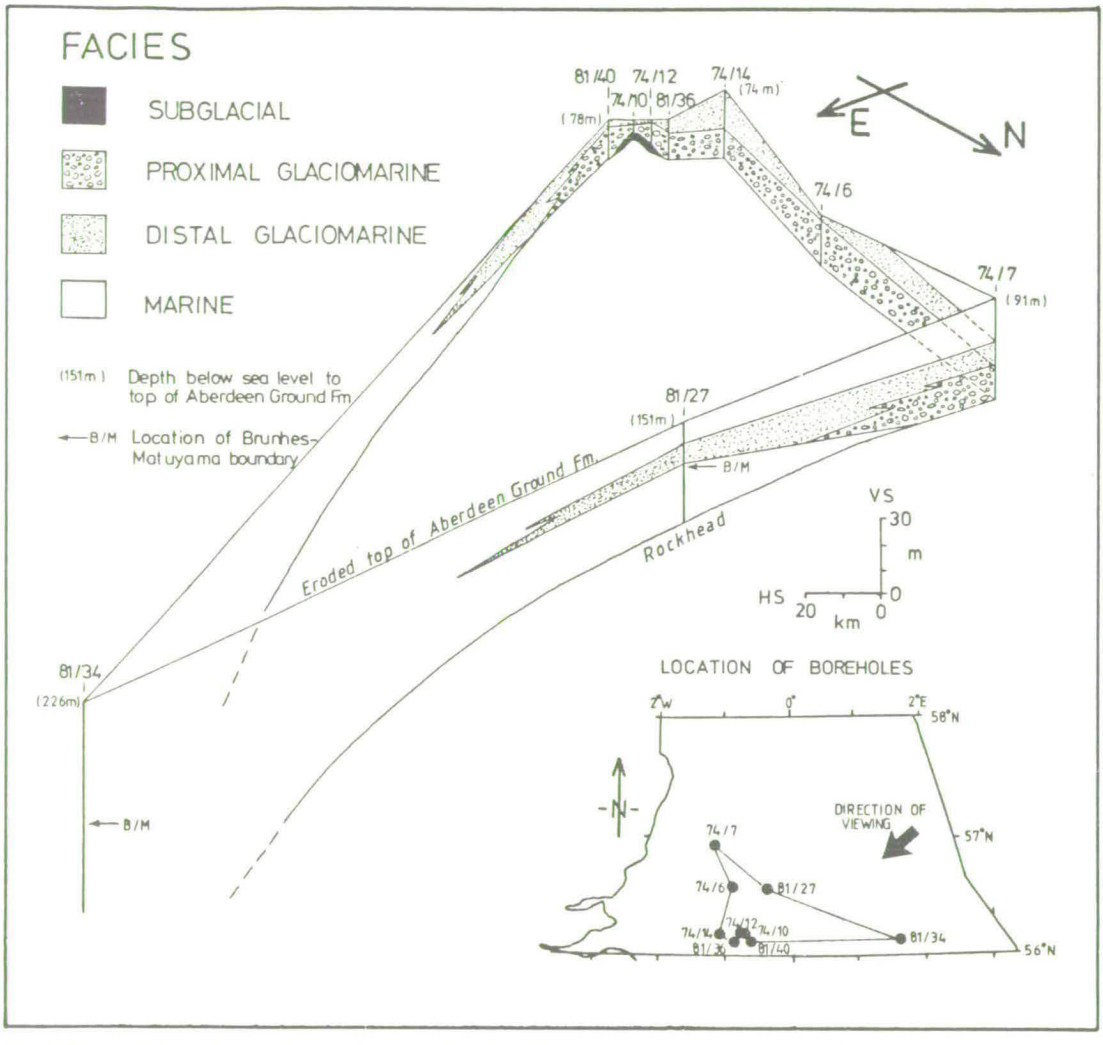

Fig. 3. Schematic fence diagram showing facies relationships. Direction of viewing is from the north-east.

be erosional as thin shale rip-up clasts are included near the base of the sequence. The top of the facies is overlain by proximal glaciomarine sediments although the exact nature of the contact is unknown.

The sediments consist of brown to olive-grey, firm, very poorly sorted, dominantly matrix-supported, gravelly sandy muds with no faunal remains. The grain-size distribution of this unit is polymodal (Fig. 4, Table 1) and texturally homogeneous (within the core). No obvious bedding structures were noted and pebble orientations varied from subhorizontal to subvertical. Clast composition is predominantly Moine/Dalradian metasediment and meta-igneous, red-purple Devonian sandstones and volcanics and grey Palaeozoic or Mesozoic sandstones, of local derivation. Fifty five percent of the pebbles were observed to be faceted and 20 % displayed striations, however, only 5 % had a distinctive 'bullet-shaped' appearance.

The textural homogeneity, unfossiliferous character, high clast content and locally erosive base suggest, collectively, that these sediments are of subglacial origin and represent some form of lodgement till. The sediments were probably deposited during the final stages of ice-advance and we suggest that their stratigraphic location

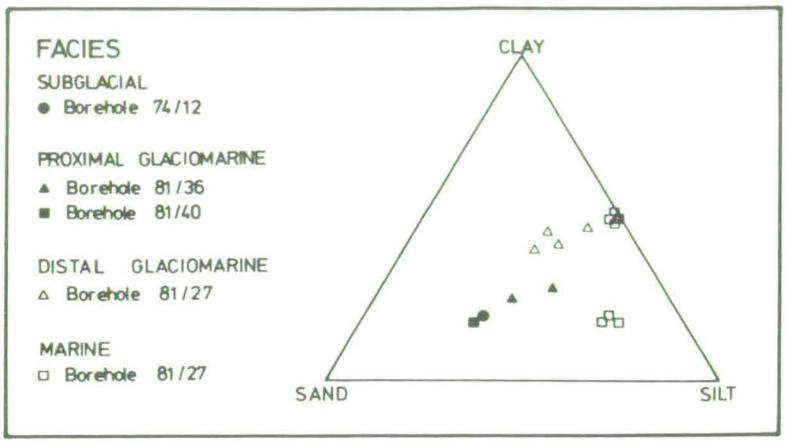

Fig. 4. Triangular diagram illustrating the grain-size distribution of the <2 μm fraction of the various facies. Each data point represents one sample.

marks the approximate easterly limit of the ice-grounding line. Proximity to the glaciomarine environment is supported by the similarities in the grain-size distribution of the subglacial and proximal glaciomarine facies (Fig. 4, Table 1). These sediments may be the preserved remnants of a previously more extensive subglacial till cover. Alternatively, the seemingly isolated till-mound may be an original feature and represent a localised ice-grounding point.

Proximal glaciomarine facies

This facies occurs in boreholes 74/6, 74/7, 74/10, 74/12, 74/14, 81/36 and 81/40 and forms an easterly thinning wedge of sediment up to 18 m thick (Fig. 3). Over most of the area the base of this facies rests on pre-Quaternary strata although in boreholes 74/10 and 74/12 it overlies the subglacial facies. Laterally and vertically the proximal glaciomarine facies passes transitionally into the distal glaciomarine facies.

The sediments of this facies consist dominantly of olive-grey to brown-grey medium-to-coarse, very poorly sorted, matrix-supported gravelly muds and gravelly muddy sands. Shell fragments are abundant although they are mostly worn and abraded and beyond recognition, however, in borehole 81/40 several specimens of *Macoma balthica* (Linné) have been identified (D. K. Graham 1982, pers. comm.). The grain size distribution of this unit is polymodal (Fig. 4, Table 1) and more texturally heterogeneous than in the subglacial facies. The bulk of the sediments lacked any obvious signs of bedding, although in borehole 74/7 a distinct pebbly sandy mud horizon, up to 2 m thick and similar to the subglacial sediments, occurs within the proximal glaciomarine sediments and probably forms a localised lens, sheet or wedge of till-like material. In borehole 81/36 the transitional passage from ice-proximal to ice-distal sediments is marked by an upwards change from coarse gravelly muddy sands through interlaminated sands and muds, with a discrete pebble band, into slightly sandy and gravelly muds. This change occurs over about one metre. The thin sandy units (approx. 1–2 cm thick) within the interlaminated sequence are rippled and laminated, and both flaser and lenticular bedding are present. Pebbles throughout this facies are dominated by Moine/Dalradian meta-igneous and metasediment, Devonian sandstones and volcanics, Palaeozoic or Mesozoic sandstones, siltstones and mudstones, and Upper Cretaceous chalk, limestone and flint, of local origin. Up to 70 % of the pebbles are faceted although only 5 % displayed striations.

Scarce foraminiferal data from borehole 81/36 suggest that deposition of the sediments occurred in a shallow-water glaciomarine environment, with the paucity of fauna indicative of unfavourable conditions (Stoker *et al.* in press a). The coarse nature of the sediments implies deposition

Table 1. Gravel fraction as a percentage of the total sediment sample.

Subglacial facies	20–30 %
Proximal glaciomarine facies	5–20 %
Distal glaciomarine facies	<5 %
Marine facies	<1 %

from powerful sediment-laden currents. The sheet-like geometry of this facies indicates that sedimentation was not constrained in any way and was able to expand laterally. We envisage a situation whereby meltwater streams issuing from the base of a glacier emerged from beneath the ice-front and deposited their load subaqueously into a shallow sea. From our limited borehole data it is impossible to identify, in detail, the sedimentary environment, e.g. subaqueous outwash fan (Cheel & Rust 1982), although the general setting is probably much the same. Some detail, however, is provided by examination of the interlaminated ice-proximal/ice-distal transitional sequence. The rippled sand units provide evidence of horizontal bottom transport while the intervening homogenous mud may have been deposited from suspension fall-out from surface sediment plumes, or from turbidity currents (associated with the sandy units). The localised occurrence of pebble bands within this sequence suggests that either powerful sediment discharges still periodically swept across this part of the sea floor or that gravity flow or ice-rafting processes were active. The existence of a till-like unit within the proximal-glaciomarine facies clearly indicates the proximity of the ice-front. The lack of any glaciodynamic deformation in the underlying sediments, however, rules out the likelihood of the till-like sediments being deposited as lodgement till during a minor readvance and suggests that these sediments were derived from slumping off, or melt-out from, the ice-margin. Iceberg calving and subsequent release of debris from the ice-front is also another likely source for much of the coarse gravel and sand which characterise this facies.

Distal glaciomarine facies

This facies is present in all boreholes except 81/34, and forms an easterly thinning sheet up to 16 m thick (Fig. 3). In the west, the base of the facies rests conformably on ice-proximal sediments, although locally it may rest directly on pre-Quaternary strata. In the east, it interfingers with, and, where not eroded, is conformably overlain by the marine facies.

The sediments are characterised by olive-grey to dark brown, stiff, very poorly sorted, matrix-supported, slightly sandy and gravelly muds, with occasional shell fragments, sandy lenses and sand-filled infaunal burrows. The grain size distribution of the sediment is essentially bimodal (Fig. 4, Table 1). Although the gravel fraction is much less in these sediments than in the subglacial and proximal glaciomarine sediments, it nevertheless forms a distinct component within the predominantly fine-grained sediments. Pebbles in this facies include Dalradian metasediment, Devonian sandstones, Palaeozoic or Mesozoic sandstones and Upper Cretaceous flints. Approximately 50 % of the clasts are faceted but none showed any striations.

The characteristics of this facies are consistent with deposition in a distal glaciomarine environment (Powell 1984). In particular, the high clay content and the lack of current indicators suggest a low energy environment, but with a subsidiary input of coarse material probably by ice rafting. The fine sediment fraction was probably carried by surface sediment plumes, originating at the ice-front, but by-passing the proximal zone and eventually being deposited from suspension fall-out. Coarser sand and gravel was carried beyond the proximal zone by icebergs which eventually melted or overturned releasing their debris to the seabed.

Marine facies

This facies has been examined in boreholes 74/7, 81/27 and 81/34 and forms an easterly thickening wedge of sediment in excess of 80 m in borehole 81/34. The interdigitatery nature of the glacigenic sequence into the marine facies is clearly illustrated in Fig. 3.

The sediments consist dominantly of very dark grey to olive-brown, hard, poorly sorted, bioturbated sandy muds, which are commonly associated with complexly laminated sands and muds and normally-graded sands, and subordinate dark brown, moderately sorted, structureless mud (Fig. 4). These sediments were deposited in a middle-to-inner-shelf environment, and micropalaeontological data from boreholes 81/27 and 81/34 indicate that favourable climatic conditions began to deteriorate up the sequence at about the level of the Brunhes/Matuyama palaeomagnetic boundary (Stoker *et al.* in press b).

A general facies model

A general facies model for the development of the glacigenic sequence is summarised in Fig. 5. The lithofacies relationships and their areal extent (tens of km rather than hundreds – cf. Fig. 6) are consistent with deposition from a ground-

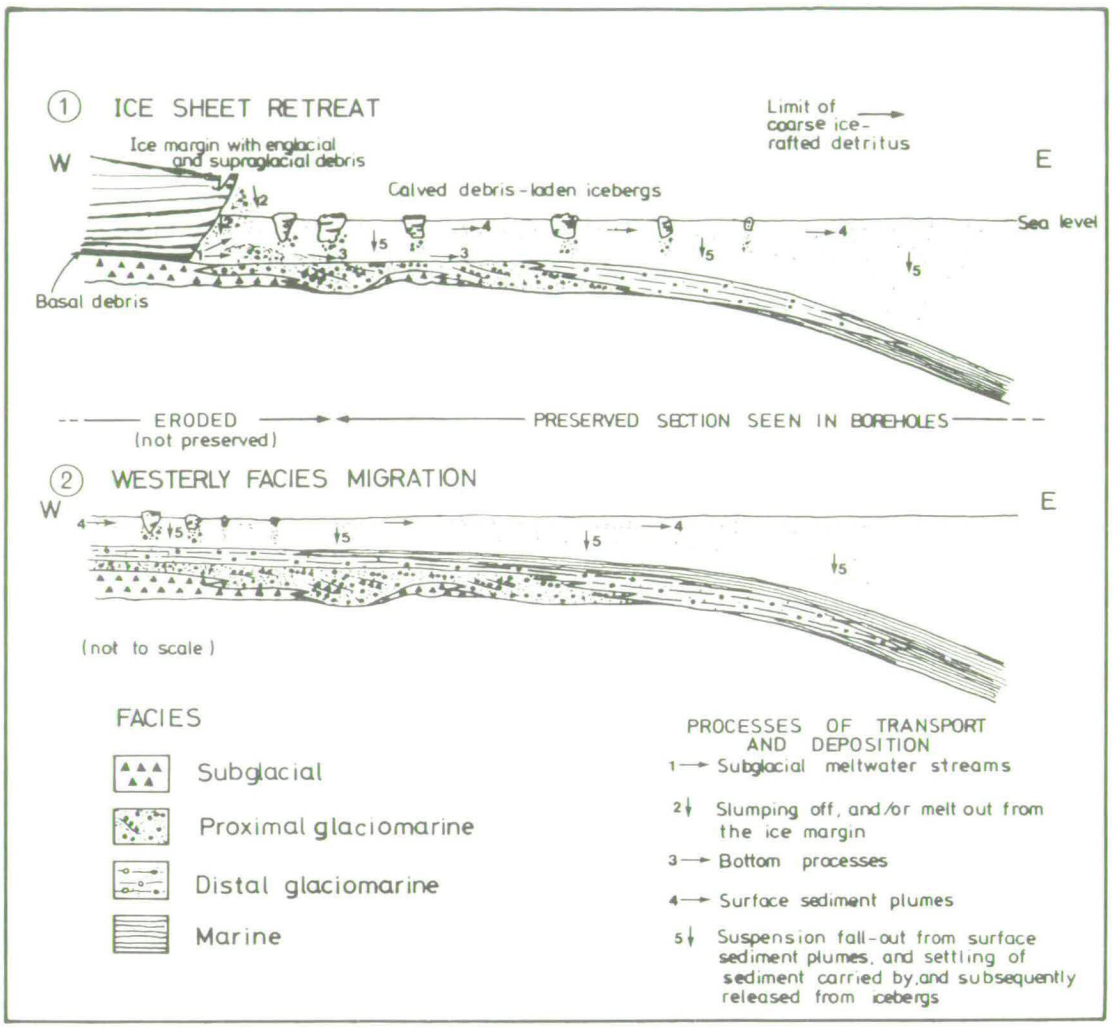

Fig. 5. Schematic model of facies development in a grounded tidewater ice-sheet environment. For explanation see text.

ed tidewater ice-sheet (cf. Powell 1984). The subglacial facies was deposited during the final stages of ice-advance while the glaciomarine facies was deposited as the ice-sheet began to melt and retreat. During ice-retreat meltwater streams discharging from tunnels beneath the ice-sheet deposited coarse proximal glaciomarine sediments immediately in front of the ice-grounding line, while the finer material was generally carried in suspension to greater distances from the ice-front, although bottom-flowing traction currents did exist. Calving of icebergs from the front of the ice-sheet carried entrapped basal and high-level debris away from the ice-margin into more distal areas, where it was eventually dumped due to melting or toppling of the iceberg and incorporated into the distal muds. Melting at the ice-front and slumping and/or melt-out of material may also have resulted in the inclusion of till-like deposits as discrete sheets or lenses within the proximal glaciomarine facies.

Overall fining of the sediments with increasing distance from the ice-front is clearly illustrated by grain-size analysis of the sand-mud fraction; the sand content clearly decreases away from the subglacial and proximal glaciomarine facies to the distal glaciomarine and marine facies (Fig. 4). A decrease in the gravel content is also appar-

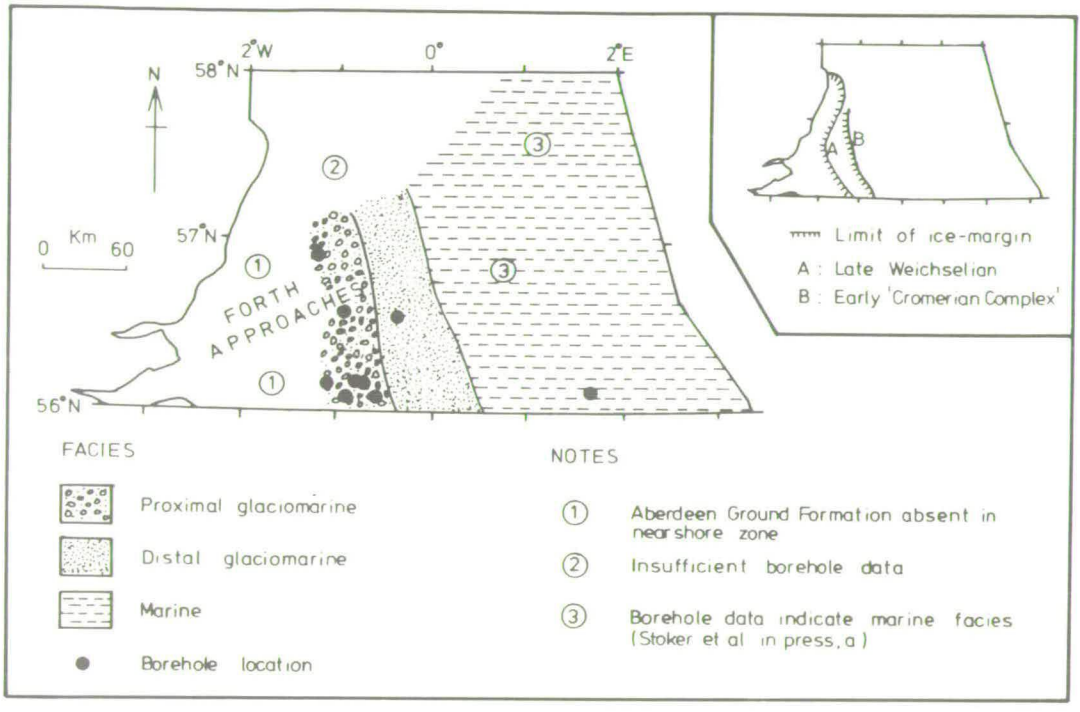

Fig. 6. Generalised palaeogeographic map of early 'Cromerian Complex' proglacial depositional environments at the onset of ice-sheet retreat. Inset shows the relative locations of the early 'Cromerian Complex' and late Weichselian ice-margins. Position of late Weichselian ice-margin after Thomson & Eden (1977) and Stoker *et al.* (in press a).

ent (Table 1). The lack of ice-rafted sandy and gravelly detritus within the marine sediments in borehole 81/34, at a level equivalent to that in borehole 81/27 (correlated by the palaeomagnetic boundary) suggests that there was a limit to the distance that icebergs were able to travel. This limit may have been due to restrictions imposed by sea ice or, as is more common under temperate tidewater conditions, to rapid melting of the icebergs (Powell 1984). Continued ice-sheet retreat led to the westerly migration of the various facies and the establishment of the overlapping facies relationships.

Correlation of the glacigenic sequence

The location of the Brunhes/Matuyama palaeomagnetic boundary in borehole 81/27 lies 1 m below the distal glaciomarine horizon. There is no evidence of any intervening erosional breaks, thus the boundary provides us with an effective stratigraphic marker for correlating the glacigenic sequence. As the Lower/Middle Pleistocene boundary is taken at the Brunhes/Matuyama boundary the sediments would appear to be of very early Middle Pleistocene age. Zagwijn *et al.* (1971) noted a correlation between the Brunhes/Matuyama boundary and the 'Glacial A' subdivision of the 'Cromerian' stage in the Dutch Quaternary sequence. The close proximity of the glacigenic sequence to the palaeomagnetic boundary suggests that these sediments may be correlatable with the 'Glacial A' subdivision, which would imply an early 'Cromerian Complex' age.

Palaeogeographic implications

The spatial distribution of the glacial and glaciomarine sediments at the onset of ice-sheet retreat is illustrated in Fig. 6. Deglaciation subsequently led to a westerly facies migration into the Forth Approaches which suggests that this area was a major outlet for glacial ice at this particular time. Clearly, however, the ice-sheet had a limited

offshore extent, and the facies distribution beyond the ice-front, even at the time of maximum ice-advance, suggests that:

(1) the ice-sheet responsible for the glacigenic sequence was restricted to the UK; and,
(2) beyond the ice-margin the central North Sea was not covered by glacial ice, hence, no Scandinavian ice-sheet was involved in the deposition of these sediments.

Conclusions

A sequence of early Middle Pleistocene glacial and glaciomarine sediments has been identified in the west central North Sea, and has been tentatively dated as early 'Cromerian Complex' in age. These sediments represent, at present, the earliest indications of glacial climatic conditions in this area. They form an easterly thinning wedge of sediment, passing laterally and vertically into marine sediments, and were deposited from a grounded tidewater ice-sheet of restricted offshore extent.

The proposed location of the ice-margin is very similar to that envisaged for the late Weichselian ice-sheet (Fig. 6), and supports the growing belief that Scottish ice-sheets may have been more localised in their occurrence.

Acknowledgements. – We thank Dr. R. A. Scrutton for his comments on an early version of this manuscript. One of us (AB) acknowledges the receipt of a NERC research grant. This paper is published with the permission of the Director, British Geological Survey (NERC).

References

Brigham-Grette, J. & Sejrup, H. P. 1984: Stratigraphic resolution of amino-acid geochronology in North Sea Quaternary sediments. *In* Aarseth, I. & Sejrup, H. P. (eds.): *Quaternary Stratigraphy of the North Sea*, 30–32. Abstract volume, Symposium Univ. of Bergen.

Butzer, K. W. & Isaac, G. K. 1975: *After the Australopithecines*. The Hague.

Cheel, R. J. & Rust, B. R. 1982: Coarse grained facies of glacio-marine deposits near Ottawa, Canada. *In* Davidson-Arnott, R., Nickling, W. & Fahey, B. D. (eds.): *Research on Glacial, Glacio-fluvial and Glacio-Lacustrine Systems*, 279–293. GEO Books, Norwich.

Folk, R. L. 1954: The distinction between grain size and mineral composition in sedimentary rock nomenclature. *J. Geol. 62*, 344–359.

Godwin, H. 1975: *History of the British Flora: A Factual Basis for Phytogeography*. 541 pp. Cambridge Univ. Press, Cambridge.

Griffin, K. 1984: Plant macrofossils from a Quaternary deposit in the North Sea. *In* Aarseth, I. & Sejrup, H. P. (eds.): *Quaternary Stratigraphy of the North Sea*, 33. Abstract volume, Symposium Univ. of Bergen.

Holmes, R. 1977: Quaternary deposits of the central North Sea, 5. The Quaternary geology of the UK sector of the North Sea between 56° and 58°N. *Rep. Inst. Geol. Sci. 77/14.*

Jansen, J. H. F. 1976: Late Pleistocene and Holocene history of the northern North Sea, based on acoustic reflection records. *Neth. J. Sea. Res. 10*, 1–43.

Jansen, J. H. F. & Hensey, A. M. 1981: Interglacial and Holocene sedimentation in the northern North Sea: an example of Eemian deposits in the Tartan Field. *Spec. Publ. Int. Ass. Sediment. 5*, 323–334.

Jansen, J. H. F., Doppert, J. W. C., Hoogendoorn-Toering, K., DeJong, J. & Spaink, G. 1979: Late Pleistocene and Holocene deposits in the Witch and Fladen Ground area, northern North Sea. *Neth. J. Sea Res. 13*, 1–39.

Johnson, R. G. 1982: Brunhes-Matuyama Reversal dated at 790,000 yr BP by marine-astronomical calculations. *Quat. Res. 17*, 135–147.

Mankinen, E. A. & Dalrymple, G. B. 1979: Revised geomagnetic time scale for interval 0-5my B.P. *J. Geophys. Res. 84*, 615–626.

Powell, R. D. 1984: Glacimarine processes and inductive lithofacies modelling of ice-shelf and tidewater glacier sediments based on Quaternary examples. *Marine Geology 57*, 1–52.

Stoker, M. S., Long, D. & Fyfe, J. A. in press a: A revised Quaternary stratigraphy for the central North Sea. *Rep. Brit. Geol. Surv.*

Stoker, M. S., Long, D. & Fyfe, J. A. in press b: The Quaternary succession in the central North Sea. *Newsl. on Strat.*

Stoker, M. S., Skinner, A. C., Fyfe, J. A. & Long, D. 1983: Palaeomagnetic evidence for early Pleistocene in the central and northern North Sea. *Nature 304*, 322–334.

Thomson, M. E. & Eden, R. A. 1977: Quaternary deposits of the central North Sea. *Rep. Inst. Geol. Sci. 77/12.*

Zagwijn, W. H. 1979: Early and Middle Pleistocene coastlines in the Southern North Sea basin. *In* Oele, E., Schüttenhelm, R. T. E. & Wiggers, A. J. (eds.): *The Quaternary History of the North Sea*, 31–42. Acta Univ. Ups. Symp.

Zagwijn, W. H., van Monfrans, H. M. & Zandstra, J. G. 1971: Subdivision of the 'Cromerian' in the Netherlands; pollen-analysis, palaeomagnetism and sedimentary petrology. *Geol. en Mijnbouw 50*, 41–58.

Marine Geology, 73 (1986) 109–123
Elsevier Science Publishers B.V., Amsterdam — Printed in The Netherlands

LATE QUATERNARY PALAEONTOLOGY, SEDIMENTOLOGY AND GEOCHEMISTRY OF A VIBROCORE FROM THE WITCH GROUND BASIN, CENTRAL NORTH SEA

D. LONG[1], A. BENT[2], R. HARLAND[3], D.M. GREGORY[3], D.K. GRAHAM[1] and A.C. MORTON[3]

[1]*British Geological Survey, West Mains Road, Edinburgh EH9 3LA (Scotland)*
[2]*Grant Institute of Geology, Edinburgh University, Edinburgh EH9 3JW (Scotland)*
[3]*British Geological Survey, Keyworth, Nottinghamshire NG12 5GG (England)*

(Received July 25, 1985; revised and accepted March 6, 1986)

ABSTRACT

Long, D., Bent, A., Harland, R., Gregory, D.M., Graham, D.K. and Morton, A.C., 1986. Late Quaternary palaeontology, sedimentology and geochemistry of a vibrocore from the Witch Ground Basin, central North Sea. Mar. Geol., 73: 109–123.

Results are detailed from analytical procedures carried out on a single closely sampled 5.7 m long vibrocore from the Witch Ground Basin, central North Sea. Information about the environmental conditions during the deposition of the Witch Ground Formation, of late Weichselian to Holocene age, was obtained by combining the various palaeontological, sedimentological and geochemical results. This has suggested that a complete glaciomarine to marine sequence from before 13,000 to after 10,000 B.P. is present in the central North Sea. An ash layer equated with the Vedde Ash of western Norway has been identified for the first time in the UK sector.

INTRODUCTION

The Witch Ground Formation is a well-layered seismostratigraphic unit clearly identified over a large area of the central North Sea (Stoker et al., 1985) and occupies the topographic low of the Witch Ground Basin. It has been examined previously by Jansen (1976) as the Witch and Fladen deposits and by Holmes (1977) as the Witch Ground Beds. They have suggested that the sediments were deposited during the late Weichselian to Holocene in a glaciomarine to marine environment, although these ages are uncertain. The base of the formation forms a distinct irregular surface scoured by sea-ice (Stoker and Long, 1984). Various ages have been suggested for the base including mid-Weichselian (Jansen, 1976), late Weichselian (Stoker and Long, 1984) and Younger Dryas (Holmes, 1977).

A core (number 58+00/111) of 5.7 m length was extracted from the Witch Ground Basin in the North Sea at 58°34.5′N, 00°24.1′E, in 140 m of water (Fig.1a) using an electrically operated vibrocorer from an anchored vessel, as part of the British Geological Survey's routine sampling programme. Sampling

0025-3227/86/$03.50

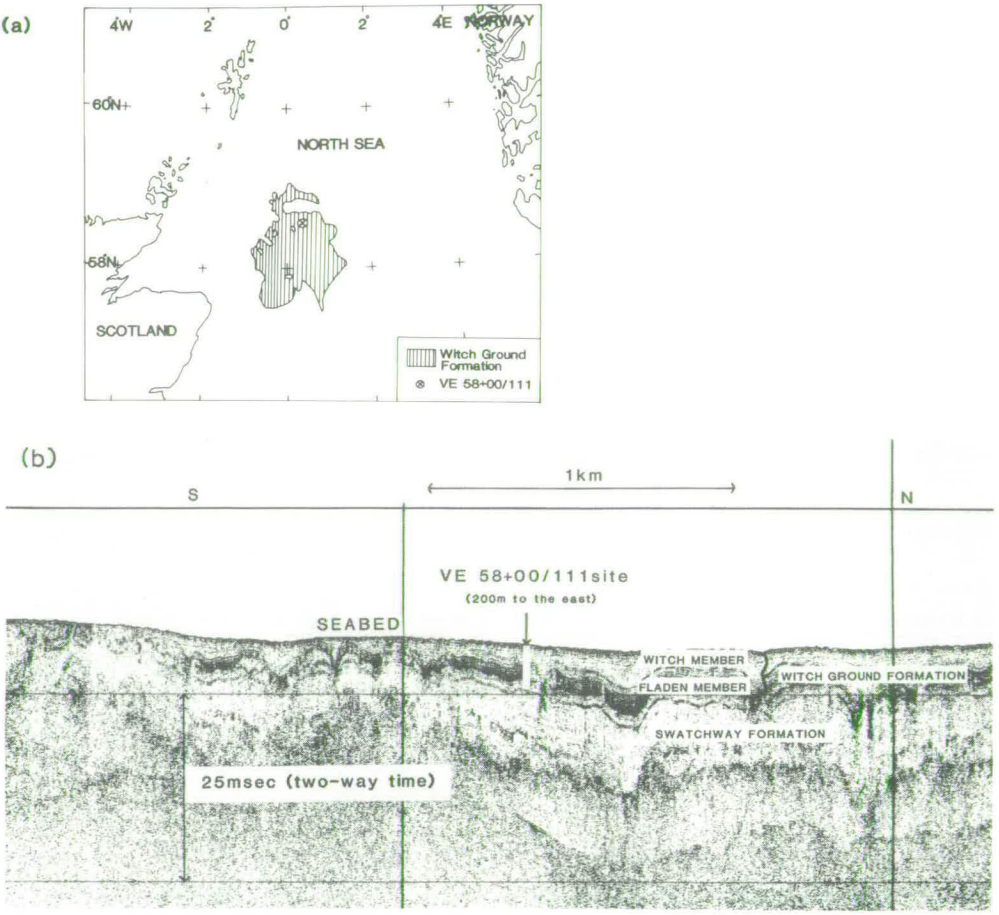

Fig.1. (a) Location of VE 58+00/111. (b) Boomer record close to vibrocore site, showing the upper, faintly layered Witch Member and the underlying, well-layered Fladen Member.

methods have previously been described by Ardus et al. (1982). The core was cut into six lengths, split longitudinally, and then photographed and described whilst on board ship. The detailed core description is based on shipboard photographs, visual description and grain-size analysis. The core was subdivided and various analyses into the particle size, sediment geochemistry and clay mineralogy (A.B.), dinoflagellate cysts (R.H.), foraminifera (D.M.G.), macrofauna (D.K.G.) and volcanic ash (A.C.M.) were carried out.

A seismic section (Fig.1b) run approximately 200 m to the east, shows that the core penetrated two distinct units but probably just failed to reach the irregular base of the formation. The upper, faintly layered unit is pitted by pockmarks at the sea bed, whereas the lower, well-layered unit is characterised by an irregular base reflector with a relief of up to 3 m. These have been

identified as the Witch and Fladen Members of the Witch Ground Formation (Stoker et al., 1985). The contact between the two units appears to be gradational, occurring at between 2.5 and 3.0 m below the sea bed. An acoustic velocity of 1550 m s^{-1} is typical for these sediments. At this locality the two units form a condensed sequence, just over 6 m thick, of the Witch Ground Formation. Elsewhere this formation has been identified up to 30 m thick. Its base is probably not a single chronostratigraphic horizon but seems to represent the last disturbance of the palaeoseabed by sea-ice as there is often little lithological or geotechnical difference between the Witch Ground Formation and the underlying Swatchway Formation.

Methods

Grain-size analyses of the sub 2 μm grades were carried out using the procedures outlined in Galehouse (1971). Samples were prepared for X-ray diffraction (XRD) analysis of the clay fraction by separating and concentrating the sub 2 μm grades using settling and centrifuge techniques, respectively. Orientated aggregates were made on glass slides. The analyses were run using a Philips diffractometer with machine settings at 40 kV, 20 mA, 1°20′ min^{-1} scanning rate, 1° receiving slit and Cu Kα radiation.

Three XRD traces were run for each sample: (1) untreated; (2) after treating the sample with ethylene glycol at 60°C; and (3) after heating the sample to 180°C. Semi-quantitative analyses were carried using the procedures outlined by Griffin (1971).

The bulk geochemistry of the sediments was determined using X-ray fluorescence spectrometry. The samples were first ignited at 1100°C to remove any volatile material and glass discs (45 mm diameter) were then made for major element analyses (after the method of Norrish and Hutton, 1969). The analyses were corrected for mass absorption effects (using the tables of Theisen and Vollach, 1967) and interference effects where appropriate.

Fifty-two samples taken at 10 cm intervals were analysed for their foraminiferal and dinoflagellate cyst content. Foraminiferal analysis was undertaken using methods similar to those described by Skinner and Gregory (1983). Walton's faunal diversity index has been applied in this study; this is the number of ranked species in an assemblage whose cumulative percentage accounts for 95% of the total. The dinoflagellate cyst samples were given a normal palynological processing technique using the sintered glass funnel procedure of Neves and Dale (1963), avoiding any oxidation which might inadvertently destroy peridiniacean cysts (Dale, 1976).

The composition of volcanic glass shards was determined by electron microprobe, using a Link Systems energy-dispersive X-ray analyser attached to a Geoscan electron microprobe.

Results

Four principal depositional environments were identified based primarily on the discovery of four distinct dinoflagellate zones (Fig.2) and to a lesser extent on foraminiferal (Fig.3) and lithological evidence (Fig.4). The discovery of an ash layer at 0.6 m similar in composition to the Vedde Ash (Mangerud et al., 1984) allowed the respective facies to be assigned to possible chronozones. The characteristics of these facies are discussed below.

Facies A — 5.3–2.8 m: This consists of thickly interbedded soft grey-brown (2.5Y 6/2, Munsell Colour Chart) muds and silty-sandy muds; contacts between the two lithologies are gradational. Monosulphide layers and partings occur throughout. Unimodal particle-size distributions in the finer beds (Fig.4) with over 50% clay and only 1% sand suggest deposition by suspension with only limited current action. The coarser beds, consisting of unimodal muddy sands

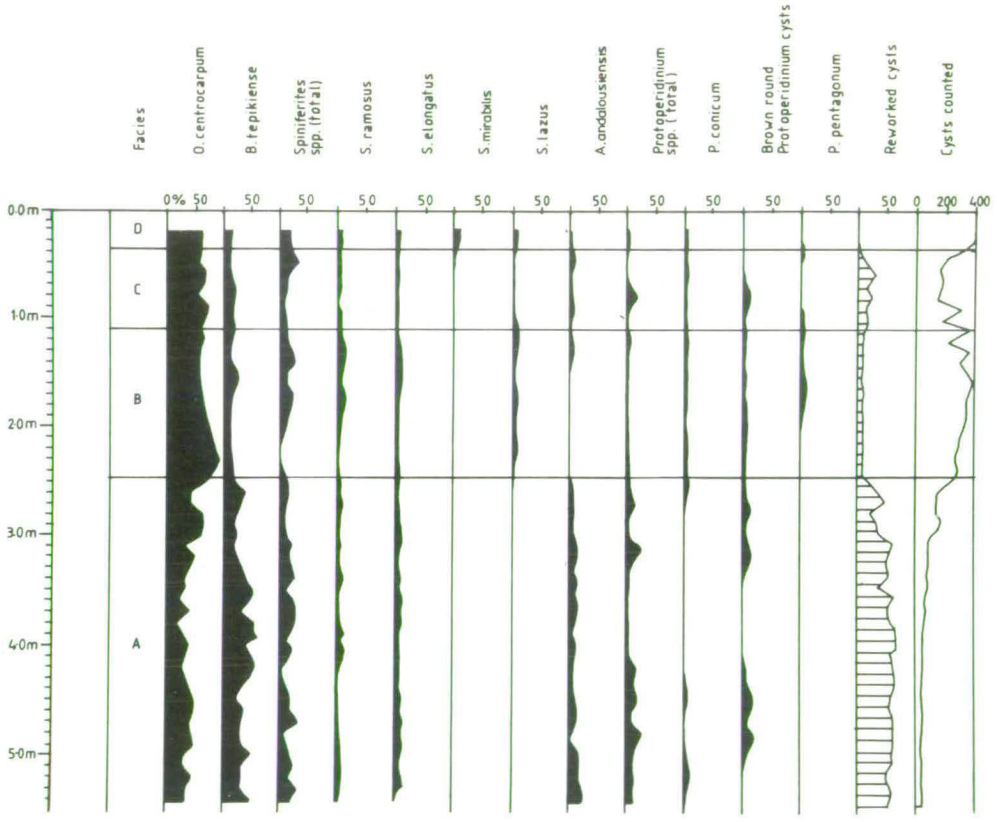

Fig.2. Dinoflagellate cyst variations of VE 58+00/111. The proportions of cysts presented are per the number counted. The number counted usually represents a total count of one microscope slide or until one species numbers a total of 125 specimens.

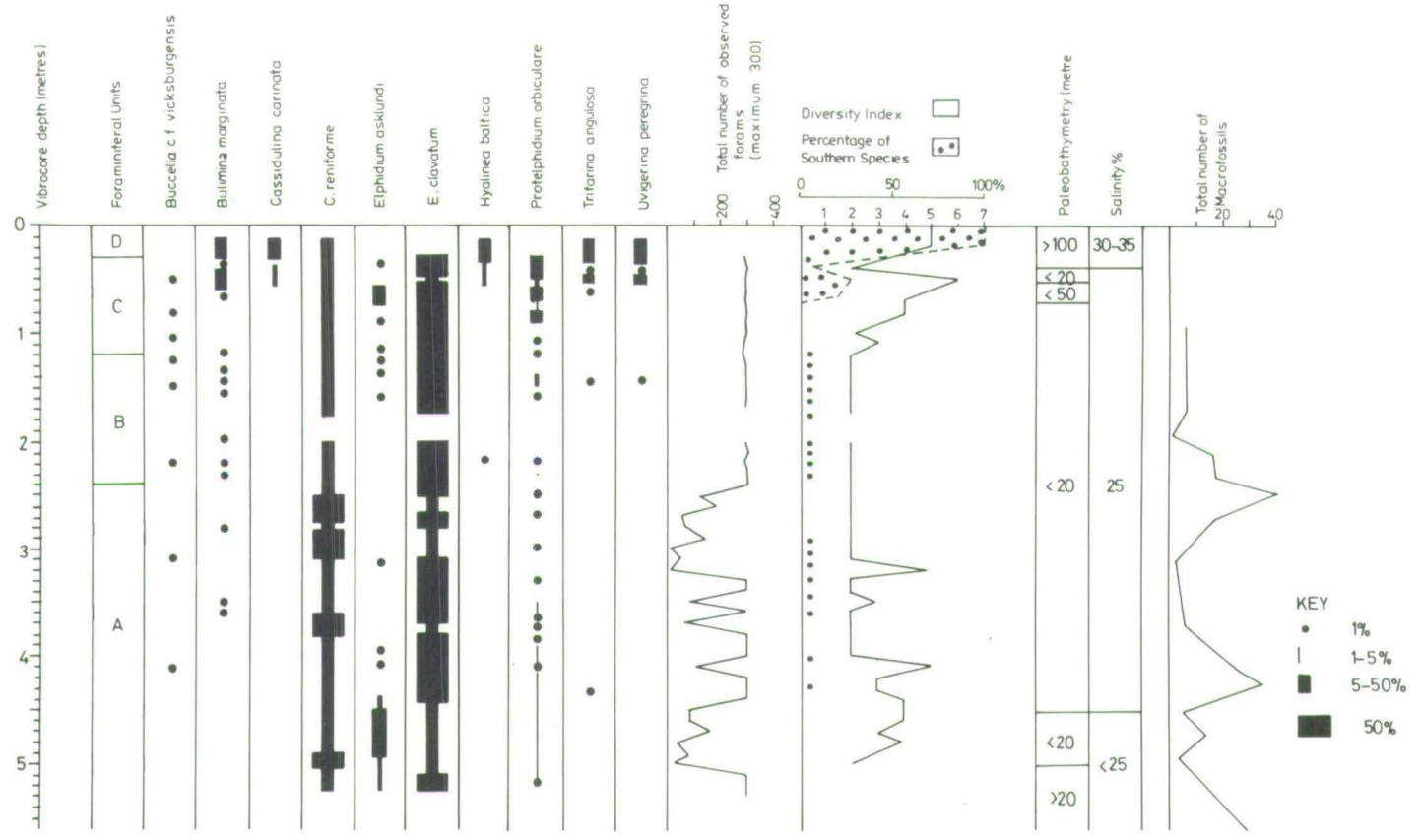

Fig.3. Foraminiferal variations of VE 58+00/111.

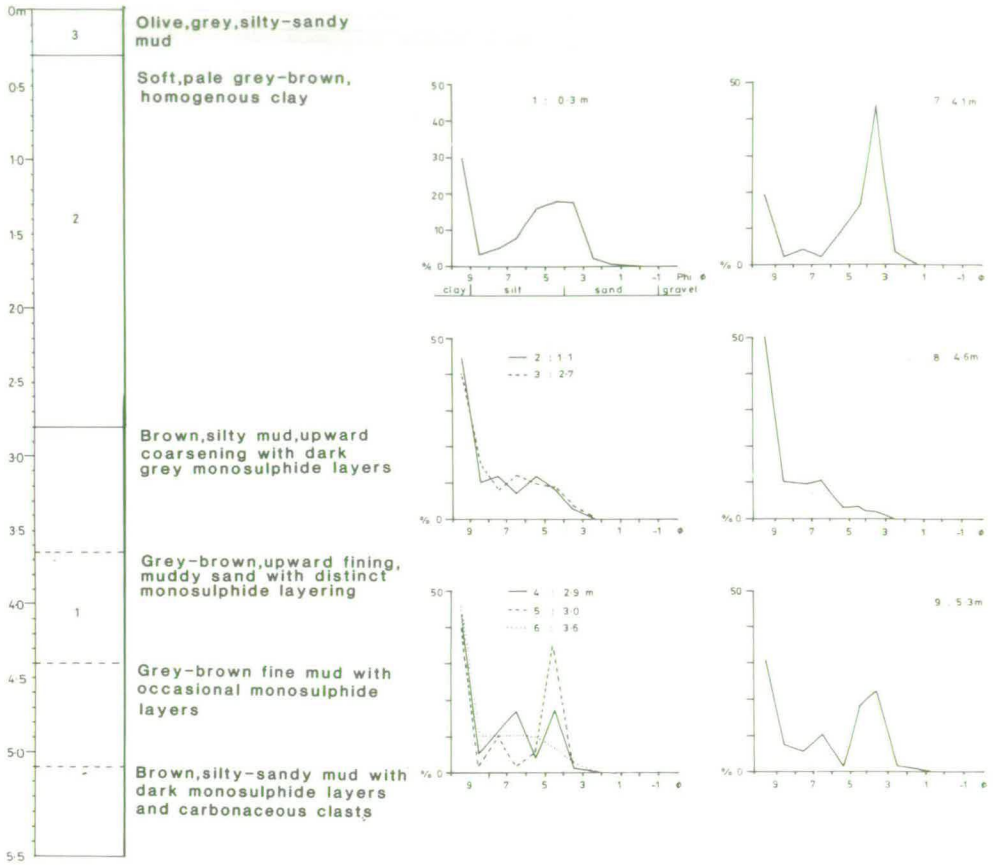

Fig.4. Sedimentology of VE 58+00/111.

and bimodal sandy muds, may indicate shallower water and stronger current activity.

The dinoflagellate cyst assemblage is characterised by a significant degree of reworking (Fig.2). *Bitectatodinium tepikense* Wilson is the dominant species and this, coupled with the presence of *Spiniferites frigidus* Harland and Reid and *Achomosphaera andalousiensis* Jan du Chêne, suggests a cold water environment with only limited contact with Atlantic waters (Reid and Harland, 1977; Harland, 1983). This conclusion is supported by the lack of more temperate species. In addition the occurrrence of significant proportions of round brown *Protoperidinium* cysts produced by non-photosynthesising dinoflagellates may indicate periods of sea-ice cover (Dale, 1985), or at least a close association with sea-ice.

Elphidium clavatum Cushman with subsidiary *Cassidulina reniforme* Norvang dominate a glaciomarine foraminiferal assemblage. Water depths of around 20 m and salinity values of 25‰ are indicated throughout (Skinner and

Gregory, 1983). Small-scale variations in the foraminiferal assemblage appear to relate to lithological changes, the coarser sandy muds and muddy sands containing a slightly richer and more diverse assemblage. Errant individuals of southern species such as *Buccella* cf. *vicksbergensis* (Cushman and Ellison) and *Bulimina* spp. occur in the upper part of this facies unit; these may be spurious or the first indications of penetration by the North Atlantic Current.

The macrofauna has a restricted diversity, dominated by the bivalves *Portlandia arctica* (Gray) and *Portlandia* (*Yoldiella*) *lenticula* (Möller). The thin shells are generally undamaged, suggesting little if any reworking and that they are in situ. Ockelmann (1958, p.25) observed that the optimum habitat of *P. arctica* to be off the mouths of rivers with meltwater and off glacier fronts where large quantities of mud and clay are deposited.

In conclusion, it is thought that facies A was deposited in a cold probably shallow glaciomarine environment cut off from the Atlantic, with low salinities maintained by glacial meltwater input. The absence of dropstones probably indicates an ice-distal location. The distinctive monosulphide layers do not contain larger amounts of organic matter and are therefore thought to relate to variations in meltwater input as described by Stevens (1985).

Facies B — 2.8–1.3 m: The sediments in this facies consist of soft brown (7.5YR 6/4) homogeneous muds containing no monosulphides. The grain-size distributions are weakly unimodal and indicate a low-energy environment with suspension-dominated sedimentation.

In the dinoflagellate flora a marked change where the species *Operculodinium centrocarpum* (Deflandre and Cookson) gains dominance over *B. tepikiense* is used to define the lower boundary of facies B. This occurs together with an increase in cyst abundance and diversity. The predominance of *O. centrocarpum* suggests a much stronger penetration of Atlantic waters than identified in the facies below (Harland, 1983) and this is concomitant with the presence of more temperate species including *Spiniferites ramosus* (Ehrenberg) Mantell, *Spiniferites elongatus* Reid and *Spiniferites lazus* Reid. Only minor levels of dinoflagellate cyst reworking were recorded (approx. 10%).

Interestingly, apart from a few errant southern species such as *B.* cf. *vicksbergensis, Bulimina marginata* (d'Orbigny) and *Hyalinea baltica* (Shroeter), in the upper half of this unit, the foraminiferal assemblage is still dominated by the cold-water species *E. clavatum* with subordinate *C. reniforme*, giving little evidence for climatic amelioration. Thus, given the dinoflagellate cyst results, it is possible that the water column was seasonally stratified or alternatively that the foraminifera are derived.

The bivalve *P. arctica*, noted in facies A, is absent within facies B, suggesting some climatic amelioration. The macrofauna is dominated by *P.* (*Y.*) *lenticula* and *Nuculana pernula* (Müller) suggesting water temperatures less than today. The fragmented nature of much of the shell material may indicate some reworking.

This facies represents an amelioration when compared to facies A with

oceanographic conditions more similar to today although the foraminiferal assemblage and the presence of *N. pernula* suggests harsher conditions than those found at present. There is no evidence of any cyclic sedimentation and deposition appears to have been continuous and rapid.

Facies C — 1.3–0.4 m: This facies is lithologically similar to facies B with no apparent sedimentological change. However this unit is characterised by a poor dinoflagellate recovery and moderate reworking (~20%) with an assemblage intermediate between facies A and B. The dinoflagellate assemblage shows continued dominance of *O. centrocarpum* over *B. tepikiense*, but in contrast to the underlying facies, the assemblage shows a significant increase in cold water species such as *A. andalousiensis* and a paucity of more temperate species. In particular the return of round brown *Protoperidinium* cysts is thought to be indicative of some sea-ice cover.

The foraminiferal assemblage continues to be dominated by cold-water species, and southern species are represented only by sporadic occurrences of *B.* cf. *vicksburgensis*, indicating shallow glaciomarine conditions. The occurrence of *Elphidium asklundi* Brotzen and *Protelphidium orbiculare* (Brady) becomes significant in the middle of this facies suggesting falling water levels. However, there is increasing diversity and the assemblage at the top of the unit with *B. marginata, Cassidulina carinata* Silvestri, *H. baltica, Trifarina angulosa* (Williamson) and *Uvigerina peregrina* Cushman suggests moderate amelioration and significant deepening.

The macrobenthos is characterised by the return of *P. arctica* in association with *N. pernula* and unidentifiable gastropod and bivalve fragments. This, together with the micropalaeontology suggests a reversion to a cold phase, though one less severe than for facies A.

Facies D — 0.4–0.2 m: This consists of an olive-grey (5GY 5/2) sandy silt. The sediment is moderately to poorly sorted and the grain-size distribution is polymodal.

The dinoflagellate assemblage, dominated by *O. centrocarpum*, contains a significant proportion of temperate species including *S. ramosus, S. lazus* and *Spiniferites mirabilis* (Rossignol), *Protoperidinium conicum* (Gran) Balech and *Protoperidinium pentagonum* (Gran) Balech. Similarly in the foraminiferal benthos, the species *B. marginata, C. carinata, H. baltica, T. angulosa* (Williamson) and *U. peregrina* are all temperate species and suggest deep-water and fully marine salinities. The macrofaunal evidence is poor, consisting of apparently reworked bivalves, including *Arctica islandica* (Linné) and *Chlamys septemradiata* (Müller), but no cold indicators were found.

Facies D is therefore indicative of temperate conditions concomitant with an increase in water depth to around 100 m, and a return to normal salinities (30–35‰) similar to the present.

Clay mineralogy

The clay fraction is consistently dominated by illite with varying subsidiary proportions of kaolinite, chlorite and smectite. Calcite, quartz, feldspar and minor amounts of amphibole also occur. Illite dominates throughout, its proportion being inversely related to smectite content. The high 10–5 Å ratio suggests that the illite is iron-rich with low crystallinity. The presence of kaolinite in high-latitude sediments has been noted by a number of workers (Bjørlykke and Elverhoi, 1977) and it seems likely that it is derived from ancient sediments deposited in a low-latitude environment. The chlorite is thought to be iron-rich on the basis of the weak nature of the (001) and (003) peaks relative to the (002) peak (Darby, 1975).

Smectite shows major variations in both abundance and the degree of crystallinity. Only 2 samples, both from facies B, displayed distinct peaks at 17 Å and this is attributed to the greater crystallinity of the smectite. This crystallinity may represent more rapid deposition or a change in source area compared with the underlying facies. In facies A and C the generally diffuse and asymmetric smectite peaks may represent the presence of mixed-layer minerals similar to those identified by Berry and Johns (1966), who suggested that when clay minerals are introduced into the marine environment some K^+ and Mg^{2+} are displaced from the illitic and chloritic phases by Na^+. In addition K^+ and Mg^{2+} are randomly fixed in exchange positions of expandable clays. Such mixed-layer minerals are thought to be more stable in the marine environment and their presence in a sediment may suggest relatively slow deposition rates. Below 2.9 m there is a small decrease in the smectite:illite ratio. This decrease may represent deteriorating conditions in an adjacent source area (Robert and Maillot, 1981).

Geochemistry

Variations in the bulk geochemistry with depth are shown in Fig.5, and certain elements were also plotted as a ratio to Al_2O_3 to preclude a false impression of element proportions. The indices S* and D* (Fig.5) permit the recognition of detrital particles (Boström and Peterson, 1969).

The Fe:Al ratio shows a slight increase with depth to a maximum of 4.45 m. The occurrence of distinct monosulphide bands in facies A (Fig.5) probably accounts for these slightly higher concentrations of iron. The ratio of Mn:Al changes markedly down the core, reaching a maximum in facies A and a minimum in facies B. Arrhenius (1963) suggested that a high Mn content may be representative of an area with a slow rate of deposition as the longer period of sediment–seawater interaction would increase the chance of Mn being absorbed onto the sediment surface. It should be noted, however, that Mn values in the vibrocore are generally much lower than those recorded from the Weddell Sea by Angino (1966) which, if the postulation of Arrhenius is correct, suggests much lower deposition rates in the latter area. Increases in the Ca:Al

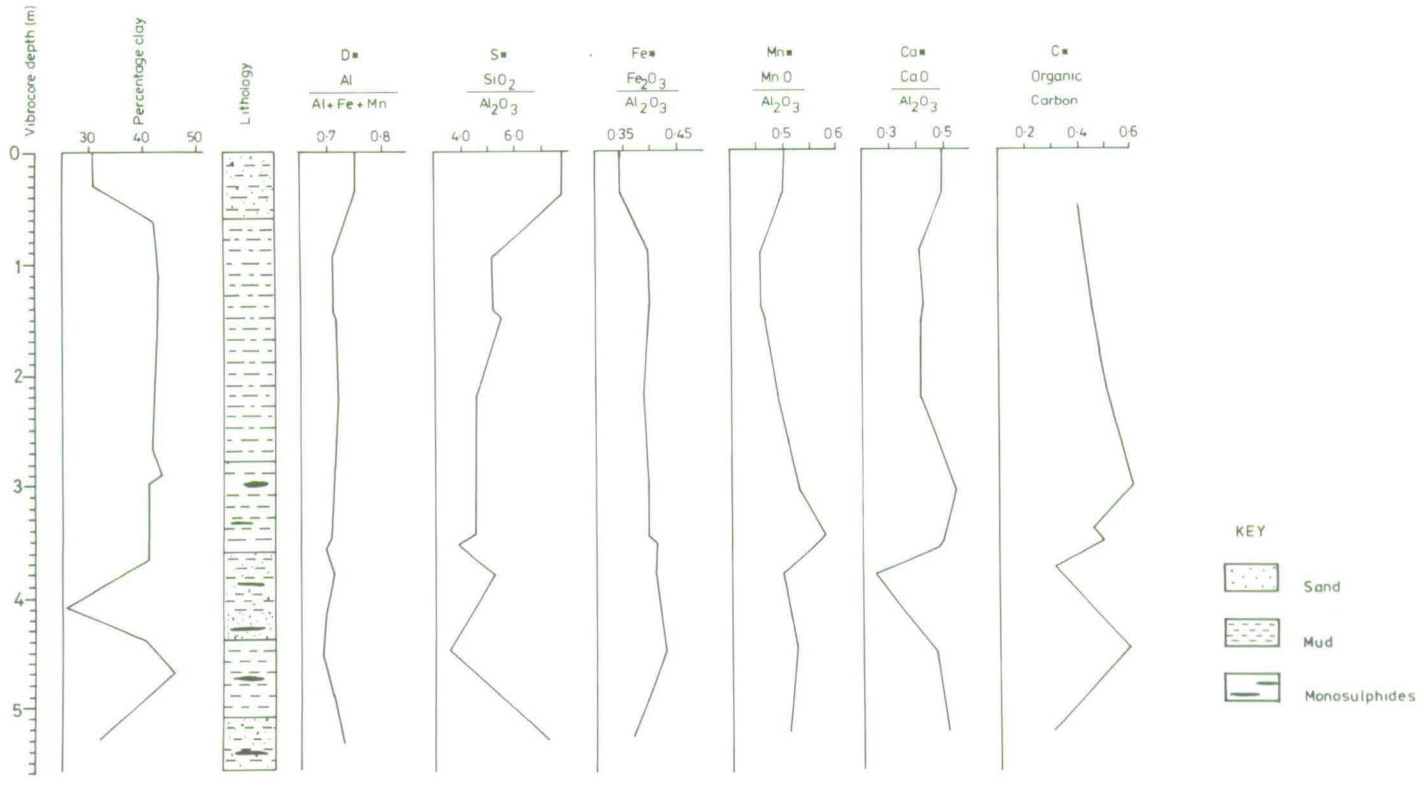

Fig.5. Geochemical parameters of VE 58+00/111.

ratio and corresponding decreases in the S* ratio probably represent reductions in detrital input and increased biogenic activity.

Ash layer

Glass shards were identified in the 63–125 μm fraction of a sample from 0.4 to 0.6 m depth (Fig.6). They are predominantly acidic with only a few highly altered basic glass shards. The acidic shards have a similar composition to those of the Vedde Ash identified in western Norway (Mangerud et al., 1984) including the characteristically high Fe content (Table 1). All the elements analysed have similar ranges to those described by Mangerud et al. (1984). This ash layer has been dated at 10,600 yrs B.P. (Mangerud et al., 1984). Although Ruddiman and McIntyre (1981) give a younger date (9800 yrs B.P.) for a similar ash layer identified in the North Atlantic, this date is now doubted (Ruddiman and Duplessy, 1985). The high iron content, typical of the Vedde Ash, is characteristic of rhyolitic obsidians erupted by the Icelandic volcano Katla (H. Sigurdsson, 1983, pers. commun., quoted by Mangerud et al., 1984, p.95).

TABLE 1

Chemical composition of the glass shards from 0.4–0.6 m (electron microprobe), compared with the composition of acidic glass from the Vedde Ash Bed in western Norway, as determined by Mangerud et al. (1984)

	Mean	Standard deviation	Range	Mangerud et al. (1984)
SiO_2	69.08	1.18	67.00–70.38	70.16–74.51
Al_2O_3	12.64	0.34	12.06–13.03	12.89–13.49
TiO_2	0.35	0.04	0.30–0.40	0.26–0.37
Cr_2O_3	0.04	0.06	0.00–0.15	
MnO	0.11	0.06	0.00–0.17	0.14–0.26
FeO_2	3.92	0.25	3.67–4.38	3.79–4.13
CaO	1.24	0.12	1.13–1.37	1.23–1.71
MgO	0.11	0.10	0.00–0.26	0.15–0.21
Na_2O	2.48	0.88	1.72–3.75	
K_2O	3.46	0.11	3.30–3.59	3.25–4.96
P_2O_5	0.09	0.06	0.00–0.14	
Total	93.52	1.22		

DISCUSSION

Using the facies types identified and with reference to earlier work by Jansen (1976) and Jansen et al. (1979), a tentative environmental model has been drawn up and possible age limits suggested (Fig.6).

It is postulated that facies A is a distal glaciomarine sediment deposited in shallow Arctic water conditions affected by sea-ice and with little or no

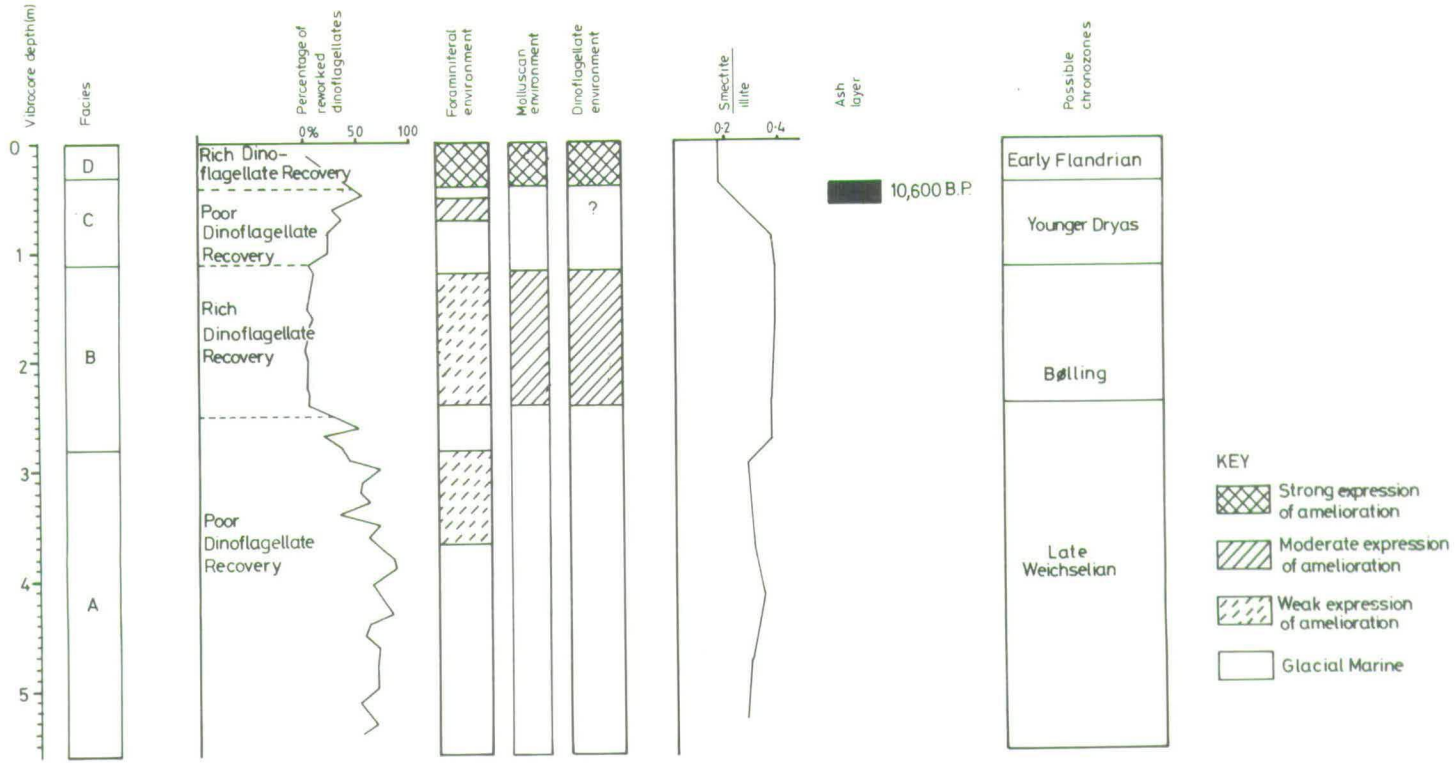

Fig.6. Palaeoenvironmental interpretation of VE 58+00/111 and possible associated chronozones.

contact with temperate North Atlantic waters. This conclusion is supported by the similarity of the faunal assemblage to that described in zone A from the Norwegian Sea by Jansen et al. (1983) who attributed the assemblage to a polar environment low in nutrients and oxygen. With regard to the age of this facies, it appears to be part of the Fladen Deposit described by Jansen (1976) and later as the Fladen Member by Stoker et al. (1985). If this assumption is correct, facies A was deposited in a cold period prior to 13,000 B.P. and may therefore be ascribed to the late Weichselian. This is older than the age suggested by McCave et al. (1977) who ascribed a Flandrian age to the entire transparent multilayered seismic unit but agrees in both age and environmental conditions to those suggested by Jansen (1976) and Jansen et al. (1979).

On this basis facies B would correlate with the distinct climatic amelioration in the North Atlantic record between 13,000 and 11,000 yrs B.P. known as the Bølling interstadial. A decrease or absence of sea-ice cover concomitant with a greater influx of warmer Atlantic waters would account for the more temperate dinoflagellate cyst fauna. However, persistent low-salinity values and evidence of rapid sedimentation are consistent with an input from meltwater sources perhaps producing water stratification and hence explaining the Arctic foraminiferal benthos. This facies may be assigned to the Witch Member of Stoker et al. (1985) and the lower Witch Deposits of Jansen (1976).

Facies C represents a colder period less severe than facies A. The waters remained in contact with the Atlantic and there was probably limited pack ice. The lack of monosulphides and the lithological similarity to facies B suggests that the prevalent nutrient- and oxygen-rich period was not greatly affected by this cooling. It therefore appears that this facies can be attributed to the Younger Dryas cooling between 10,000 and 11,000 yrs B.P. The existence of glass shards at the top of this unit, similar to those found in western Norway (Mangerud et al., 1984) and in the Norwegian Sea (Jansen et al., 1983) dated at 10,600 yrs B.P. fits the proposed time scale. The fact that this ash layer occurs within the colder facies C, fits with Mangerud's date of 10,600 yrs B.P. better than Ruddiman and McIntyre's date of 9800 yrs B.P.

The palaeontological evidence indicates that facies D represents the onset of the Holocene with conditions similar to those occurring at present.

CONCLUSION

Our results represent a continuous record of the marine environment from late Weichselian to Holocene times in the central North Sea and provide evidence of changes in salinity, hydrographic regime and amount of ice cover up to the present day. The Younger Dryas is evident in the micropalaeontological data and an ashfall corresponding to the Vedde Ash has been identified in the UK sector. The interpretation of facies B and C suggests sedimentation rates of about 800 mm ka^{-1}. However, it should be noted that vibrocore VE 58+00/111 was obtained from a condensed sequence based on seismic evidence.

The identification of the Vedde Ash horizon in the UK sector is important as

APPENDIX 9

QUATERNARY STRATIGRAPHY OF THE FLADEN AREA, CENTRAL NORTH SEA: A MULTIDISCIPLINARY STUDY

By: Sejrup, H.P., Aarseth, I., Ellingsen, K.L., Lovlie, R., Reither, E., Bent, A., Brigham-Grette, J., Jansen, E., Larsen, E., Stoker, M. (in press). J. Quaternary Sci.

Abstract

Detailed stratigraphic investigations have been performed on a 200, 6m-long core (81/26) from the Fladen Ground area, British sector, central North Sea. In addition, core material from the Sleipner field (Norwegian sector) and shallow seismic profiles between the core sites have been studied. The geochronology of the cores is based on radiometric dates, amino acid chronology, palaeomagnetism, faunal extinctions and correlation of climatic events with surrounding areas and the deep-sea record.

The following palaeoenvironmental changes have been recorded in the cores, which span appr. 1 mill. year:

1. The North Sea was glaciated sometime during the later part of Matuyama reversed period. A complete glacial-interglacial-glacial cycle is recorded in these sediments. The interglacial is tentatively correlated with the Leerdam interglacial (in the Bavelian stage) in Netherlands (Zagwijn 1985).

2. In a period of marine sedimentation in the Middle Pleistocene, a transgression-regression cycle under boreo-arctic regime is recorded. The upper part of this sequence was deposited at 0-10 m water depth. This suggests that this part of the North Sea has subsided at a rate of between 0,9 and 0,6 m/ka through the later parts of the Quaternary.

3. A major glacial event dated at between 130 and 200 ka is recorded as a thick till unit in 81/26. This till which was deposited by ice moving from the southwest (Scotland), probably represents a period when the Scandinavian and British ice sheets coalesced in the North Sea.

4. No conclusive evidence was found in core 81/26 that the Scandinavian and British ice sheets coalesced in the Fladen area in the Late Weichselian. However, based on the seismic data and the

stratigraphy of the Sleipner core, a Late Weichselian scenario with an ice free, open embayment/dry land, is favoured for the central North Sea.

Also, some general conclusions can be drawn concerning the Quaternary sedimentation. First, especially from the amino acid data, it is shown that there has been an episodic style of sedimentation. Periods with high sedimentation rates were interrupted by large hiatuses representing erosion and/or nondeposition. Secondly, the interglacials play a relatively insignificant role in terms of sedimentation through the Quaternary. Of the investigated sediment appr. 98% have been deposited under arctic to boreo-arctic conditions.

APPENDIX 10

LOWER PLEISTOCENE DELTAIC AND MARINE SEDIMENTATION IN THE UK SECTOR OF THE CENTRAL NORTH SEA

By: Stoker, M.S., and Bent, A.J.

(in press). J. Quaternary Sci.

Abstract

A sequence of Lower Pleistocene deltaic and marine sediments has been identified in the UK sector of the central North Sea. The sediments comprise delta front, distributary mouth bar facies, prodelta facies, marginal marine estuarine and subtidal chanel facies, and sub-littoral marine and possible tidal sand ridge facies. Facies sequences and relationships indicate that deltaic sedimentation is associated with a major regressive episode resulting from the influx of coarse clastic detritus into a predominantly argillaceous marine basin. The delta-related sediments form part of a massive northerly progradation of the delta systems of eastern Britain and north-west Europe throughout early Pleistocene time. Sedimentation was controlled by a combination of isostatic and eustatic influences. Uplift around the margin of the basin was compensated by extensive subsidence in the North Sea enabling up to 500m of sediment to accumulate. However, the sequence is punctuated by a series of basin-wide unconformities which reflect glacio-eustatic changes in sea level. the bulk of the sequence was deposited during interglacial periods associated with rising sea levels, although high sedimentation rates resulted in an overall regressive regime. During low sea level stands much of the basin may have been an area of sediment by-pass.

Fig. 2.6. Line interpretations of north-south seismic profiles in the study area. Vertical scale is in metres below sea level, horizontal scale is 1:500,000. Figure numbers (circled) show location of the respective profile.

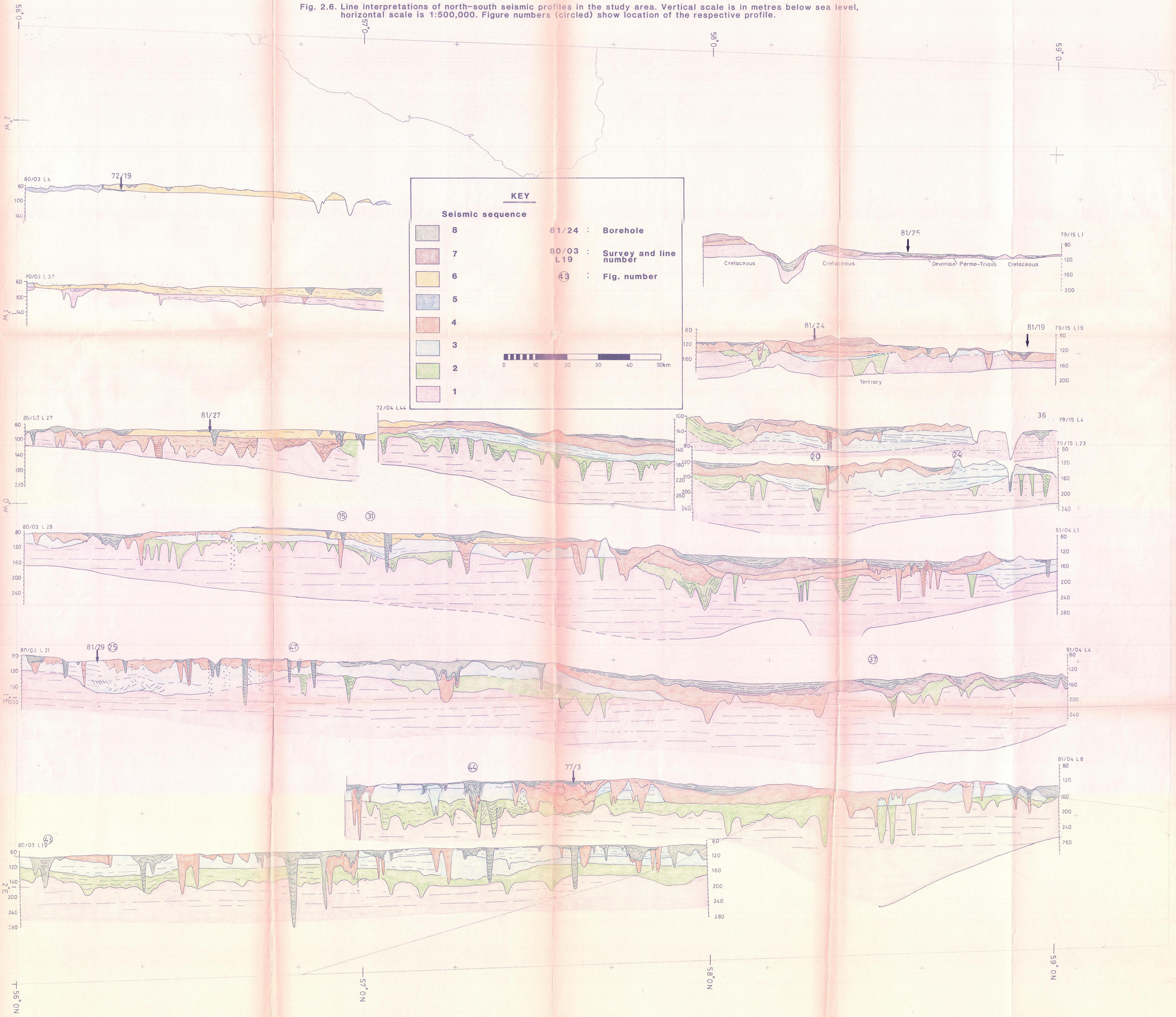

Fig. 2.5. Line interpretations of east-west seismic profiles in the study area. Vertical scale is in metres below sea level, horizontal scale is 1:500,000. Figure numbers (circled) show location of the respective profile.

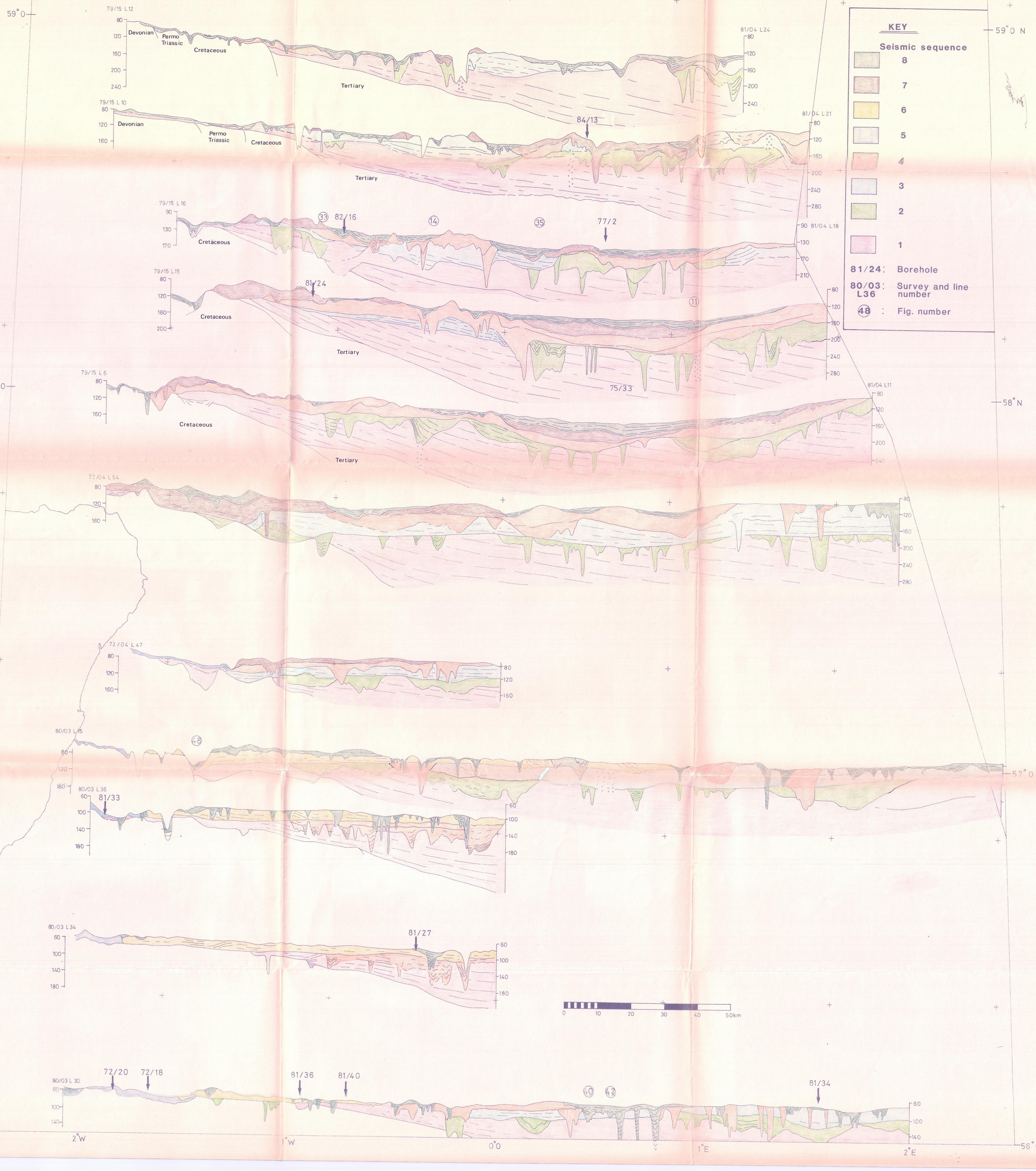

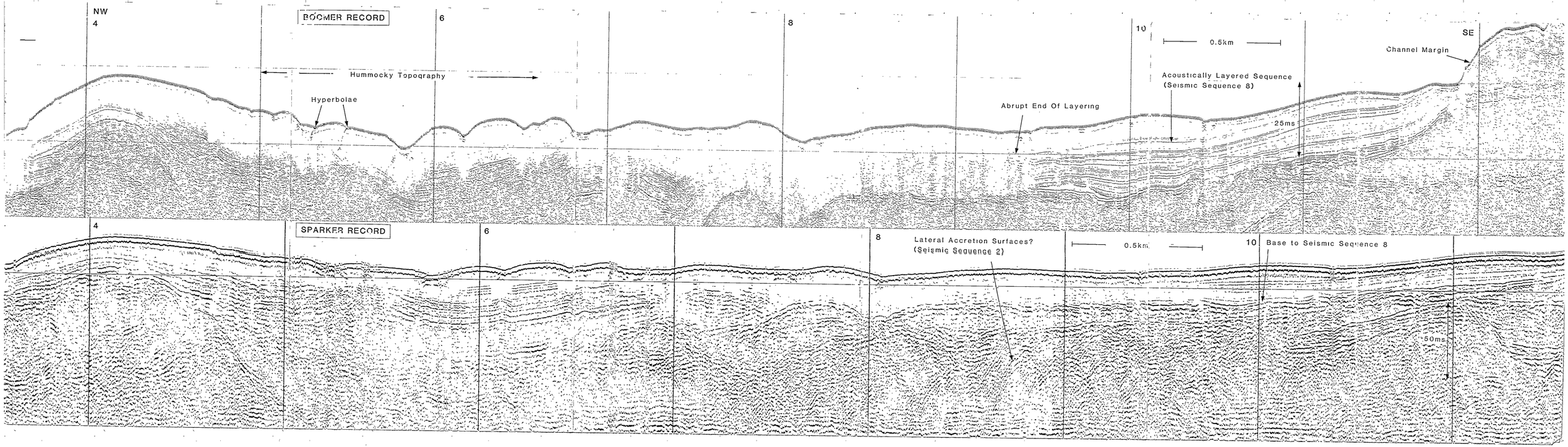
NW
4
BOOMER RECORD
6
8
10
0.5km
SE
Channel Margin
Hummocky Topography
Hyperbolae
Acoustically Layered Sequence
(Seismic Sequence 8)
Abrupt End Of Layering
25ms
4
SPARKER RECORD
6
8
Lateral Accretion Surfaces?
(Seismic Sequence 2)
0.5km
10
Base to Seismic Sequence 8
50ms

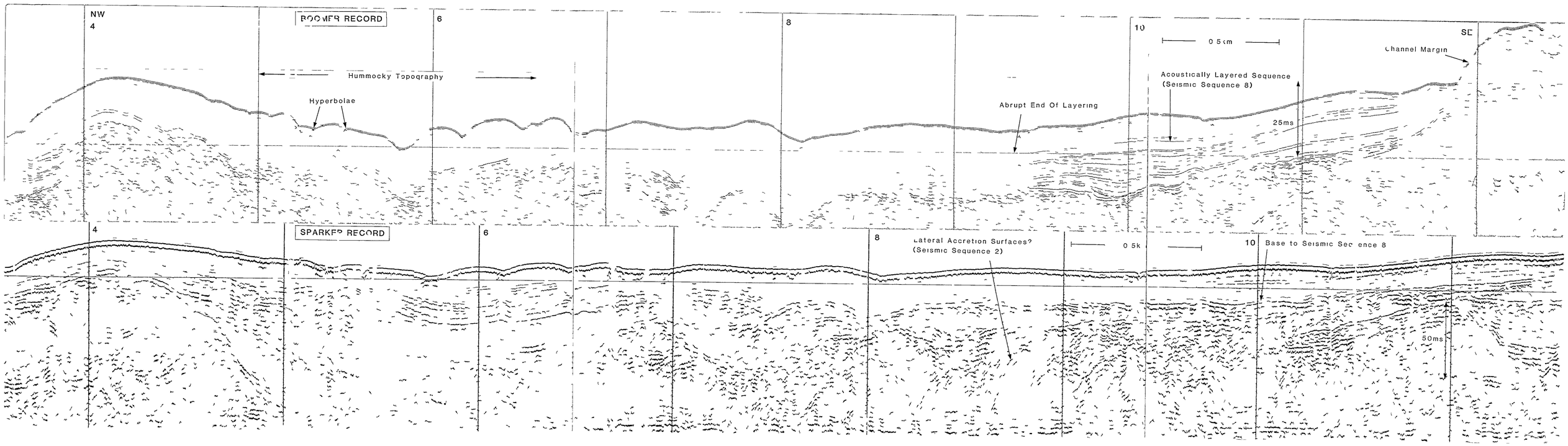
NW
4
BOOMER RECORD
6
8
10
0 5km
SE
Channel Margin
Hummocky Topography
Hyperbolae
Abrupt End Of Layering
Acoustically Layered Sequence
(Seismic Sequence 8)
25ms
4
SPARKER RECORD
6
8
Lateral Accretion Surfaces?
(Seismic Sequence 2)
0 5k
10
Base to Seismic Sequence 8
50ms